UNIVERSIDAD AUTÓNOMA DE NUEVO LEÓN
FACULTAD DE INGENIERÍA MECÁNICA Y ELÉCTRICA

THESIS

"*SYNTHESIS AND CHARACTERIZATION OF METAL NANOPARTICLES BY PULSED LASER ABLATION IN LIQUID MEDIA (PLAL)*"

BY

M.C. MARÍA ISABEL MENDIVIL PALMA

SUBMITTED IN PARTIAL FULFILLMENT OF THE REQUIREMENTS FOR THE DOCTORAL DEGREE IN MATERIALS ENGINEERING

N O V E M B E R, 2 0 1 5

UNIVERSIDAD AUTÓNOMA DE NUEVO LEÓN
FACULTAD DE INGENIERÍA MECÁNICA Y ELÉCTRICA

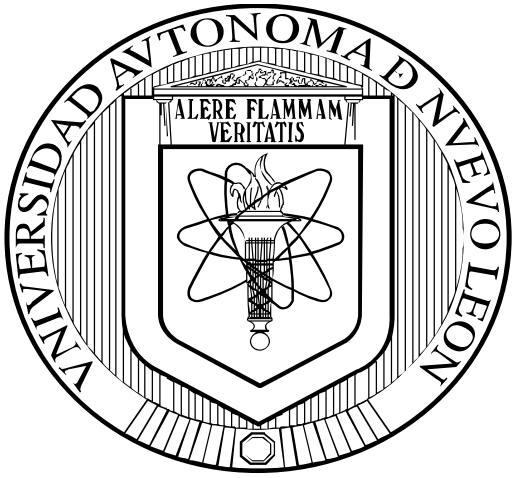

THESIS

"*SYNTHESIS AND CHARACTERIZATION OF METAL NANOPARTICLES BY PULSED LASER ABLATION IN LIQUID MEDIA (PLAL)*"

BY

M.C. MARÍA ISABEL MENDIVIL PALMA

SUBMITTED IN PARTIAL FULFILLMENT OF THE REQUIREMENTS FOR
THE DOCTORAL DEGREE IN MATERIALS ENGINEERING

N O V E M B E R, 2 0 1 5

UNIVERSIDAD AUTÓNOMA DE NUEVO LEÓN
FACULTAD DE INGENIERÍA MECÁNICA Y ELÉCTRICA
SUBDIRECCIÓN DE ESTUDIOS DE POSGRADO

THESIS

"*SYNTHESIS AND CHARACTERIZATION OF METAL NANOPARTICLES BY PULSED LASER ABLATION IN LIQUID MEDIA (PLAL)*"

BY

M.C. MARÍA ISABEL MENDIVIL PALMA

SUBMITTED IN PARTIAL FULFILLMENT OF THE REQUIREMENTS FOR THE DOCTORAL DEGREE IN MATERIALS ENGINEERING

SUPERVISED BY
DR. SADASIVAN SHAJI

SAN NICOLÁS DE LOS GARZA, NUEVO LEÓN, MÉXICO NOVIEMBRE, 2015

UNIVERSIDAD AUTÓNOMA DE NUEVO LEÓN

FACULTAD DE INGENIERÍA MECÁNICA Y ELÉCTRICA
SUBDIRECCIÓN DE ESTUDIOS DE POSGRADO

The Thesis Committee members recommended that the thesis ***"SYNTHESIS AND CHARACTERIZATION OF METAL NANOPARTICLES BY PULSED LASER ABLATION IN LIQUID MEDIA (PLAL)"*** by student **M. C. María Isabel Mendivil Palma** with registration number **1148300** be accepted as an option for its defense to the degree of Doctor of Engineering in Materials.

Thesis Committee members

Dr. Sadasivan Shaji
Research guide

Dr. Víctor Manuel Coello Cárdenas
Reviewer

Dr. Manuel García Méndez
Reviewer

Dra. Bindu Krishnan
Reviewer

Dr. David Avellaneda Avellaneda
Reviewer

Dr. Simon Martínez Martínez
Sub-Director, Post-Graduate Studies

San Nicolás de los Garza, Nuevo León November, 2015

A C K N O W L E D G E M E N T S

Thanks to God for all his love…

I would like to thank **CONACYT** for the assistance and support through a research fellowship.

To **FIME**, UANL for the scholar preparation and facilities to the use of laser laboratory.

Thanks to **CIIDIT**, especially to Dr. Domingo Garcia and Dr. Alejandro Torres for their training, help and support in the use of Transmission Electron Microscope (TEM).

I would like to thank my assessor *Dr. Sadasivan Shaji*, for sharing his knowledge, all the comments during this project and principally the continuous motivation for improvement personally and scientific area.

Thanks to *Dra. Bindu Krishnan* for lean my academic achievements.

Thanks to my thesis revisers, *Dr. Víctor Manuel Coello Cárdenas, Dr. Manuel García Méndez* and, *Dr. David Avellaneda Avellaneda* for their help in the corrections and comments to this thesis.

Thanks to Dr. Alan Castillo and Dr. Tushar Kanti Das Roy for their advice and support.

The next part of acknowledgments will be in Spanish in consideration to the persons to whom it is directed.

Agradezco infinitamente a mi familia que ha sido mi mayor aliento para continuar con mi preparación académica, pero sobre todo por enseñarme lo maravillosa que es la vida y lo afortunada que soy al tenerlos a todos ustedes.

Quiero agradecer y dedicar muy especialmente este trabajo a mi nana Rosa Cruz Mendoza, por todas sus bendiciones que nos siguen llegando aún después de su partida.

Al amor de mi vida, Edgar Adrian Castro por estar ahí siempre para apoyarme. Me encanta poder compartir contigo cada instante de mi vida. Te amo.

A mis hijas, Isabella e Itzel quienes son las propulsoras de mi vida y de todos mis proyectos. Las amo.

A mi MADRE, por su incansable fe en mí, su apoyo, correcciones y consejos. No estaría aquí sin su infinito amor de madre.

Gracias a mi PADRE, porque sé que siempre cuento con él en todo lugar y todo momento.

Mis herman@s y cuñad@s; Jorge mi dador de felicidad favorito, eres fuerte para proteger lo que amas y sensible cuando ocupamos consuelo y apoyo. Carlos mi inventor predilecto, se que pronto salvaremos el mundo. Ana mi comadre y hermana, he descubierto en ti a una gran amiga. Isaí, Laila y Lupita gracias por su gran cariño.

Gracias a Carlos Almanza por acompañarnos en este viaje y aguantar a esta singular familia.

Gracias por todo su apoyo y amor a toda mi bella familia, abuela María Peraza, tíos, primos y sobrinas.

Gracias a los grandes amigos que conocí durante esta etapa, Grisel, Ernesto, Linda, Dorian, Daniel, Shadai, Karina, Gaby, Pao, Dana, ha sido un placer trabajar con ustedes y haberlos conocido.

Dedicado a mi enfermera favorita…

(†) Rosa Cruz Mendoza

ABBREVIATIONS

(0-3) D	(0-3) Dimension
BF-TEM	Bright Field TEM
CIS	Copper-Indium-Selenide
CNT	Carbon Nanotubes
CVD	Chemical Vapor Deposition
CW	Continuous Wave
DC	Direct Current
DLTT	Distance from Lens to Target
DNA	Deoxyribonucleic Acid
DP-LA	Double Pulsed Laser Ablation
DW	Distilled Water
EDX	Energy Dispersive X-Ray
EG	Ethylene Glycol
FCC	Face-Centered-Cubic
GNS	Graphene Nano-Sheet
HAADF	High Angular Annular Dark Field
HEX	Hexagonal
HRTEM	High Resolution TEM
IR	Infrared
ITO	Indium Tin Oxide
KrF	Krypton Fluoride
LAL	Laser Ablation in Liquids
Laser	Light Amplification by Stimulated Emission of Radiation
LCVD	Laser CVD
LDI	Laser Deposition Ionization
LED	Light Emitting Diode
LIFT	Laser-Induced Forward Transfer
LPCVD	Low Pressure CVD
LVCC	Laser Vaporization Controlled Condensation
MBE	Molecular Beam Epitaxy
MOVPE	Metal-Organic Vapor Phase Epitaxy
MRI	Magnetic Resonance Imaging
MWCNT	Multi Walled Carbon Nanotubes
Nd:YAG	Neodymium-Doped Yttrium Aluminum Garnet
NEMS	Nano-Electromechanical Systems
NIR	Near Infrared

NPs	Nanoparticles
NW	Nanowire
PACVD	Plasma-Assisted CVD
PEG	Poly Ethylene Glycol
PL	Pulsed Laser
PLAL	Pulsed Laser Ablation in Liquid
PLD	Pulsed Laser Deposition
PLM	Pulsed Laser Melting
PVA	Poly Vinyl Alcohol
PVD	Physical Vapor Deposition
PVP	Polyvinylpyrrolidone
RF	Radio Frequency
SAED	Selected Area Electron Diffraction
SDS	Sodium Dodecyl Sulphate
SERS	Surface Enhanced Raman Scattering
SPR	Surface Plasmon Resonance
STEM	Scanning Transmission Electron Microscope
STM	Scanning Tunneling Microscope
TEM	Transmission Electron Microscopy
TEOS	Tetraethyl Orthosilicate
TTM	Two Temperature Model
UV-Vis	Ultra Violet-Visible
XPS	X-Ray Photoelectron Spectroscopy
YDFL	Ytterbium Doped Fiber Laser

CONTENTS

SUMMARY

Pulsed laser ablation as a novel technique had been employed in this work for the synthesis of Ag, Au, Pd and Pt nanoparticles with different experimental conditions. The different conditions of PLAL such as variation of laser parameters and liquid media were selected based on the literature review and previous knowledge obtained in master studies for this thesis work Silver and gold nanoparticles were obtained by PLAL in distilled water using 1064 and 532 nm output wavelengths. The experiments (single-PL, in-situ and post CW) were performed to study the effect of continuous laser irradiation over the final properties of nanoparticles synthesized by PLAL. Pd nanoparticles were synthesized by PLAL at 1064 nm of wavelength with different energy fluence (40.5, 26.5, 18, 12.5 and 8 J/cm^2). Palladium nanoparticle colloidal solutions were obtained in different liquid media such as distilled water (DW), methanol-water mixture, ethylene glycol (EG) and in aqueous solution of sodium dodecyl sulphate (SDS) at 0.001 M. Pd NPs obtained by PLAL in water and methanol-water mixture were treated with pulsed laser post-irradiation using 532 of wavelength with focused and unfocused beam. Ultrasonic treatment was used as a simple alternative to re-disperse and recover the optical properties of Pd NPs obtained by PLAL after their precipitation. All the samples of Pd NPs produced by PLAL in DW, methanol-water mixture and SDS (with and without post-irradiation treatment) were taken to an ultrasonic bath treatment to explore their effect in re-dispersion and the optical properties of the ablated products. Platinum nanocolloids were synthesized by pulsed laser ablation in methanol, ethanol and acetone, respectively at different energy fluence (25, 19 and 9 J/cm^2) and time of ablation (5, 10 and 15 minutes for 25 J/cm^2 of fluence). For all the sets of nanoparticles obtained by PLAL, morphology, crystalline structure, elemental composition and optical properties were characterized by using TEM, EDX, XPS and UV-Vis absorption spectroscopy techniques.

CHAPTER 1

INTRODUCTION TO NANOMATERIALS AND PULSED LASER ABLATION IN LIQUID

1.1 GENERAL INTRODUCTION TO NANOMATERIALS

1.1.1 Introduction

Nanotechnology is an important topic that implies design, fabrication and application of nanostructures or nanomaterials, and the fundamental understanding of the relationships between physical properties or phenomena and material dimensions [1]. The recent advances in their synthesis methods, characterization techniques and applications have been of great utility. Another important aspect of nanotechnology is the miniaturization of current and new instruments, sensors and machines. We can find their applications in a great variety of areas as nanoscale electronics and optics, nanobiological systems, nanomedicine, technology, biology, disease treatments, etc. Therefore requires contribution from multidisciplinary teams of physicists, chemists, materials scientists, engineers, molecular biologists, pharmacologists, etc. In this thesis we report an easy, fast, alternative-novel and one-step method for the preparation of pure and stable (in some cases) noble metal nanoparticles, viz Pulsed Laser Ablation in liquid media; this method presents significant advantages over chemical routes as: pure metal nanoparticles production, less aggregation, non-vacuum requirements, non-toxic agents are required, size and shape tunability, between others. Pulsed laser ablation in liquid media will be described in detail in the next part,

1.1.2 Properties of Nanomaterials

At nanometer scale, materials or structures may possess new physical properties or exhibit new physical phenomena different from that of bulk. For example, Crystal structures stable at elevated temperatures are stable at much lower temperatures in nanometer sizes; bulk gold (Au) does not exhibit catalytic properties, Au nanocrystal demonstrates to be an excellent low temperature catalyst. Some physical properties of

nanomaterials are related to large fraction of surface atoms, large surface energy, spatial confinement and reduced imperfections. For examples: 1) lower melting point or phase transition temperature and appreciably reduced lattice constants of nanomaterials are due to a huge fraction of surface atoms in the total amount of atoms. 2) Mechanical properties of nanomaterials may reach one or two orders of magnitude higher than that of single crystals in the bulk form due to the reduced probability of defects. 3) Optical properties of nanomaterials can be significantly different from bulk crystals. For example, the optical absorption peak of a semiconductor nanoparticle shifts to a shorter wavelength, due to an increased band gap (by varying material dimension). Surface plasmon resonance is characteristic of metal nanoparticles, which can be appreciated in different color of metallic NPs by varying their sizes. 4) Electrical conductivity decreases with a reduced dimension due to increased surface scattering. However, electrical conductivity of nanomaterials could also be enhanced appreciably, due to the better ordering in microstructure, e. g. in polymeric fibrils. 5) Magnetic properties of nanostructured materials are different from that of bulk materials. Ferromagnetism of bulk materials disappears and transfers to superparamagnetism in the nanometer scale due to the huge surface energy [1].

1.1.3 Applications

Nanomaterials had a great diversity of fields of applications due to their novel properties. These applications are based principally on size dependence of physical properties and huge surface area. Some examples or area of applications can be mentioned as follows. In **molecular electronics**, which are sensors that translate unique molecular properties into electrical signal. Various electronic devices based on Au nanoparticles and Au_{55} clusters have been as the single electron transistor action, that contain ideally only one nanoparticle in the gap between two electrodes separated by only a few nanometers [2]. Single-walled carbon nanotubes have also been intensively studied for nanoelectronic devices, due to the semiconducting behavior of different allotropes. In **medicine** is another important field of application of nanotechnology which is often referred as nanomedicine. For example, the creation of nanoscale devices for improved therapy and diagnostics namely as nanobots. Their principal function briefly is to serve as vehicles for delivery of therapeutic agents, detectors or guardians against early disease and perhaps repair of metabolic or genetic defects. The fix delivered by the nanobots may be that of releasing a

drug in a localized area, thus minimizing the potential side effects of generalized drug therapy [3-5]. Nanobiotechnology is the use of nanostructures as highly sophisticated scopes, machines or materials in biology and/or medicine, and the use of biological molecules to assemble nanoscale structures. Some other applications of nanomaterials in **biology** or medicine are: fluorescent biological labels, bio detection of pathogens, detection of proteins, probing of DNA structure, tissue engineering, tumor destruction via heating (hyperthermia), separation and purification of biological molecules and cells, MRI contrast enhancement and phagokinetic studies [6, 7]. Industrial **catalysis** is other important field of application of nanoparticles. Their applications include as chemical manufacturing, energy conversion and storage. Catalytic activity of NPs is dependent of their size, shape and surface sites [8]. As mentioned previously, properties of materials were completely different at nanoscale dimensions. For example, bulk gold is chemically inert but gold NPs have excellent catalytic properties. Gold NPs have been reported in catalysis and photocatalysis processes due to their effectiveness in degrading and mineralizing organic compounds [9, 10]. Other metals as Pd and Pt nanoparticles exhibit excellent catalytic properties [11-14]. The energy sector is an important topic in which the principal goal is to obtain a more effective and efficient process as nano-based technology. Nanomaterials in energy applications would include: lithium-ion battery, fuel cell, light emitting diode (LED), ultracapacitor and solar cells [15] to obtain better performance. For example, nanostructures are advantageous for photoelectrochemical **cell devices** for high efficient conversion of light to electrical power due to its large surface area at which photoelectrochemical processes take place. The fabrication of **solar cells** has passed through a large number of improvement steps considering the technological and economic aspects. Different generations of solar cells had been development as based on Si wafers, thin films of amorphous Si and CIS (Copper-Indium-Selenide), nanocrystals and nano-porous materials and quantum dot solar cells based on CdSe-TiO_2structures, among others [16, 17]. As example of as smart nanostructures can increase the yield of solar cells, Sandeep et al. [18] reported the use of linked quantum dots. These researchers reported a new design, in which the empty space between quantum dots was filled with aluminum oxide. This approach allows more contact between the quantum dots and higher mobility of the electrons. **Plasmonic sensing** is another important research field which was based on

surface plasmon resonance typical of metal nanoparticles. These plasmon sensors were applied for example in miniaturized optical devices, sensors, photonic circuits and detection of trace molecules in chemistry and biology. The sensing techniques are based on surface-enhanced spectroscopies and surface plasmon resonances (SPRs) [19, 20]. Semiconductor **nanowires** (NWs) are nanomaterials that through controlled growth and organization are used on novel nanoscale photonic and electronic devices. Then semiconductor NWs offer many opportunities for the assembly of nanoscale electronic and optoelectronic devices. **Electronic and optoelectronic** devices are present in a great range of areas since simple household appliances and multimedia systems to communications, computing, and medical instruments [21, 22]. Bhattacharya et al. [23] reported the growth and electronic properties of InGaAs quantum dots for optoelectronic devices. Self-organized In(Ga)As/GaAs quantum dots are grown by molecular beam expitaxy (MBE) or metal-organic vapor phase epitaxy (MOVPE) on GaAs, InP, and other substrates and are being incorporated in microelectronic and opto-electronic devices. Another important field is **nano-electromechanical systems** (NEMS) which are suitable for a multitude of technological applications such as ultrafast sensors, actuators, and signal processing components [24, 25]. However, an important NEMs engineering challenge is the detection of displacements in the picometer or even femtometer range at gigahertz frequencies [26]. By this brief summary, it is possible to note that the applications of nanotechnology in different fields have distinctly different demands and challenges, which require different approaches. And their technological advances depend on many factors as understanding nanomaterial properties, nano-manipulation and characterization techniques, among others.

1.1.4 Synthesis of Nanomaterials

Synthesis of nanomaterials is an important aspect of nanotechnology. Synthesis methods of nanomaterials rely on search for new physical properties and applications of nanomaterials and nanostructures. The principal goal of synthesis method is to allow a desired size, morphology, crystal microstructure and chemical composition. There are two principal classification of synthesis methods; top-down and bottom-up process. Top down means taking bulk material and fragment it. Top-down process had advantages as universality and low cost, but the main disadvantages are polydispersity of final products and the introduction of many defects [26]. Bottom-up process refers to the build-up of a

material from the bottom: atom-by-atom, molecule-by-molecule, or cluster-by-cluster. Advantages of bottom-up are to obtain nanostructures with less defects, more homogeneous chemical composition, and better short and long range ordering. This introduction presents some examples of synthesis techniques according this classification. By top-down techniques includes milling or attrition which can produce nanoparticles of tens to several hundred nanometers in diameter. However, nanoparticles produced by **attrition** have a relatively broad size distribution and varied particle shape or geometry. Also lithography and their variant as photolithography, optical and X-ray lithography, electron beam lithography, focused ion beam lithography, dip-pen lithography, extreme UV lithography and scanning probe lithography are very useful top-down techniques to nanofabrication. **Lithography** is the process of transferring a pattern into a reactive polymer film (termed as resist) which will be used to replicate that pattern into a thin film or substrate. Some examples of use of lithography are the fabrication of nanowires by electron beam lithography, ion beam lithography, STM lithography, X-ray lithography, proxial-probe lithography and near-field photolithography. Electron beam lithography is the most powerful tool for the fabrication of features as small as 3-5 nm. Photolithography is the most widely used technique in microelectronics fabrication [27]. Bottom-up synthesis techniques can be divided into chemical process (**as sol-gel, chemical vapour deposition (CVD**), **plasma or flame spraying**, homogeneous nucleation from liquid or vapour and atomic or molecular condensation) and physical process (as **physical vapour deposition (PVD) and laser ablation**). Self-assembly is another important bottom-up process used in nanotechnology. Some of the mentioned synthesis techniques will be briefly described as follows. **Sol-gel** is a wet chemical route for the synthesis of colloidal dispersions which has been widely used in the fields of materials science, ceramic engineering and especially in the preparation of photocatalysts. From such colloidal dispersions, powders, fibers, thin films and monoliths can be readily prepared. The fundamentals and general approaches in the synthesis of colloidal dispersions are well established and vary specific considerations to the different forms of final products. Some advantages for this technique are the low processing temperature and molecular level homogeneity [28, 29]. **Chemical Vapor deposition (CVD)** consists in activating an in situ chemical reaction between the substrate surface and a gaseous precursor. Chemical vapor deposition and its variants such as low

pressure CVD (LPCVD), plasma-assisted CVD (PACVD), and laser CVD (LCVD) have been active areas of research for many years. In CVD a solid material is deposited from gaseous precursors onto a substrate. The substrate is typically heated to promote the deposition reaction and/or provide sufficient mobility of the adatoms to form the desired structure. CVD is widely used to produce carbon nanotubes. There are reports of many phases deposited by CVD, which include most of the metals and many carbides, nitrides, borides, silicides, and sulfides [30, 31]. **Plasma of flame spraying** is a branch of thermal spray process. A high temperature flame is used to heat the feedstock material as well as spray it into a condensation chamber, where it will condense as nano-sized particles. Plasma spray allows process of multilayered structures in a successive spray process using only one piece of equipment, allowing deposition of several materials with controlled porosity and microstructure [32, 33]. Formation of metal quantum dots in glass matrix by annealing at moderate temperatures is a good example of the formation of nanoparticles by **homogeneous nucleation** in which a supersaturation of growth species must be created. Supersaturation would be generating through in situ chemical reactions by converting highly soluble chemicals into less soluble chemicals. Nanoparticles can be synthesized through homogeneous nucleation in three media: liquid, gas and solid; however, the fundamentals of nucleation and subsequent growth processes are essentially the same [34, 35]. **Physical vapor deposition (PVD)** is a process in which the materials are deposited from a source or target onto a substrate to form a film. The process mostly involves no chemical reactions and proceeds atomistically (the individual atoms or clusters removed from the surface are deposited on the substrate). The thickness of the deposits can vary from angstroms to millimeters. The removal of growth species from the source or target is achieved by two physical principles: evaporation and sputtering. In evaporation, the growth species are removed from the source by thermal means. In sputtering, atoms or molecules are dislodged from solid target through impact of gaseous ions (usually Argon). The inert ions bombarding the target are produced by DC or RF plasma. A very large number of inorganic materials (metals, alloys and compounds) as well as some organic materials can be deposited using PVD technologies [36-38]. **Self assembly** is an approach that ordered arrangement of molecules and small components such as small particles occurred spontaneously under the influence of certain forces such as chemical reactions, electrostatic

attraction and capillary forces. Self-assembled monolayers are molecular assemblies that are formed spontaneously by the immersion of an appropriate substrate into a solution of an active surfactant in an organic solvent. One of the important applications of self-assembly is the introduction of various desired functionalities and surface chemistry to the inorganic materials. Self-assembled organic monolayers are widely used to link different materials together; to the synthesis and fabrication of nanomaterials and nanostructures, particularly the core-shell structures [39-41]. **Laser ablation** of solid materials has been studied intensively due to their great potential in laser-based material processing [42]. In general techniques of laser processing of nanostructures are simple, quick, one-step and green, and produce materials having surfaces free from chemical contamination [43]. Laser-based nanomaterial processing methods can produce 0D, 1D, 2D, and 3D nanostructures in the gaseous or liquid phases, and can produce nano-/microstructures at the selective sites of bulk solid materials. Pulsed laser deposition [44, 45], laser vaporization controlled condensation (LVCC) [46], laser pyrolysis [47-49], laser chemical vapor deposition [50, 51], laser-induced direct surface writing for nano-/microfabrication [52, 53], two-photon polymerization [54], laser-induced forward transfer (LIFT) [55], laser ablation in liquids (LALs) [56, 57], laser-induced melting [58-60], laser fragmentation for resizing and reshaping of particles [61-68] and laser-induced photo dissociation of liquid precursors [69] are some of these processes. Laser ablation is easily carried out in conventional deposition chambers with vacuum or filled gas. Laser ablation has proven to be an effective technique for the deposition of complex films including complex metal oxides such as high T_c superconductor films [70, 71]. One of the great advantages that laser ablation offers is the control of the vapor composition. In principle, the composition of the vapor phase can be controlled as that in the source. The disadvantages of laser ablation include the complex system design, not always possible to find desired laser wavelength for evaporation, and the low energy conversion efficiency [1]. Pulsed laser ablation in liquids (PLAL) is an important technique for the synthesis of a great diversity of materials as metals, alloys, oxides, semiconductors and composites [72-75]. This is a simple, rapid and one step approach which can be developed at ambient pressure, without chemical agents. Nanomaterials synthesized by PLAL are charged and thus possess extremely high colloidal stability without the use of surfactants. Since no chemical precursors are used, NPs are free

from any type of chemical contamination. Then nanomaterials obtained by PLAL are excellent for their use in biocompatibility, functionalization, drug loading, environmental sensing and medical applications.

1.2 PULSED LASER ABLATION IN LIQUID

1.2.1 Introduction

Pulsed laser ablation in liquid (PLAL) is an important method for the synthesis of nanoparticles with tunable morphology and size. After the invention of the first pulsed Ruby laser by Maiman [76] laser-matter interactions has been studied by many researchers. Pulsed laser ablation in a vacuum or dilute gas was the technique which preceded PLAL [77]. Pulsed laser ablation in liquid is a versatile technique with the capacity to use different target materials (elemental, alloys, powders) and most recently researchers used different target geometry [78, 79] to improve the productivity of the laser ablation process. Another remarkable advantage is the devoid of toxic agents in the synthesis of nanoparticles as in comparison with chemical methods. There are many reports on synthesis of stable nanomaterials in colloidal solution by PLAL without the addition of any surfactant for size control. It is possible to use liquids which allow applications of biocompatibility [80, 81] (water, alcohols, etc.) of the nanomaterials synthesized by PLAL. A relevant advance in this topic, is the use of liquid flow [82, 83] or liquid with special properties (polymers [84] or supercritical fluids [85, 86]). The variation of implicit parameters of PLAL as: laser wavelength, pulse duration, frequency and fluence are other important aspects to produce a wide variety of nanomaterials [73, 74, 77, 87].

1.2.2 Fundamental Aspects of PLAL

PLAL has become a feasible synthesis technique of nanomaterials in colloidal solution by choosing appropriate target material, confining liquids and laser parameters. In comparison with other conventional methods of synthesis as vapor deposition, vapor phase transport, pulsed laser ablation in vacuum and hydrothermal methods, PLAL has interesting advantages. These advantages are:

1) clean and green synthesis, the ablated products are usually obtained without by-products and no need of posterior purification;

2) no need of vacuum system, rapid (only few minutes) and one step process;

3) confined conditions of high pressure and temperature in the plasma plume which favors the formation of unusual metastable phases.

The yield of nanoparticles is dependent not only of the laser parameters (pulse duration, frequency, energy and wavelength) but also of the target properties and the liquid media. The final properties of nanoparticles are also characteristics of the plasma plume properties. The general configuration of PLAL is a laser beam focused onto a metal target which is submerged in liquid environment to produce colloidal suspensions of the nanomaterials synthesized. Figures 1 and 2 show the typical setup configurations of horizontal and vertical PLAL, respectively. In these configurations, the laser beam was focused and directed with convex lens and mirrors (99% reflective), respectively. To vary the energy fluence over the metal target, the distance between convex lens and sample is changed. Energy fluence (in J/cm^2 units) was defined as the laser energy output (Joules) per unit area (cm^2). Our laser laboratory is equipped with a Q-switched Nd:YAG pulsed laser operating at 1064 nm for the first harmonic and 532 nm for the second harmonic. The laser beam properties are: 10 ns pulse width, 10 Hz pulse repetition and output energy of 600 and 230 mJ/pulse for IR and visible wavelength, respectively. Two continuous wave lasers (CNI Lasers), one of 532 nm (variable to 0-10 Watts of laser power) and the other of 457 nm (fixed at 4 Watts of laser power) of wavelength are available. An optical power and energy meter (Model PM100D, Thorlabs Inc.) was used to measure the output energy of the Nd:YAG pulsed laser and the continuous lasers. To improve the ablation productivity and to avoid continuous irradiation at same place of the target, a translation system (designed by mechatronics students of FIME, UANL) with linear movement was employed. The range of velocity of the scanning system was 20 to 3000μm/s.

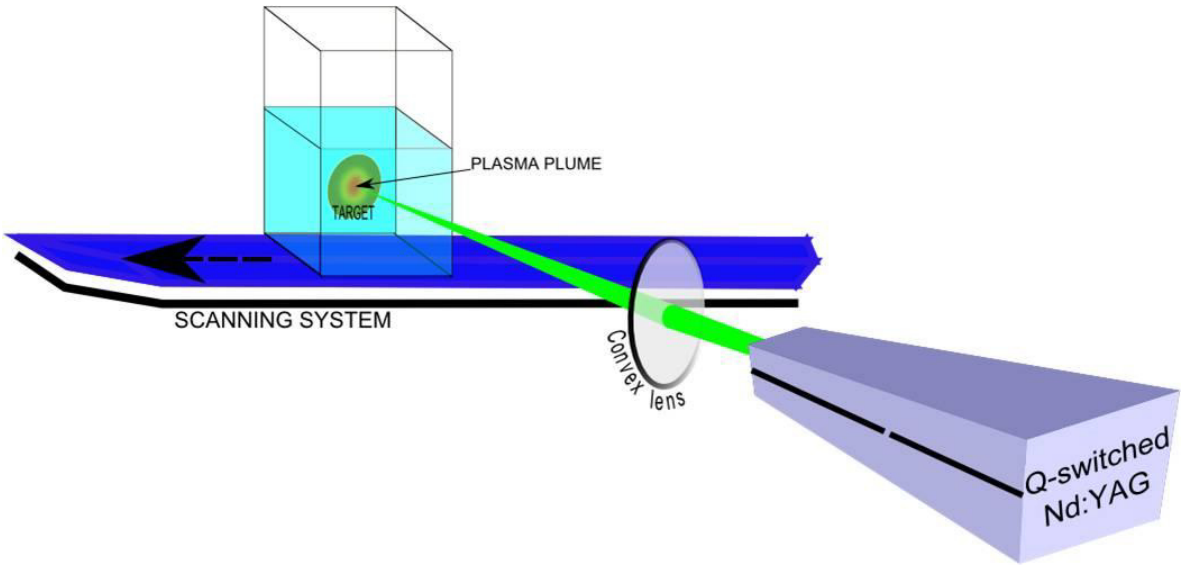

Figure 1. General experimental set-up of pulsed laser ablation in liquid (PLAL) in horizontal configuration.

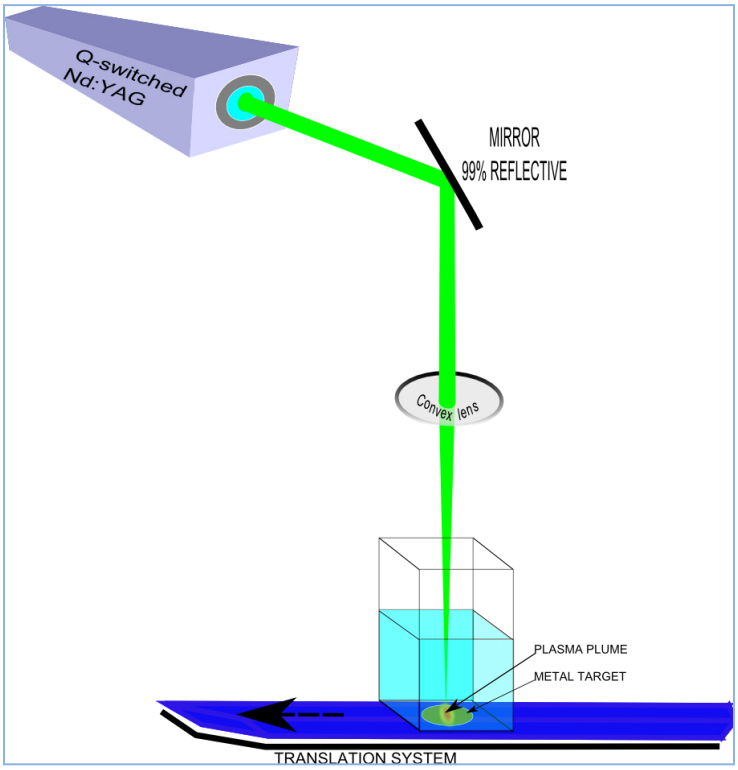

Figure 2. General experimental set-up of pulsed laser ablation in liquid (PLAL) in vertical configuration.

1.2.3 Proposed Mechanisms

The process of laser interaction with the target is similar for pulsed laser deposition in vacuum (PLD) and for pulsed laser ablation in liquid (PLAL). The production of plasma and formation of a strong confinement of the emission species is characteristic in both processes. The crucial difference is the free expansion of plasma in vacuum in PLD, while in PLAL the plasma is confined by the liquid layer. The liquid layer delays the expansion of the plasma plume, generating a high plasma pressure and temperature in the irradiated zone [77]. This leads to the vaporization of both the solid target and the liquid, which allows the formation of novel materials because the products can contain atoms from the target and the liquids. The basic mechanism and the particle formation of PLAL starts with the absorption of the laser pulse by the target. An analytical study of the energy deposition process was described by S. Hachimoto et al. [88], in three stages. First, part of the laser beam was absorbed by the electronic system. Second, after a few hundreds of femtoseconds, a thermal equilibrium was reached to transfer the electron energy to the lattice via electron-phonon coupling. Third, the lattice energy is given to the surrounding liquid, resulting in the cooling of the NPs. Due to the nature of the pulsed laser irradiation, PLAL is very fast and far-from equilibrium process. Therefore all metastable and stable phases formed in the ablation process could be maintained in the final products [89]. This phenomenon resulted for the laser-matter interaction which is largely determined by: the laser parameters (pulse duration τ, wavelength λ), fluence F, the optical (absorption coefficient, α), mechanical and thermal properties of the target material. A brief description about the impact of each parameter in the ablation process is given as the following. In terms of wavelength, it is considered the emission range of the most common lasers any wavelength is appropriate for laser ablation of metals due to the fact that the optical constants of metals are similar. But, in another way, the ablated products or NPs produced could interact or absorb part of the incoming laser irradiation. Then the UV-Vis wavelength region is preferred because the majority of metal NPs absorb in this range. The pulse repetition rate can impact in the yield of nanoparticles during the ablation process, due to that the NPs are ejected at each pulse. But, higher repetition rate can provide a target screening due to the effect of the previous pulses. This effect can be avoided by using liquid flow or high scanning velocity. It was reported that the production of approximately

1 mg of ablated products requires 105 laser pulses, that correspond to ablation times of 20 minutes at 10 Hz (nanosecond or picoseconds) or 100 seconds at 1 KHz (femtoseconds) [90]. When the laser beam impacts the target, its surface reflects part of this incoming energy. The absorbed energy (photons) is transferred to the electrons in the target, leading to the formation of hot carriers which transfer their energy to the ions into the material (page 114 of [56]). The ions and the electron hot carriers eventually reach equilibrium (when the temperature of the electron gas T_e and the lattice T_l are equal) in a timescale $\tau_E = 10^{-12} - 10^{-11}$s [91]. This timescale is an important factor to determine the possible routes to ablation, thermal or non-thermal for "long" or "short" pulses. When the laser pulse is absorbed by the target, a plasma plume is created. This plasma plume contains the ablated material and expands into the liquid media. Due to the confining effect of the liquid media, the plasma plume expands and collapses continuously releasing energy to the liquid solution and emitting a shockwave. During this event a cavitation bubble is generated, which also expands and collapses in a time scale of hundreds of microseconds emitting a second shockwave [92]. Fabbro et al. studied the thermodynamics of the plasma plume created by PLAL by emission spectroscopy [93]. **Thermal evaporation**, is the proposed mechanism for long pulses as in the case of nanosecond pulsed laser, (where $\tau_L \gg \tau_E$) electron and phonons reach at equilibrium during the heating stage. Then the material ejection and phase change is dominated by thermal process. Due that the heat diffusion from the lattice takes place on a timescale shorter than the pulse width. Liu et al. reported the **laser induced heating and melting** (not vaporized) of the target material via heat conduction inside the material. Where the temperature distribution is governed by the heat conduction equation:

$$\rho C_p \frac{\partial T}{\partial t} = \nabla \cdot (K \nabla T) + (1 - R) I_o \alpha e^{\alpha z} \qquad \text{Eq. 1}$$

Where, ρ= density, Cp= specific heat, K= thermal conductivity and T= temperature. The second term represents the source which is the laser energy absorbed by the material at a depth z from the surface. R= surface reflectivity, I_o= laser irradiance and α= absorption coefficient [57]. The melting, boiling, vaporization and eventually formation of plasma are characteristic of the thermal process. The ablated products are contained in the plasma plume and expand into the liquid media, generating a shockwave. Due the confining effect

of the liquid media, the plasma plume cools and release energy to the liquid media during the expansion. NPs are formed during this process due the condensation of the vapor atoms. The nucleation and growth of the NPs are related principally by the laser parameters. The nucleation time is double that the laser pulse width used (for nanosecond lasers). There is an inverse relation between the pressure and time of nucleation and a direct relation between the velocity and the temperature of nucleation [94]. **Explosive boiling** takes places when a very high energy pulsed laser irradiate the target, as ultra-short pulses (femtoseconds and picoseconds). The transmitted energy to the electrons by femtosecond laser pulses is on a time-scale much shorter than the electron-phonon thermalization process. Then for ultra-short pulses, the material is into a highly non-equilibrium state and temperature of the electron gas that is much higher than the lattice temperature. By thermodynamic analysis, if the surface target is heated upper the limit of its thermodynamic stability during ultra-short pulse laser, the surface experiment a rapid transition from superheated liquid to a mixture of vapor and liquid droplets. Another approach to PLAL technique is the size reduction or shape modification by the irradiation of colloidal solutions by a selected pulsed laser beam. Either with nanosecond [63, 66-68], femtosecond [62, 95] or picosecond [61, 96] pulsed laser irradiation. Different mechanism had been proposed to fragmentation process. **Coulomb explosion** model presumes ejection of a quite number of electrons to generate multiply ionized NPs to undergo spontaneous fission because of the charge repulsion. Werner and Besner [62, 95] reported that femtosecond laser-induced fragmentation is dominated by the Coulomb explosion mechanism. **Photothermal evaporation** is another mechanism of fragmentation process. Pyatenko et al. [97] reported that the photothermal mechanism prevails at low laser intensities in their studies based on the observation of a size reduction of chemically prepared aqueous gold NPs by exposure of the SPR band to various intensities and numbers of 532 nm nanosecond pulsed laser beam. **Two temperature model** proposed that the transferred laser energy into the electron and lattice sub-systems is described by two temperatures, electron temperature (Te) and lattice temperature (T_l) to determine the energy distribution inside the system. Giammanco et al. [61] proposed a two temperature model (TTM) to explain the fragmentation of gold NPs by picoseconds laser irradiation. They concluded that the

evaporation of NPs was not predominant compared to Coulombic explosion resulting from thermionic electron emission and photoelectric effect.

1.2.4 Methodologies

Pulse laser ablation in liquid media had been successfully used for the synthesis of different materials in a great variety of liquid media. This section will present some alternative configurations in the set-up of the PLAL experiments. These modifications are reported with the firm intention to improve the production of nanoparticles or to modify the final properties of the ablated products.

Double pulsed laser ablation (DP-LA): During the ablation process and the interaction of the laser beam with the target a plasma plume was created. This plasma plume generates a cavitation bubble which expands and collapses due the confining effect of the liquid media. These phenomena affect the production of nanoparticles during the ablation process due that the plasma plume generated by a first laser pulse could absorb part of the energy of the next laser pulse. De Giacommo and Burakovet al. [98, 99], respectively reported the use of DP-LA to improve the productivity and selectivity of nanoparticles produced by PLAL. De Giacommo reported in the case of DP-LA at 1atm, the laser induced plasma expansion occurs inside the cavitation bubble, thus allowing the plasma to longer preserve its energy. This results in a longer plasma lifetime and in a thermodynamic course of particles aggregation. **Target geometry**: Barcikowski et al. [78, 79, 100] proposed the use of a wire target of defined diameters instead of a planar target for pulsed laser ablation in liquid to allow increase in the ablation efficiency and nanoparticle productivity. The wire target acts as a one-dimensional heat conductor with slower heat dispersion which might enhance laser ablation efficiency. Then, the optimal combination of laser fluence, pulse duration and target geometry could increase the ablation efficiency. Other advantage to use a wire target is the possibility of feeding the wire continuously inside a chamber combined with the use of a liquid flow. **Pulsed laser melting (PLM)**: With a low fluence of only several hundreds of mJ/cm^2, PLM can be employed for the production of spherical particles of several hundreds of nm in size. Koshizaki et al. [58, 59, 101] reported the production for various kinds of materials as metals, oxides and semiconductors. They reported that with a non-focused laser beam at moderate fluence, transformed the NPs to submicron-sized spherical particles. These spherical sub-micron

particles are in use in various functional materials such as cell markers and photonic materials.

1.2.5 Applications

Nanomaterials obtained by PLAL in colloidal solution had important characteristics as purity, stability without surfactants and narrow size distribution. **Biotechnology applications**: In biotechnology research [6], had been reported nano-gold applications [102] as the conjugation with biomolecules (for example in the case when antibody, DNA or aptamer-targeting) and fluorescence imaging [103]. The use of PLAL products showed important results in medical technology due their high reactivity and less toxicity (than chemically synthesized). S. Barcikowski et al. [81, 104, 105] reported some studies of in-situ conjugation during laser ablation of gold nanoparticles with biomolecules. They demonstrated that laser-ablation-based in situ conjugation is a rapid, one-step production method in comparison to the conventional bio-functionalization using chemical synthesis, being highly pure gold colloids possessed some advantages for biological applications as an efficient binding to biomolecules (higher yield), higher ligand load (relevant to specificity of targeting) and less cleaning effort (no interfering chemical residuals). **Catalysis**: The great variety and the purity of nanoparticles produced by PLAL imply advantages for catalytic application. The absence of a ligand layer due the electrostatic stabilization of laser-generated particles is a positive effect on the affinity of nanoparticles to the carrier surface. Nanoparticles synthesized by PLAL had higher deposition efficiency in comparison with chemically synthesized nanoparticles (containing residual citrate) [106]. The use of metal nanoparticles also had been explored in the catalytic reduction of CO and photocatalytic hydrogen production [107]. Wu et al. [108] examined the effect of hydrogen-thermal reduction process time on TiO_2–Pd based catalysts for the performance of photocatalytic decomposition of organic dyes and photocatalytic production of hydrogen. Pd nanoparticles obtained by PLAL also had been reported in studies of heterogeneous catalysis [109]. **Nanocomposites**: An additional advantage of PLAL technique is the feasibility to produce/synthesize composites in-situ the ablation process. As reported in [110] which produced nanohybrids formed by multiwalled carbon nanotubes (MWCNTs) and Au NPs by PLAL. By a two-step method of PLAL had been reported the synthesis of bimetallic (Au/Al [111]) and core/shell (ZnO/Ag and ZnO/Au [112]) nanocomposites.

PLAL also had been explored to produce nanoparticle-polymer nanocomposites due the purity of laser-generated colloids which allow the binding of the particles to the polymer. For example, Ana Menéndez-Manjón et al. [84] reported the formation of ligand-free gold–silver nanoparticle alloy polymer composites by picosecond laser ablation in liquid monomer.

1.2.6 Materials

PLAL, as mentioned is an effective, rapid, simple and versatile technique that could be used to synthesize a great variety of nanostructures with various compositions (metals, alloys, oxides, carbides, hydroxides, etc.) and morphologies (nanoparticles, nanocubes, nanorods, nanocomposites, etc.). Another important branch of PLAL is post laser irradiation of suspended nanomaterials that can be applied to further modify their size, shape, and composition. This section is a brief summary of the different materials reported by PLAL. Pulsed laser ablation of **noble metals** as Ag, Au, Pd, Pt, etc. had been reported by many authors and will be discussed in detail in the next part. **Metal oxide** compounds formed via the reaction of ablated metal with liquid media are another important research field [113]. For example the synthesis of ZnO [114-119], TiO_2 or TiO [120-126], CuO [59, 127-130], Aluminum oxide [131, 132], SnO [133], Sb_2O_3 [134, 135], NiO [136], Bi_2O_3 [137], Fe_3O_4/FeO [138-141]. Also different morphologies also had been reported as ZnO nanorods [142, 143]. The synthesis of different **alloys** by PLAL is another alternative to nanomaterial synthesis reported by some researchers [94]. There are two main ways reported, one is the direct irradiation of an alloy target and the second is a two-step method. Basically, two-step method consists in a first step in which metal nanoparticles are obtained by PLAL. The second step is the irradiation of another metal immersed in the previous colloidal solution obtained. Some example of nanocolloid alloys synthesized by PLAL are Ag/Pd [144], Au/Ag [145-149], Pt/Ir [150], Ni/Ti [80], Fe/Pt [151], Ag/Pd [152]. Hybrid nanostructured materials formed by **carbon nanotubes** (CNTs) and nanoparticles have attracted the attention of research groups due to their novel chemical-physical properties. There are some reports of synthesis of CNTs as composites with noble metal nanoparticles as Au [110, 153] or Ag/Pd [154]. G. Forte et al. [155] reported the synthesis of linear carbon chains by PLAL in different liquid media (water, acetonitrile, methanol and cyclohexane) starting from graphite roads. Another examples of **carbon structures**

synthesized by PLAL are Cyanopolyynes in acetonitrile [156], linear carbon chain colloid mixed with silver nanoparticles [157], core-shell CdS/carbon NPs [158], carbon-based nanostructures [98] as (diamond-like carbon or nanodiamonds) [159] and carbon NPs [160]. The versatility of PLAL technique allowed the synthesis of a great diversity of nanomaterials, nanocompounds, nanocomposites, etc. For this reason, the field of synthesis, methodologies and future applications will be helpful to fulfill the new requirements and scientific curiosity.

1.3 METAL NANOPARTICLES BY PLAL – AN OVERVIEW

1.3.1 Introduction

In recent years, nanotechnology have been attracted much attention due to all novel properties and applications of the nanostructured materials. Nanotechnology implies design, fabrication and application of nanostructures or nanomaterials [1]. The understanding of the relationship between physical properties and material dimensions is fundamental for all the potential applications. Nanotechnology has a broad range of potential applications as nanoscale electronics and optics, nanobiological systems, nanomedicine, etc. Materials or structures at nanometer scale possess new physical properties or exhibit new physical phenomena. For example, some noble metals at nanometer scale have a surface resonant plasmon at a frequency in the visible light range. Due the Mie`s theory which explained the red color of gold nanoparticle colloidal in 1908 by resolving Maxwell´s equation for an electromagnetic light wave interacting with small metallic spheres. By resolving these equations they concluded that the plasmon resonance depends explicitly on the particle size, *r*. The larger the particles, the more important the high-order modes as the light can no longer polarize the nanoparticles homogeneously. These higher-order modes peak at lower energies. Therefore, the plasmon band red shifts with increasing particle size. At the same time, the plasmon bandwidth increases with increasing particle size. The situation concerning the size dependence of the optical absorption spectrum is more complicated for smaller nanoparticles for which only the dipole term is important. For nanoparticles much smaller than the wavelength of incident light ($2r < \lambda_{max}/10$), only the dipole oscillation contributes to the extinction cross-section [1]. For the fabrication of nanoparticles, a small size is not the only requirement. For any practical application, the processing conditions need to be controlled in such a way that

resulting nanoparticles have the following characteristics: i) identical size distribution (monosized or uniform size distribution); ii) identical shape or morphology; iii) identical chemical composition and crystal structure that are desired among different particles and within individual particles, such as core and surface composition must be the same and iv) individually dispersed or monodispersed, i.e. no agglomeration. If agglomeration does occur, nanoparticles should be readily re-dispersible [1]. There are a wide range of techniques to obtain nanostructured materials as chemical methods (sol-gel, chemical vapor deposition, chemical routes) and physical methods (sputtering, laser ablation, thermal evaporation, etc.). **Pulsed laser ablation in liquid** (PLAL) has been applied in recent years to generate, excite, fragment and conjugate metals, semiconductors or ceramic nanoparticles. In general, advantages of laser-generated nanomaterials can be summarized as: i) metal nanoparticles generated are charged and thus have an extremely high colloidal stability; ii) nanoparticles in colloidal solution are not inhalable (like dry nanopowders), then is a safety condition during product handling; iii) the colloids produced are free of chemical precursors and it can be obtained in biocompatible liquids as distilled water and alcohols; iv) crystalline nanoparticles can be obtained during this process with no heat treatments and v) this technique can be applied universally with an almost unlimited variety of materials and solvents. These advantages are of value in comparison to specific conventional synthesis [161]. Low product yield is one of the main disadvantages associated with PLAL, but a solution can be to optimize both laser (ablation time, fluence and frequency) and medium (liquid layer, density, surface tension and viscosity) parameters [87]. Another problem attached to PLAL is the control of nanoparticle size and size distribution, especially when pure nanoparticles without ligands are desired, although by exploiting the plasmon absorption or interband transitions with a selected wavelength of irradiation, is possible to control the size without the use of surfactants or chemical reagents [162]. Since the past time to the recent years, noble metals have been extensively applied for medical or decorative purposes [163]. Gold and silver have been the most coveted precious metals since the time of Pharaohs. Moreover their well-known uses in currency and jewelry, metalworkers found that the properties of gold were more than meets the eye [164]. For example, nanoparticles of gold in the famous Lycurgus cup, c. a. 4^{th} century AD, cause the color to change from green for reflected light to red for transmitted light [165].

Actually, noble metal nanoparticles are of interest in various technological areas like sensing, catalysis, electronic and plasmonics due some features as: i) the presence of optically activate plasmonic modes which originate intense absorption and scattering bands in the visible-near infrared interval, the local field amplification due to plasmon resonance is also at the basis of surface enhanced Raman scattering (SERS); ii) the easy surface functionalization with a wide series of organic molecules, and iii) the chemical and physical stability and biocompatibility. Important catalytic properties derive from the chemical stability and surface chemistry of noble metal nanoparticles [90].

1.3.2 Gold Nanoparticles in Colloidal Solution

Colloidal gold has been studied extensively for a long time. Faraday published a study on the synthesis and properties of colloidal gold in 1857 [166]. In recent years there are a wide range of applications as: biotechnology [167-170], industries [171], optical [172], pharmaceutical [173], medical [174, 175] and agricultural fields [176]. A number of diseases were diagnosed by the interaction of colloidal gold with spinal fluids obtained from the patient [177]. Au nanoparticles can function as carrier vehicles to accommodate multiple functionalities through attaching various functional organic molecules or bio-components [178]. Although bulk gold does not exhibit catalytic properties, Au nanocrystals demonstrate to be an excellent low temperature catalyst [164]. Due the ability of gold to produce heat after absorbing light provides a medicinal usage named as photothermal therapy [179]. Gold nanoparticles have been developed by chemical, physical (dc magnetron sputtering [180]), physicochemical and biological [181] methods. The most commonly used chemical method is the sodium citrate reduction of chloroauric acid at 100 °C which was developed more than 50 years ago [182]. Turkevich method [183], wet chemical synthesis [184] and chemical reduction method are other examples of chemical routes of synthesis. Sonochemical and sono-electrochemical methods [185] are physicochemical routes also employed. Some examples of physical methods are the UV irradiation, laser [186] and plasma synthesis. Due to the size dependence of novel properties of gold nanoparticles and the free-ligands needed for several applications, it is necessary to control these important properties; size (and size distribution) and purity. The production of gold nanoparticles by PLAL has been widely reported; the main parameters used are the liquid nature, focusing conditions, wavelength and pulsed width duration. Here

is a brief summary of these reports in which the studies are first arranged by the pulse width employed due that the mechanism of formation predominant is different for each one; femtosecond, picosecond and nanosecond. There are studies of mechanism for pulsed laser ablation using femtosecond lasers which will be separated according to the specific studies as: Povarnitsyn et al. [89] which developed the two-temperature wide range hydrodynamic model to explain the **femtosecond** laser interactions with the metal target in liquid water. They attributed the bimodal size distribution of NPs to the two stages of ablation: one at the ablated metastable liquid layer and the other one inside the cavitation bubble. There were other studies with more focusing on control of the average size by varying the principal parameters of PLAL or the liquid media as J. Sylvestre et al. which had been produced Au nanoparticles partially oxidized with controlled surface chemistry [187]. They proposed the use of different salts (KCl, NaCl and NaOH) to limit the coalescence of the gold nanoparticles and as consequence to control the size of the nanoparticles. Andrei V. Kabashin et al. [188] reported the synthesis of gold nanoparticles in high α-cyclodextrin concentration by femtosecond pulsed laser. In comparison with the reports of Au NPs synthesized by nanosecond with a broad size distribution, they obtained an average size of 2 - 2.4 nm with a narrow size distribution. S. Barcikowski et al. [189] reported the properties of nanomaterials by femtosecond pulsed laser in air and water. They obtained the optimum parameters to control the size and improve the ablation productivity. M. A. Sobhan et al. [190] realized a systematic studies in order to clarify the impact of each laser parameter over the final properties of the ablated materials. They varied the laser pulse energy, exposure time, energy fluence, scan speed and pulse repetition rate. They concluded that the combined effect of pulse repetition rate, pulse energy and the spot size determined the properties of the nanoparticles. In another study, G. A. Torchia et al. [191] proposed optical extinction technique to determine with more accuracy the size distribution of gold nanoparticles synthesized by PLAL (or another technique), complementary to TEM analysis. Effect of water temperature during the generation of nanoparticles by PLA was explored using an IR femtosecond laser in water at different stabilized liquid temperatures [192], also reported a study about bio-functionalization [81]. S. Petersen et al. also reported studies of in situ conjugation during laser ablation in liquids with Au NPs [104]. R. Intartaglia et al. applied the PLAL with a **picosecond** pulsed laser technique to obtain Au-

Ag bimetallic NPs by the irradiation of a silver target immersed in a colloidal solution of Au NPs [145]. The final properties of the bimetallic nanoparticles were dependent of the initial concentration of the gold colloidal solution. They used these bimetallic nanoparticles in plasmonic applications. Other application of gold, silver and gold-silver nanoparticles synthesized by picosecond laser ablation was reported by S. Dengler et al. [146]. They reported studies of non-linear optical properties of these metal nanoparticles. Also, Menéndez et al. [84] reported the generation of Au, Ag, and Au-Ag alloy nanoparticle acrylate composites by picosecond pulsed laser ablation of the respective metal target in the liquid monomer. Synthesis of (PAMAM G5)-capped gold nanoparticles by picosecond laser ablation in water [61] also reported. The most published investigations of PLAL is using the **nanosecond** pulsed laser in comparison with femtosecond and picosecond pulsed laser ablation. Mafune et al. demonstrated the synthesis of gold nanoparticles by nanosecond pulsed laser ablation of a gold target in SDS aqueous solution. They obtained gold with an average size of 1-5 nm after centrifugation and photo-induced reshaping of the colloidal solution [193]. They concluded the direct relation between the concentration of the surfactant and the energy fluence over the size and size distribution of the gold nanoparticles. K. Elsayed et al. [194] presented a study about the influence of laser parameters (as laser wavelength, focusing conditions of laser beam) and ablation parameter (laser fluence,) on the size and morphology of the gold nanoparticles prepared in de-ionized water by pulsed laser ablation. N. Mirghassemzadeh et al. [195] analyzed the effect of laser fluence over size and morphology of gold NPs synthesized by PLAL. They reported dependence between size and laser energy, with smaller NPs at high laser fluence. But there is a limit for the increase in laser fluence. If the laser pulse energy increases beyond the threshold, would not lead to decrease in the nanoparticles size because a large amount of laser pulse energy is absorbed in liquid environment. The effect of the post-irradiation of the colloidal solution by a wavelength near the plasmon resonance of metal NPs had been described. Mafune et al. [196] reported the laser-assisted size reduction of gold nanoparticles; effect of post-irradiation. They [197, 198] studied the synthesis of gold nanoparticles in SDS surfactant by PLAL and the additional irradiation by a nanosecond pulsed laser beam to control the size of these NPs. They observed the fragmentation as the principal mechanism predominant to size control of the NPs. N. V. Tarasenko et al. [199]

also reported the variation of mean size and stability by select parameters of laser ablation and post-irradiation, specifically with wavelengths near of the SPR of metal NPs. Kim Kuk Ki et al. [200] reported a similar study of gold NPs synthesized by PLAL and post-irradiation treatment. The additional information consisted in the comparison of average size and stability of both as-prepared and post-irradiated NPs with different wavelengths (266, 355, 532 and 1064 nm). They reported that 355 nm was the best wavelength for preparation of size reduced and stable Au NPs solution using post-irradiation method with ns lasers at 16 mJ/cm^2. Studies on different mechanisms of size reduction due post-irradiation of colloidal Au and Ag NPs with nanosecond pulsed lasers [97] also presented, showing the dependence of the electron ejection process on the laser energy flow density (W/cm^2) which in turn was a function of particle diameter and laser wavelength. D. Werner et al. [88] reported a model to investigate the relation of laser wavelength and fluence over laser-induced size reduction of Au NPs. They concluded that the fragmentation mechanism strongly depends on the pulse duration. For femtosecond laser, the fragmentation mechanism is caused by Coulomb explosion meanwhile, for nanosecond pulsed laser heating of gold NPs is dominated by photothermal evaporation mechanism. In case of picosecond laser both mechanisms can take place depending on the laser fluence. Also have been reported the studies of effects on size and shape induced by laser irradiation for NPs synthesized previously by chemical methods. For example the size reduction of gold NPs (synthesized by chemical methods) by pulsed laser irradiation also have been reported by K. Hideaki et al. [201]. V. Resta [202] worked with the size reduction of gold nanoparticles (synthesized by other methods) by the irradiation of a nanosecond pulsed laser, in order to control or modify the morphological/ optical properties of NPs. D. Riabinina has explored the laser-induced optical properties modifications as the blue-shift of plasmon resonance of gold nanoparticles via excimer laser irradiation [203]. They have explained the different mechanisms present in the present blue-shift as the shape modification, fragmentation and the modification of the refractive index due the chemical agents presents in the solution. S. Link have demonstrated the shape modifications of gold nanoparticles by nanosecond and femtosecond pulsed laser [143]. They studied the different mechanisms for each pulsed width in relation with the time of melting, photo-absorption, etc. The use of specific liquid media in PLAL experiments to allow size control or some specific application has been

reported. For example, Rehbock et al. proposed the use of highly diluted electrolytes for size control [204] of gold nanoparticles by nanosecond PLAL. J. Sylvestre et al. [205] reported the synthesis of gold NPs by PLAL in aqueous cyclodextrins. A. F. M. Y. Haider et al. [206] worked with nanosecond PLAL of Au NPs in pure water to study the effect of the laser parameters over final properties of the colloidal solution without the effect of any surfactants. But the size and size distribution were higher in comparison with the Au NPs obtained in other liquids. They also explored the time of irradiation as Riabinina et al. [108] and observed a decrease in the size of the nanoparticles due the fragmentation process. Recently, T. X. Phuoc have [207] reported the synthesis of biocompatible gold nanoparticle suspensions using two-beam PLAL in deionized water containing natural polymers as chitosan and starch. There are other specific studies as the formation of alloys, composites or applications. E. Messina et al. [208] reported the formation of Ag/Au nanoalloy by PLAL in two step method. They reported that plasmon resonance of metallic nanoalloys was tuned from 400 nm to 520 nm using the laser irradiated technique. Synthesis of Al-Au alloy by PLAL in two step process [111] in both pure water and aqueous poly(N-vinyl-2-pirrolidone) solution was reported. They synthesized nanocomposites in the polymer matrix and in water; and studied the effect of polymer on the size, size distribution and stability of the nanocomposites as Au (core)-Al (shell) or Al (core)-Au (shell) bimetallic nanoparticles. A. S. Nikolov et al. [209] reported the formation of gold nanowire networks by PLAL at different wavelengths (532 and 355 nm) and laser fluence in double-distilled water. T. Salminen et al. [210] reported the formation of core-shell structures. By coating of individual and agglomerated gold nanoparticles with silica shells by a single step PLAL process in the presence of TEOS (tetraethyl orthosilicate) and ammonia in 2-propanol. They used two wavelengths (515 and 1030 nm) and reported that at 515 nm was the best to initiate the formation of the shell. L. Lascialfari et al. [110] reported the production of nanohybrids formed by oxidized multiwalled carbon nanotubes (MWCNTs) and gold nanoparticles by PLAL. They reported an optimal interaction between Au NPs and CNTs mediated by a linker namely a pyrene derivative. Fabrication and properties of bio-functional coatings with NPs synthesized by PLAL were reported by C. Streich et al. [105]. Some modifications have been proposed by researchers either on set-up configuration, characterization, etc. For example, Maciulevičius M. et al. [211] designed a complete

system to do online characterization of the production of nanoparticles by nanosecond pulsed laser ablation and to complement the information obtained by TEM. Other important feature for this work was the use of a double pulsed laser system as the reported by De Giacomo [98] and V. S. Burakov [99]. They reported that the time delay between the laser pulses increases the productivity of the ablation process. The variation of wavelength also was reported for the synthesis of gold nanoparticles as O. V. Overschelde et al. [212]. They reported the synthesis of gold nanoparticles by 248 nm of excimer KrF nanosecond pulsed laser ablation in water and some alcohols. Werner et al. [213] added high pressure to control the size of gold nanoparticles by laser-induced size reduction. They observed an effect of the energy fluence on the size reduction of these gold NPs especially at high pressures. They ascribed their results to the formation of a supercritical water layer surrounding the liquid droplet NP transformed by laser heating. They previously worked with laser-induced fragmentation of gold nanoparticles by a femtosecond pulsed laser. They proposed that the Coulombic explosion was the dominant mechanism in the presented studies [95]. Another methodology is laser melting in liquids to synthesize submicron-sized spherical particles. Tsuji [58] reported the fabrication of gold sub-micron spherical particles by laser melting using citrate as stabilizer. Also reported the synthesis of gold sub-micron particles by this technique in another less toxic stabilizer as NaCl solution [101].

1.3.3 Silver Nanoparticles in Colloidal Solution

Various methods have been developed for the synthesis of silver nanoparticles. One of them is by the UV illumination [214] of aqueous solution containing $AgClO_4$, acetone, 2-propanol and various polymer stabilizers. There are another methods of synthesis as green synthesis [215], electrical synthesis [216], derived seed-growth method [217], chemical methods [218], sonochemical reduction [219], among others. But the principal disadvantage of chemical methods is the non-purity of the synthesized nanoparticles due the inherent role of the chemical reagents. For this reason an alternative and promising technique to obtain pure nanoparticles in colloidal solution is PLAL. Silver was of the first noble metal studied by this technique. Different studies on formation of NPs, mechanisms and effect of laser parameters over the final properties of silver NPs have been reported. The next part presents some investigations on silver nanoparticles synthesized by PLAL. Takeshi Tsuji et al. [73] presented a review on the synthesis of silver nanoparticles by

pulsed laser ablation in liquids. This review also presented the applicability of silver nanoparticles in colloidal solution, the role of a famous polymer (PVP) as stabilizer and the advantages of post laser irradiation. The synthesis of silver NPs by PLAL was found with different pulse width of the laser beam used as follows; E. Akman et al. [220] reported the synthesis of silver NPs and their subsequent fragmentation by a **femtosecond** pulsed laser. Their results showed that post-irradiation had an effect by decreasing size and agglomeration of silver NPs. N. Barsch et al. [221] reported the synthesis of silver NPs by PLAL with 50 W **picosecond** laser source with a high yield of NPs produced (several hundred milligram per hour). E. V. Zavedeev et al. [222] reported the formation of nanospikes by picosecond pulsed laser ablation of a silver target immersed into water or ethanol. **Nanosecond** laser sources have been the most popular source used in PLAL experiments. Different researchers studied the mechanisms and effects induced by laser as cavitation bubble in order to have a better understanding on the formation of NPs. As reported by P. Wagener et al. [223] the formation of nanoparticles is within the laser-induced cavitation bubble studied by in situ small angle X-ray scattering during PLAL experiments. They reported that after laser ablation, two different particle, consisting of compact primary particles (8–10 nm size) and agglomerates (40–60 nm size) are formed and their abundance is strongly influenced by the dynamics of the oscillating cavitation bubble. Studies on effects of laser parameters (wavelength), energy fluence and liquid media have been reported. For example, E. Solati et al. [224] reported the synthesis of Ag NPs by pulsed laser ablation in acetone with 1064 and 532 nm of wavelength. Their results showed that nanoparticles produced with 1064 nm laser wavelength, at higher laser fluence resulted in an increase in the average size of Ag NPs. Our group [134] described the synthesis of silver NPs in aqueous solution of SDS surfactant using the second harmonic of a nanosecond pulsed laser. A. I. Talukder et al. [225] also reported the dependence between size and laser energy. They reported that Ag NPs with smaller size resulted with higher laser pulse power at 532 nm of wavelength. They attributed this result to that at higher laser power, increases the temperature of the ablated material and a faster quenching rate may be involved which would cause the reduction of the sizes of nanoparticles. R. M. Tilaki [226] studied the effects of the liquid media on the size and optical properties of silver nanoparticles prepared by PLAL at 1064 nm. Ag NPs were synthesized in acetone,

deionized water and ethanol and concluded that high polar molecules provided a strong surrounding electrical double layer, which prevents growth, aggregation and precipitation. A. Pyatenko et al. [227] reported the synthesis of silver NPs by PLAL in pure water and studied the effect of laser power and spot size (which was related to energy fluence). They observed that at high laser power and small spot sizes, small silver nanoparticles with a narrow size distribution were obtained. R. A. Ganeev et al. [228] also reported the synthesis of Ag NPs by PLAL in different liquid media (ethylene glycol, water and ethanol). They observed that the viscosity of surrounding liquid had an important effect on the stabilization of structural and nonlinear optical properties of Ag nanocolloids. F. Mafune et al. [229] reported the synthesis of silver NPs by PLAL (532 nm) using different surfactants to study the stability of nanocolloids. In another study [230], they observed the formation of smaller silver NPs with increase in the concentration of sodium dodecyl sulfate and with a decrease in the irradiation laser power. There are reports on the synthesis of complex structures, alloys or nanostructures by PLAL technique as follows. Z. Yan et al. [231] obtained the formation of Ag-Ag_2O complex structures by excimer laser ablation of Ag in water. Yun-Hung Chen et al. [149] reported the synthesis of Ag/Au bimetallic alloy by the irradiation of silver and gold colloids mixtures prepared separately by chemical methods. Recently the target geometry was changed in order to increase the productivity of nanoparticles by pulsed laser ablation, G. C. Messina and co-workers, reported an increase in a factor of 15 in the efficiency of NPs production during the ablation of a silver wire (instead of a planar target) as a target in liquid flow for high yield production of silver nanoparticles [79]. Post-irradiation for silver nanoparticles was reported by Zamiri et al. [232], they produced the colloidal solution by PLAL (at 1064 nm, 5 ns) in ethanol and post-irradiate it by a pulsed laser beam at 532 nm. They reported the formation of microbelts and microrods after the post-irradiation treatment and ascribed this formation to the fusion of the aggregated nanoparticles. There are other reports of post-irradiation treatment of silver nanoparticles as the one by P. V. Kamat et al. [96] in which they synthesized Ag NPs by chemical reduction in aqueous solution. Silver nanocolloids were subjected to laser-pulse excitation (355 or 532 nm) and reported that electron ejection is one of the primary photochemical events that lead to the photo-fragmentation process. Also L. C. Courrol et al. [233] studied a photo-induced method for obtaining silver nanoparticles using UV LED, xenon lamp and sodium

lamp excitation. Silver colloidal were synthesized by using auto-polymerizable resin and $AgNO_3$ in an ethanol solution. They produced spherical silver nanoparticles (5–8 nm) with the combination of pulsed laser ablation with UV–visible illumination. Another important example is the report of K. G. Stamplecoskie et al. [234] of a photo-chemically synthesis method of silver nanoparticles with the shape control of these NPs under the irradiation of a light emitting diode at different wavelength. Pulsed laser ablation in liquid had many advantages, as result a great number of applications and specific studies had been reported; F. Neri and co-workers published results on the enhanced nonlinear optical response of linear carbon chain colloid mixed with silver nanoparticles [157]. E. Messina et al. [147] reported the synthesis of gold/silver alloy by PLAL in colloidal solution. The obtained solution was observed with tuneable plasmon resonance and proposed for applications in bio-sensing experiments, frequency selected photo thermal therapy, nonlinear optics, SERS applications, and spectroscopic characterization of nanomaterials and composites. Other applications of silver nanoparticles in colloidal solution synthesized by PLAL had been reported as; in biological field some applications as for mosquito control [235], antimicrobial [236], protein reduction [237]. SERS enhancement due to the superficial plasmon resonance of novel metals like silver also was reported, for example: palladium-doped silver nanoparticles [238]. In photo-catalysis field, in some composites like titanium dioxide nanotubes modified with silver and palladium nanoparticles [154], catalytic activity of silver nanoparticles supported on manganese oxide [171].

1.3.4 Palladium Nanoparticles in Colloidal Solution

Palladium and platinum nanoparticles are heavily studied for many catalytic applications as such as C-C bond formations, hydrogenation of alkenes and allylamines, oxidation and reduction reactions in fuel cells, etc. In catalysis studies, the catalytic active material has to be as small as possible with high accessible surface. It has been studied a different activity and selectivity are dependent of facets and presence of kinks and steps of the bulk crystals. This characteristic was found to be related with the concentration of catalytically active atoms on the different types of surfaces. As nanoparticles of different shapes are enclosed by different facets, there are different fractions of atoms located at different faces, corners, edges and often defects. Therefore is expected that catalytic properties will be different and interesting, in terms of both activity and selectivity. For

these reasons, research has been focused on the development of this nanocatalysis by the formation with fine control of both size and shape. Catalytic activity of the nano-catalyst in the nano-colloid depends not only on size and shape; another important characteristic is the surface environment, which is often dramatically influenced by the use of reducing agents. The use of protective agents had been reported as n-alkanethiols, phosphines, linear polymer such as poly(vinylpyrrolidone), polyvinyl alcohol [14], sodium polyacrylate and dendrimers. The catalytic activity of Pd nanoparticles are well understood, however the costs of this material has been increasing in the last years. Therefore the studies in which Pd is employed as nanoparticles can allow the fabrication of chemical sensors using a very small amount of this material. Pt and Pd NPs of different morphologies have been reported in the growing area of shape-controlled synthesis and shape-dependent catalytic studies. Pt and Pd NPs have a face-centered-cubic (FCC) crystal structure. The literature reports calculations that predicted thermodynamic equilibrium shape for an FCC nanocrystal is a truncated octahedron bound by six {100} and eight {111} planes. There are catalytic studies showing shape-dependent effects of Pt and Pd NPs [13], between them faceted polyhedral nanocrystals, porous-like, branched nanostructures, 1-D nanorods and nanowires. Pd nanoparticles had been coated with cationic isocyanides, thiolated β-cyclodextrin, N,N,N-trimethyl (8-mercapto octyl) ammonium chloride, mercapto ammonium ligand, polyvinyl alcohols [14], among others. Palladium nanoparticles are applied in many industrial applications as in the reduction of automobile pollutants and catalyst for many organic reactions, such as C-C coupling of Heck, Suzuki, hydrogenation of alkenes and allylamines. Palladium nanoparticles have a special sensitivity to absorb hydrogen, make them appropriate as gas sensor [12, 239] and as hydrogen storage materials in fuel cells or batteries. There are reports on the use of Pd NPs as hydrogen and humidity sensors which were fabricated by laser ablation direct writing [240]. Wei-Fang et al. reported the photo catalytic performance of TiO_2-Pd based nanoparticles [108]. Jianzhong Chen and co-workers studied the determination of biological compounds by mimic enzyme palladium nanoparticles [241]. Pd nanoparticles have been produced by pulsed laser ablation in different liquid media. Also there are studies on Pd or Pd compounds produced by PLAL for different applications of this material. For example, the advantages of PLAL are in agreement with the needs of catalysis industry as: shape and size control of the

nanoparticles synthesized. Some research groups studied the effect of the different ablation parameters over the final properties of the Pd nanomaterials and their potential applications. Pd nanoparticles produced by PLAL can be separated mainly in two groups: first when they used an IR laser irradiation with different conditions. J. Pou and co-workers produced pure Pd nanoparticles using both, CW (monomode Ytterbium doped fiber laser YDFL, @ 1075 nm, irradiance ranged 2 x 10^5 and 10^6 W/cm^2) and pulsed laser (Nd:YAG @1069 nm, 1-2 ms pulse width, 10 Hz, pulse energy 2-8 J) ablation in de-ionized water [242]. M. Muniz-Miranda et al. [243] reported the production of palladium nanoparticles by pulsed laser ablation in water. Laser ablation was performed using a Nd:YAG pulsed laser (λ= 1064 nm, τ= 12 ns, 10 Hz, laser energy 3-158 mJ) in an aqueous solution (with and without the addition of SDS) and an energy fluence between 1.6-2000 J/cm^2. Through the variation of the fluence, it was observed the optimal conditions for the NPs productions at an intermediate fluence (~21 J/cm^2) and by strongly defocusing the laser beam. Pd NPs had SERS activity observed by spectroscopic analysis of their precipitates. Soghra Mirershadi et al. [244] studied the wavelength dependence on the nanoparticle formation mechanisms during PLAL. They applied an IR Nd:YAG pulsed laser (λ= 1064 nm) and UV ArF excimer laser (λ= 193 nm) for the synthesis of Pd NPs in deionized water. Both lasers had the same laser properties as pulsed width (10 ns), repetition rate (5 Hz), pulsed energy (50 mJ), and energy density (5 J/cm^2). The other group, when the second harmonic (532 nm) was used to ablate the metal target. T Motohiro et al. [245] synthesized Pd nanoparticles with larger magnetic susceptibility properties than commercial Pd powders. They used a pulsed laser system (Nd:YAG, λ= 532 nm, 10 Hz, 7 ns, laser energy 400 mJ) for the ablation of a Pd disc in heavy and light water. L. Guetaz and co-workers [246] synthesized pure Pd nanoparticles in DIW and palladium hydride nanoparticles (PdHx) in acetone or ethanol using PLAL. To the PLAL process a picosecond (12 ps) pulsed laser source at 532 nm of wavelength was used. They varied both average power (2.6 or 1.6 W) and the high pulse repetition rate (200, 80 or 10 kHz). The resulted nanoparticles can be used in hydrogen storage applications. In this work, Pd NPs were synthesized by pulsed laser ablation in different liquid media. The ablation parameters (fluence), nature of the liquid and stability of the Pd NPs were reported. Pd NPs were characterized by TEM, EDX, XPS and UV-Vis Absorption spectroscopy to study the morphology, size, size distribution,

structure, elemental composition, chemical state and optical properties of the ablated products.

1.3.5 Platinum Nanoparticles in Colloidal Solution

Platinum and its alloy nanoparticles have attracted much attention because of their potential application in many catalytic reactions as to eliminate NO generated in combustion process [247]. There are various synthesis routes for the fabrication of Pt and Pt-compounds at nanoscale as: Henglein et al. [248] studied and compared three different methods for the preparation of Pt nanoparticles: radiolysis, hydrogen reduction and citrate reduction. By pulsed laser ablation deposition had been synthesized Pt compounds with different application in catalysis, as Daniel Guay and co-workers [249] synthesized a series of Pt_xSn_{100-x} NPs by PLD method by varying the background pressure during the deposition. They reported the characterization of their physic-chemical and electrochemical properties. It was found that the surface composition and structure of the resulted catalysts NPs has a high effect on the electrocatalytic activity of the catalysis for ethanol oxidation. Synthesis of Pt and Pt compounds by PLAL have been reported by different researches groups as; Zheng-Wen Fu et al. [250] reported the preparation of highly dispersed platinum nanoparticle-graphene nanosheet (PtNP-GNS) hybrid colloidal solution by pulsed laser ablation in liquid. A Nd:YAG pulsed laser (λ= 355 nm, frequency 10 Hz, τ= 5 ns, fluence 2 J/cm^2) was used for the ablation of a platinum plate (99.99%) which was immersed in 5 ml of aqueous graphene dispersions. Air cathodes were prepared by dispersing drops of PtNP-GNS onto the ITO substrate and drying in air for the film deposition. PtNP-GNS hybrids showed a high electro-catalytic activity for discharge and charge process as air electrode which is important for applications for Li-air battery. Stephan Barcikowski et al. [150] were successful in the synthesis of charged Pt-Ir alloy nanoparticles by femtosecond laser ablation in acetone. These PtIr obtained nanoparticles had the same composition as the Pt_9Ir target used in PLAL and was confirmed by EDX (in TEM), STEM-EDX maps, HRTEM and SAED. These NPs were used to make electrodes by electrophoretic deposition with enhanced surface roughness in comparison with other techniques. The ablation process was developed with a femtosecond laser system (λ= 800 nm, τ= 120 ps, pulse energy = 300 μJ/, 5 Hz). Marta Castillejo et al. [251] reported the fabrication of Pt NPs by pulsed laser ablation in liquids and explored the application to laser desorption ionization. The laser

system employed was a Q-switched Nd:YAG (λ= 1064, 532 and 266 nm, τ= 5 ns, 10 Hz) for the ablation of a Pt target immersed in citrate and some polymers as PEG (poly ethylene glycol), PVA (polyvinyl alcohol) and PVP (polyvinylpyrrolidone) as stabilizing agents. They observed shape modifications of the Pt NPs which were related with the wavelength selected. The nanoparticles were employed to develop films capable of assisting the laser deposition ionization (LDI) of a model peptide. Stable Pt nanoparticles were synthesized [252] by pulsed laser ablation in water and aqueous solution of sodium dodecyl sulfate (SDS). The abundance of the Pt NPs was changed with the concentration of surfactant. The laser system used in this experiment was a Nd:YAG pulsed laser (λ= 532 nm and 1064 nm, 10 Hz). Naoto Koshizaki et al. [253-255] reported a complete study of Pt NPs produced by pulsed laser ablation in liquids. Laser ablation was carried out at normal incidence of the laser beam Nd:YAG (λ= 1064, 532 and 355 nm, τ= 10, 8 and 7 ns, respectively) of a platinum metal immersed in filtered, doubly de-ionized water (> 18 MΩ). They covered different aspects in the ablation process: first the ablation mechanisms (variation of the target surface morphology versus laser fluence and wavelength). They observed an important difference between the ablation in the IR and the UV region, meanwhile the ablation in the visible region showed a combination of the other two wavelengths. They concluded that the nature of the liquid could affect the ablation mechanism and the products of ablation. Therefore the surface conditions is an important parameter due that the surfactant may affect the growth and also the ablation mechanism. Further, they analyzed the ablation rate and size distributions (the effect of the laser wavelength and fluence on the mass yield and size distribution of the nanoparticles). The resulted bimodal size distribution of the nanoparticles was attributed to the thermal vaporization (smaller) and explosive boiling mechanisms (larger). Also found a higher yield of Pt nanoparticles for 1064 nm wavelength used in PLAL. The third paper described the laser induced reactions (laser-target-liquid interactions occurring in PLAL) and demonstrated that an advantage of PLAL is the tunability in the reactivity between the solution and the ablated species. In this thesis, Pt NPs were synthesized by pulsed laser ablation in different liquid media. The ablation parameters (fluence), nature of the liquid and stability of the Pt NPs were reported. Pt NPs were characterized by TEM, EDX, XPS and UV-Vis Absorption spectroscopy to study the

morphology, size, size distribution, structure, elemental composition, chemical state and optical properties of the ablated products.

1.3.6 Other Metal Nanoparticles Synthesized by PLAL

There are nanomaterials of other metals, non-metals, lantanides, semiconductors etc. that had been synthesized by PLAL in different liquid media. This is due to the great advantages of this technique and the potential applications of the obtained nanoparticles/nanocomposites. PLAL of a **Pb** target in primary alcohols [256] resulted in synthesis of ($Pb_3(CO_3)_2(OH)_2$). The second harmonic of an Nd:YAG laser was used for the PLAL experiments to obtain the nanostructured hydrocerussite with hexagonal morphology. Santillan et al. [127] synthesized **Cu** and Cu oxide nanoparticles by femtosecond pulsed laser ablation of Cu in water and acetone. They reported significant differences in the composition and structure depending on the liquid media and the energy fluence used. Hongqiang Wang et al. [59] reported the synthesis of submicrometer sized particles of **CuO** by pulsed laser ablation of colloidal NPs. They proposed the heating-melting fusion as the predominant mechanism. They reported that the size and phase of ablated products could be controlled by the input laser fluence. Seung Won Lee et al. [128] also reported the synthesis of **CuO** nanofluid to critical heat flux (CHF) measurements. They used a Nd:YAG laser system at 532 nm of wavelength for 8 hours. P. G. Kuzmina et al. [257] produced porous nanoparticles of **Al** or **Ti** by PLA in ethanol, water and n-propanol saturated with hydrogen. They used two different pulsed laser systems, a Ti:Sapphire (180 fs at λ=800 nm) and a Nd:YAG (70 ns at λ=1064 nm). They reported that the morphology of NPs and its cavities depend on the nature of the metal and on the pulse duration. Cobalt sulfate nanoparticles [258] were synthesized by PLAL using a pure **Cobalt** slice as metal target immersed in SDS solution. They used a Nd:YAG laser system with the fundamental wavelength for 1 hour of irradiation. Important changes in the optical and magnetic properties of the synthesized NPs were observed in comparison with the bulk material. Qiang Li et al. [259] reported the formation of core–shell $Ta_xO@Ta_2O_5$ (x =1/2) composite nanoparticles by the irradiation of **tantalum** metal plate in ethanol. In the characterization to the photocatalytic activity of the Ta_xO/Ta_2O_5 core–shell NPs present higher activity compared with pure micrometer-scale Ta_2O_5 powders. In the case of non-metals, some researches has been explored carbon as started material to obtain a desired

compound as Tomonari Wakabayashi et al. [156] which reported the synthesis of Cyanopolyynes by pulsed laser ablation in liquid acetonitrile. The carbon powders were irradiated with an Nd:YAG 532 nm laser system at 0 °C during 5 hours. In the same group of carbon materials, S. Z. Mortazavi et al. [260] reported the synthesis of **graphene** by pulsed laser ablation in liquid nitrogen. They used a q-switched Nd:YAG laser at 1064 nm of wavelength and observed the relation between the number of graphenes and the energy fluence used. They proposed that the mechanism for the graphene formation is the penetration of liquid nitrogen and the subsequent expansion to gas phase during laser heating. Also there are studies on some **lantanides** as reported by K. Hasna et al. [261] describing the synthesis of Europium doped HAp (hydroxyapatite ($Ca_{10}(PO_4)_6(OH)_2$) nanoparticles for applications as imaging of tumor cells and also for targeted drug delivery. They reported the laser ablation in liquid phase of europium doped HAp target using the third harmonic of the Nd-YAG laser system at a wavelength of 355 nm. Some results on semiconductor NPs synthesized by PLAL is described as follows: Nikolai V. Tarasenko et al. [262] reported the synthesis of **Ga-Si** nanoparticles by PLA in ethanol. They used a Nd:YAG pulsed laser at 1064 nm and 8 ns of pulse width. The Gd−Si nanoparticles obtained were of approximately 5-15 nm of diameter exhibit a superparamagnetic behavior. Saitow K. [85] reported the synthesis of **Silicon** nanoclusters by laser ablation in supercritical fluid. Blue luminescent ultra-fine Si-nanocrystals [263] also synthesized by pulsed laser ablation in de-ionized water. P. A. Perminov et al. [264] reported the synthesis of silicon nanocrystals by laser ablation of monocrystalline silicon targets in water, glycerol at the different temperatures and liquid nitrogen. Synthesis of Si nanocrystals [265] was reported in a two-stage process of PLAL. First, the nanosecond laser ablation of Si target in an organic liquid (chloroform). And second, an ultrasonic post-treatment of Si NPs in the presence of HF. The post-treatment was responsible for disintegration of composite Si NPs due to HF induced etching of the Si oxide surface. P. Chewchinda et al. [266] studied the effect of energy fluence on laser ablation of Silicon target in liquid. They reported that production of silicon nanoparticles resulted at higher energy fluence. R. Intartaglia et al. [267] reported the ultrafast laser ablation of a Si target in deionized water. They synthesized isolated Si-NPs with pseudospherical morphology and smooth surface. E. V. Barmina et al. [268] also reported the nanostructuring of a single crystal Si wafers by

femtosecond PLAL in ethanol. They obtained two types of nanostructures namely, ripples and self-organized nanostructures (SONS). V. Švrček et al. [67] reported the synthesis of Si nanocrystals by nanosecond PLAL in ethanol and water. Their results showed that the fragmentation time in both liquids determines the photoluminescence (PL) intensity and red-shifts the PL maxima of the Si-nanocrystals. This group developed two different types of solar cells employing surface-engineered Si-nanocrystals. Other important semiconductor nanoparticle synthesized by PLAL is Ge nanoparticles, due to their novel properties in comparison with bulk material. For example, S. Vadavalli et al. [269] synthesized **Ge** NPs in acetone using pulsed laser ablation. They observed that the average size of Ge NPs decreases with the increment of laser energy as reported by other authors. Synthesis of Ge nanoparticles by PLAL and the study of the thickness of liquid layer upon the final properties of NPs [270] was described. It was found that the average size decreases with the thickness of water, and reported an optimum thickness to improve the yield of nanoparticles. Yilu Li. [271] studied the synthesis of germanium NPs by PLAL in water and ethanol in an externally applied electric field. The study reported a correlation between particle size and the magnitude of externally applied electric field. There is a great diversity of materials reported by PLAL as was mentioned previously, which is one of the interesting characteristics of this technique, in addition to the interest of researchers to allow increase in the productivity of PLAL and the applicability of ablated products. Based on these studies of PLAL in terms of applications, properties, mechanisms of formation and methodologies, the following hypothesis and objectives are selected.

1.4 HYPOTHESIS

The morphology and properties of noble metal nanoparticles synthesized by pulsed laser ablation in liquid media is determined by laser parameters, ablation parameters (energy fluence, liquid media and ablation time) and in-situ irradiation process.

1.5 OBJECTIVES

1. To synthesize Au and Ag nanoparticles by PLAL.
2. To study the effect of in-situ irradiation of continuous laser during the pulsed laser ablation of Ag and Au metal targets in different liquid media.
3. To characterize Ag and Au nanoparticles by TEM, SAED and UV-Visible absorption spectroscopy.
4. To characterize chemical state and elemental composition of Ag and Au nanoparticles by XPS and EDX spectroscopy.
5. To synthesize Pd and Pt nanoparticles by PLAL.
6. To characterize Pd and Pt nanoparticles by TEM, SAED and UV-Vis absorption and XPS analysis.
7. To study the effect of ablation parameters (energy fluence) in the formation of Pd and Pt nanoparticles.
8. To study effect of liquid media and concentration in final size and size distribution of Pd and Pt nanoparticles

1.6 JUSTIFICATION

Pulsed laser ablation in liquid media is a novel and versatile technique for fabrication of a great variety of nanomaterials in one step as metals, oxides, alloys or nanocomposites. Other important advantage of PLAL is the high purity of nanocolloids produced. Due to these characteristics the range of possible application of nanomaterial produced by PLAL involves many areas of investigation as medical, biological, catalysis, optoelectronics, solar energy, between others. Study of the different parameters over the final properties of nanomaterials obtained in PLAL is an important topic. Noble metal nanoparticles as Au, Ag, Pt and Pd are of interest in various technological areas like sensing, catalysis, electronic and plasmonics due their novel properties at nanoscale dimensions. Gold nanoparticles have found a wide range of applications as: biotechnology, industries, optical, pharmaceutical, medical, agricultural fields and low temperature catalyst. Some applications of silver nanoparticles as anti-bacterial agents in the health industry, food storage, textile coatings, catalysis and a number of environmental applications had been reported. Antibacterial activity of silver NPs is closely related to their size, structure, shape, size distribution, and chemical–physical environment. Palladium and platinum nanoparticles are heavily studied for many catalytic applications, oxidation and reduction reactions in fuel cells. Also platinum and its alloy nanoparticles were used in many catalytic reactions as to eliminate NO generated in combustion process. For all this novel and important applications the control over the size and size distribution is an important task. Another important factor is the chemical environment and purity of synthesized nanoparticles. Thus, this study focus on synthesis and characterization of nanoparticles of Ag, Au, Pd and Pt nanoparticles by pulsed laser ablation in liquid media. Advantages of PLAL were made use to obtain noble metal nanoparticles in liquids such as water and alcohols. The study of different laser parameters and liquid media to control size, size distribution, shape and crystalline structure of these noble metal nanomaterials was carried out.

CHAPTER 2

SYNTHESIS AND CHARACTERIZATION OF GOLD NANOPARTICLES BY PLAL

2.1. INTRODUCTION

Metal nanoparticles have been investigated because of their novel chemical and physical properties. These novel properties are strongly dependent on their size and structure. Specifically, Au nanoparticles have been used in a wide range of applications such as: biotechnology [167-170], industrial [171], optical [172], pharmaceutical [173], medical [174, 175] and agricultural fields [176]. Also in treatment of arthritis [177], by attaching various functional organic molecules or bio-components [178] or in photothermal therapy [179]. Although bulk gold does not exhibit catalytic properties, Au nanocrystals demonstrate to be an excellent low temperature catalyst [164]. Recently, pulsed laser ablation in liquid media (PLAL) has been studied due to their advantages over other synthesis methods [181, 272, 273] for gold nanoparticles [74, 87]. PLAL allows us to synthesize nanoparticles with high purity in common liquids as water, alcohols, acetone, surfactants, etc. without contamination by reducing agents. This advantage is important for biological and biocompatible applications [81, 173, 181, 274]. Additionally, the photo-excitation induced by pulsed [196, 197, 201, 275] and continuous [276] laser irradiation over colloidal solutions of metal nanoparticles also has been well studied. The absorption spectrum of Au nanoparticles exhibit peaks at 520 nm due to the surface plasmon resonance. Different laser parameters as the pulse width (picosecond and femtosecond) had been studied in PLAL experiments of synthesis of gold NPs [62, 64]. In this chapter, synthesis and characterization of gold nanoparticles by pulsed laser ablation in distilled water and the effects of in-situ irradiation of a continuous wave laser during the synthesis of Au nanoparticles by PLAL is explained. Pure gold target was irradiated using both, the fundamental and second harmonic (1064 and 532 nm, respectively) outputs of a Nd:YAG pulsed laser (10 Hz, 10 ns). During PLAL experiments the solution was irradiated by continuous laser using 532 and 457 nm wavelengths (at same output power of 4 W). For a comparison, the colloidal nanoparticles obtained by pulsed laser ablation were post-irradiated by 457 nm and 532 nm continuous lasers. For in-situ experiments, the continuous

laser was expanded over the colloidal solution near to the irradiated zone of the metal target, where the plasma plume and the initial stage of the ablated material occur. A detailed description of experimental conditions is given below. The shape, mean size, size distributions, elemental composition and optical properties of gold nanoparticles synthesized at different irradiation configurations were examined. These nanoparticles were characterized by transmission electron microscopy (TEM), X-ray photoelectron spectroscopy (XPS) and UV-Visible absorption spectroscopy.

2.2. EXPERIMENTAL SECTION

Gold nanoparticles were obtained by PLAL in distilled water using 1064 and 532 nm output wavelengths. Pulsed laser ablation experiments were performed using a q-switched pulsed laser Nd:YAG (Solar Laser System LQ929A) of 10 ns (pulse width), 10 Hz (repetition frequency) and output energies of 600 and 230 mJ/pulse at 1064 and 532 nm wavelengths, respectively. Two continuous wave (CW) lasers (CNI lasers Ltd.) at 457 and 532 nm were employed for the in-situ and post-irradiation experiments. The CW laser source of 457 nm had an invariable output power of 4W. The CW laser source of 532 nm had an output power variable in the range of 0 – 10 W. The gold target was a 99.99% pure Au metal plate. The experiments were named as single PL (1064 or 532), in-situ CW532, in-situ CW457, post CW532 and post CW457, respectively. Single PL consisted of an experimental configuration as in conventional PLAL experiments where the target was directly irradiated with the pulsed laser using 1064 or 532 nm. In-situ CW (532 or 457) consisted of the CW irradiation of the liquid media during PLAL (single PL1064 or 532 nm) of Au target. Post CW (532 or 457) was done in two steps, first the gold nanoparticles were obtained with pulsed laser ablation (at 1064 or 532 nm). In the second step, these Au nanocolloids (after PLAL experiments) were irradiated with continuous wave lasers. Figure 3 shows a) photograph and b) schematic diagram of the PLAL experimental setup for 1064 nm ablation. A vertical configuration was used in which the metal target was placed at the bottom of a glass beaker (50 ml of volume). For all the experiments, we used 30 ml of distilled water (DW) with a liquid layer height of 2.5 cm. Mirrors 1 and 2 were used to direct the laser beam on to the metal target. One mirror was 99% reflective for the selected wavelength and the second one 50% reflective at this wavelength. The output energy of the laser beam was 600 and 280 mJ/pulse, for the first and the second mirror, respectively. The

pulsed beam was focused with a convex lens to the target at its focal distance (200 mm) and the calculated energy fluence was 40.5 J/cm^2. The CW laser was placed near to the glass beaker where the laser beam was expanded with a concave lens over the liquid media (for in-situ or post-irradiation experiments). Both continuous wave lasers (457 and 532 nm) were fixed at 4 W output power. Single, in-situ CW and post CW experiments were carried out for 10 minutes. Figure 4 shows, a) photo and b) schematic of the setup of PLAL experiments for 532 nm laser output. A horizontal configuration was used in which the metal plate was fixed parallel to the wall of a beaker. The beaker was filled with 30 ml of distilled water. The normal distance between target surface and liquid surface, namely as liquid layer was 3 cm for all experiments. The pulsed beam was focused with a convex lens to the target at its focal distance (200 mm). The second harmonic (532 nm) with output energy of 230 mJ/pulse was used and the calculated energy fluence was 27.6 J/cm^2. The CW laser was placed near the glass beaker where the laser beam was expanded with a concave lens over the liquid media (for in-situ and post-irradiation experiments). Both continuous lasers (457 and 532 nm) were kept with an output power of 4 W. Single, in-situ CW and post CW experiments were carried out for 10 minutes. In all these experiments, the glass beaker was attached to a translation system (developed by Mechatronics students of FIME, UANL) to improve the ablation productivity. The scan velocity can be varied from 50 to 5000 μm/s; in this experiment we selected 50 μm/s. Figure 5 shows Au colloidal solutions obtained by PLAL in both sets 1064 and 532 nm of wavelength.

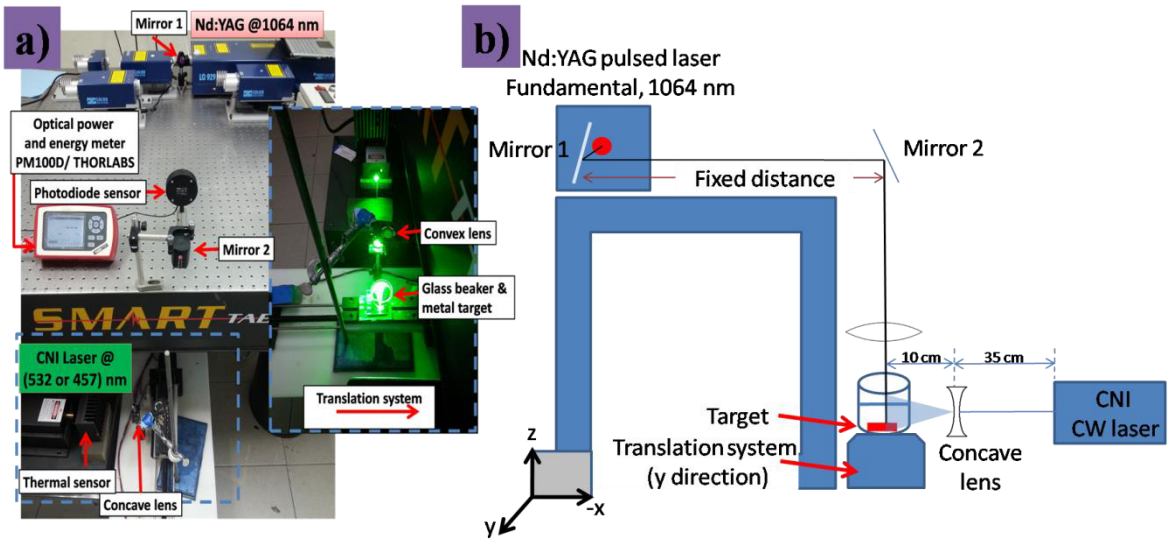

Figure 3. a) Photo of experimental set-up for PLAL using 1064 nm. The inset corresponded to PLAL experiment with in-situ / CW532 nm irradiation; b) schematic of vertical configuration (1064 nm).

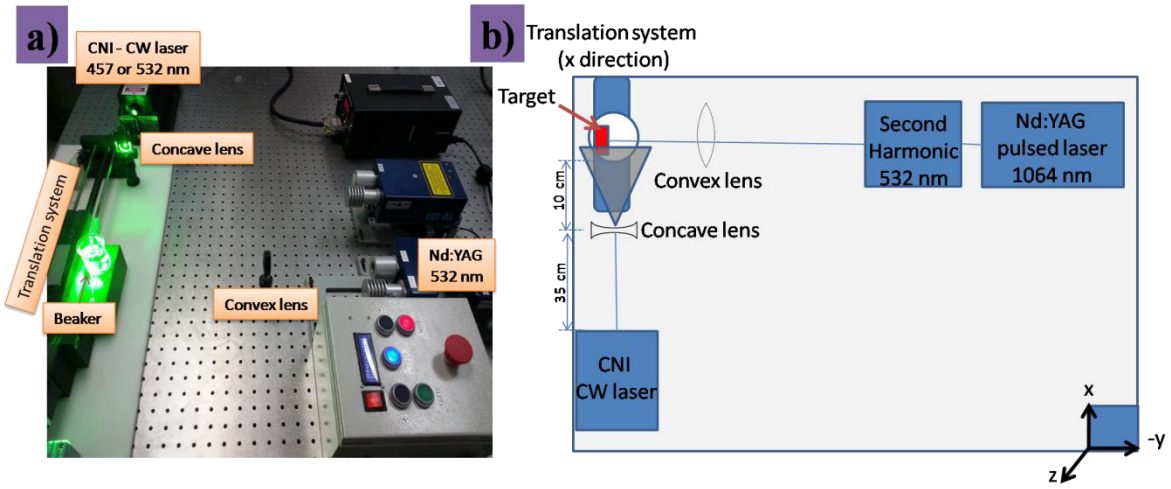

Figure 4. a) Photo of experimental and b) schematic set-up for PLAL at 532 nm experiment with in-situ CW532 nm irradiation.

Figure 5. Au colloidal solutions obtained by PLAL for 1064 and 532 nm of wavelength under different configurations.

2.3. RESULTS AND DISCUSSION

Gold nanocolloids obtained by PLAL experiments (single, in-situ and post) were red color and stable for 6 months after their synthesis. UV-Vis absorption measurements were carried out after PLAL experiments in a UV-Vis-NIR spectrometer (Shimadzu UV-1800) in a wavelength range of 200 to 1000 nm. For the optical measurements, the colloidal samples were taken in a quartz cuvette of 1 cm of length, using water as reference. Immediately after each experiment, a TEM grid was prepared by placing a drop of the colloidal solution on a copper grid and dried at ambient temperature. TEM analysis was performed in a FEI Titan G2 80-300 in bright field (BF) and STEM mode (with the high angle annular dark field and EDX detector). For XPS analysis a few drops of each solution were placed on a Cu tape and dried at room temperature. The samples were subjected to X-ray photoelectron spectroscopy (XPS) analysis in a Thermo Scientific K-Alpha XPS instrument. The samples were excited by a monochromatized Al K_α X-ray radiation of energy 1486.6 eV. All the spectral peaks were recorded with reference to C 1s peak (284.6 eV).

2.3.1. Morphology by TEM

The morphology of Au NPs produced in the two sets of PLAL experiments (1064 or 532 nm) was analyzed by BF-TEM micrographs. Average size (diameter), size distribution and shape for the gold nanoparticles obtained under different experimental conditions were analyzed from the TEM images. Figures 6 and 7 show the TEM micrographs, size and size

distribution of Au NPs obtained by the two sets of PLAL at 1064 and 532 nm, respectively. Figure 6 shows TEM micrographs and size distributions of Au NPs obtained by PLAL using 1064 nm under five experimental conditions: Single PL1064, in-situ CW (532 and 457) and post CW (532 and 457). Au nanoparticles were in general spherical for all the conditions with average size of Ø= 13±6 nm for single PL1064, Ø= 16±6 and 11±6 nm for in-situ and post CW 532, respectively. For in-situ and post CW 457 the average size measured was Ø=14±6 nm with more agglomerated nanoparticles. As mentioned, Au NPs were smaller in size and well dispersed for post CW 532 in comparison with other conditions using the fundamental wavelength (1064 nm). This phenomenon is in agreement with reports of size reduction of nanoparticles using irradiation near to SPR band of the metal [90, 95, 201]. Figure 7 shows TEM micrographs and size distributions of Au NPs obtained by PLAL using 532 nm for five experimental conditions: single PL, in-situ CW (532 and 457) and post CW (532 and 457). A plot with the mean size and size distribution vs. the different PLAL configurations at 532 nm, is also included. Au nanoparticles presented spherical as well as elongated morphologies with an average size of Ø=9±2 nm for all the conditions. The average size and size distribution for the gold nanoparticles prepared in set of PLAL at 532 nm were smaller than that obtained at 1064 nm, as reported by K. A. Elsayed et al. [194]. They attributed this effect to two factors: the value of the absorption coefficient and the photon energy. The value of the absorption coefficient for bulk gold is higher in the case of 1064 nm. The photon energy of 532 nm is higher than the photon energy of 1064 nm. This leads to the fragmentation of gold nanoparticles prepared at 532 nm and consequently results in the generation of smaller size gold nanoparticles. Figure 8 shows TEM micrographs at higher magnifications leading to the presence of elongated gold nanoparticles resulted from the experiments of in-situ and post- irradiation of CW lasers (532 and 457 nm) in set using 532 nm. TEM micrographs of Au NPs with in-situ irradiation of CW457 show interconnected gold nanoparticles as nanowires with a diameter of ~5 nm. In the case of Au nanoparticles obtained with post CW457 the presence of NPs of around 5 nm were observed. Nikolov, A. S. et al. reported the synthesis of gold nanowires by PLAL with post-irradiation by pulsed lasers at 355 nm of wavelength [209], similar to the elongation effect of in-situ irradiation in our Au NPs. They attributed the formation to this structure to the positioning of wavelength of irradiation near to SPR band

by self- absorption condition. Then in-situ and post CW 457 irradiation had an effect over the growth of gold nanoparticles. Probably for in-situ CW 457, the additional energy helped the formation of nanowires meanwhile; only small nanoparticles were produced by post CW 457 irradiation.

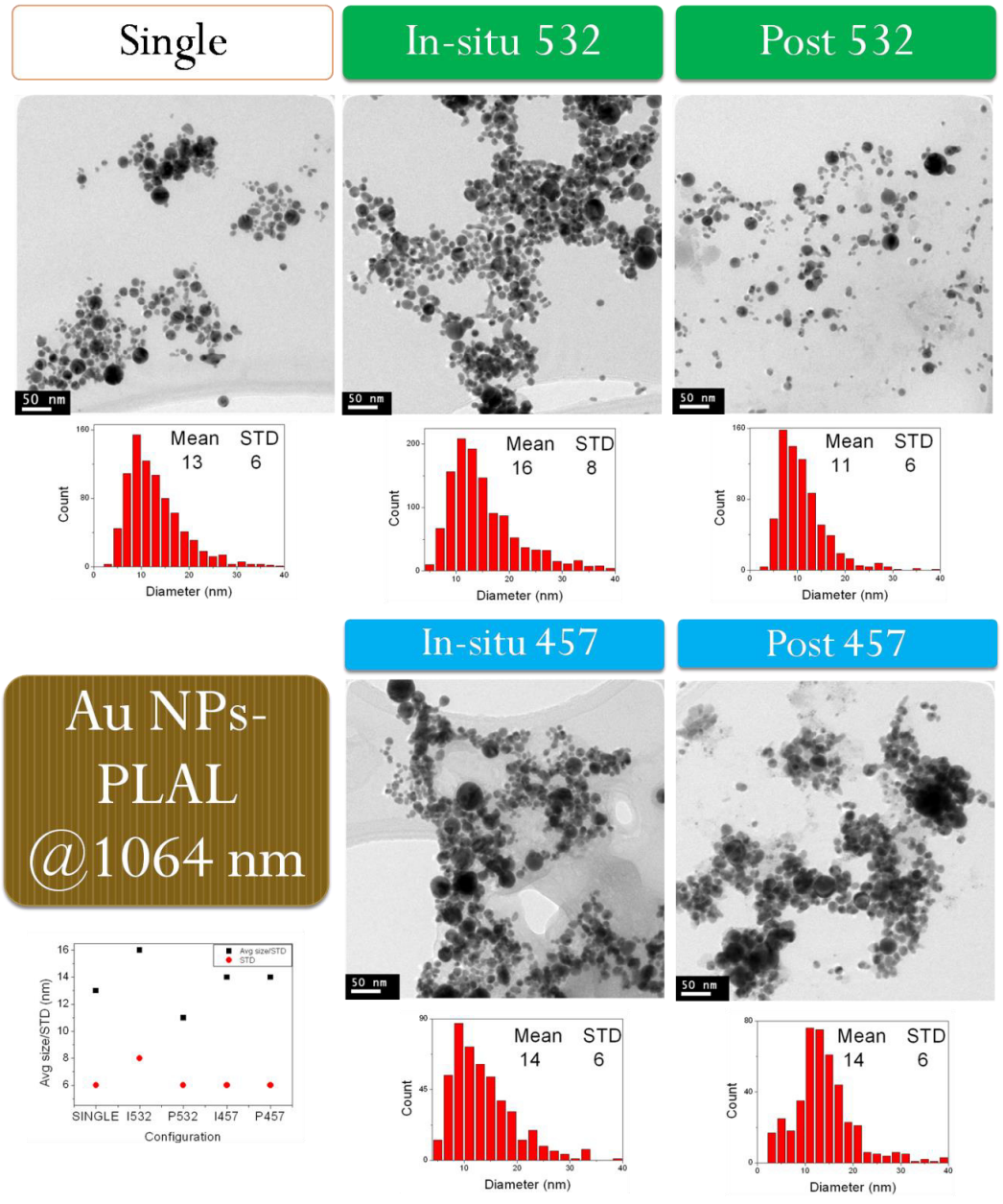

Figure 6. TEM micrographs and size distribution of Au NPs obtained in DW by PLAL using 1064 nm in Single, In-situ and Post-irradiation configuration with CW lasers of 532 and 457 nm

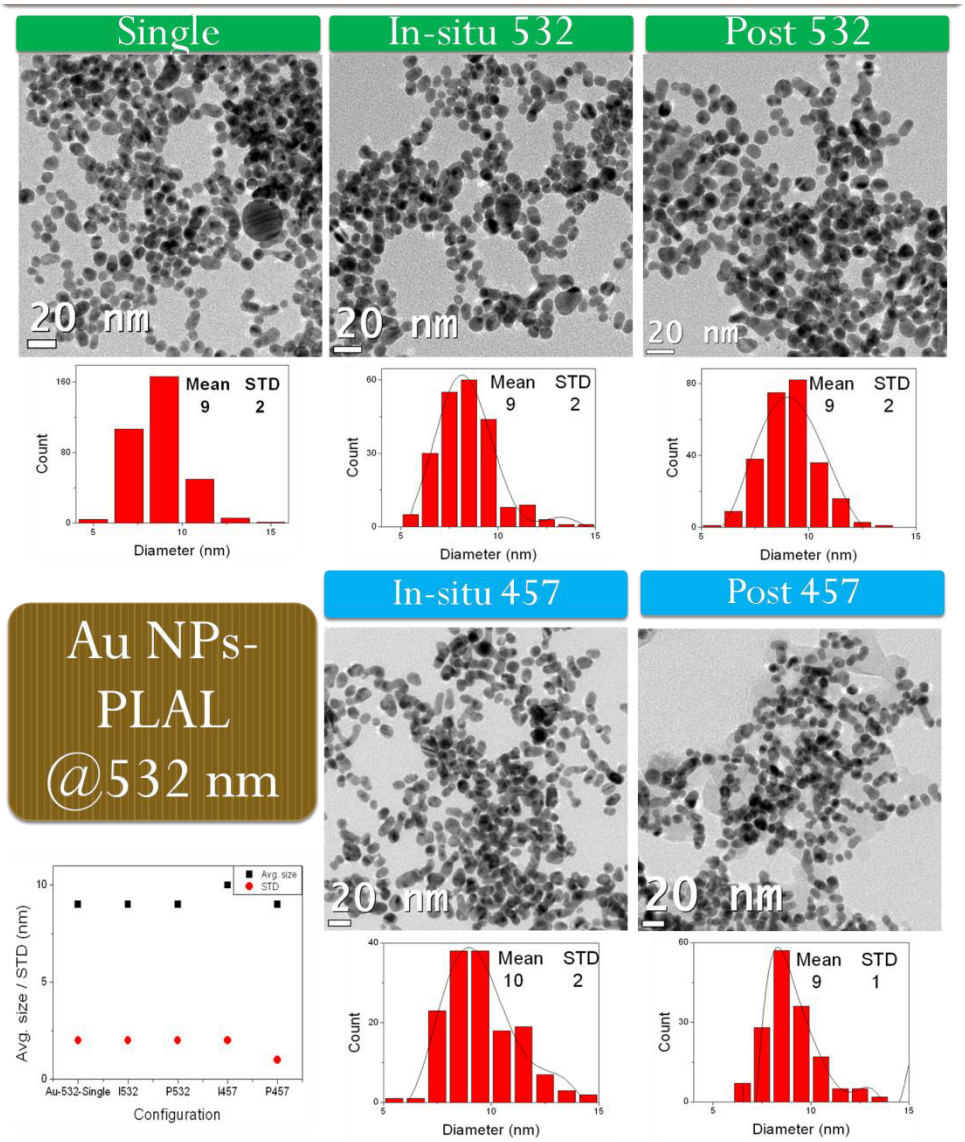

Figure 7. TEM micrographs and size distribution of Au NPs obtained in DW by PLAL using 532 nm in Single, In-situ and Post-irradiation configuration with CW lasers of 532 and 457 nm.

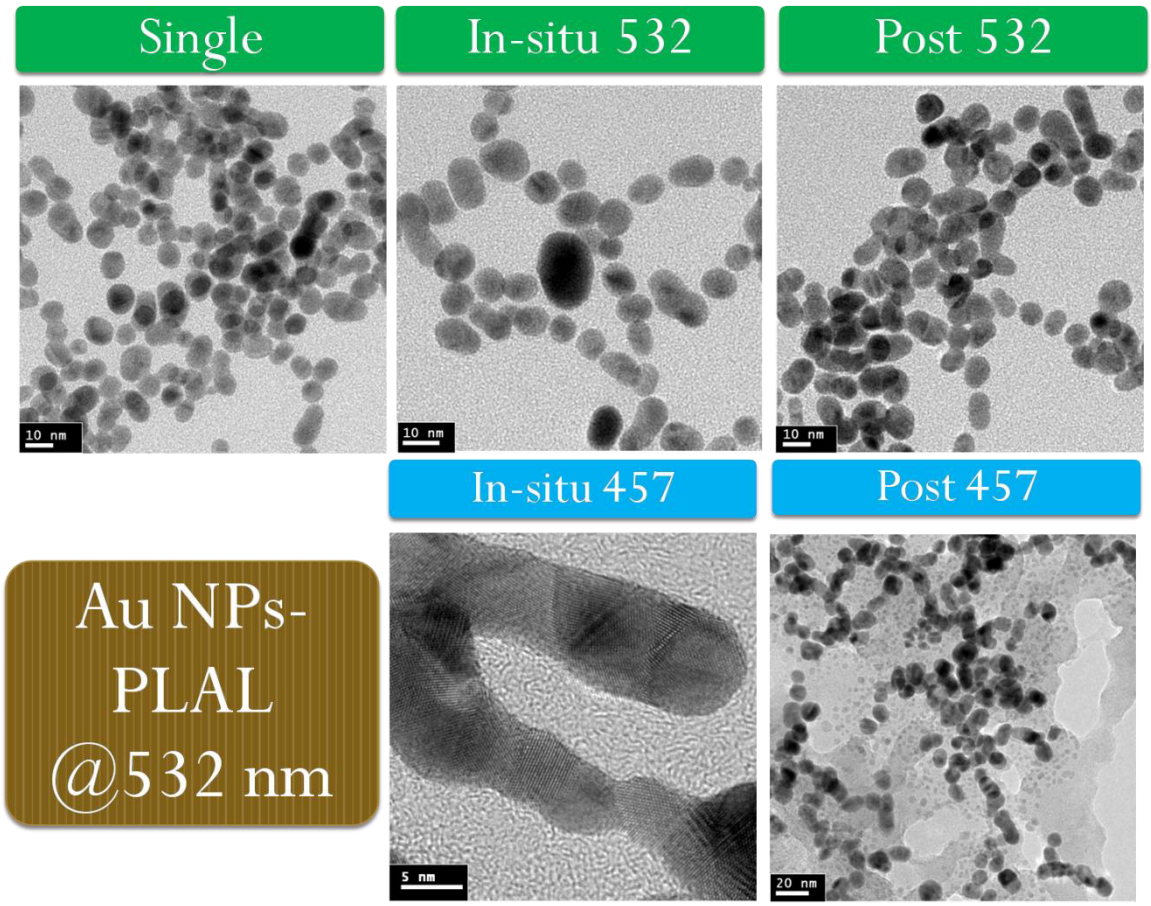

Figure 8. TEM micrographs of Au NPs obtained in DW by PLAL using 532 nm in Single, In-situ and Post-irradiation configuration with CW lasers of 532 and 457 nm

Crystalline structure of Au NPs obtained by PLAL using 1064 and 532 nm was analyzed by high resolution transmission electron microscopy (HRTEM) and selected area electron diffraction (SAED) and the results are presented in figures 9 and 10, respectively. The planes indexed for all SAED were (111), (200), (220) and (311). The interplanar distances measured in HRTEM micrographs were 2.3 Å (111) and 2.03 Å (200). Electron diffractions and high resolution TEM micrographs were indexed using the PDF No. 04-0784 that corresponds to cubic FCC structure of gold. All the measurements were performed using the DigitalMicrograph software. These results showed that the Au nanoparticles synthesized by PLAL experiment were crystalline and the crystalline

structure was not affected by the in-situ or post-irradiation of the different CW lasers (532 and 457).

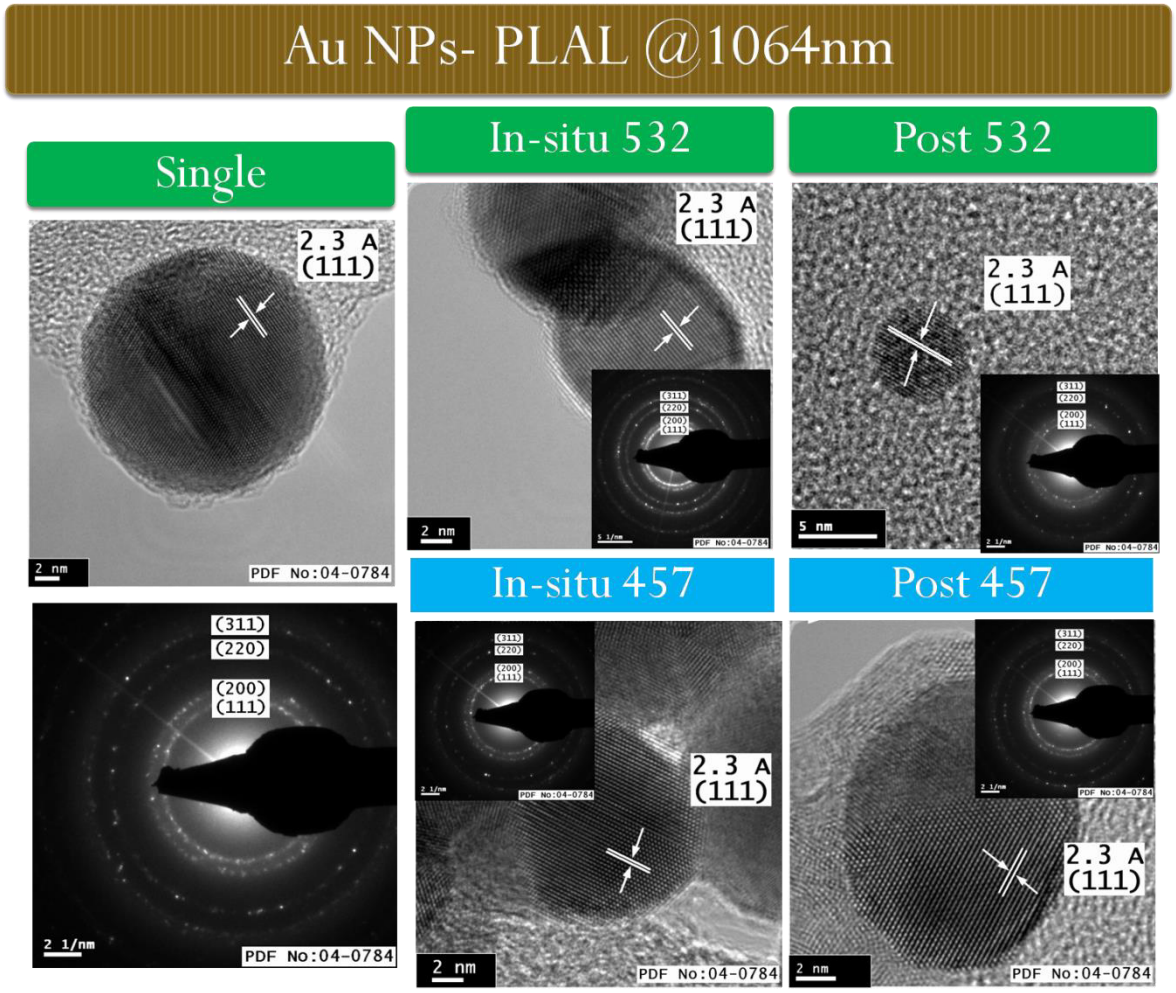

Figure 9. HRTEM and SAED micrographs of Au NPs obtained in DW by PLAL using 1064 nm in Single, In-situ and Post-irradiation configuration with CW lasers of 532 and 457 nm.

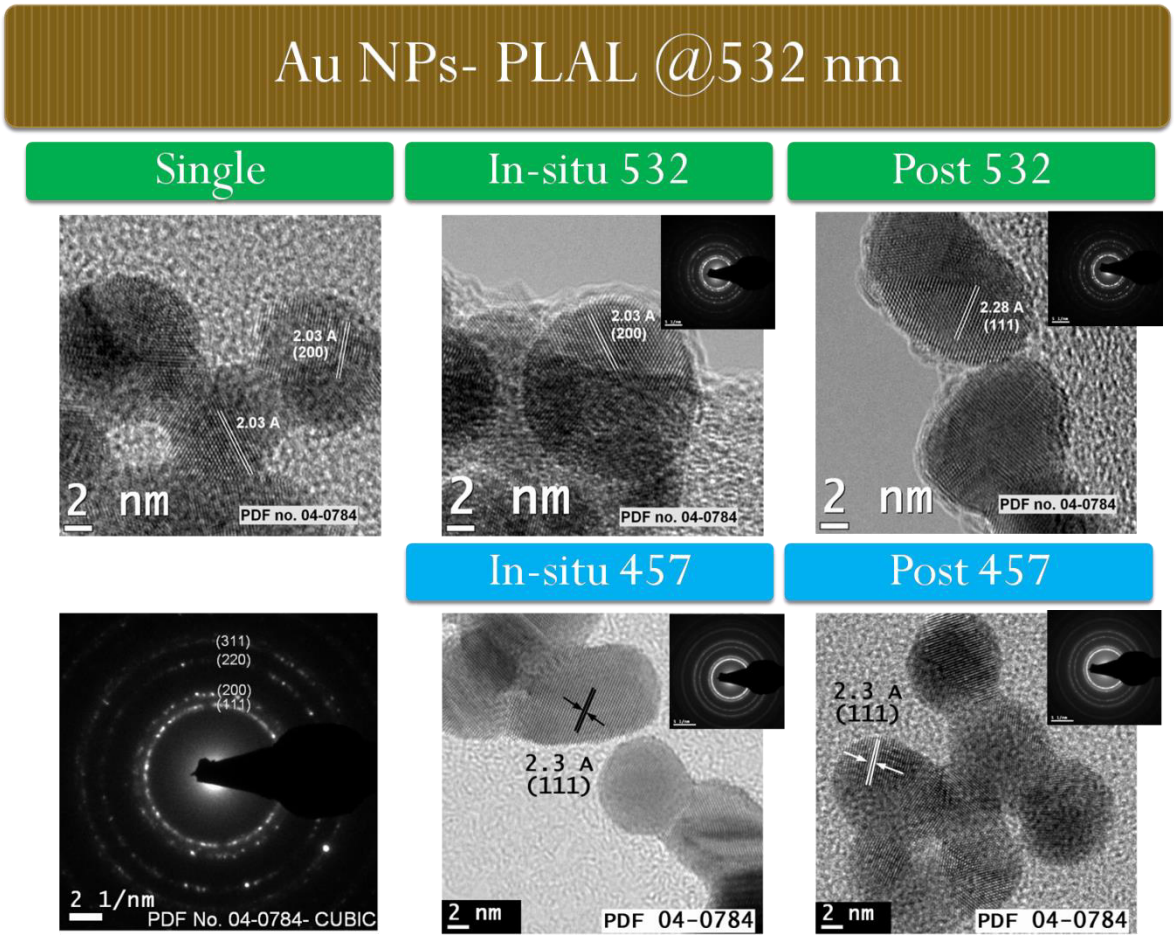

Figure 10. HRTEM and SAED micrographs of Au NPs obtained in DW by PLAL using 532 nm in Single, In-situ and Post-irradiation configuration with CW lasers of 532 and 457 nm.

2.3.2. *Elemental Composition by XPS*

Elemental composition of gold nanoparticles was analyzed by XPS technique. For XPS analysis some drops of Au nanocolloids were dried at room temperature on a Cu tape. This was repeated many times to recollect sufficient material for analysis. Figure 11 shows the high resolution Au 4f for gold nanoparticles obtained by PLAL in the set of 532 nm of wavelength. The Au $4f_{7/2}$ at 83.97, 83.48 and 83.70 eV corresponded to single-PL532, in-situ CW 457 and 532 configurations; all doublets had a splitting energy Δ= 3.67 eV. In the case of Au NPs with in-situ CW 532 showed a broadening peak in comparison with other

ones. This result shows the high purity of Au nanoparticles in colloidal solution obtained by PLAL, same as the results reported by this technique [64, 197, 276]. Sample preparation of in-situ CW (532 and 457) were performed using precipitates at bottom of the solution, meanwhile single PL532 was completely stable. Then, the little chemical shift between them can be attributed to the difference between core level binding energies of surface atoms with respect to those of bulk material (in reference to precipitates of gold in the solution) [277].

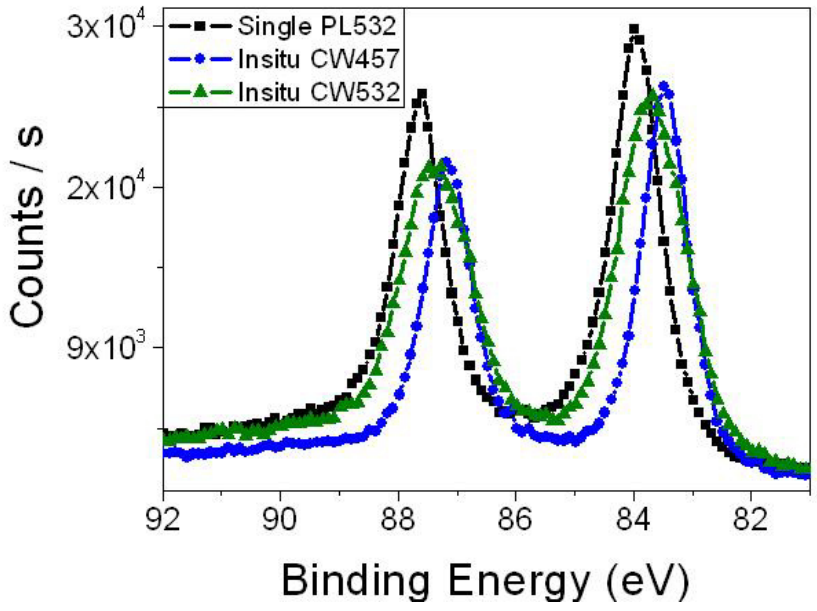

Figure 11. High resolution Au 4f XPS spectrum of gold nanoparticles obtained by PLAL using 532 nm of wavelength in distilled water with single and in-situ (532 and 457) configurations.

2.3.3. *Optical Properties by UV-Vis*

Optical properties of gold nanoparticles obtained by PLAL were analyzed by UV-Visible absorption spectroscopy. Figures 12 and 13 show the UV-Vis absorption spectra of Au colloidal solution obtained by PLAL at 1064 and 532 nm, respectively, with the different configurations (single PL, in-situ and post-irradiation of the continuous wave lasers). In general, the absorption intensity was higher for 1064 nm in comparison with 532 nm, as was mentioned in the reference [194] in which the ablation productivity increases

when wavelength increases. Figure 12 shows plasmon peaks around 520 nm for Au NPs obtained by the set of PLAL using 1064 nm for the five configurations, these results are in accordance with the surface plasmon peak reported in literature for Au nanoparticles. Then in-situ and post-irradiation of CW did not affect the plasmon peak of Au NPs as confirmed by TEM analysis; without a significant change in average size of nanoparticles. Absorption intensity was higher for in-situ and post CW (532 and 457) in comparison to single PL1064. In the absorption spectrum of figure 13 are shown gold nanoparticles obtained by the set of PLAL using 532 nm of wavelength. The plasmon peak position of Au NPs obtained by PLAL using 532 was affected by the different configurations of PLAL (single PL, in-situ and post). For single PL the spectrum showed a plasmon peak at 522 nm, whereas for the samples in-situ and post irradiated with CW 532 nm the plasmon peak was at 519 nm. A little shift was observed for the samples in-situ and post irradiated with CW 457 nm with plasmon peaks at 523 and 521 nm, respectively. The little blue shift of post CW 457 could be related to smaller nanoparticles observed in TEM images on figure 8. Absorption intensity of Au NPs synthesized by PLAL using 532 was higher for in-situ and post-irradiation CW conditions in comparison to single PL532 (with the exception of in-situ CW 457) as the results obtained in the set using 1064 nm. The plasmon peaks for all Au NPs obtained in this work by PLAL were around 519-523 nm, which indicates the formation of nanoparticles in the range of 5-30 nm, which was in accordance with the TEM images (figures 6-8). Figure 14 shows the UV-Vis absorption spectra of gold NPs synthesized by PLAL in the set using 532 nm after 43 days. For the samples obtained by single and In-situ 532 the peak presented some broadening which could be due to agglomeration of the smaller spherical Au NPs to bigger ones. Meanwhile, for the other samples (in-situ CW457, post CW532 and post CW457) an additional plasmon peak was present which could be related to agglomerated spherical or ellipsoidal NPs [199].

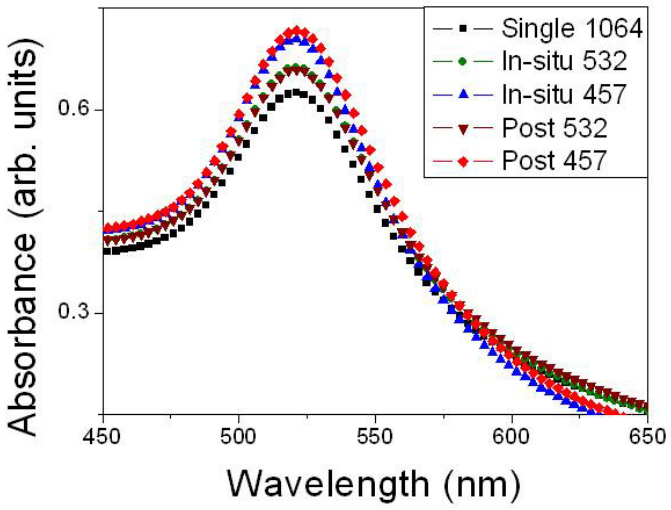

Figure 12. UV-Vis Absorption spectra of gold nanoparticles synthesized by PLAL using 1064 nm in DW at different configurations of experiments (Single PL1064, In-situ CW457, In-situ CW532, post CW457 and post CW532)

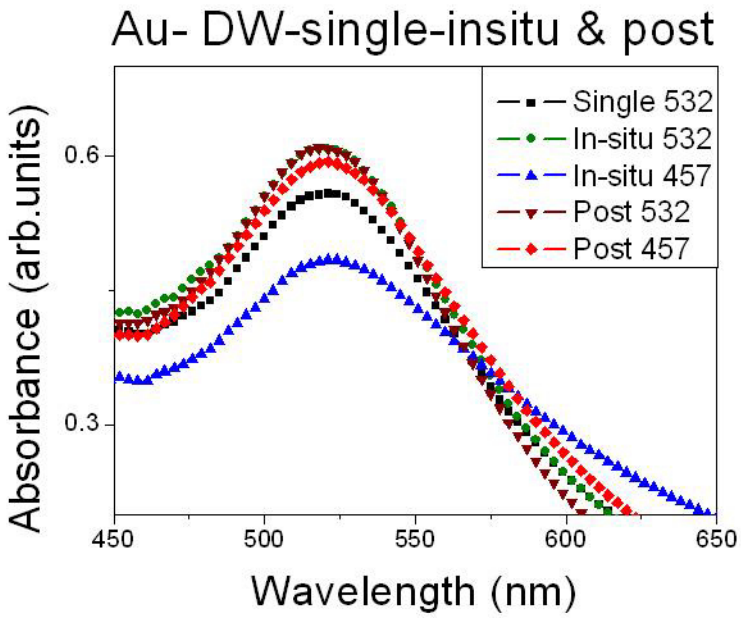

Figure 13. UV-Vis Absorption spectra of gold nanoparticles synthesized by PLAL using 532 nm in DW at different configurations of experiments (Single, In-situ 457, In-situ 532, post 457 and post 532).

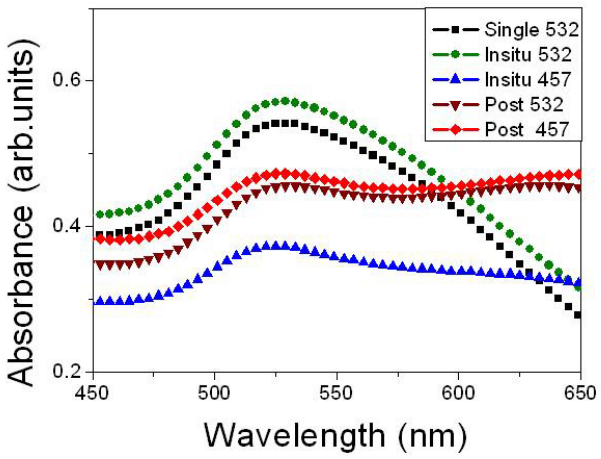

Figure 14. UV-Vis Absorption spectra of gold nanoparticles synthesized by PLAL using 532 nm in DW at different configurations of experiments (Single, In-situ 457, In-situ 532, post 457 and post 532) after 43 days of PLAL experiments.

The conclusions of the synthesis of Gold nanoparticles by PLAL using 1064 and 532 nm of wavelength in DW (in which traditional PLAL experiment was modified with the in-situ irradiation of a continuous wave laser at 532 and 457 nm of wavelength and a post-irradiation) were the following: i) The average size and ablation productivity of gold nanoparticles was higher for the higher wavelength as reported in previous studies [194]; ii) In-situ and post CW (532 and 457) PLAL configuration in the set using 1064 nm did not affect morphology of gold nanoparticles as confirmed by TEM micrographs and UV-Vis absorption spectrum; iii) In the set using 532 nm, in-situ and post CW 457 produced nanowires and small NPs (~5nm), respectively. This change in morphology was observed in HRTEM micrographs and a little blue shift in the plasmon peak of absorption spectrum; iv) Crystalline structure of gold nanoparticles (indexed as FCC structure for all the experimental condition of PLAL) was not affected by the in-situ and post CW irradiation for all conditions; v) The absorption intensity of gold nanoparticles was higher for in-situ and post-irradiation conditions with respect to single PL in both sets (using 1064 and 532 nm); vi) Optical properties of gold NPs (using 532 nm) after 43 days showed an additional peak at ~650 nm (except to single-PL532 and in-situ 532) showing the growth of spherical and ellipsoidal NPs according to literature; and finally vii) The chemical nature of metallic state of gold nanoparticles was confirmed by XPS spectroscopy, which is in accordance with the non-reactive nature of PLAL of gold nanoparticles.

CHAPTER 3

SYNTHESIS AND CHARACTERIZATION OF SILVER NANOPARTICLES BY PLAL

3.1. INTRODUCTION

This chapter presents the synthesis and characterization of Ag NPs by pulsed laser ablation in distilled water (DW). Effects of in-situ and post-irradiation with CW lasers to the silver nanocolloids during and after PLAL experiments were studied. Ag NPs were characterized by TEM, EDX, XPS and UV-Vis Absorption spectroscopy to explore the morphology, size, size distribution, structure, elemental composition, chemical state and optical properties of the ablated products.

3.2. EXPERIMENTAL SECTION

Silver nanoparticles were obtained by PLAL in distilled water using 1064 and 532 nm output wavelengths. Pulsed laser ablation experiments were performed using a pulsed laser q-switched Nd:YAG (Solar Laser System LQ929A) of 10 ns, 10 Hz and output energy of 600 and 230 mJ/pulse for 1064 and 532 nm of wavelengths, respectively. Two continuous wave lasers (CNI lasers Ltd.) at 457 and 532 nm were employed for the in-situ and post-irradiation experiments. The CW laser of 457 nm source has a constant output power of 4W, whereas the CW laser source of 532 nm has a variable output power between 0 – 10 W. The target used for ablation was Ag metal plate (99.99% pure). The experiments were named as single PL (1064 or 532), in-situ CW532, in-situ CW457, post CW532 and post CW457. Single PL consisted of experimental configuration as in conventional PLAL experiments where the target is directly irradiated with the pulsed laser output of 1064 or 532 nm. In-situ CW (532 or 457) consisted of the CW irradiation of the liquid media using an expanded laser beam during PLAL (single PL1064 or 532 nm) of Ag target. The silver nanocolloids obtained with pulsed laser ablation using 1064 or 532 nm were post irradiated with CW laser of 532 and 457 nm, labeled as post CW532 and post CW457, respectively. Figure 15 shows the setup of PLAL experiments at 1064 nm. A vertical configuration was used in which the metal target was placed at the bottom of a glass beaker (50 ml of volume). For all experiments, we used 30 ml of DW with a liquid layer height of 2.5 cm.

Mirrors 1 and 2 were used to direct the laser beam on to the metal target. One mirror was 99% reflective for the selected wavelength and the second one 50% reflective at this wavelength (because it was not special for 1064 nm). The output energies of the laser beam were 600 and 280 mJ/pulse for the first and the second mirror, respectively. The pulsed beam was focused with a convex lens to the target at its focal distance (200 mm) and the calculated energy fluence was 40.5 J/cm^2. The CNI laser was placed near to the glass beaker where the CW beam was expanded with a concave lens over the liquid media (for in-situ or post-irradiation experiments), keeping 4 W output power for both continuous lasers (457 and 532 nm). Figure 16 shows the laboratory experimental setup of PLAL experiments using 532 nm. For ablation procedure, a horizontal configuration was used in which the metal plate was fixed parallel to the wall of the beaker, and this was filled with 30 ml of distilled water. The liquid layer was 3 cm for all experiments. The second harmonic (532 nm) with output energy of 230 mJ/pulse was used and the energy fluence calculated was 27.6 J/cm^2. The pulsed beam was focused by a convex lens onto the target at its focal distance (200 mm). The CW laser was placed near the glass beaker where the CW beam was expanded with a concave lens over the liquid media (for in-situ or post-irradiation experiments). Both continuous lasers 457 and 532 nm were kept with an output power of 4 W. To improve the ablation productivity in all these experiments, the beaker was attached to a translation system (developed by Mechatronics students of FIME, UANL). All ablation experiments were carried out for 10 minutes and with 50 μm/s of scan velocity. Figures 17 and 18 show the Ag colloidal solutions obtained by PLAL in the sets using 1064 and 532 nm, respectively. Immediately after each experiment a TEM grid was prepared by placing a drop of the colloidal solution obtained on a copper grid and dried it at room temperature. UV-Visible absorption measurements were carried out in a UV-Vis spectrophotometer (Shimadzu UV-1800). For XPS analysis some drops of each solution were placed on a Cu tape and dried at room temperature. These samples were analyzed by X-ray photoelectron spectroscopy, XPS (K-Alpha, Thermo Scientific). The samples were excited by a monochromatized Al K_α X-ray radiation of energy 1486.6 eV. All the spectral peaks were recorded with reference to binding energy of adventitious carbon, C 1s (284.6 eV).

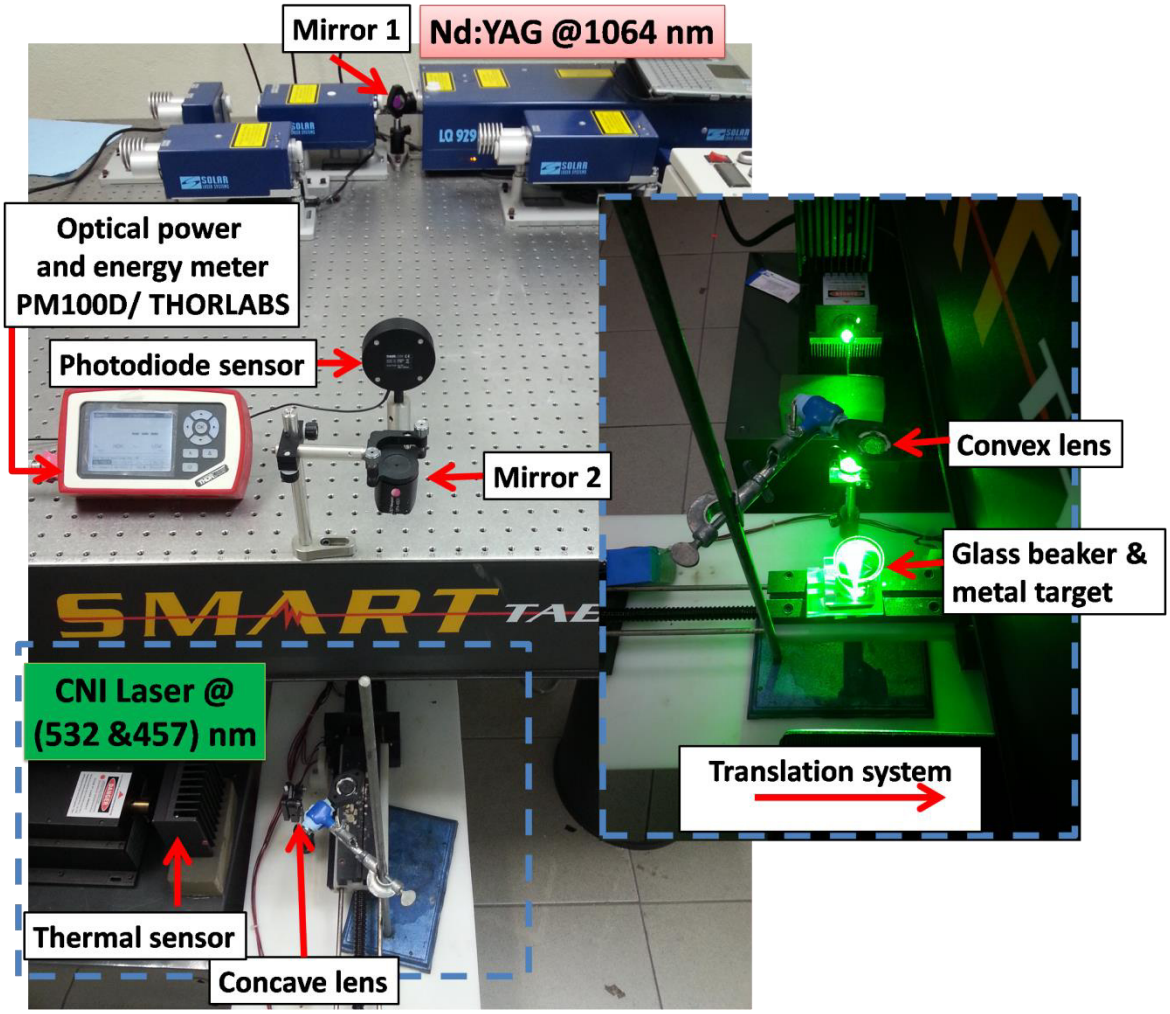

Figure 15. Photo of the experimental set-up for PLAL using 1064 nm. The inset corresponded to a PLAL at 1064 nm experiment with in-situ CW irradiation.

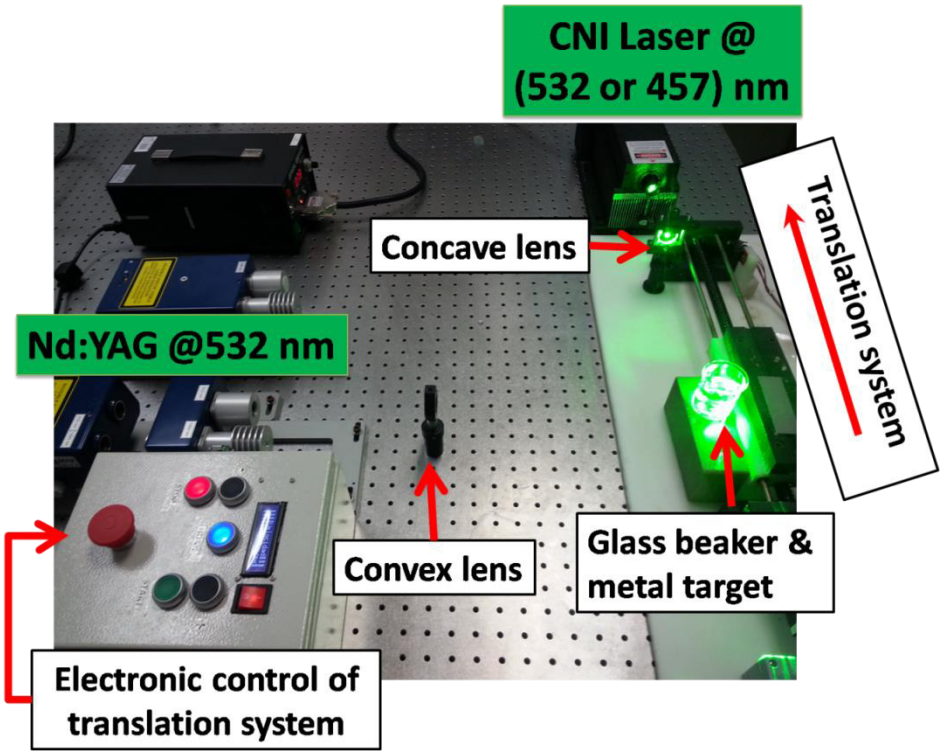

Figure 16. Photo of experimental set-up for PLAL (using 532 nm) and the five configurations (single, in-situ CW and post CW).

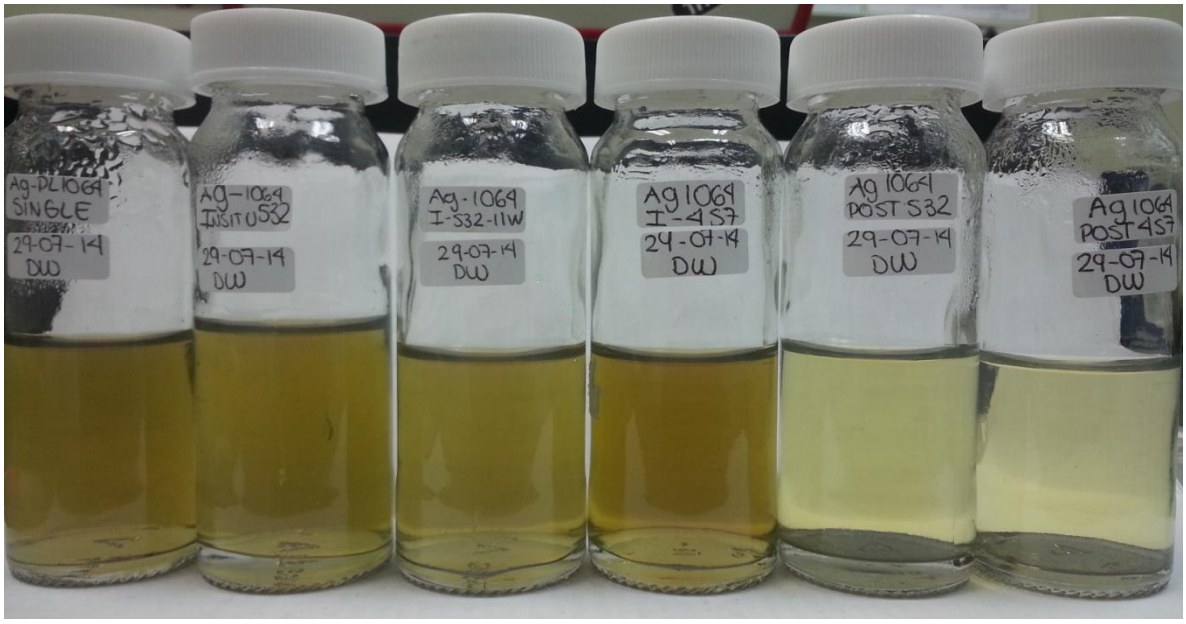

Figure 17. Photograph of silver colloids synthesized by PLAL using 1064 nm and in-situ and post- irradiation of continuous wave laser of 532 and 457 nm.

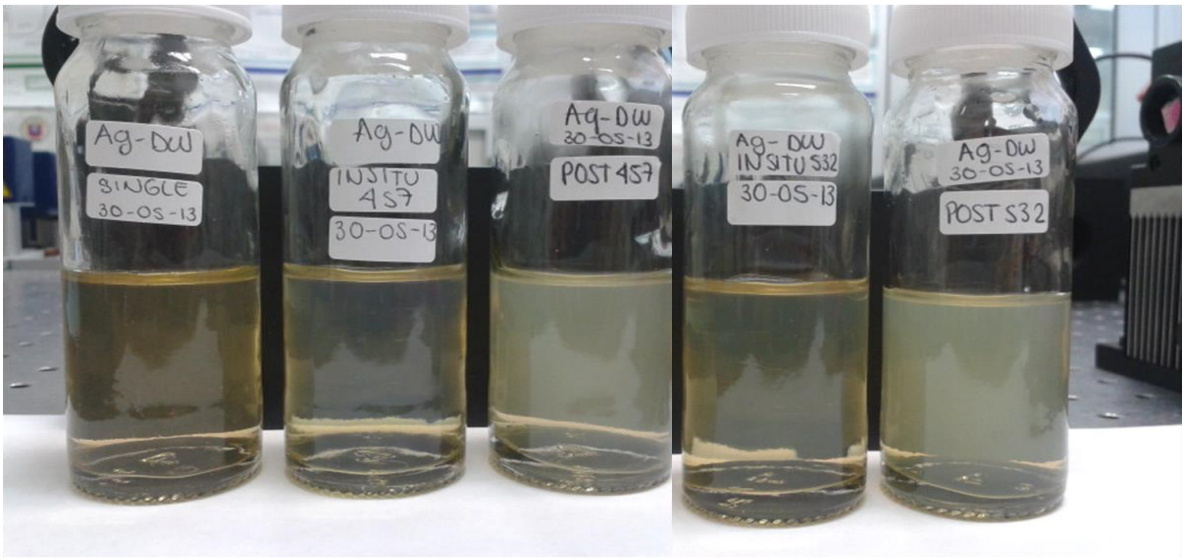

Figure 18. Photograph of silver colloids synthesized by PLAL using 532 nm and in-situ and post- irradiation of continuous wave lasers of 532 and 457 nm.

3.3. RESULTS AND DISCUSSION

Silver nanoparticles synthesized by PLAL using single 1064 and 532 nm as well as with in-situ and post-irradiation of CW lasers were characterized by TEM, EDX, XPS and UV-Vis absorption spectroscopy. Silver NPs obtained in different PLAL configurations as single, in-situ and post- irradiation of the different wavelengths were characterized by these techniques to study the effect of irradiation of continuous wave laser on their final properties. Morphology (shape, size and size distribution) was analyzed by bright field images of TEM. BF-TEM micrographs were analyzed by image processing software´s as ImageJ and Gatan Digital Micrograph. Silver nanoparticle diameters were measured directly from the BF-TEM micrographs to obtain the mean size and size distribution for each experiment. Crystalline structure of Ag NPs was analyzed by HRTEM and SAED micrographs. Elemental composition of ablated products was confirmed by EDX in TEM and XPS spectroscopy. Optical absorption properties of silver nanoparticles as their characteristic surface plasmon resonance were obtained by UV-Vis spectroscopy.

3.3.1. Morphology by TEM

Morphology of silver nanoparticle obtained in the two sets of PLAL using 1064 and 532 nm was analyzed by BF -TEM images. More than 300 NPs for each experimental condition of PLAL were measured to obtain the mean size and size distribution of silver nanoparticles. Silver nanoparticles with spherical shapes were obtained in both sets of PLAL by 1064 and 532 nm. As in the results of gold nanoparticles (chapter 2), smaller silver nanoparticles and lower ablation productivity were obtained for 532 nm of wavelength [194] in comparison to IR wavelength. Figure 19 shows shape, size and size distribution of Ag NPs obtained by the set of PLAL using 1064 nm. The mean size and size distribution of Ag NPs obtained by PLAL using 1064 nm for single-PL1064, in-situ CW532, post CW532, in-situ CW457 and post CW457 were Ø= 19±10, 15±7, 11±5, 24±9 and 8±4 nm, respectively. Smaller size and size distribution were obtained for silver nanocolloids post-irradiated with CW laser 532 and 457 nm. Meanwhile, a higher average size was obtained for in-situ CW 457 nm. Figure 20 shows shape, size and size distribution of Ag NPs obtained by the set of PLAL using 532 nm. The mean size and size distribution of Ag NPs obtained by PLAL using 532 nm for single- PL532, in-situ CW532, post CW532, in-situ CW457 and post CW457 were Ø= 5±1, 6±2, 5±2, 12±4 and 6±1 nm, respectively. In the same way, as that observed for the set of PLAL using 1064 nm, the higher average size was obtained for in-situ CW 457 nm. Figure 21 shows the crystalline structure of silver nanoparticles obtained by the set of PLAL using 1064 nm. In SAED of single-PL1064 and in-situ CW (532 and 457 nm) irradiation, the planes of FCC structure (111), (200), (220), (311) and (420) were indexed. The interplanar distances measured in HRTEM micrographs for in-situ CW (532 and 457 nm) were 2.3 and 2.5 Å, which corresponds to (111) plane of FCC and (100) plane of hexagonal crystalline structures, respectively. FCC and hexagonal structure were indexed with PDF No. 04-0783 and 87-0598, respectively. For silver nanocolloids with post-irradiation CW532 and 457 nm, SAED appeared without well-defined rings, probably due the diffraction spots corresponded to both crystalline structures (FCC and HEX). Figure 22 shows the crystalline structure of silver nanoparticles obtained by the set of PLAL using 532 nm. For single-PL532 the diffraction spots of SAED match with that of (111), (220), (311) and (331)

planes of FCC structure and the interplanar distance of 2.35 Å of HRTEM image to (111) plane of the same structure. For Ag NPs with in-situ and post-irradiation CW532 nm SAED micrographs presented both FCC and HEX structures. For FCC structure, the planes (200) and (420) were indexed of SAED (in-situ CW532 and post CW532, respectively). For hexagonal structure of silver NPs a higher number of planes (101), (102), (103), (105), (202) and (114) were indexed for the same conditions. SAED micrographs of Ag NPs with in-situ and post-irradiation CW457 nm were indexed as FCC and HEX structures, respectively. SAED and HRTEM micrographs of FCC and hexagonal crystalline structures were indexed with PDF No. 04-0783 and 87-0598, respectively. Crystalline structure of silver nanoparticles was affected by in-situ and post CW (532 and 457 nm) in both sets (1064 and 532 nm) of PLAL. In single PL (for each set), the crystalline structure was FCC meanwhile a combination between FCC and hexagonal was obtained for other conditions.

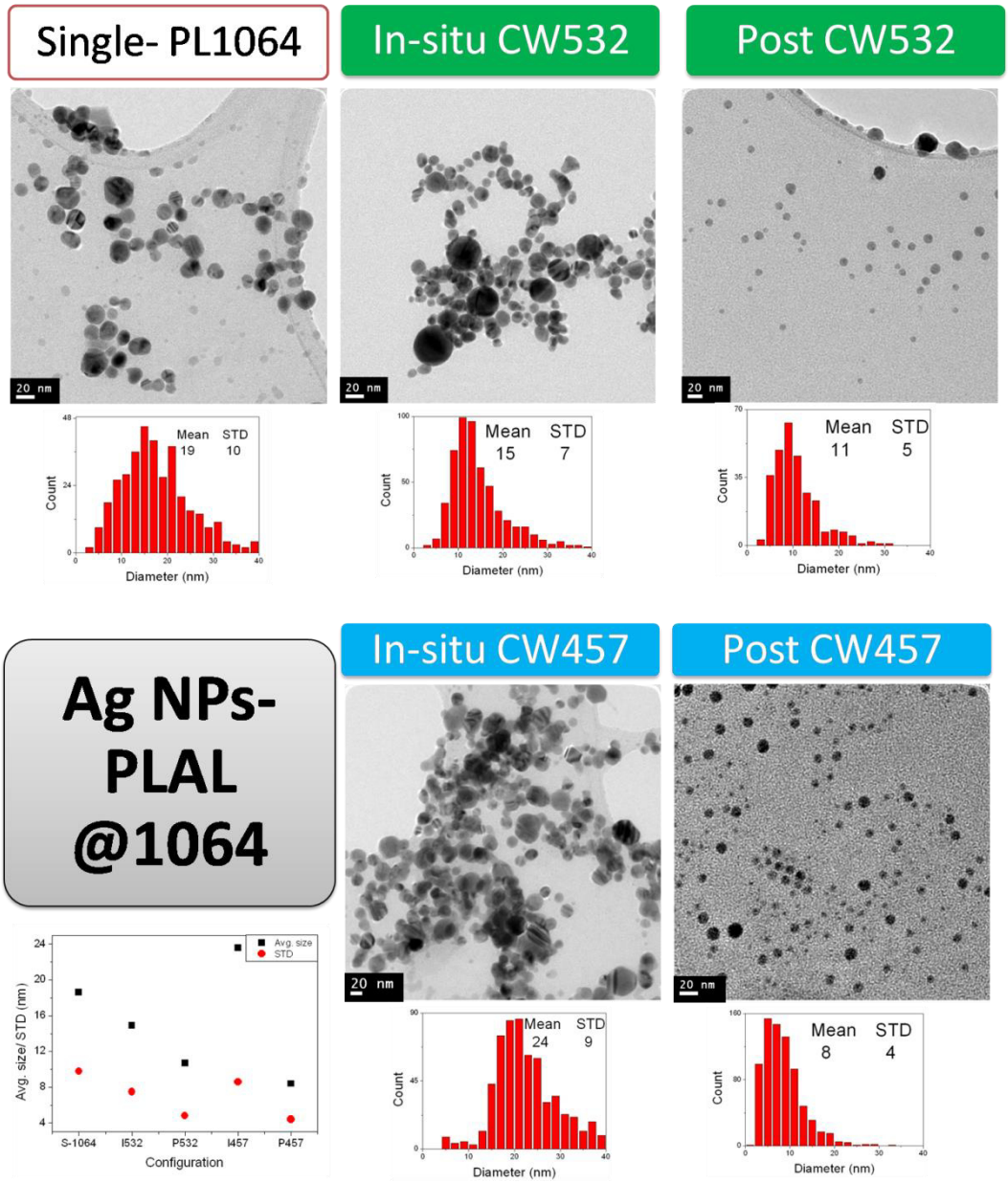

Figure 19. TEM micrographs and size distribution of silver nanoparticles synthesized by PLAL using 1064 nm and the in-situ and post-irradiation of the continuous wave lasers of 532 and 457 nm.

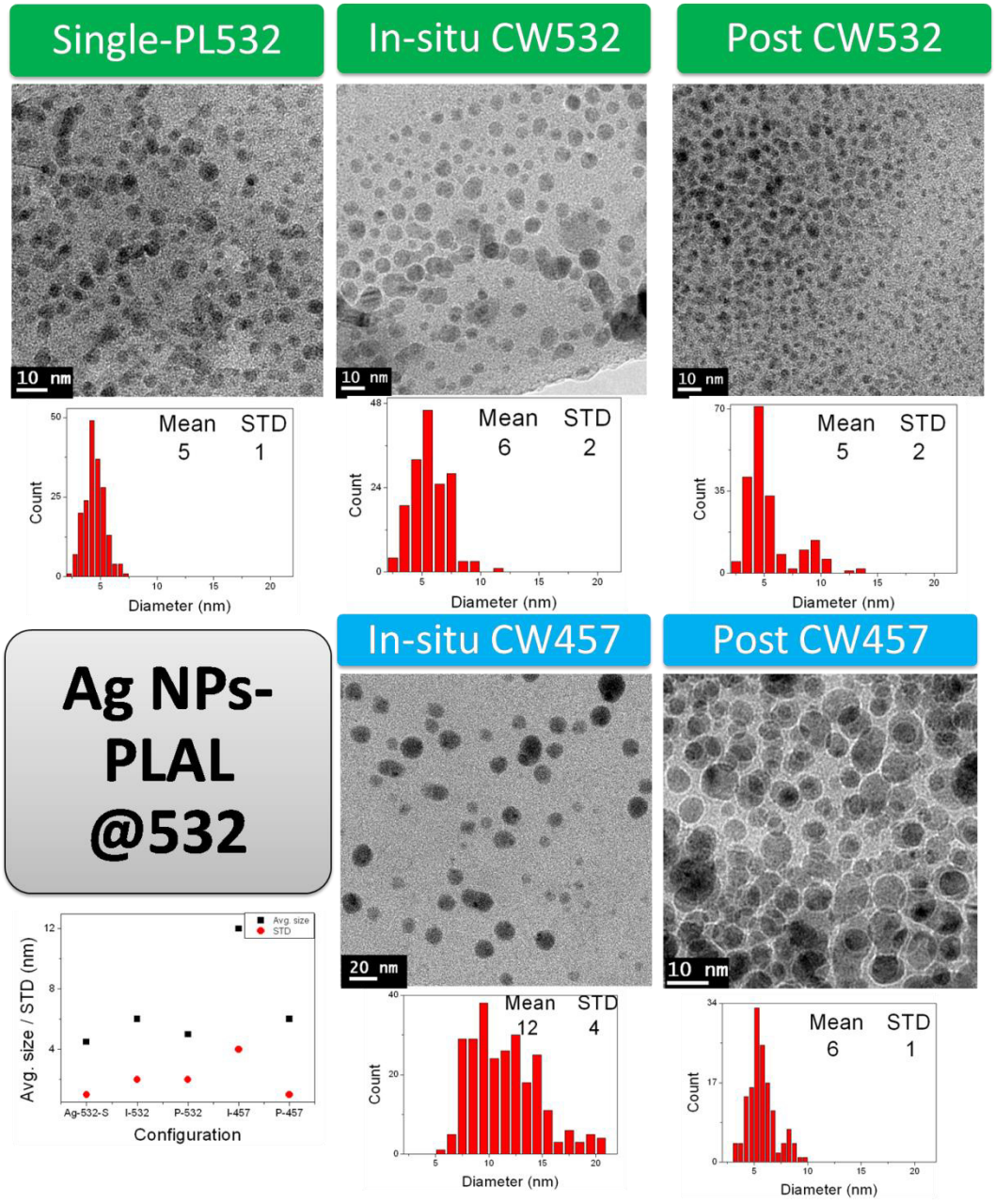

Figure 20. TEM micrographs and size distribution of silver nanoparticles synthesized by PLAL using 532 nm and the in-situ and post-irradiation of the continuous wave lasers of 532 and 457 nm.

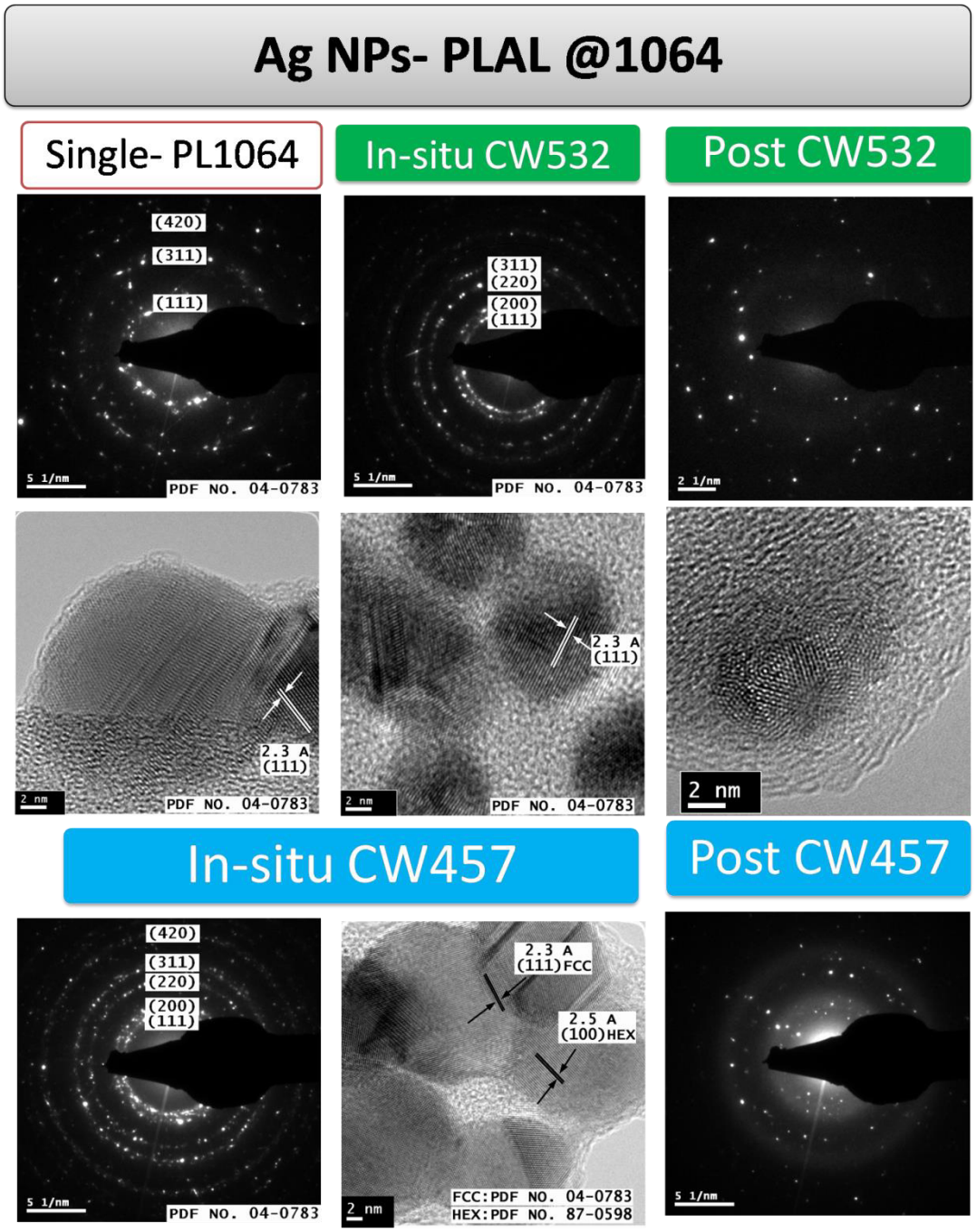

Figure 21. Electron diffraction and high resolution TEM micrographs of silver nanoparticles synthesized by PLAL using 1064 nm and the in-situ and post-irradiation of the continuous wave lasers of 532 and 457 nm.

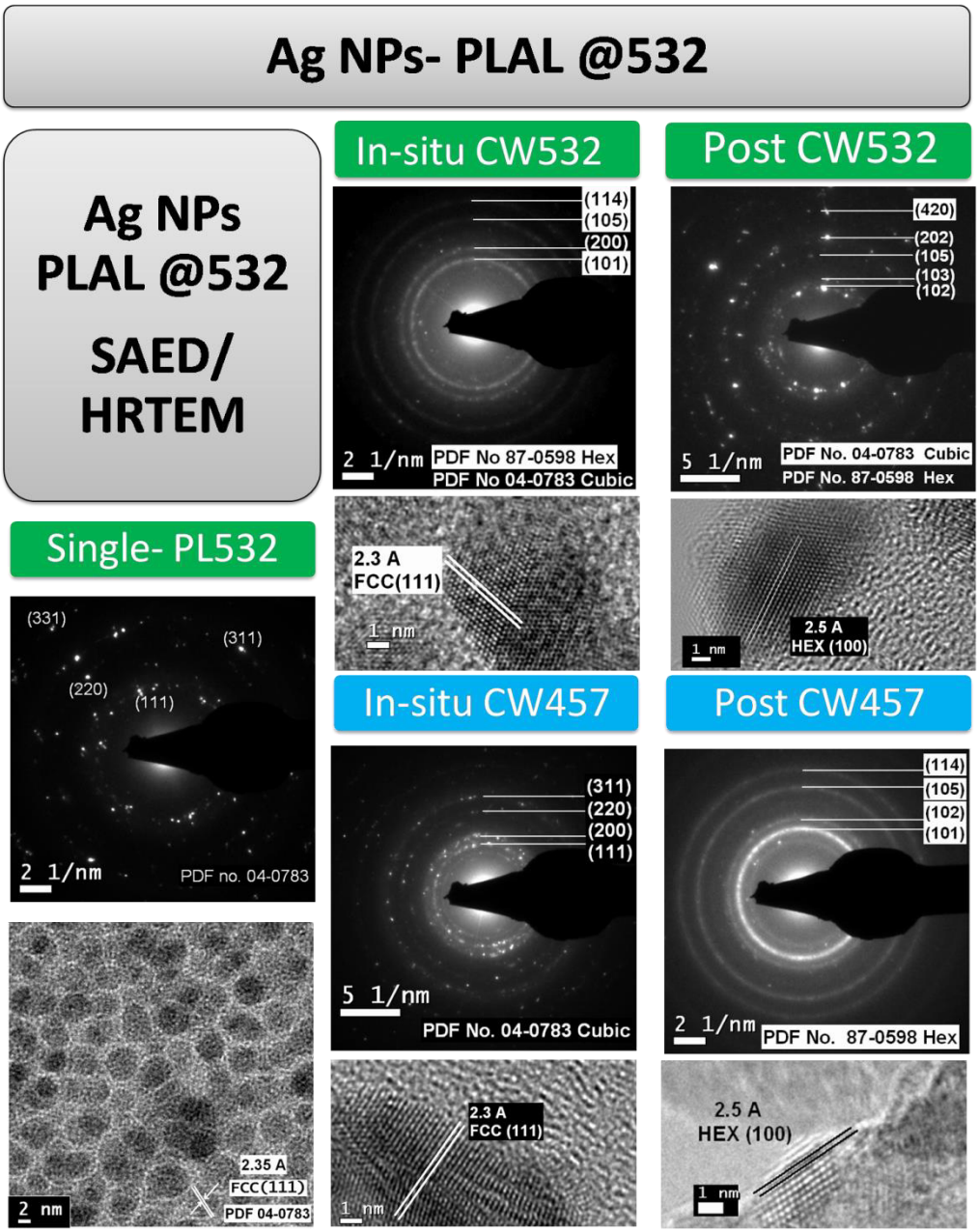

Figure 22. Electron diffraction and high resolution TEM micrographs of silver nanoparticles synthesized by PLAL using 532 nm and the in-situ and post-irradiation of the continuous wave lasers of 532 and 457 nm.

3.3.2. Elemental Composition by XPS and EDX

EDX and XPS measurements were performed to analyze the elemental composition of silver nanoparticles obtained by PLAL at different irradiation configurations. For XPS analysis some drops of silver nanocolloidal solution of the different PLAL experiments were used. EDX analysis was performed with Ag NPs on Cu grid in STEM mode of TEM. Figure 23 shows the high resolution photoelectron spectrum of Ag 3d for silver nanoparticles obtained by PLAL using 532 nm in DW. The Ag $3d_{5/2}$ and $3d_{3/2}$doublet at 368.3 and 374.3 eV, respectively corresponds to metallic state of silver nanoparticles. Figures 24 and 25 show EDX spectra and STEM images of silver nanoparticles obtained by PLAL using 532 nm with in-situ CW457 and post CW 457, respectively. In both spectra the presence of silver was predominant which confirmed the composition of silver nanoparticles.

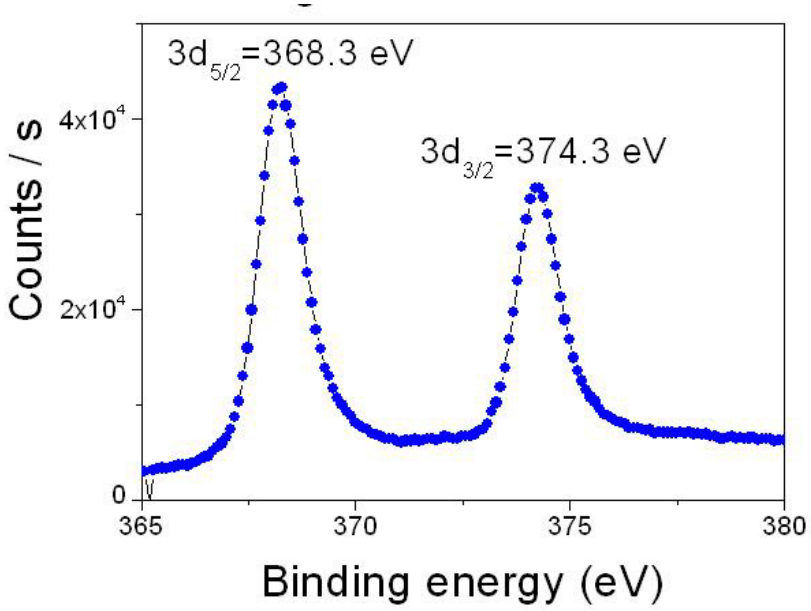

Figure 23. High resolution Ag 3d XPS spectrum of silver nanoparticles obtained by PLAL using 532 nm in distilled water.

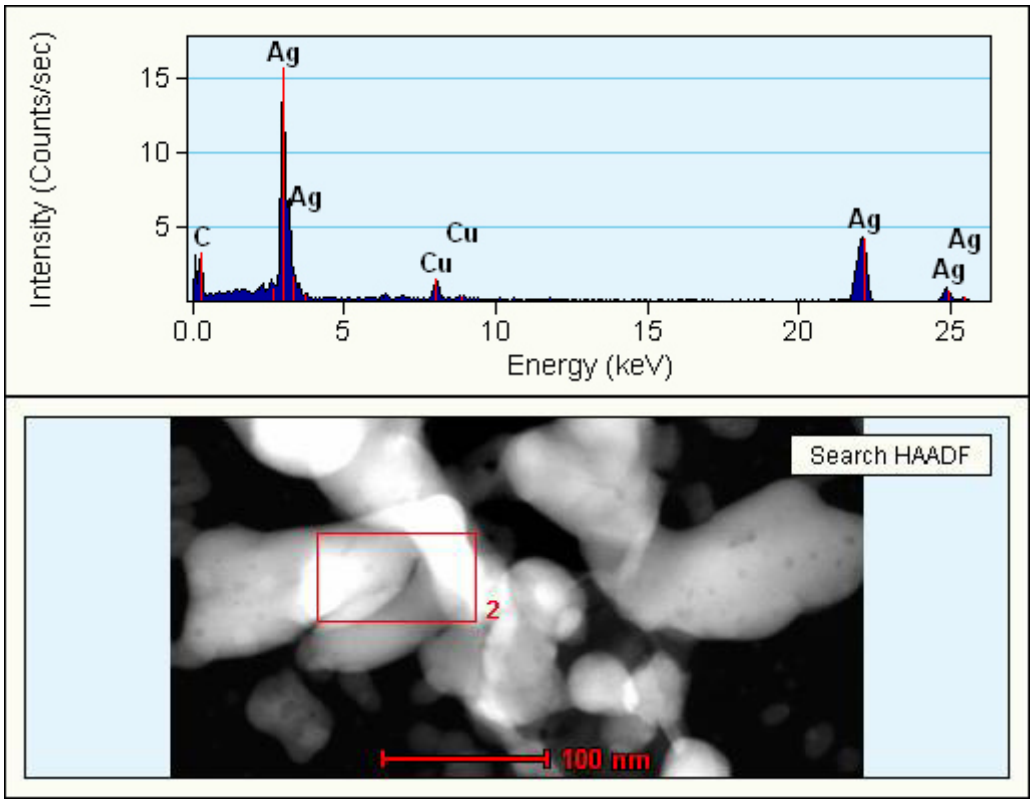

Figure 24. . EDX spectrum of silver nanoparticles obtained by PLAL using 532 nm and in-situ CW457.

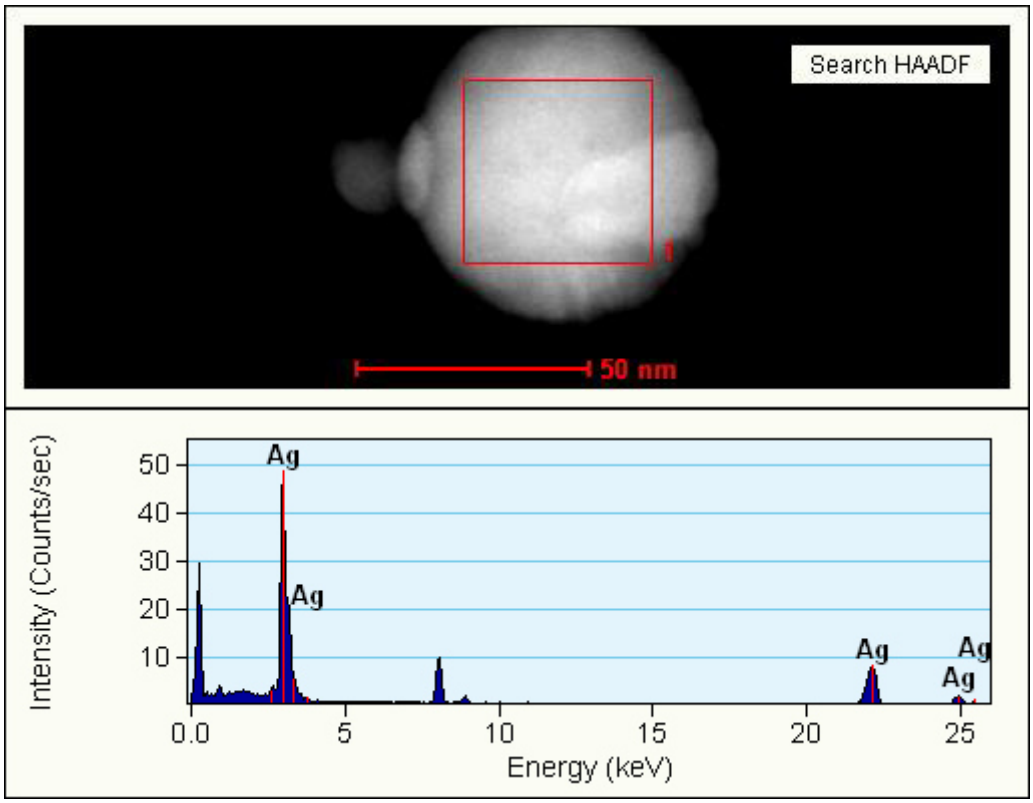

Figure 25. EDX spectrum of a single silver nanoparticle obtained by PLAL using 532 nm and post CW457.

3.3.3. Optical Properties by UV-Vis

Optical properties of silver nanocolloids were studied by UV-Vis absorption spectroscopy. Silver NPs in colloidal solution were measured immediately after its synthesis by PLAL. Figure 26 shows the absorption spectra for the set of colloidal solutions obtained by PLAL using 1064 nm at single-PL, in-situ CW (532 and 457) and post CW (532 and 457) irradiation conditions. The plasmon peak for single PL1064 and in-situ CW532 was detected at 396 and 395 nm, respectively. Meanwhile, for the other conditions (in-situ CW 457 and post CW at two wavelengths) the plasmon peak appeared at 394 nm. This little blue shift in the plasmon peak for post CW could be in accordance with the decrease on average size of those samples, as mentioned in discussion of BF-TEM micrographs (figure 19). In the same way as reported in [194], a higher production of Ag NPs was observed with 1064 nm of wavelength (with respect to 532), which was related to

the higher absorption intensity in the UV-Vis spectra. Figure 27 shows UV-Vis spectra for the set of colloidal solution of silver nanoparticles obtained by PLAL using 532 nm at single-PL532, in-situ CW (532 and 457) and post CW (532 and 457) irradiation. For single-PL and in-situ CW (532 and 457) the plasmon peak appeared at 398 nm, whereas, for post CW (532 and 457) the plasmon peak appeared at 402 and 400 nm, respectively. For both sets of PLAL (1064 and 532) higher absorption intensity was obtained for in-situ and post irradiation of CW lasers in comparison with single PL. The UV-Vis absorption spectrum in figure 28 corresponds to Ag NPs after 13 days of its synthesis by the set of PLAL using 532 nm. Spectra of silver nanocolloids with post-irradiation at both CW wavelengths appeared more broadened with respect to those with in-situ CW irradiation. In general, samples retained their optical properties and stability, similar to the as-prepared Ag nanocolloids.

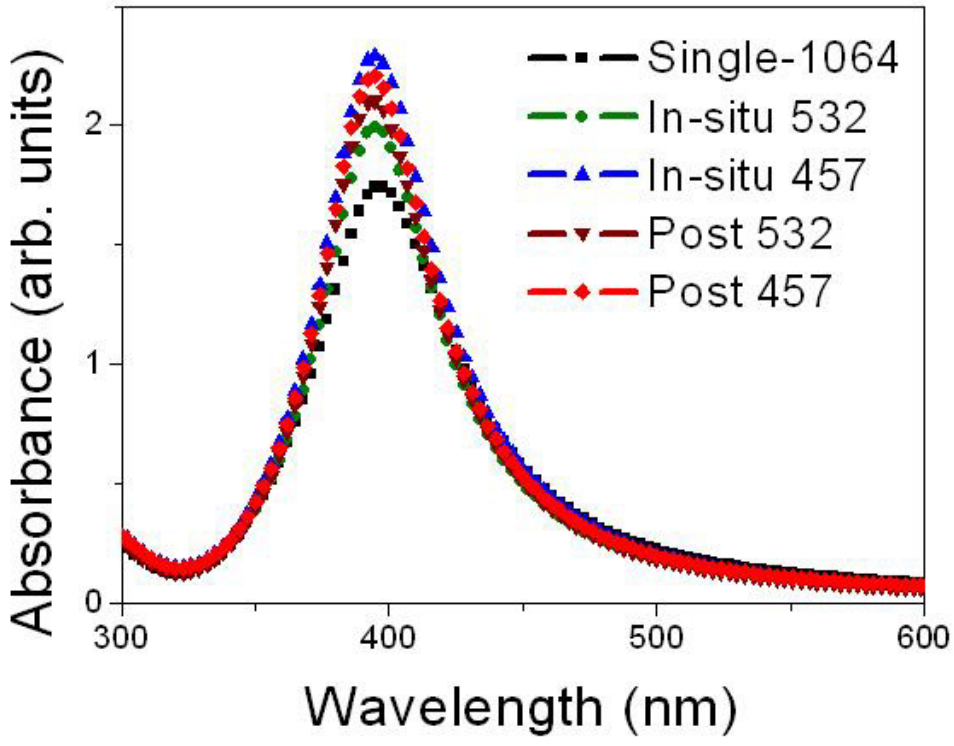

Figure 26. UV-Vis absorption spectra of silver nanoparticles obtained by PLAL using 1064 nm with single-PL532, in-situ and post-irradiation of the CW lasers of 532 and 457 nm.

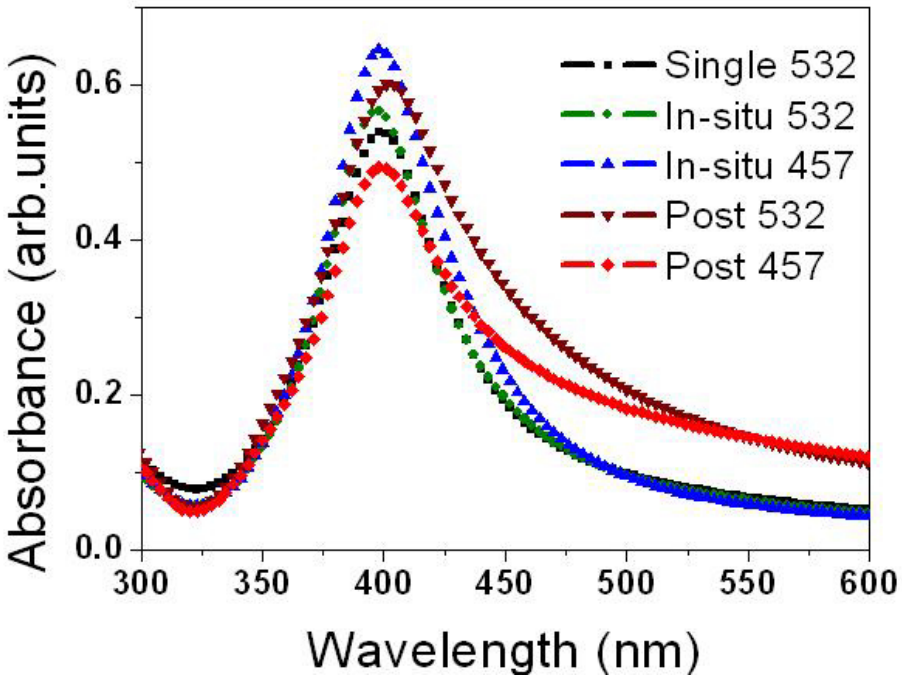

Figure 27. UV-Vis absorption spectra of silver nanoparticles obtained by PLAL using 532 nm with single-PL532, in-situ and post-irradiation of the CW lasers of 532 and 457 nm.

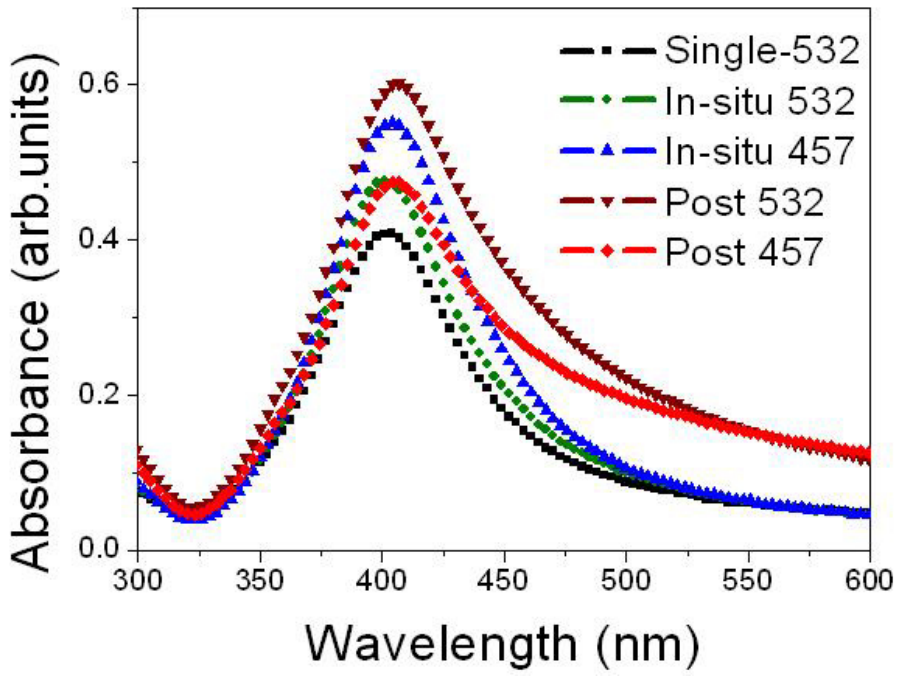

Figure 28. UV-Vis absorption spectra of silver nanoparticles obtained by PLAL using 532 nm with single-PL532, in-situ and post-irradiation of the CW lasers of 532 and 457 nm after 13 days.

In this chapter, silver nanoparticles were synthesized by PLAL in distilled water with two different wavelengths (1064 and 532 nm). And In-situ irradiation/ post-irradiation of continuous wave laser was performed at each selected wavelength to study its effect over the final properties of gold nanoparticles. The conclusions were the following: i) The production and average size of silver nanoparticles was higher for infrared wavelength (1064 nm) than the visible wavelength (532 nm) as the reported in literature [194]; ii) Spherical silver nanoparticles were observed in the two sets of PLAL at 1064 and 532 nm by BF -TEM images; iii) There is an effect of in-situ and post-irradiation of CW laser over the final size and crystalline structure of silver NPs produced by PLAL; iv) Elemental composition of silver nanoparticles was confirmed by EDX and XPS; and finally v) In-situ and post-irradiation of CW lasers showed an effect over the optical properties and the SPR peak position, ablation productivity and stability of silver nanocolloids as a function of the selected wavelength.

CHAPTER 4

SYNTHESIS AND CHARACTERIZATION OF PALLADIUM NANOPARTICLES BY PLAL

4.1. INTRODUCTION

Palladium (Pd) is a material well studied principally in the field of catalysis. There are different techniques reported for the synthesis of Pd nanoparticles. This chapter presents the synthesis of Pd nanoparticles by PLAL in different liquid media as water, methanol-water mixture (1:1), SDS and ethylene glycol. The synthesis was performed at a selected wavelength output of 1064 nm (fundamental) of a Nd:YAG pulsed laser at different energy fluence. Further, studies on effects of post-irradiation and ultrasonic treatment of the colloidal solution after their precipitation were performed. Pd nanoparticles obtained were characterized for their morphology, size, elemental composition, chemical state and optical properties by TEM, EDX, XPS and UV-Visible absorption spectroscopy techniques.

4.2. EXPERIMENTAL

Pulsed laser ablation experiments to synthesize Pd nanoparticles were performed using a q-switched pulsed Nd:YAG laser (Solar Laser System LQ929A) with output energy of 600 mJ/pulse at 1064 nm of wavelength. The pulse width and repetition rate for this laser were 10 ns and 10 Hz, respectively. For the selected wavelength (1064 nm), we used a vertical configuration for PLAL experiments. In the experiment, we employed two mirrors for aligning the laser beam with experimental setup and one convex lens of 200 mm of focal length for focusing the laser output on the target. One mirror was 99% reflective for the selected wavelength (1064 nm) and the second one was not a special mirror for this wavelength. As a consequence, the output energy of the laser beam was 600 and 280 mJ/pulse for the first and the second mirror, respectively. Then, the energy fluence was calculated for the output energy of 280 mJ/pulse. The energy fluence was varied by adjusting the distance between the surface of the target and the convex lens. The energy fluence calculated for the different distance from lens to target (DLTT) surface were 40.5,

26.5, 18, 12.5 and 8 J/cm^2 for 20, 19, 18, 17 and 16 cm, respectively. Figure 29 shows the schematic of PLAL experimental setup for the synthesis of Pd nanoparticles.

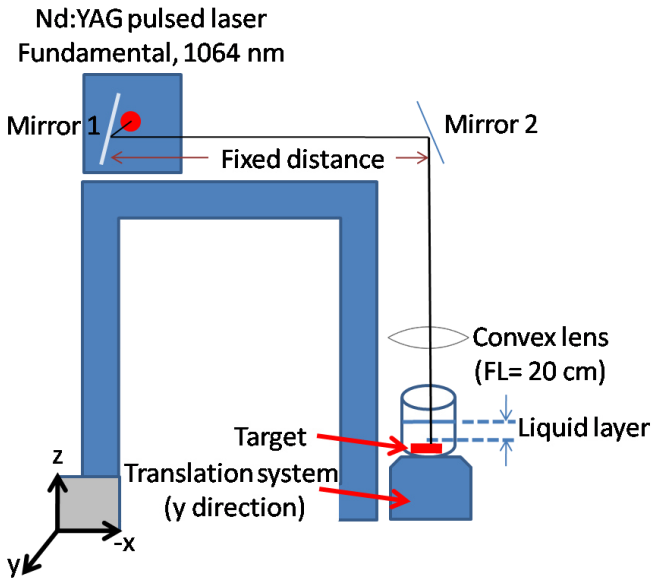

Figure 29. Schematic of vertical configuration of PLAL used to synthesize Pd NPs in different liquid media and energy fluence.

The metal target used was a pure Pd plate of 99.9% purity which was placed at bottom of a glass beaker of 50 ml volume. To improve the ablation productivity, the glass beaker was attached to a linear translation system at a fixed velocity (50 μm/s) for all these experiments. All the experiments were carried out for ablation duration of 10 minutes. Palladium nanoparticle colloidal solutions were synthesized by pulsed laser ablation in different liquid media such as distilled water (DW), methanol-water mixture, ethylene glycol (EG) and sodium dodecyl sulphate (SDS) in aqueous solution at 0.001 M. Since, methanol is highly inflammable; methanol was mixed with DW at the ratio of 1, for ablation using the high energy of the pulsed laser beam. Figure 30 shows the images of the colloidal solutions obtained by the pulsed laser ablation of Pd metal target in all liquid media at different energy fluence.

Pd NPs	Energy Fluence (J/cm^2) 40.5 26.5 18 12.5 8
DW	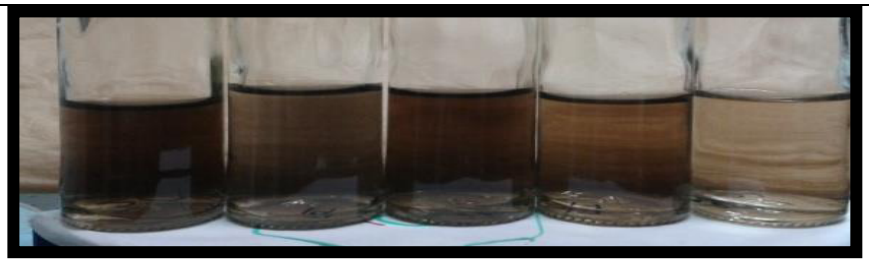
SDS 0.001 M	
Methanol/ Water	
Ethylene Glycol	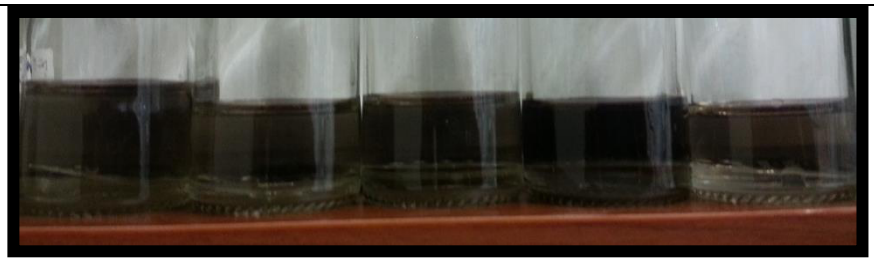

Figure 30. Photographs of colloidal solution of Pd NPs synthesized by PLAL in different liquid media at different energy fluence.

Post-irradiation treatment

The colloidal solutions of Pd NPs obtained in DW and methanol-water mixture were least stable, rapidly precipitated in approximately 15 minutes and 1 hour, respectively. For SDS and EG, the colloidal solutions were more stable for a few days. Then, after a week all the samples were completely precipitated and the aggregates were observed at the bottom of the glass container. Laser post-irradiation has been reported as a feasible

technique for the size and shape manipulation of different nanomaterials [62, 68, 197, 200, 275, 278]. In the present work, post-irradiation treatment was applied (represented in figure 31) as following: the pulsed Nd:YAG laser system at wavelength of 532 nm was used with output energy of 230 mJ/pulse for a time of 5 or 10 minutes for the selected samples. Before the post-irradiation treatment, the sample was decanted to increase the concentration of aggregates in the solution. The resulted colloidal solution was poured into a beaker of 15 ml and stirred continuously during the post-irradiation treatment. The pulsed laser beam was directed over the solution. A convex lens with a focal length of 20 cm was used to focus the pulsed laser beam over the solution, keeping the focal point out of the solution. The pulsed laser beam used to post-irradiate the colloidal solution was used unfocused (direct beam irradiation) and focused (not at focal point) to find the optimal condition of post-irradiation. For focus condition, the colloidal solution was placed at 30 and 10 cm of the convex lens with an energy fluence of ~2 J/cm^2. The focal point was kept out of the colloidal solution to avoid the effects of high energy irradiation at this point. Only the solutions obtained in DW and methanol-water mixture were post-irradiated. Table 1 shows the selected samples and experimental details of the post-irradiation treatment.

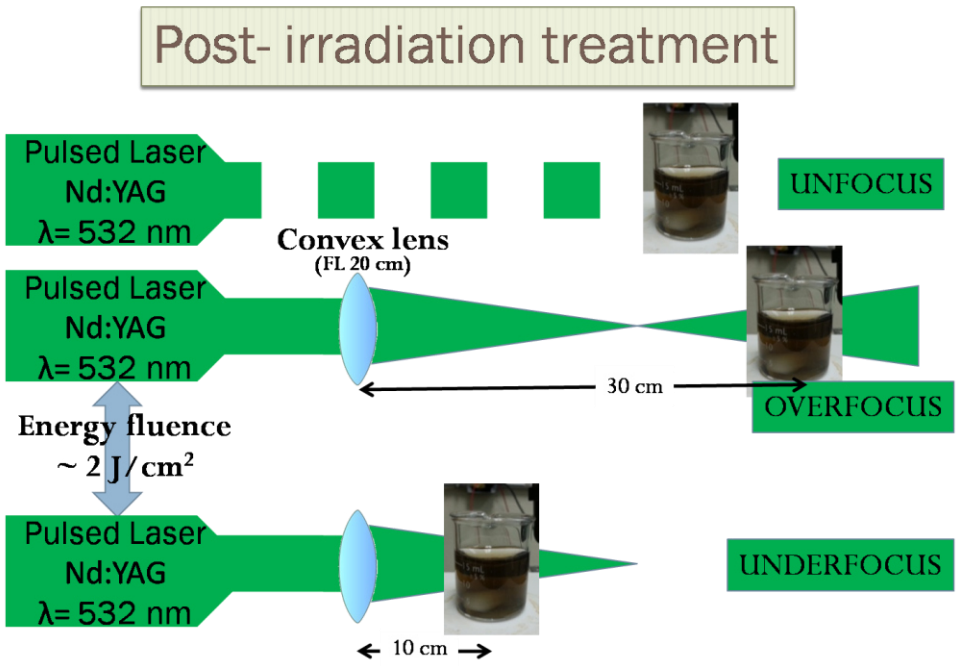

Figure 31. Schematic representation of post-irradiation treatment for Pd NPs.

Started sample/Energy fluence (J/cm^2) of PLAL	Focusing conditions for post irradiation (distance between the convex lens and the solution)	Time (min)
Pd DW (40.5)	Unfocused	5
Pd DW (26.5)	Focused (30 cm)	5
Pd methanol-water(40.5)	Unfocused	5
Pd methanol-water(26.5)	Focused (30 cm)	5
Pd methanol-water(18)	Focused (10 cm)	5
Pd methanol-water(12.5)	Unfocused	10

Table 1. Samples selected for post-irradiation treatment and their respective experimental conditions.

Ultrasonic treatment

Another simple alternative to re-disperse and recover the optical properties of Pd NPs was ultrasonic bath treatment. All the samples of Pd NPs produced by PLAL in DW, methanol-water mixture and SDS (with and without post-irradiation treatment) were taken to an ultrasonic bath treatment to explore their effect in re-dispersion and the optical properties of the ablated products. The precipitated samples were immersed in the ultrasonic bath for 10 minutes (Aquasonic Model 75T from VWR-Scientific). After the ultrasonic treatment, the samples which were precipitated changed to its characteristic brown color as obtained by the PLAL experiments. These samples were immediately characterized by UV-Visible absorption spectroscopy. Also TEM grids were prepared to study the changes in morphology after ultrasonic treatment. To characterize the morphology, size and distribution and crystalline structure, TEM grids were prepared after each experiment by placing a drop of the colloidal solution on a copper grid and dried at room temperature. TEM analysis was carried out using a FEI Titan G2 80-300 TEM and elemental analysis using an Energy Dispersive X-ray Analyzer (EDAX) associated with TEM. To obtain the elemental composition and chemical state of the ablated products, some drops were placed onto a Cu tape and dried at room temperature for XPS analysis. X-ray photoelectron spectroscopy (XPS) analysis was done using a Thermo Scientific K-

Alpha XPS instrument with monochromatized Al Kα radiation (hν=1486.68 eV). All the spectra reported were recorded with reference to adventitious carbon, C 1s peak (284.6 eV). To characterize the optical properties, the UV-Visible absorption measurements were carried out in a UV-Vis spectrometer (Shimadzu UV-1800).

4.3. RESULTS AND DISCUSSION

Colloidal solutions of Pd NPs were obtained by PLAL using 1064 nm in different liquid media and energy fluence. Post-irradiation and ultrasonic treatment was done after a few months to the precipitated samples. As-prepared nanocolloids and samples with post-irradiation and ultrasonic treatment were characterized by TEM, XPS and UV-Visible absorption spectroscopy. Morphology of Pd NPs as prepared by PLAL was analyzed for each liquid media in terms of the energy fluence used. After the characterization of the as prepared samples, the effect of post-irradiation and ultrasonic treatment on the morphology of Pd NPs was analyzed. Elemental composition of Pd NPs obtained in each liquid media was characterized by XPS and EDX. Optical properties of Pd NPs obtained by PLAL, with post-irradiation and ultrasonic treatment were analyzed by UV-Visible absorption spectroscopy and correlated with the morphology characterization by TEM.

4.3.1. Morphology and Crystalline Structure by TEM

Pd nanoparticles were synthesized by PLAL using 1064 nm in four different liquid media (as distilled water, methanol-water mixture, 0.001 M of aqueous solution of SDS and ethylene glycol) with different energy fluence for each liquid media (40.5 to 8 J/cm^2). The morphology (shape, size and size distribution) was analyzed by bright field images of TEM. BF-TEM micrographs were analyzed by image processing softwares such as ImageJ and Gatan Digital Micrograph. Pd nanoparticle diameters were measured directly from the TEM micrographs to obtain the mean size and size distribution for each experiment. The crystalline structure of Pd NPs was analyzed by both HRTEM and SAED micrographs. The interplanar distances were measured from HRTEM image and SAED pattern and indexed with their corresponding PDF data. In STEM mode of TEM, an elemental analysis of Pd NPs for each liquid media was done to confirm the elemental composition of the ablation products.

4.3.1.1. Pd Nanoparticles: as Prepared

Pd NPs were obtained by PLAL using 1064 nm in distilled water (DW), methanol-water mixture (1:1), aqueous solution of SDS at 0.001 M and ethylene glycol (EG). The effects of energy fluence on the morphology of Pd NPs for each liquid media were studied by TEM micrographs. Immediately after PLAL experiments, TEM grids were prepared to characterize the morphology and crystalline structure of Pd NPs by BF-TEM, HRTEM and SAED micrographs.

4.3.1.1.1. Pd Nanoparticles in Distilled Water

Figure 32 shows the morphology of Pd nanoparticles obtained by PLAL using 1064 nm in distilled water. The BF-TEM micrographs (left column) and the corresponding size distribution graphs (right column) corresponds to the different energy fluence (J/cm^2) (a, b) 40.5, (c, d) 26.5, (e, f) 18, (g, h) 12.5 and (i, j) 8 J/cm^2. The morphology of the Pd NPs obtained in distilled water was predominantly spherical and well dispersed. The average size shows an increase from 17 nm to 27 nm with the decrease in energy fluence. In the same way, the size distribution calculated was a little broader for the lower energy fluence, as reported by K. A. Elsayed et al. [194] where a similar range of energy fluence in DW was used.

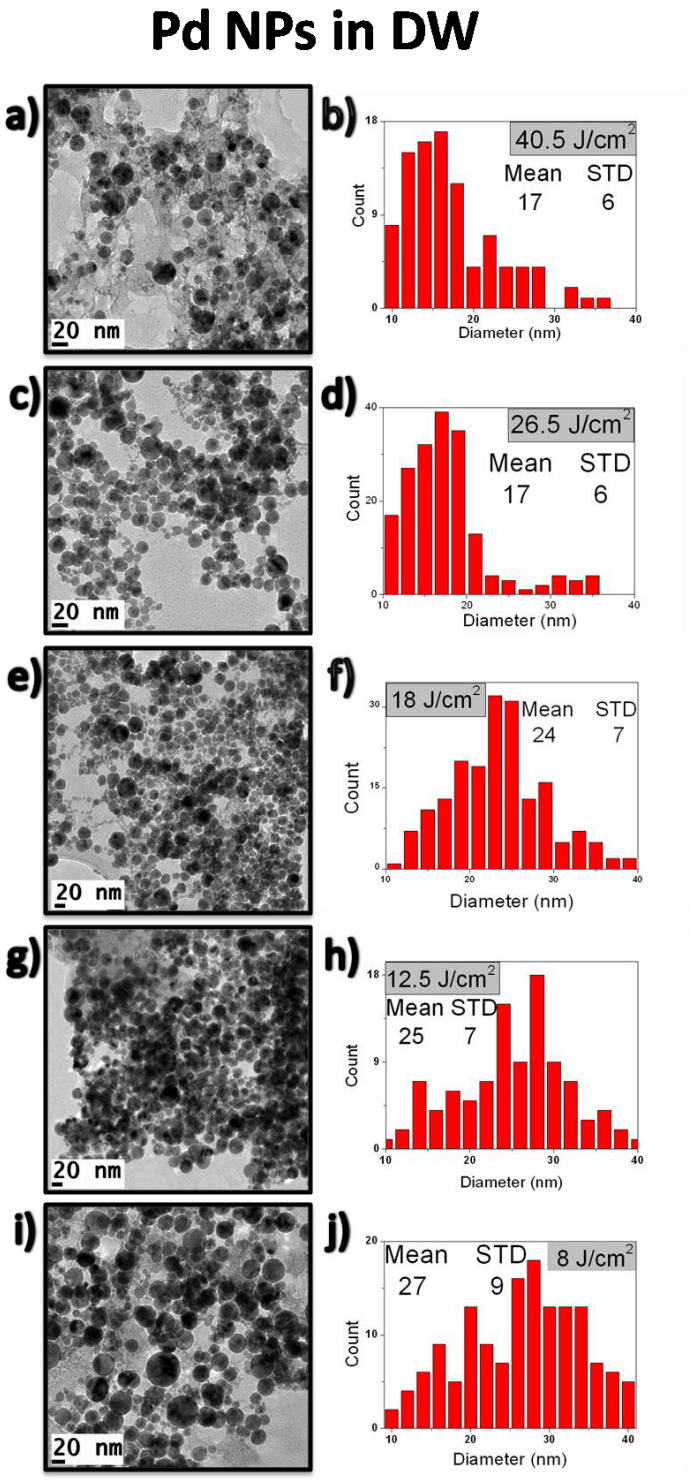

Figure 32. TEM (BF) micrographs and size distribution of Pd nanoparticles synthesized by PLAL using 1064 nm in DW at (a, b) 40.5, (c, d) 26.5, (e, f) 18,(g, h) 12.5 and (i, j) 8 J/cm^2 of energy fluence.

Figure 33 shows the resume of average size and size distribution at the different energy fluence for the Pd NPs obtained by PLAL using 1064 nm in DW. The average size and size distribution showed a decrease as the energy fluence of ablation increased.

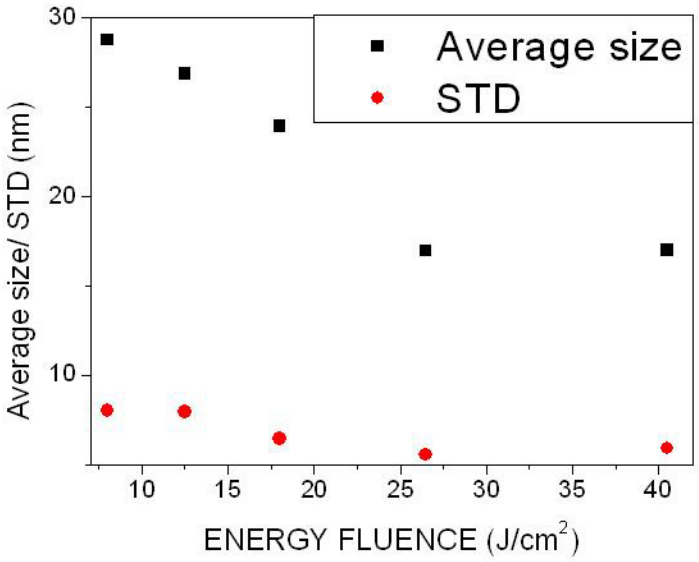

Figure 33. Graph of averages size and standards deviation of Pd NPs obtained by PLAL using 1064 nm in DW at different energy fluence.

The crystalline structure of Pd NPs analyzed by HRTEM and SAED was cubic for all the samples obtained in DW (using 1064 nm) at different energy fluence (figure 34). Figure 34 (a, c, e, g and i) corresponds to HRTEM micrographs of Pd NPs in DW obtained at 40.5, 26.5, 18, 12.5 and 8 J/cm^2 of energy fluence, respectively. The interplanar distances (2.26 and 2.3 Å) of HRTEM micrographs (measured in the Digital Micrograph software) were indexed as the plane (111) of FCC structure of Pd with the PDF No. 04-016-3309. In figure 34 (b, d, f, h and j) the planes in the SAED (111), (200), (220), (311), (331) and (420) were indexed with the PDF No. 03-065-6174 corresponding to cubic FCC crystalline structure of Pd. Table 2 lists the experimental measurements for the SAED obtained of Pd NPs at 18 J/cm^2.

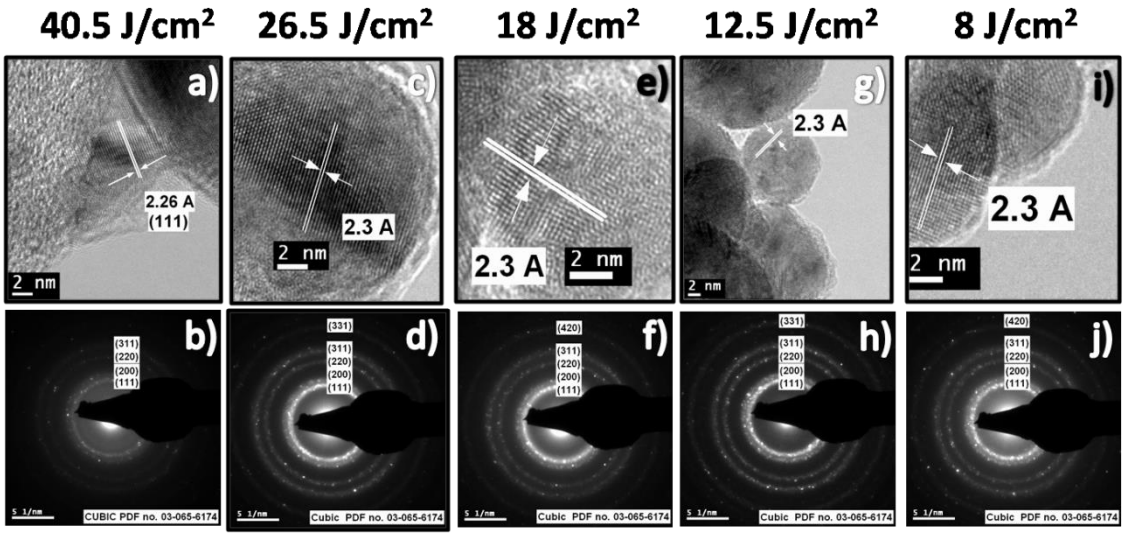

Figure 34. HRTEM and SAED micrographs for Pd NPs obtained by PLAL using 1064 nm in DW at different energy fluence.

Experimental data	CUBIC FCC PDF No. 03-065-6174	
d(Å)	d(Å)	Plane
2.26886	2.24439	(111)
1.94156	1.9437	(200)
1.36902	1.3744	(220)
1.167202	1.1721	(311)
0.877616	0.869249	(420)

Table 2. Experimental measurements of SAED for Pd NPs obtained at 18 J/cm^2 in DW and PDF No. 03-065-6174 reported data for cubic FCC Pd.

4.3.1.1.2. Pd Nanoparticles in Methanol-Water Mixture

Figure 35 shows the TEM micrographs and size distributions of Pd NPs obtained by PLAL in methanol-water mixture at (a, b) 40.5, (c, d) 18 and (e, f) 8 J/cm^2 of energy fluence. Pd NPs obtained in this mixture of methanol-water (1:1) were spherical and interconnected by chains formed by the smaller NPs. The average size and size distribution calculated for the different energy fluence were 12-14 nm and 4-5 nm respectively. The average size and size distribution of Pd NPs maintained very similar for all the range of energy fluence. In this case, there was no effect of energy fluence in the final size of nanoparticles, as reported by G. Cristoforetti et al. [279] for Pd NPs in alcohols (ethanol and 2-propanol). The crystalline structure analyzed by SAED in TEM for the sample obtained at 8 J/cm^2 is a representative for the other energy fluence. Figure 36 a) shows the SAED micrograph corresponded to Pd NPs obtained by PLAL in methanol-water mixture using 8 J/cm^2. The table in figure 36b presents the interplanar distances calculated from SAED micrograph and the reported data of the PDF No. 03-065-6174 which matches FCC structure of Pd. The planes indexed in the SAED micrograph are (111), (200), (220) and (311).

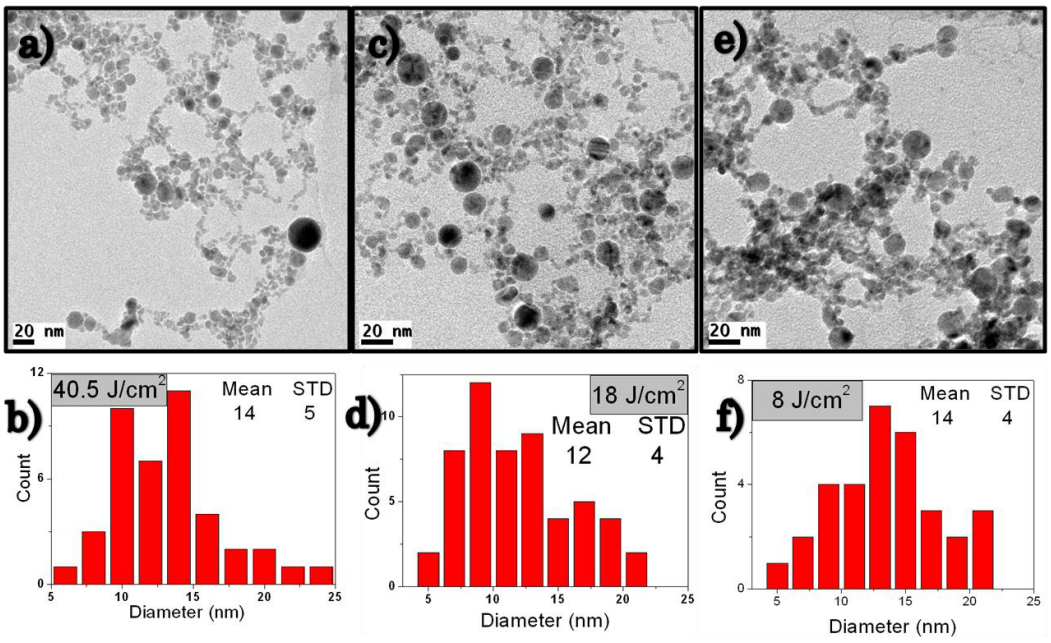

Figure 35. TEM images and size distribution of Pd NPs synthesized by PLAL using 1064 nm in methanol-water mixture at (a, b) 40.5, (c, d) 18 and (e, f) 8 J/cm^2 of energy fluence.

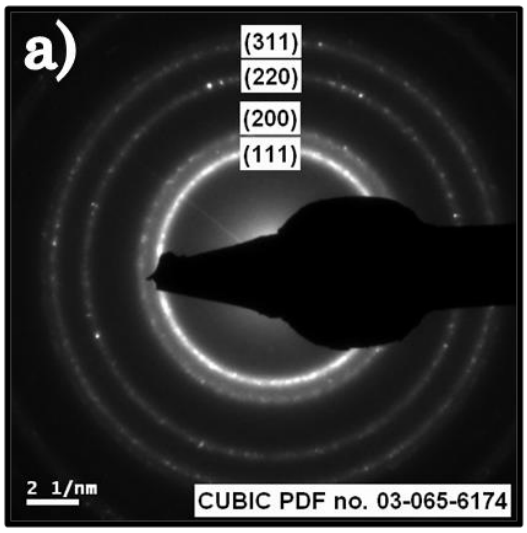

b)

Interplanar distance	Cubic FCC 03-065-6174	
d(Å)	d(Å)	Plane
2.2277	2.2458	(111)
1.9370	1.9451	(200)
1.3779	1.3753	(220)
1.1828	1.1729	(311)

Figure 36. a) SAED of Pd NPs obtained in diluted methanol by PLAL; b) Table with the cubic FCC structure was indexed with the PDF No. 03-065-6174

4.3.1.1.3. Pd Nanoparticles in SDS

Figure 37 shows the TEM micrographs and size distributions of Pd NPs obtained by PLAL in the 0.001 M aqueous solution of SDS at (a, b) 40.5, (c, d) 18 and (e, f) 8 J/cm^2 of energy fluence. The morphology of Pd NPs obtained in the SDS surfactant solution was spherical and well dispersed. The average size calculated was Ø= 33±10, 28±13 and 21±9 nm for Pd NPs obtained in the surfactant at 40.5, 18 and 8 J/cm^2 of energy fluence, respectively. The lowest average size and size distribution were for the low energy fluence, opposite to the case of Pd NPs produced in DW. This effect was reported by F. Mafune et al. [80] also in SDS surfactant. Figure 38a) shows the HRTEM micrograph of Pd NPs obtained by PLAL at 40.5 J/cm^2 of energy fluence in SDS. The interplanar distance of 2.26 Å corresponded to (111) plane of FCC structure of Pd NPs. Figure 38b) shows the SAED micrograph of Pd NPs formed by 18 J/cm^2 of energy fluence in the surfactant. The rings observed in the SAED corresponded to FCC structure of Pd. The HRTEM and the SAED were indexed with the PDF No. 03-065-6174.

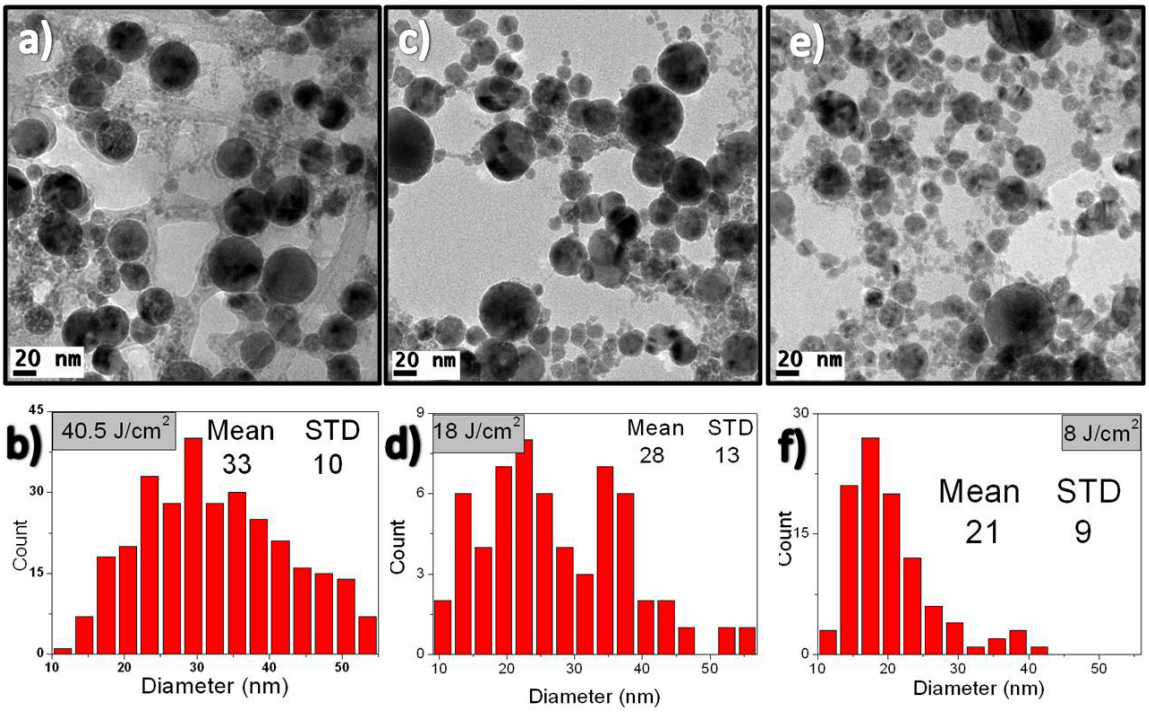

Figure 37. TEM images and size distribution of Pd NP synthesized by PLAL using 1064 nm in SDS at (a, b) 40.5, (c, d) 18 and (e, f) 8 J/cm^2 of energy fluence.

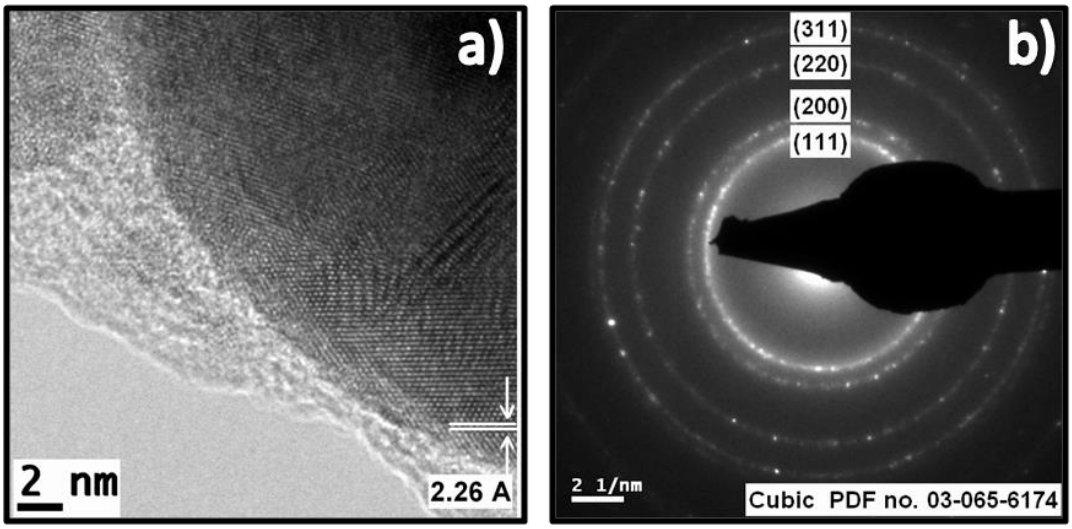

Figure 38. a) HRTEM image of a single Pd NPs and b) SAED of Pd NPs obtained by PLAL in aqueous solution of SDS

4.3.1.1.4. Pd Nanoparticles in Ethylene Glycol

Pd nanoparticles were synthesized by PLAL in ethylene glycol at different energy fluence (40.5 – 8 J/cm^2). Figure 39 (a, c, e, g and i) shows the morphology of Pd NPs at the different energy fluence in the BF mode of TEM. In these micrographs, Pd NPs were not well distinguished because they were embedded in EG. Therefore, STEM images with the mode of high angular annular dark field (HAADF) were collected. Figure 39 (b, d, f, h and j) shows the STEM micrographs of Pd NPs in EG at the same energy fluence of the BF images. The Pd NPs in the BF and STEM images were spherical and completely embedded in EG and well separated. Figure 40 shows the crystalline structure of Pd NPs obtained by PLAL in EG at: a) 40.5, b) 26.5, c) 18, d) 12.5 and e) 8 J/cm^2 of energy fluence. Figure 40 (a, b and d) shows the HRTEM micrographs of Pd NPs. In HRTEM (figure 40b) Pd NPs were found in the range of 2-8 nm of diameter. The interplanar distance measured in figure 40d) was 2.27 Å that corresponds to the plane (111) of the Pd FCC structure. Figure 40 (c and e) shows the electron diffraction of Pd NPs obtained by PLAL in EG at 18 and 8 J/cm^2 of energy fluence, respectively. A table with the experimental measurements of the SAED rings and the reported data of the PDF No. 03-065-6174 are in figure 40f). The SAED and HRTEM were indexed with the PDF No. 03-065-6174 which corresponded to the FCC structure of Pd. In our experiments, Pd NPs obtained in all types of liquid media got precipitated in a few days as reported by Cristoforetti G. et al. [243] in the case of Pd NPs by PLAL in DW and SDS. They reported stable colloidal solution of Pd NPs in organic solvents [279] (acetone, ethanol, toluene and n-hexane) probably due to the formation of amorphous carbon on the nanoparticle surface.

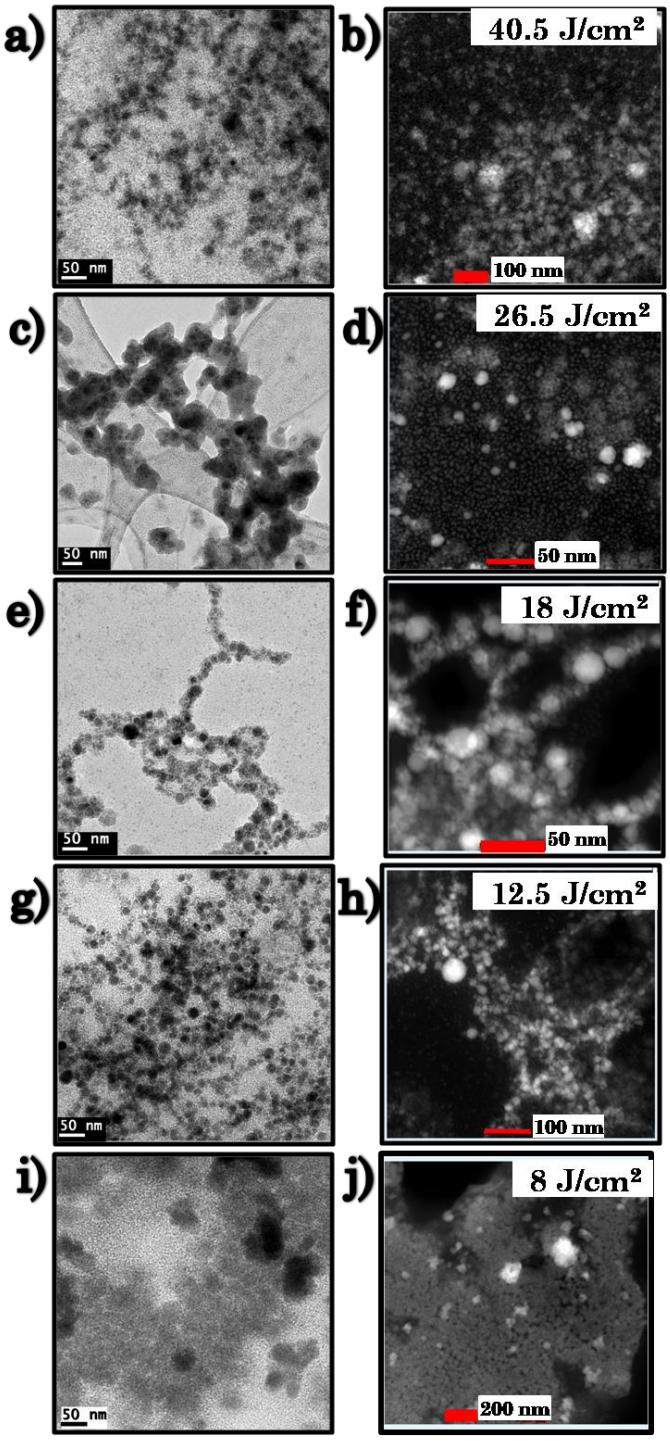

Figure 39. Bright Field TEM (left column) and STEM (right column) micrographs of Pd NPs obtained by PLAL in Ethylene glycol at (a, b) 40.5, (c, d) 26.5, (e, f) 18, (g, h) 12.5 and (i, j) 8 J/cm^2 of energy fluence.

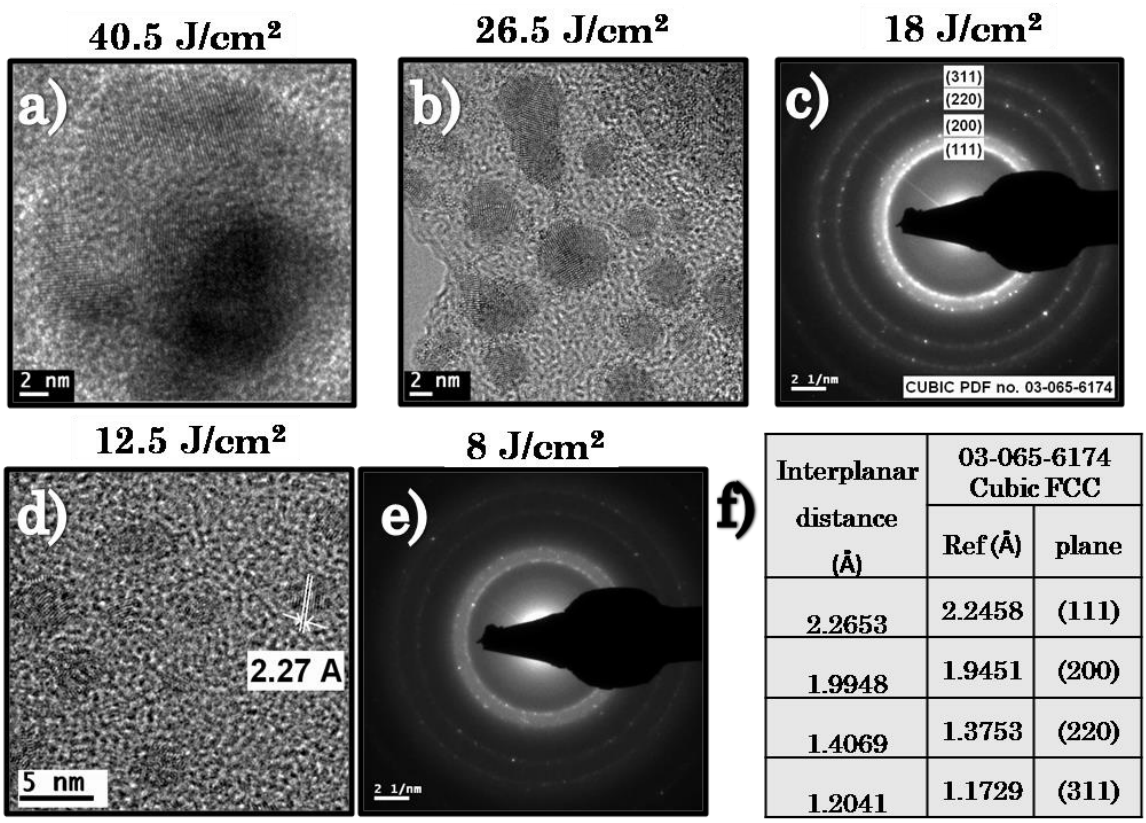

Interplanar distance (Å)	03-065-6174 Cubic FCC	
	Ref (Å)	plane
2.2653	2.2458	(111)
1.9948	1.9451	(200)
1.4069	1.3753	(220)
1.2041	1.1729	(311)

Figure 40. (a, b and d) HRTEM and (c, e) SAED of Pd NPs obtained by PLAL in Ethylene Glycol at 40.5, 26.5, 18, 12.5 and 8 J/cm^2 of energy fluence as mentioned.

4.3.1.2. Pd Nanoparticles with Post-Irradiation and Ultrasonic Treatment

4.3.1.2.1. Pd NPs in Distilled Water

The effect of post-irradiation of pulsed laser in the morphology of Pd NPs was studied in this work. Aggregates of Pd NPs obtained initially by PLAL in DW were post-irradiated with 532 nm output (second harmonic) of the Nd:YAG laser. The pulsed laser beam was used for irradiation as focused and unfocused (direct) over the solution of aggregates which were under continuous agitation. Figure 41 (a-c) shows the characterization of Pd NPs (obtained initially by PLAL at 40.5 J/cm^2) post-irradiated with unfocused (direct, 0.3 J/cm^2) pulsed laser output. The BF image in figure 41a) shows spherical Pd NPs well dispersed with a broad size distribution of Ø= 32±8 nm (figure 41b). Figure 41c) shows the SAED of Pd NPs after the post-irradiation treatment with un-focus

condition. The crystalline structure evaluated corresponded to FCC structure indexed with the PDF No. 03-065-6174. Figure 41 (d-f) shows Pd NPs (initially prepared by PLAL at 26.5 J/cm^2) post-irradiated with focused condition at energy fluence of 2 J/cm^2 (not at focal point). Figure 41d) shows spherical and well dispersed Pd NPs after the post-irradiation treatment with focused pulsed laser beam. Figure 41e) shows a little bimodal size distribution with an average size of Ø= 25±9 nm, as evident in the corresponding BF-TEM image. The crystalline structure of Pd NPs post-irradiated with focus condition was confirmed with the HRTEM micrograph (figure 41f). The interplanar distance of 2.26 Å corresponded to (111) planes of FCC structure of Pd indexed with the PDF No. 03-065-6174. The average size of Pd NPs was smaller with bimodal size distribution for those obtained in solutions irradiated with the focused pulsed laser beam. The focused beam allowed the fragmentation of Pd NPs. In this bimodal size distribution the bigger particles were attributed to re-dispersed nanoparticles and the smaller ones to photo-fragmentation process [65] during the post-irradiation. Meanwhile, the average size obtained by direct post-irradiation (unfocused) was very near to as prepared Pd NPs in distilled water. Therefore post-irradiation by direct beam only re-disperse the aggregates. But in general, post-irradiation treatment allowed to re-disperse or to recover the mean size of Pd NPs after its agglomeration. Pd NPs in DW after post-irradiation treatment recovered and retained its optical properties (as observed in the UV-Vis absorption spectra) for nearly 24 h. After a day these samples were agglomerated and precipitated. Ultrasonic bath treatment was tested as an alternative simple method to re-disperse those nanoparticles. Samples of Pd NPs with and without laser post-irradiation treatment were taken to an ultrasonic treatment for 10 minutes. First, the samples of Pd NPs obtained by PLAL at 40.5 J/cm^2 and then post-irradiated subjected to an ultrasonic bath treatment. Figure 42a) shows the spherical morphology of Pd NPs in BF images, well dispersed with a size distribution of Ø= 33±8 nm (figure 42b). Figure 42c shows the SAED micrograph obtained for post-irradiated Pd NPs and those with the post ultrasonic treatment. After this treatment, the average size of Pd NPs (which previously were post-irradiated with the un-focused pulsed laser beam) was like to that of NP formed by post-irradiation treatment (Ø= 32±8 nm). Aggregates of Pd NPs obtained by PLAL at 18 J/cm^2 (without post-irradiation treatment) were selected for the ultrasonic bath treatment. Figure 42d) illustrates the spherical morphology of Pd NPs in

BF images where the NPs are well dispersed with a size distribution of Ø= 34±6 nm (figure 42e). Figure 42f shows the interplanar distance of 2.26 Å in the HRTEM micrograph which corresponds to (111) plane of FCC structure of Pd NPs after its ultrasonic treatment. With the ultrasonic bath treatment, the average size of Pd NPs (without post-irradiation treatment) was slightly higher to the average size of as-prepared Pd NPs.

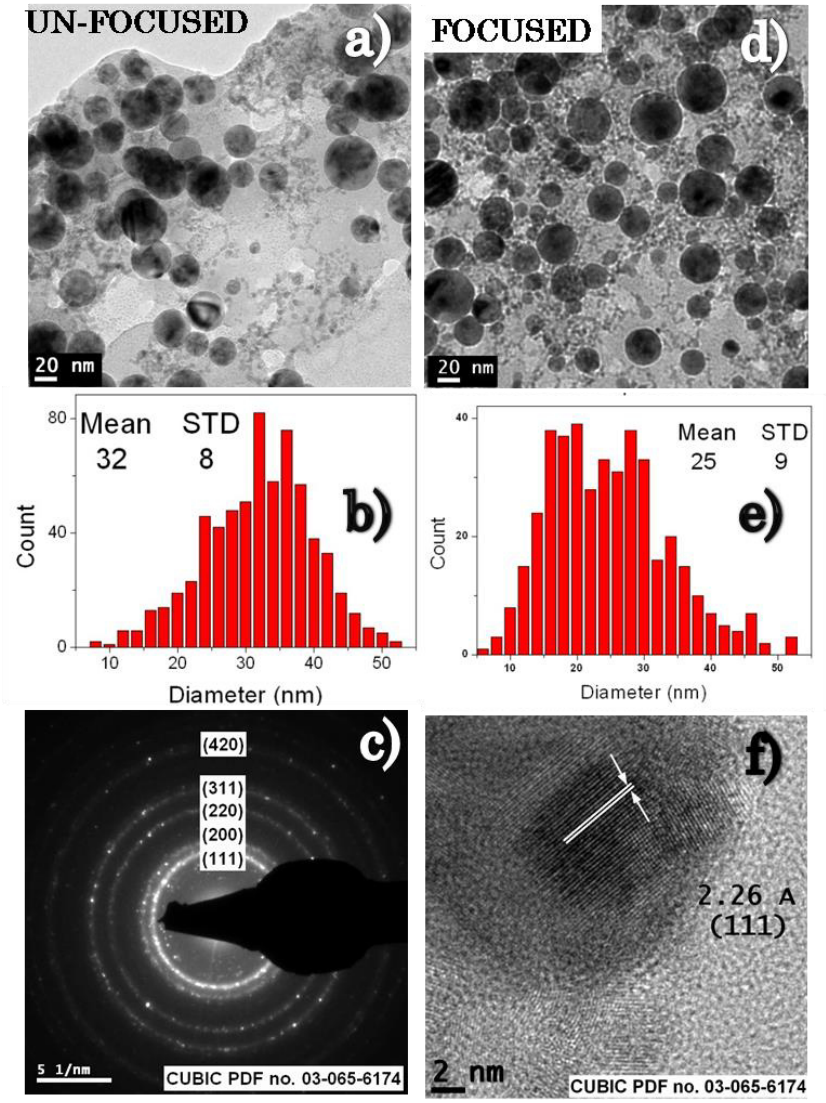

Figure 41. Pd NPs obtained by PLAL in DW with post-irradiation (a-c) unfocused and (d-f) focused condition.

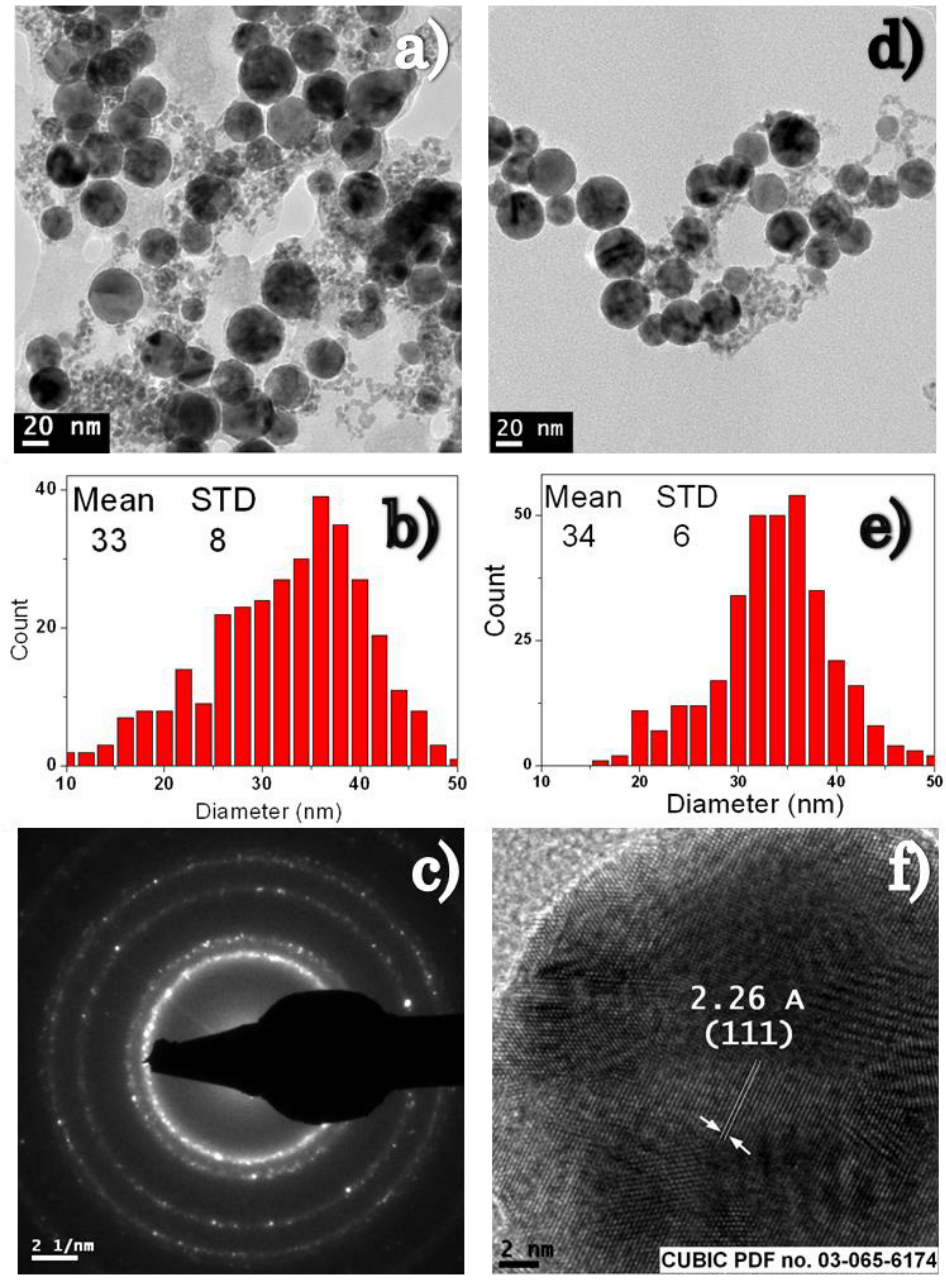

Figure 42. Morphology, size distribution and crystalline structure of Pd NPs obtained by PLAL in DW after (a-c) post-irradiation/ultrasonic and (d-f) only ultrasonic treatment.

4.3.1.2.2. Pd NPs in Methanol-Water Mixture

After the precipitation of Pd NPs obtained by PLAL at 40.5 and 26.5 J/cm^2 in methanol-water mixture, these solutions were post-irradiated with focused and unfocused pulsed laser beam (532 nm), respectively. The BF micrograph of figure 43a) shows the spherical morphology of Pd NPs post-irradiated with unfocused pulsed laser. A bimodal size distribution was observed in the BF image and presented in the size distribution plot of figure 43c). The mean size of 14±6 nm was very near to the as-prepared Pd NPs by PLAL in methanol-water mixture. The crystalline structure was confirmed by the HRTEM image of figure 43e) in which the interplanar distance of 2.24 Å corresponded to (111) plane of FCC structure of Pd. Figure 43b) shows the spherical morphology of Pd NPs post-irradiated with focused pulsed laser beam. A uniform size and narrow size distributions of Pd NPs were identified from the BF image and plotted in figure 43d). The mean size of Ø= 9±2 nm was even smaller than the as-prepared Pd NPs by PLAL in this solution. The SAED micrograph of figure 43f) shows that the FCC structure of Pd NPs did not change after its post-irradiation treatment. The HRTEM and SAED micrographs showed the crystallinity of Pd NPs which were indexed with the PDF No. 03-065-6174. Similarly to the results obtained in DW, post-irradiation with 0.3 J/cm^2 re-dispersed the aggregates of the solution and post-irradiation treatment with focused (2 J/cm^2) beam produced a reduction on average size of Pd NPs. The stability of Pd NPs post-irradiated (with focused and unfocused pulsed laser) was maintained for one day approximately. After this time Pd NPs precipitated again at the bottom of the glass container. The precipitated samples of Pd NPs in methanol-water mixture with and without post-irradiation treatment treated ultrasonically. Figure 44 (a, b) shows the morphology and size distribution, respectively of Pd NPs (which previously were obtained by PLAL at 12.5 J/cm^2 and post-irradiated with unfocused PL) with ultrasonic treatment. The spherical Pd NPs presented a bimodal size distribution with an average size of Ø= 13±7 nm similar to the as-prepared Pd NPs. Figure 44 (c, d) shows the morphology and size distribution, respectively of Pd NPs (obtained by PLAL at 8 J/cm^2 of energy fluence without post-irradiation treatment) which were treated in an ultrasonic bath. The BF image shows spherical and well dispersed Pd NPs after the ultrasonic treatment. The average size of Ø= 14±4 nm was in the range of the as-prepared Pd NPs by PLAL in methanol-water mixture.

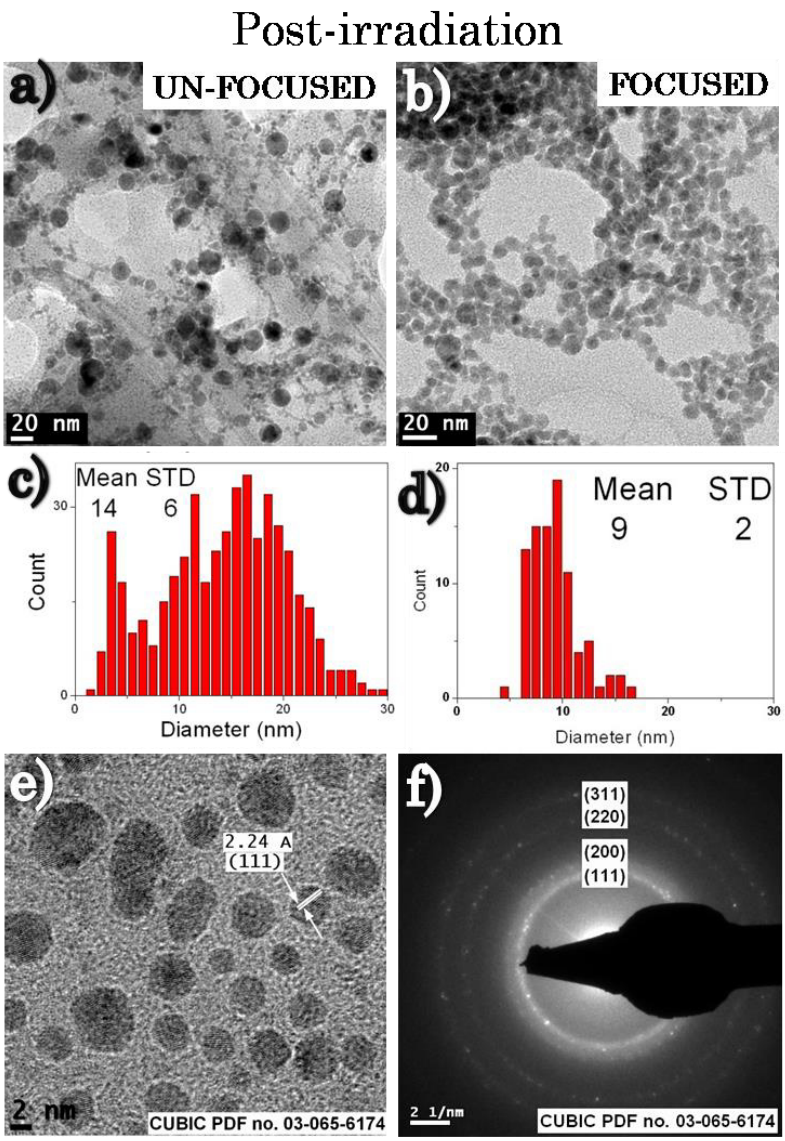

Figure 43. (a, b) BF-TEM, (c, d) size distribution, e) HRTEM and f) SAED of Pd NPs obtained by PLAL in methanol-water mixture with post-irradiation treatment.

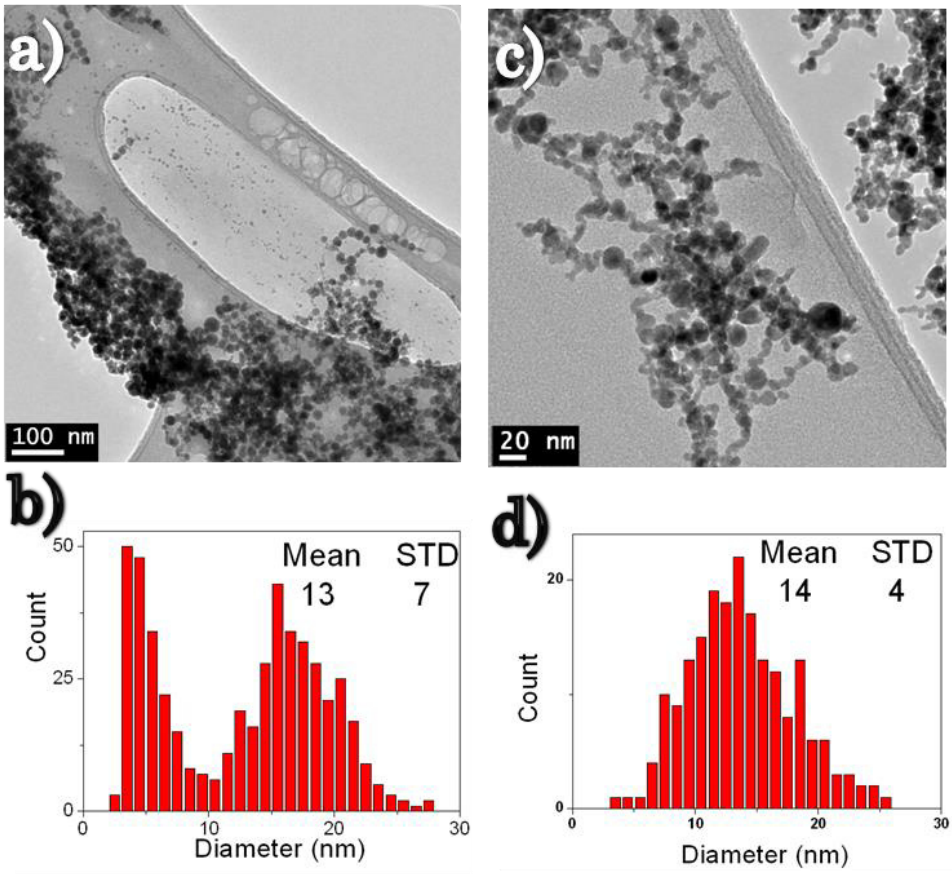

Figure 44. Pd NPs obtained by PLAL in methanol-water mixture after (a, b) post-irradiation/ultrasonic and (c, d) only ultrasonic treatment (BF-TEM and size distribution, respectively).

4.3.1.2.3. Pd NPs in SDS

Pd NPs obtained in 0.001 M solution of SDS at different energy fluence (40.5, 26.5, 18, 12.5 and 8 J/cm^2) were stable for a few days and then got precipitated. All the samples were put in ultrasonic bath to study the effect of ultrasonic treatment on the morphological and optical properties of the colloidal Pd nanoparticles. Figure 45a) shows that Pd NPs in SDS (obtained initially by PLAL at 8 J/cm^2) solution maintained the spherical morphology and the average size of Ø= 21±10 nm (figure 45b) after the ultrasonic bath treatment. Figure 45c) shows the crystalline structure of Pd NPs in the HRTEM micrograph in which the interplanar distance of 2.2 Å corresponded to (111) planes of FCC structure of Pd. The SAED in figure 45d) shows the planes (111), (200), (220) and (311) of FCC crystalline

structure of Pd NPs after the ultrasonic bath. SAED and HRTEM micrographs were indexed with the PDF No. 03-065-6174.

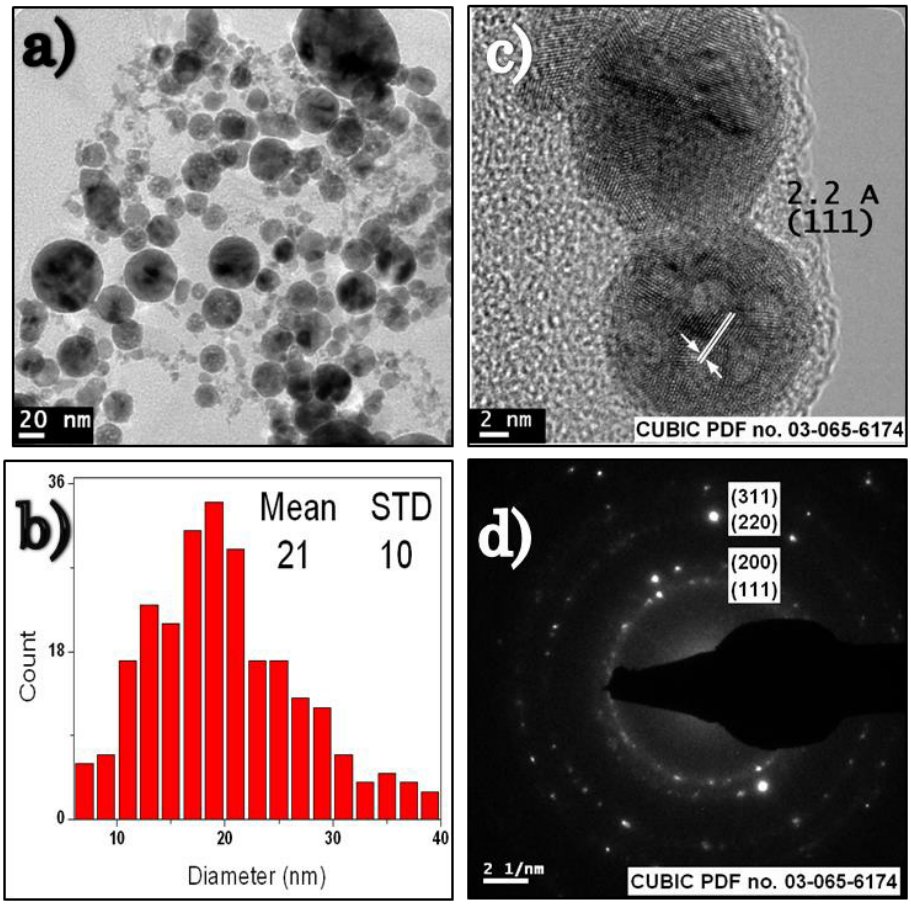

Figure 45. BF-TEM, size distribution, HRTEM and SAED of Pd NPs obtained by PLAL in SDS with ultrasonic treatment.

4.3.2. Elemental Composition by EDX and XPS

Elemental composition of Pd NPs synthesized by PLAL using 1064 nm in DW, methanol-water mixture, 0.001M of SDS and EG was characterized. A qualitative analysis was done by Energy dispersive X-ray spectroscopy in TEM microscope with the samples prepared onto the Cu grids over single Pd nanoparticle due the inherent capability in resolution of TEM microscopy. A complementary analysis was performed by XPS to confirm the chemical state of Pd NPs in DW, methanol-water mixture and SDS.

4.3.2.1. Pd NPs Obtained in DW

The elemental composition of Pd NPs obtained by PLAL using 1064 nm in DW was performed in TEM with the EDX detector. Figure 46 shows (a) STEM image of a group of Pd NPs attached to the carbon film and the area of EDX analysis. Figure 46 b) presents the EDX spectrum obtained for the selected Pd NP in DW. The elemental composition of Pd is identified for Pd NPs obtained in DW with the EDX spectrum in which it is possible to observe the presence of Pd, and other small peaks, corresponding to O, and the Cu and C from the Cu grid, and C film, respectively. The elemental analysis of Pd nanoparticles obtained by PLAL using 1064 nm in DW was complemented with the XPS spectroscopy and the chemical state analysis. Figure 47shows the high resolution spectra of Pd doublet $3d_{5/2}$ and $3d_{3/2}$ core levels of Pd NPs in distilled water (synthesized at 26.5 J/cm^2) showing the peak position at 335.48 eV and 340.78 eV, respectively separated by 5.3 eV. This binding energy corresponds to elemental Pd [279, 280]. The peaks were fitted by Gaussian–Lorentzian sum function and also, care was taken to maintain the intensity ratio of Pd $3d_{5/2}$– Pd $3d_{3/2}$ as 3:2.

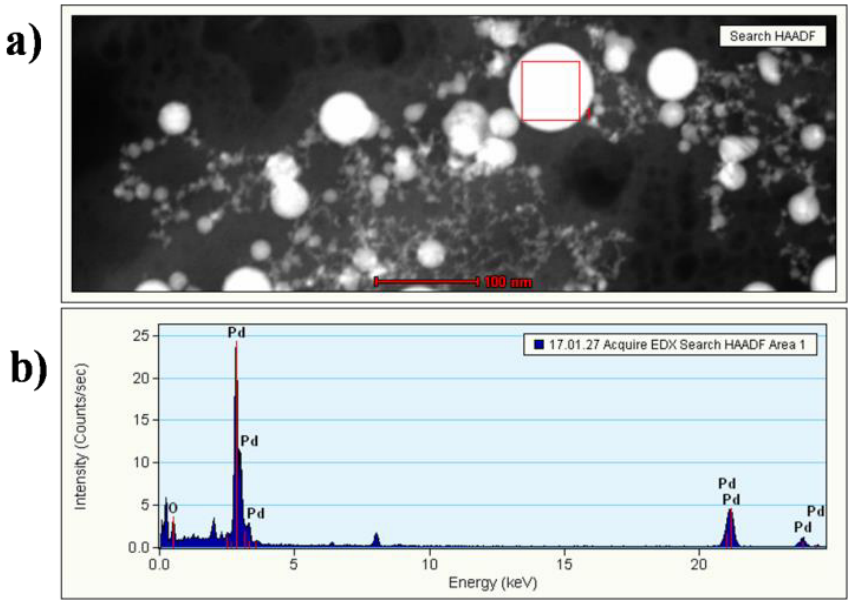

Figure 46. a) STEM image and b) EDX spectrum of Pd NPs obtained by PLAL in distilled water

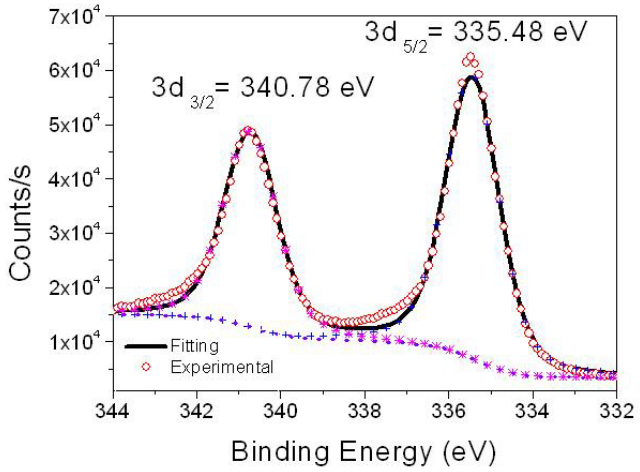

Figure 47. High resolution XPS spectrum of Pd 3d for Pd NPs obtained by PLAL in DW.

4.3.2.2. Pd NPs Obtained in Methanol-Water Mixture

The elemental composition of Pd NPs obtained by PLAL using 1064 nm in the methanol-water mixture was analyzed using energy dispersive X-ray spectroscopy (EDX) attached to TEM. Figure 48 shows the STEM micrograph of a group of Pd NPs (a) and EDX spectrum (b). EDX spectrum obtained for the selected Pd NP in methanol-water mixture corresponded to the presence of Pd as its pure elemental state. In the EDX spectrum, it is possible to observe the presence of Pd and other elements as Cu and C, from the Cu grid and C film, respectively. The elemental and chemical state analysis of Pd nanoparticles obtained by PLAL using 1064 nm in methanol-water mixture was done with the XPS spectroscopy. Figure 49 shows the high resolution spectra of Pd doublet $3d_{5/2}$ and $3d_{3/2}$ core levels of Pd NPs in methanol-water mixture (synthesized at 8 J/cm^2) showing the peak position at 335.47 eV and 340.75 eV, respectively separated by 5.28 eV. The binding energy values obtained for Pd NPs in the methanol-water mixture are corresponding to Pd in elemental state according to the reported results [279, 280]. The peaks were fitted by Gaussian–Lorentzian sum function and also, care was taken to maintain the intensity ratio of Pd $3d_{5/2}$–Pd $3d_{3/2}$ as 3:2.

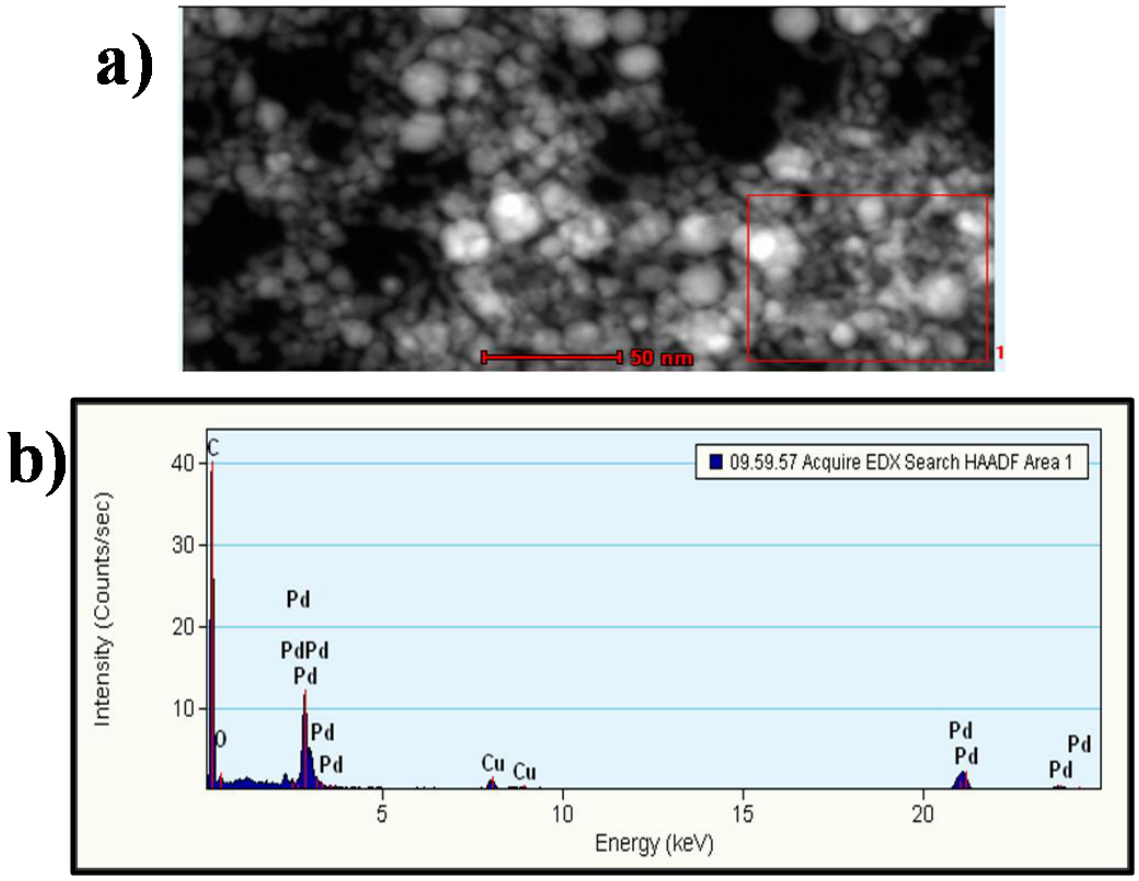

Figure 48. a) STEM image and b) EDX spectrum of Pd NPs obtained by PLAL in methanol-water mixture

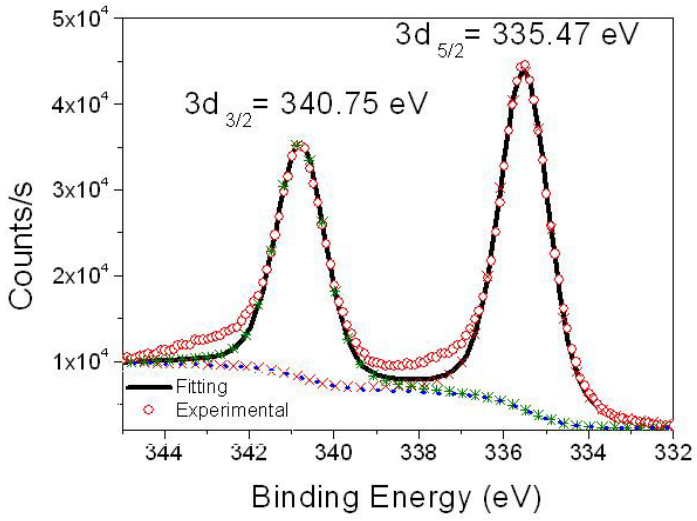

Figure 49. High resolution XPS spectrum of Pd 3d for Pd NPs obtained by PLAL in methanol-water mixture.

4.3.2.3. Pd NPs Obtained in SDS

The elemental composition of Pd NPs obtained by PLAL using 1064 nm in 0.001 M of SDS in aqueous solution at 40.5 J/cm^2 was analyzed using energy dispersive X-ray (EDX) detector within TEM microscope. Figure 50 shows the STEM micrograph of a single Pd NPs (a) and EDX spectra (b). The EDX spectrum shows the elemental composition of Pd NPs and also the presence of S, C and O related to the surfactant probably adsorbed to the nanoparticle surface. The chemical analysis of Pd nanoparticles obtained in 0.001 M of SDS surfactant showed the presence of palladium (elemental state), along with traces of oxidized form, as seen in figure 51. The figure shows two doublets peaks for Pd NPs in 0.001 M SDS (synthesized at 26.5 J/cm^2) located at 335.04 eV and 340.33 eV corresponding to Pd $3d_{5/2}$ and $3d_{3/2,}$ respectively separated by 5.29 eV. These B.E. values are reported for Pd^0 (metallic, elemental state) [279, 280]. The second one at 336.41 eV ($3d_{5/2}$), and 341.64 eV ($3d_{3/2}$), corresponded to Pd in the +2 oxidation state (PdO) [246]. The presence of PdO in the XPS spectra and the traces of oxygen in the EDX spectra (assigned to the surfactant), implies that the nanoparticles surfaces have been partially oxidized because the spectra was measured several days after PLAL experiments and their air-exposure. The peaks were de-convoluted into single states by Gaussian–

Lorentzian sum function and also, care was taken to maintain the intensity ratio of Pd $3d_{5/2}$– Pd $3d_{3/2}$ as 3:2.

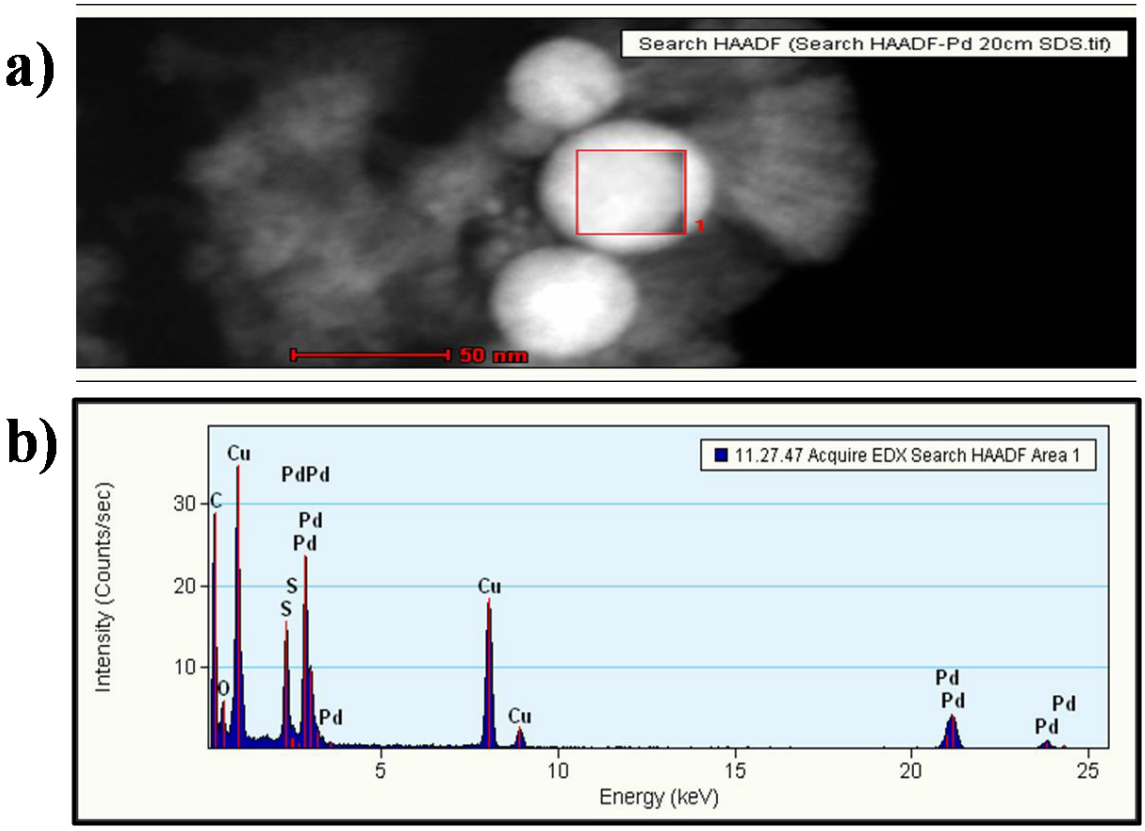

Figure 50. a) STEM image and b) EDX spectrum of Pd NPs obtained by PLAL in 0.001 M of SDS

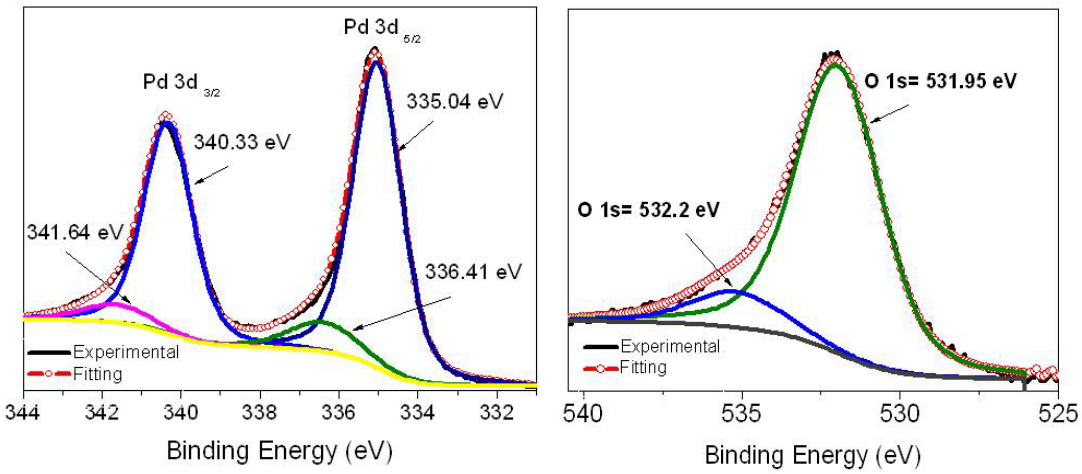

Figure 51. High resolution XPS spectrum of left) Pd 3d and right) O1s for Pd NPs obtained by PLAL in 0.001 M of SDS.

4.3.2.4. Pd NPs Obtained in Ethylene Glycol

The elemental composition of Pd NPs obtained by PLAL using 1064 nm in EG at 18 J/cm^2 was analyzed by energy dispersive X-ray spectroscopy (EDX) associated with the TEM analysis of the sample. In STEM mode, it is possible to obtain Z-contrast images (with the HAADF detector) which provides qualitative atomic resolution elemental analysis, in addition to atomic-resolution detail at interfaces between regions of different Z. A higher intensity could be related to Pd NPs and the lower to the chemical compound. In the STEM micrograph of figure 52a), Pd NPs appeared with spherical morphology (high signal intensity) and embedded in the ethylene glycol (with low signal intensity). EDX spectrum (b) of figure 52 shows the presence of Pd, which confirms the elemental Pd NPs produced.

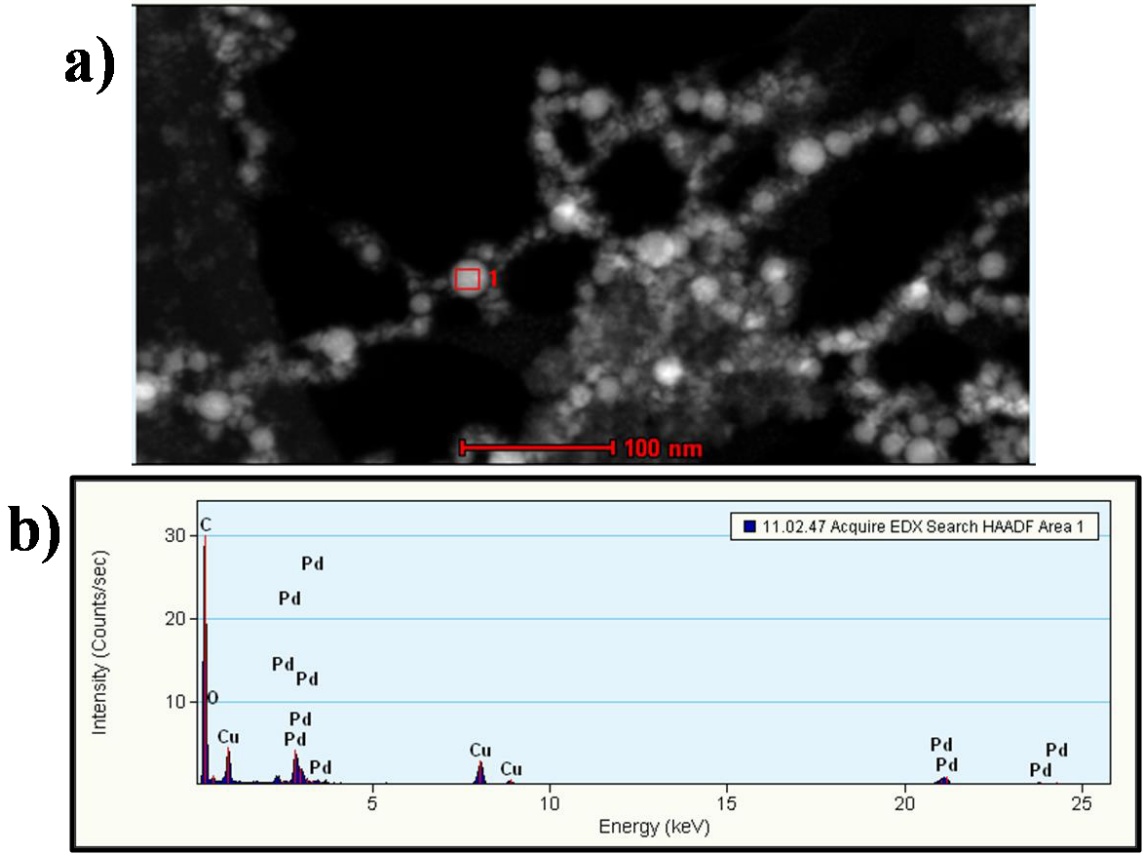

Figure 52. a) STEM image and b) EDX spectrum of Pd NPs obtained by PLAL in Ethylene Glycol.

4.3.3. Optical Properties by UV-Vis

Due to the excitation of plasma resonances or interband transitions, colloidal dispersions of metals exhibit absorption bands or broad regions of absorption in the ultraviolet-visible range. Such broad absorption is a characteristic property of metallic nature of the particles [281].

4.3.3.1. As-prepared Pd NPs

The as-prepared colloids of Pd NPs in distilled water, methanol-water mixture, 0.001 M of SDS and EG, were analyzed by UV–Vis spectroscopy immediately after PLAL experiments. The as-produced colloids in the different liquid media were turned to precipitate after approximately one hour (for DW and methanol-water mixture) or a few days (in the case of SDS and EG). Post-irradiation and ultrasonic treatments were done after 3 months of PLAL experiments with the Pd precipitates in the different liquid media.

The post-irradiation and ultrasonic treatment effects on the optical properties of Pd NPs were studied by UV-Vis absorption spectroscopy, immediately after the treatments. Pd nanoparticles were produced by PLAL using 1064 nm in distilled water, methanol-water mixture, SDS and ethylene glycol. A range of high (40.5 J/cm^2), medium (26.5, 18 and 12.5 J/cm^2) and low (8 J/cm^2) energy fluence were used for PLAL experiments. The optical properties of the resulted nanocolloids as a function of energy fluence and liquid media were studied, immediately after their synthesis, especially in case of DW and methanol-water mixture due to their fast precipitation.

4.3.3.1.1. Pd NPs Obtained in DW

Figure 53 shows the UV-Visible absorption spectra of Pd NPs synthesized by PLAL using 1064 nm in DW at 40.5, 26.5, 18, 12.5 and 8 J/cm^2 of energy fluence. The higher optical absorption peak observed at ~201 nm for 40.5 J/cm^2 has been reported as Pd^{2+} [242, 243, 279, 282]. But in other reports on synthesis of Pd NPs by similar method [246] or even chemical methods [283], the optical absorption peak at ~200 nm was assigned to superimposed interband transitions characteristics of the metallic state. Then, Pd NPs obtained in DW were assigned as metallic Pd NPs according to our results of EDX and XPS analysis. The broadening of absorption peak can be originated by the interaction between NPs due to their high concentration [242]. In the case of other energy fluence presented weak absorption broadening curve in the UV range, in which 18 and 12.5 J/cm^2 showed prominent intensity. These results are in accordance with size measurement by TEM analysis where the average size and size distribution are related to the energy fluence. The yield of nanoparticles in DW showed dependence on the energy fluence: absorption intensity increases with higher energy fluence.

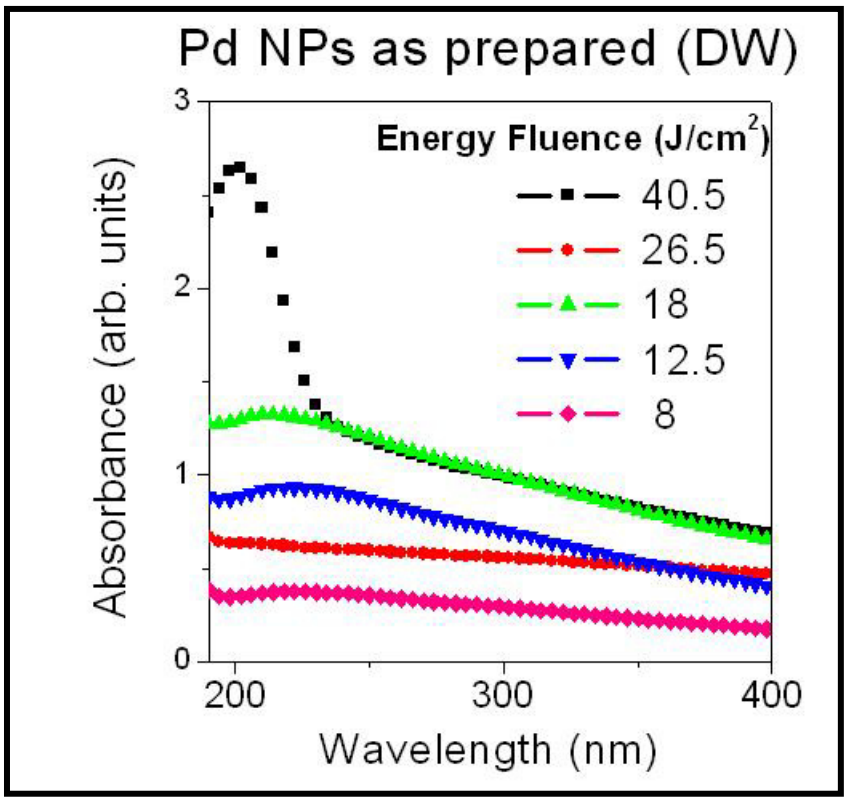

Figure 53. UV-Vis Absorption spectrum of Pd NPs synthesized by PLAL in DW at different energy fluence for 1064 nm.

4.3.3.1.2. Pd NPs Obtained in Methanol-Water Mixture

Figure 54 shows the UV-Vis absorption spectra of Pd NPs synthesized by PLAL in methanol-water mixture at 40.5, 26.5, 18, 12.5 and 8 J/cm^2 of energy fluence. All the absorption peaks were observed at ~228 nm, with a continuous absorption in the UV range. These optical peaks could be attributed to superimposed interband transitions characteristic of the metallic state [246, 283]. The yield of Pd NPs by PLAL was higher at lower energy fluence (8 J/cm^2). For medium values of energy fluence (26.5 – 12.5 J/cm^2) the concentration of Pd NPs was very similar. And the lower yield of Pd NPs was for the higher energy fluence (40.5 J/cm^2). The yield of Pd NPs in methanol-water mixture showed dependence as function of the energy fluence, opposite to the Pd NPs in DW. This behavior can be attributed to the change in the nature of the liquid media (mixing methanol and DW, 1:1) and to the increase in the irradiated area at lower energy fluence.

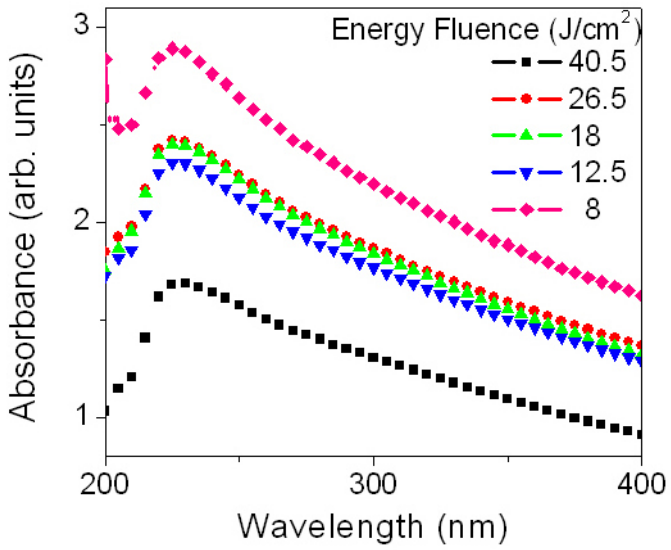

Figure 54. UV-Vis Absorption spectrum of Pd NPs synthesized by PLAL in methanol-water mixture at different energy fluence, 1064 nm.

4.3.3.1.3. Pd NPs Obtained in SDS

Figure 55 shows the UV-Vis spectra of Pd NPs synthesized by PLAL in SDS at 40.5, 26.5, 18, 12.5 and 8 J/cm^2 of energy fluence. From the figure, all the samples present broadened absorption peaks at ~240 and 300 nm with a continuous absorption. The first optical peaks can be attributed to superimposed interband transitions characteristic of the metallic state of Pd [246, 283]. There is a little red shift in the first optical peak of Pd NPs obtained at between 40.5 and 26.5 J/cm^2 of energy fluence and the other ones. This is in agreement with the average size change as a function of energy fluence observed in TEM analysis. This behavior was different from Pd NPs in distilled water. The second peaks may be attributed to the oxidized Pd species [243, 284] in SDS surfactant, or the rapid surface oxidation as observed in the XPS analysis. The absorption intensity was higher for higher energy fluence, and then the yield of Pd NPs by PLAL changed as function of the energy fluence, similar to the case of Pd NPs produced by PLAL in DW.

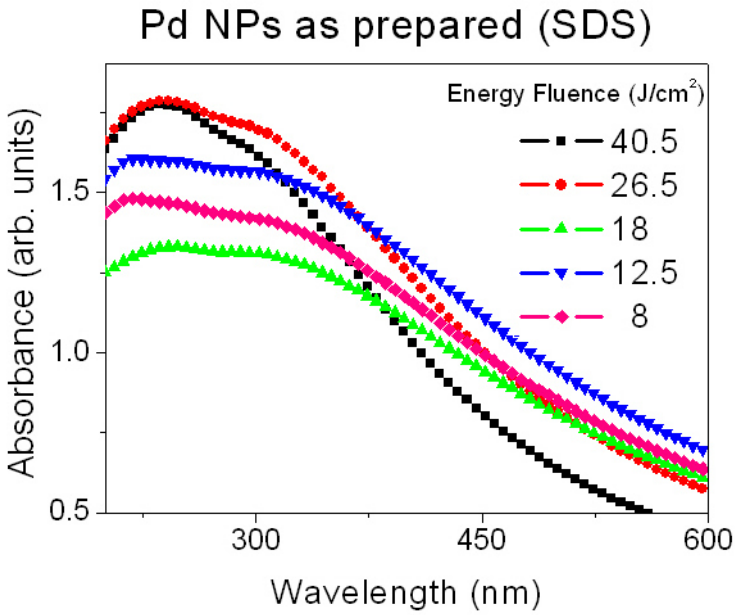

Figure 55. UV-Vis Absorption spectrum of Pd NPs synthesized by PLAL using 1064 nm in 0.001 M of SDS at different energy fluence

4.3.3.1.4. Pd NPs Obtained in EG

Figure 56 shows the UV-Vis spectra of Pd NPs synthesized by PLAL at 1064 nm in EG at 40.5, 26.5, 18, 12.5 and 8 J/cm^2 of energy fluence. All the samples presented optical absorption peaks at ~260-280 nm, and continuous absorption in the UV range as reported in literature for Pd NPs in EG synthesized by chemical methods [284]. The optical peaks could be attributed to superimposed interband transitions characteristic of the Pd metallic state [246, 283]. There is a little blue shift in the optical peak of Pd NPs obtained at energy fluence of 8 J/cm^2, an also for the other conditions. The higher absorption intensity was obtained in the sample with lower energy fluence; then the yield of Pd NPs in EG showed dependence as function of the energy fluence similarly to the Pd NPs in methanol-water mixture.

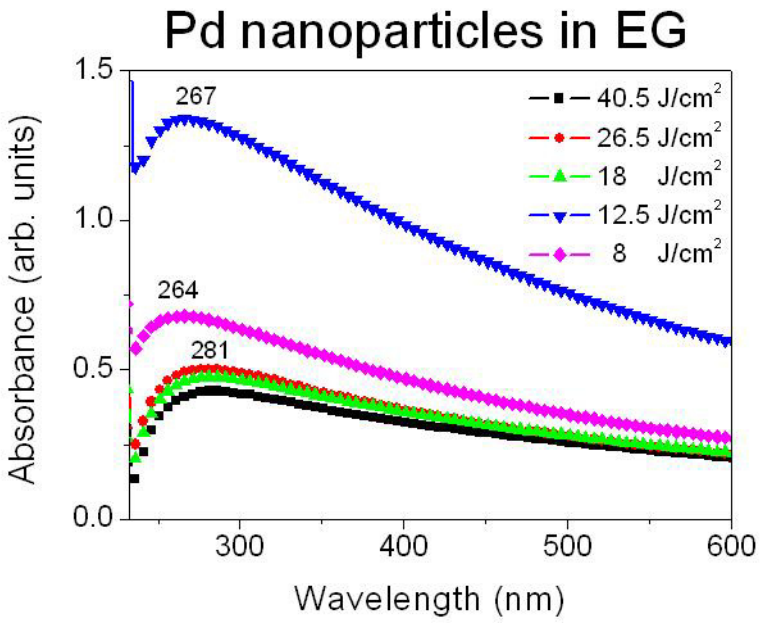

Figure 56. UV-Vis Absorption spectrum of Pd NPs synthesized by PLAL in Ethylene glycol at different energy fluence, 1064 nm.

4.3.3.2. Pd NPs with Post-Irradiation and Ultrasonic Treatment

4.3.3.2.1. Pd NPs Obtained in DW

Figure 57 a) shows the UV-Vis spectra of Pd NPs synthesized by PLAL in DW at 40.5 J/cm^2 of energy fluence with the spectrum of the as-prepared and post-irradiated nanoparticles. The optical absorption peak re-appeared after the post-irradiation treatment. The absorption intensity decreased due to the agglomeration of Pd NPs. These precipitates were used for XPS characterization. The post-irradiated sample presented a weak additional peak at ~300 nm, which is probably due to an increase in particle size, or to the partial oxidation of Pd nanoparticles after long time storage [243, 284]. This effect was related to the broad size distribution observed in TEM images of these samples. Figure 57 b) shows the UV-Vis spectra of Pd precipitates in DW with ultrasonic treatment. All the samples (with and without post-irradiation treatment) were put in the ultrasonic bath. The UV-Vis absorption spectra show the same optical peak for the as-prepared sample obtained at 40.5 and 26.5 J/cm^2 (which also were post-irradiated); additionally, the other samples also showed broadened optical peaks. This probably means that ultrasonic treatment is a fast,

efficient and cheap technique to re-disperse this aggregate Pd NPs into colloidal solution with similar optical properties.

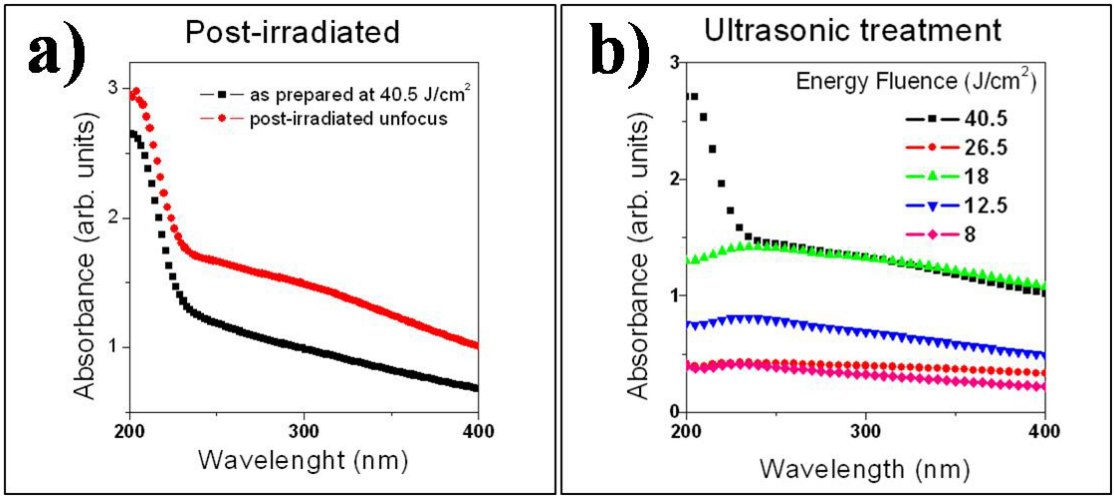

Figure 57. UV-Vis Absorption spectrum of Pd NPs synthesized by PLAL in DW with a) post-irradiation and b) ultrasonic treatment.

4.3.3.2.2. Pd NPs Obtained in Methanol-Water Mixture

Figure 58 (a) shows the UV-Vis spectra of Pd NPs synthesized by PLAL using 1064 nm in methanol-water mixture after their post-irradiation treatment. The optical absorption peaks appeared at ~226-229 nm for all the samples, near to the absorption peaks of the as-prepared samples. Figure 58 (b) shows the UV-Vis spectra of Pd NPs synthesized by PLAL using 1064 nm in methanol-water mixture after their ultrasonic treatment (as well as samples with previous post-irradiation treatment). The UV-Vis absorption spectra show narrower peaks and a blue shift with respect to the as-prepared and those that were post-irradiated samples. The absorption peaks appeared at ~208 nm for all energy fluence. The different behavior and blue shift in the absorption spectrum may be due to structural changes; however further studies are needed to prove this effect.

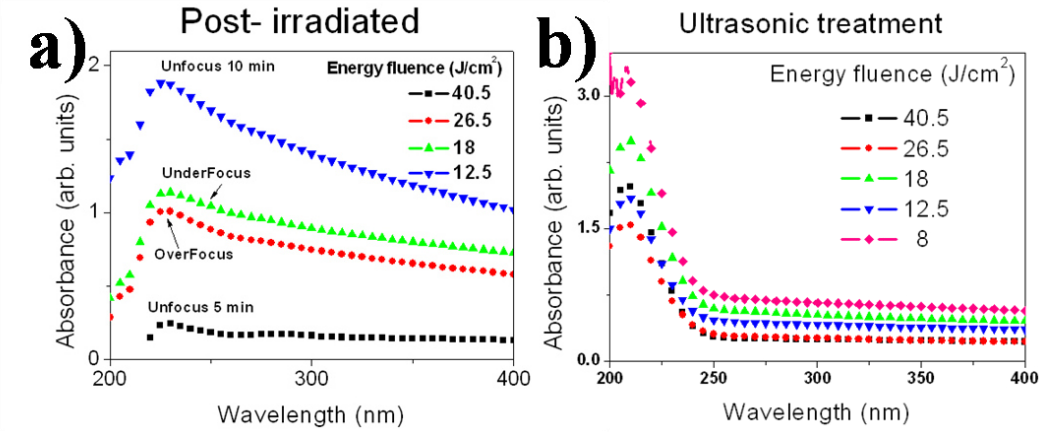

Figure 58. UV-Vis Absorption spectrum of Pd NPs synthesized by PLAL in methanol-water mixture with a) post-irradiation and b) ultrasonic treatment

4.3.3.2.3. Pd NPs Obtained in SDS

Figure 59 presents the UV-Vis absorption spectrum of Pd precipitates (which were previously synthesized by PLAL at 1064 nm in SDS) after their ultrasonic treatment. The UV-Vis absorption spectra show similar peaks compared with that of the as-prepared Pd NPs. The absorption peaks appeared at ~200 and 300 nm for all the conditions of energy fluence, showing a red shift for the high energy fluence (40.5 and 26.5 J/cm^2) in comparison with the lower (12.5 and 8 J/cm^2) fluencies. In the case of the sample of 18 J/cm^2, a negligible absorption was observed due to the very low concentration of the sample used in the measurement. These results are similar to that obtained in DW, in which ultrasonic treatment is a fast, efficient and cheap technique to re-disperse this Pd aggregate into colloidal.

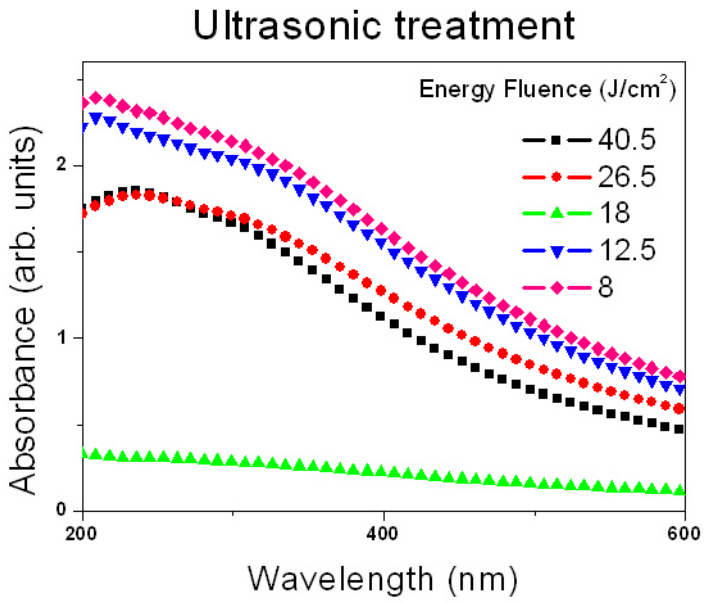

Figure 59. UV-Vis Absorption spectrum of Pd NPs synthesized by PLAL in 0.001 M of SDS with ultrasonic treatment.

Conclusions of the synthesis of Pd nanoparticles by PLAL using 1064 nm in DW, methanol-water mixture, SDS and ethylene glycol were the following; i) Results suggest that the nature of liquid affects the laser ablation process and the growth process of the nanoparticles; therefore, their dimensions and concentration changed; ii) The average size and yield of Pd nanoparticles showed dependence on the variation of energy fluence; iii) For as-prepared Pd NPs, in DW the average size increased with decrease in fluence while in SDS showed a decrease with decrease in fluence; iv) In methanol-water mixture there was no effect on the nanoparticle size for the ablation fluence; v) The yield of Pd NPs in DW and SDS was higher for higher energy fluence, opposite to methanol-water mixture and EG; vi) Smaller sizes of as-prepared Pd NPs were obtained in methanol-water mixture compared to other liquid media; vii) Laser post irradiation and ultrasonic treatment were effective to re-disperse the nanoparticles in solution and to regain their optical properties; viii) For ultrasonic treatment, Pd NPs in DW, methanol-water mixture and SDS recovered the initial size to the as-prepared NPs; and finally ix) The crystalline structure after post-irradiation and ultrasonic treatment remained as FCC structure.

CHAPTER 5

SYNTHESIS AND CHARACTERIZATION OF PLATINUM NANOPARTICLES BY PLAL

5.1. INTRODUCTION

This chapter describes the synthesis of Pt NPs by pulsed laser ablation of a Pt target in acetone, methanol and ethanol. Effects of laser energy fluence, nature of the liquid, time of ablation and stability of Pt NPs are reported. Pt NPs were characterized by TEM, EDX, XPS and UV-Visible Absorption spectroscopy to study the morphology, size, size distribution, structure, elemental composition, chemical state and optical properties of the ablated products.

5.2. EXPERIMENTAL SECTION

Pulsed laser ablation experiments were performed using a pulsed laser Nd:YAG (Solar Laser System LQ929A) with output energy of 230 mJ/pulse for 532 nm of wavelength. The pulse width was 10 ns and the repetition rate was 10 Hz for this laser. The target was a metal plate of Pt with high purity (99.9%). PLAL experiments were developed in vertical configuration as shown figure 60, in which the laser beam was deflected with a mirror (99% reflectivity for 532 nm) onto the target surface. Figures 61, 62 and 63 show photographs of platinum nanocolloids synthesized by pulsed laser ablation in methanol, ethanol and acetone, respectively at different energy fluence and time of ablation. To study the effect of the liquid media and to obtain comparative results, three different fluencies for each one were used. The liquids selected were methanol, ethanol and acetone. Due the high flammability, the selected liquids were diluted with DW in a ratio of 4:1 in order to avoid the combustion by the highly intense pulsed laser beam. The target was placed at the bottom of a glass beaker with 10 ml of the liquid (liquid layer height of 9 mm). To vary the energy fluence of pulsed laser ablation, the working distance lens to target (DLTT) was varied as 19, 18 and 17 cm. Therefore the energy fluence calculated were 25, 19 and 9 J/cm^2, for output energy of 230 mJ/pulse for 532 nm wavelength. The experiments were carried out for 5 minutes for the three energy fluence. For the high energy fluence (25 J/cm^2), time of ablation was varied in 5, 10 and 15 minutes. Table 3 summarizes the

experimental conditions of Pt NPs synthesized by PLAL. To improve the ablation productivity, a translation system (developed by Mechatronics students of FIME, UANL) was employed and all the experiments were carried at the same velocity (50 μm/s). Immediately after each experiment, a TEM grid was prepared placing a drop of Pt nanocolloids on a Cu grid and dried it at room temperature. For optical property studies UV-Visible absorption measurements were carried out using a UV-Vis spectrometer (Shimadzu UV-1800).

Liquid media	25 J/cm^2	19 J/cm^2	9 J/cm^2
Methanol	5, 10 and 15 min	5 min	5 min
Ethanol	5, 10 and 15 min	5 min	5 min
Acetone	5, 10 and 15 min	5 min	5 min

Table 3. Summary of experiments of Pt NPs synthesized by PLAL with different liquid media, focusing conditions and time of ablation.

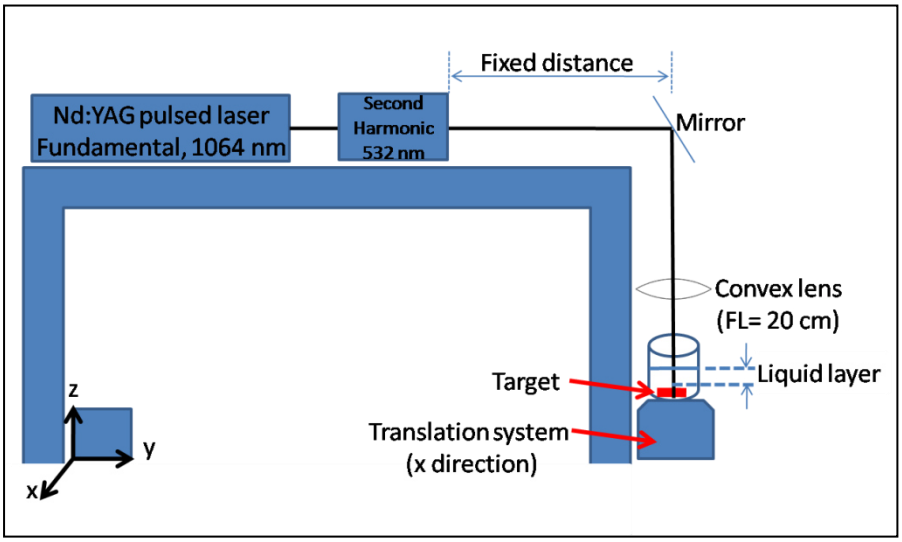

Figure 60. Set-up of vertical configuration of PLAL experiments to Pt nanocolloids synthesis.

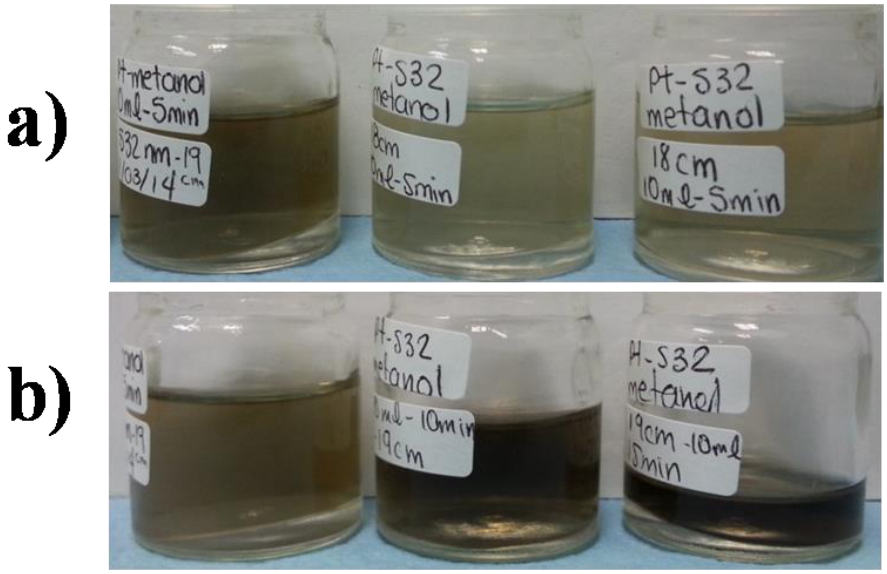

Figure 61. a) Colloidal solution of platinum nanoparticles obtained by PLAL in methanol for 5 minutes at 25, 19 and 9 J/cm^{2}of energy fluence (532 nm), respectively; b) Colloidal solution of platinum nanoparticles obtained by PLAL in methanol at 25 J/cm^2 for 5, 10 and 15 minutes, respectively

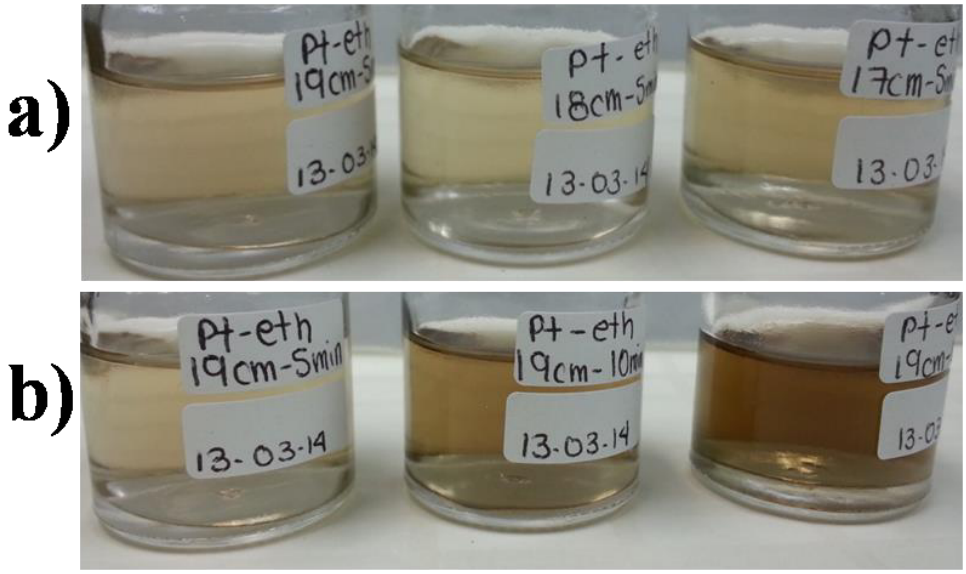

Figure 62. a) Colloidal solution of platinum nanoparticles obtained by PLAL in ethanol for 5 minutes at 25, 19 and 9 J/cm^2, respectively (532 nm); b) Colloidal solution of platinum nanoparticles obtained by PLAL in ethanol at 25 J/cm^2 for 5, 10 and 15 minutes, respectively

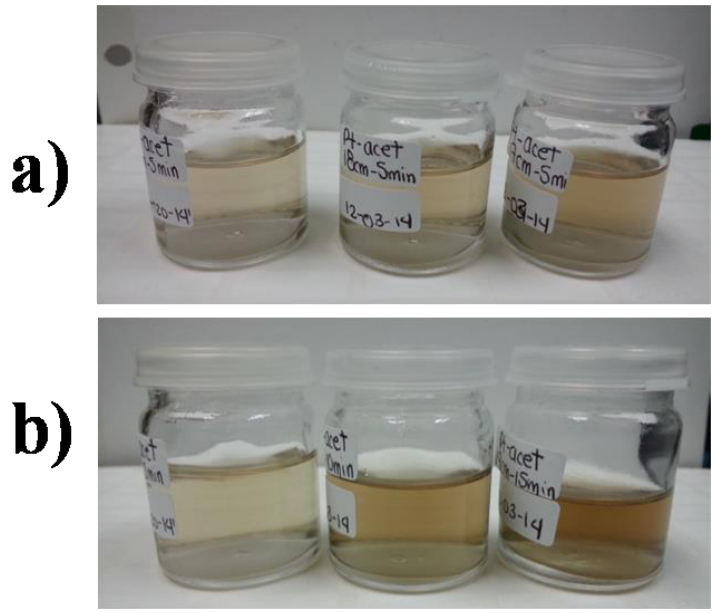

Figure 63. a) Colloidal solution of platinum nanoparticles obtained by PLAL in acetone for 5 minutes at 25, 19 and 9 J/cm^2, respectively (532 nm); b) Colloidal solution of platinum nanoparticles obtained by PLAL in acetone at 25 J/cm^2 for 5, 10 and 15 minutes, respectively.

5.3. RESULTS AND DISCUSSION

Platinum nanoparticles obtained by PLAL in methanol, ethanol and acetone were characterized to analyze their morphology, crystalline structure, elemental composition, chemical state and optical properties as a function of energy fluence, liquid media and time of ablation.

5.3.1. Morphology

Details of analysis for the shape, size and crystalline structure of Pt NPs obtained at different liquid media and energy fluence were analyzed first at different energy fluence, and then, at specific energy fluence ablated for different durations. Morphology of Pt nanocolloids obtained by PLAL in acetone, ethanol and methanol was characterized by STEM, BF and HRTEM micrographs and size distribution calculations were done. TEM and STEM micrographs in figure 64 corresponds to Pt NPs obtained by PLAL in acetone at a-c) 9, d-f) 19 and g-i) 25 J/cm^2 of energy fluence. Spherical NPs with a diameter of 2±1

nm were obtained in acetone for low and medium energy fluence. In the case of higher energy fluence size distribution of Ø= 6±3 nm was observed as seen in the micrographs. For all energy fluence, Pt NPs smaller in size and well dispersed, along with some agglomerates. HRTEM micrographs of NP obtained at all energy fluence how small NPs clustered to form bigger particle of ~6 nm in size. Figure 65 presents morphologies for Pt NPs obtained at 25 J/cm^2 of energy fluence at a-c) 5, d-f) 10 and g-i) 15 minutes of ablation. There was an effect of ablation time over the coalescence of Pt NPs. For 5 minutes Pt NPs were likely to coalesce to form bigger NPs. Meanwhile NPs synthesized for 10 minutes were well dispersed as observed in the BF and HRTEM micrographs, yielding a size distribution of Ø= 2±1 nm. In case of 15 minutes, the NPs coalesced having a size distribution of Ø= 3±1 nm as shown in the STEM micrograph (figure 65-g). Figure 66 (a, b and c) shows the crystalline structure of Pt nanoparticles in acetone formed at 9, 19 and 25 J/cm^2 ablated for 5 minutes, respectively. Figure 66 (d and e) corresponds to Pt NPs obtained by ablating for 10 and 15 minutes, respectively using at 25 J/cm^2. SAED micrographs of figure 66b) and inset of figure 66c) represent the results obtained at different energy fluence and time of ablation. The diffracted planes were identified as (111), (200), (220), (311) and (422) corresponding to FCC structure of Pt NPs by comparing with PDF file No. 040802. HRTEM micrographs showed that Pt NPs had an interplanar distance of 2.26 Å which represented (111) plane of FCC structure in agreement with the indexed planes in SAED. Figure 67 shows TEM micrographs of Pt NPs obtained in ethanol at a-c) 9, d-f) 19 and g-i) at 25 J/cm^2 of energy fluence Pt NPs obtained in ethanol were spherical and well dispersed. Smaller Pt NPs of average size Ø= 2±2 nm was obtained for lower energy fluence of 9 J/cm^2 (similar to Pt NPs obtained in acetone). Pt NPs obtained at 19 and 25 J/cm^2 showed an average size of Ø= 5±3 nm, considerable agglomeration. Figure 68 illustrates Pt NPs obtained at 25 J/cm^2 energy fluence ablated for a-c) 5, d-f) 10 and g-i) 15 minutes. As in the case of acetone, 10 minutes of ablation produced smaller average size (Ø= 3±2 nm) of Pt NPs. After this time NPs tended to grow again by the higher concentration of NPs in the solution as well as laser irradiation of the solution. In figure 68-d is possible to observe flakes with polygonal morphology moreover of spherical nanoparticles. The inset on figure 68-d shows the HRTEM micrograph and crystallinity of these flakes. The inset of figure 68-e shows the NPs agglomerated to form

islands. For 15 minutes of ablation Pt NPs morphology was spherical with an average size of Ø= 4±3 nm. For 15 minutes, the size distribution of the bigger NPs ~6-8 nm was higher than that of NPs obtained at other conditions. Such result was similar to that for Pt NPs in acetone higher time of ablation lead coalescence of Pt NPs. These results may be due to the continuous irradiation and therefore fragmentation of Pt nanoparticles in the colloidal solution with increase in ablation time. Figure 69 (a, b and c) presents the crystalline structure of Pt nanoparticles in ethanol at 9, 19 and 25 J/cm^2, respectively for 5 minutes. It also shows Pt NPs obtained at 25 J/cm^2 for (d and e) 10 and f) 15 minutes. SAED micrographs (a, f and inset of e) showed FCC structure similar to Pt NPs in acetone as indexed in the pattern: (111), (200), (220) and (311). HRTEM micrographs (b, c and e) showed an interplanar distance of 2.27 Å corresponding to (111) plane of FCC. For Pt NPs obtained at higher energy fluence for 10 minutes ablation, a slightly different morphology was detected as observed in TEM micrographs. Such flakes NPs are indexed as PtO_2 with hexagonal crystalline structure in the SAED of figure 69d) and the HRTEM micrograph on the inset of this figure. The interplanar distance of 2.5 Å (101) and planes (002), (101), (004), (104), (202) and (204) were indexed with reference to PDF No. 732360. Figure 70 shows TEM micrographs of Pt NPs obtained in methanol at a-c) 9, d-f) 19 and g-i) 25 J/cm^2 of energy fluence. In general Pt NPs obtained in methanol were spherical and well dispersed. As in the case of Pt NPs obtained in acetone and ethanol, average size for Pt NPs of Ø= 2±1 nm was shown at lower energy fluence of 9 J/cm^2. The inset of figure 70a) at this lower energy fluence shows the agglomerated islands (similar to ethanol). For 19 and 25 J/cm^2 NPs the average sizes were Ø= 3±1 and 4±2 nm, respectively. Figure 71 shows Pt NPs obtained at 25 J/cm^2 for energy fluence at a-c) 5 and d-f) 15 minutes of ablation with average size of Ø= 4±2 and 5±3 nm, respectively. Figure 72 (a, b and c) shows the crystalline structure of Pt nanoparticles in methanol at 9, 19 and 25 J/cm^2, respectively for 5 minutes. Figure 72 (d and e) illustrates the crystalline nature of Pt NPs obtained at 25 J/cm^2 for 15 minutes. SAED micrographs (a, d) represent the results obtained at different energy fluence and time of ablation. The planes (111), (200), (220), and (311) were identified and indexed in the pattern, corresponding to FCC structure of Pt NPs. HRTEM micrographs (b, c and e) show the interplanar distance of Pt NPs of 2.27 Å which correspond to (111) plane of FCC structure, indexed also with SAED.

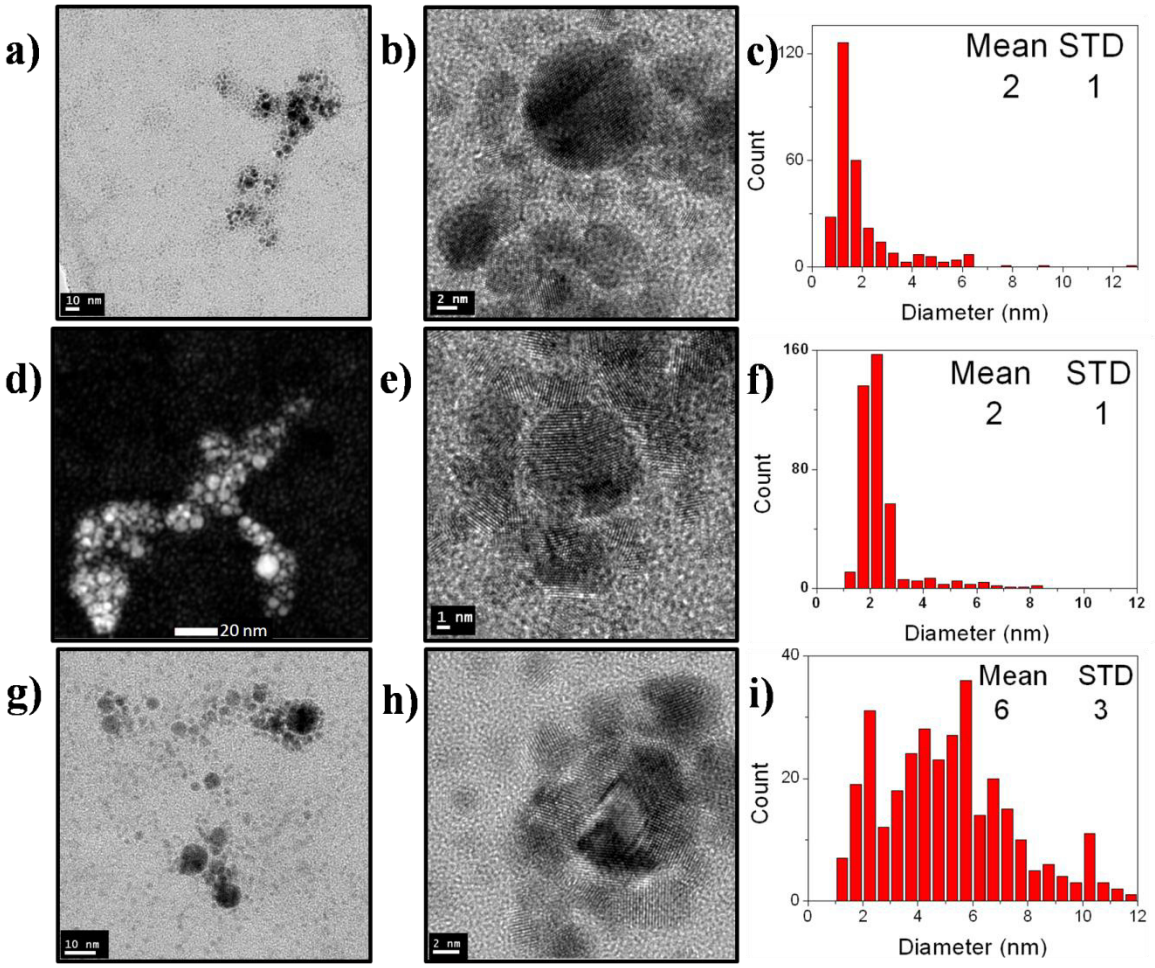

Figure 64. BF, STEM micrographs and size distribution of Pt nanoparticles obtained by PLAL using 532 nm in acetone at (a, b, c) 9, (d, e, f) 19 and (g, h, i) 25 J/cm^2 of energy fluence.

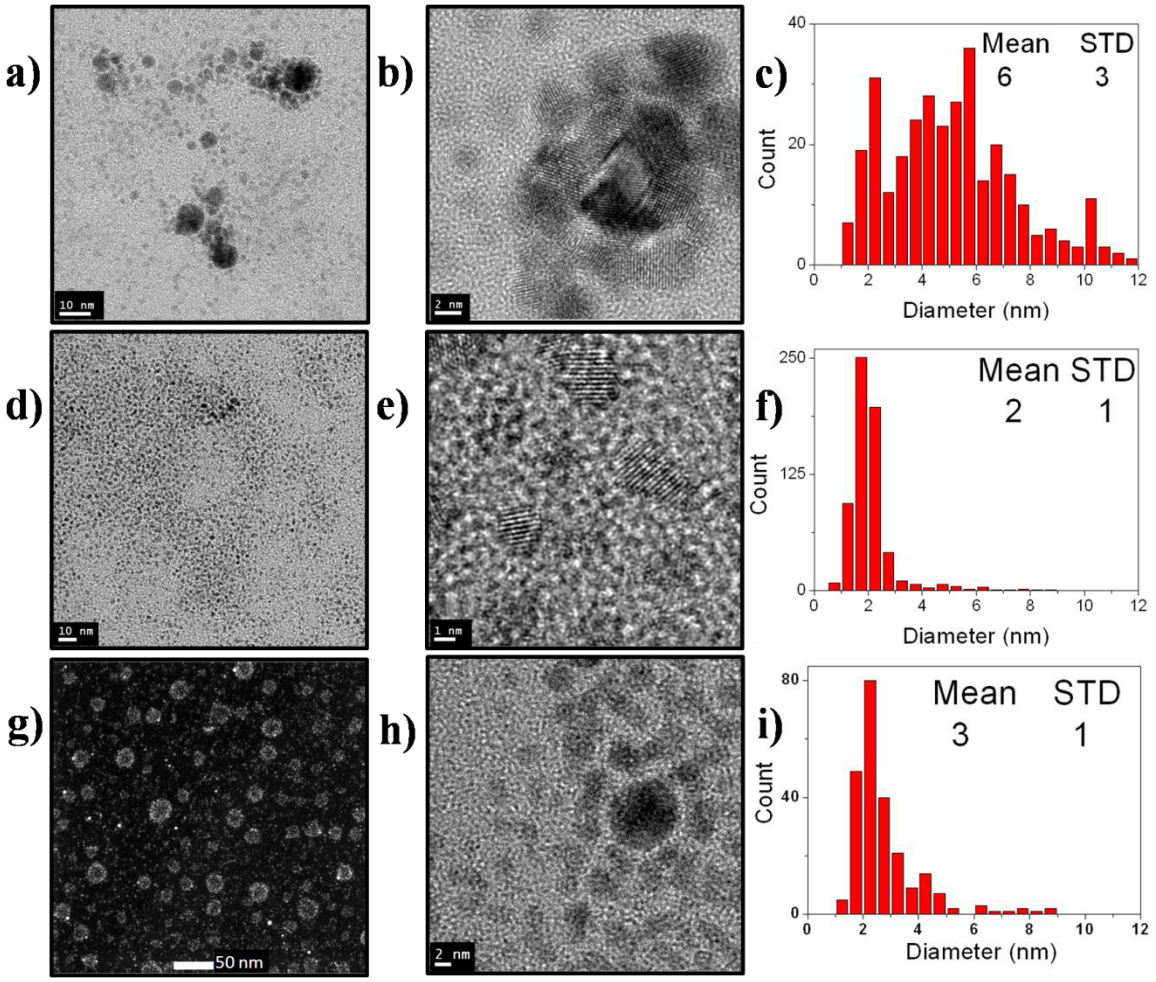

Figure 65. BF, STEM micrographs and size distribution of Pt nanoparticles obtained by PLAL using 532 nm in acetone at 25 J/cm^2 of energy fluence with (a, b, c) 5, (d, e, f) 10 and (g, h, i) 15 minutes of laser ablation.

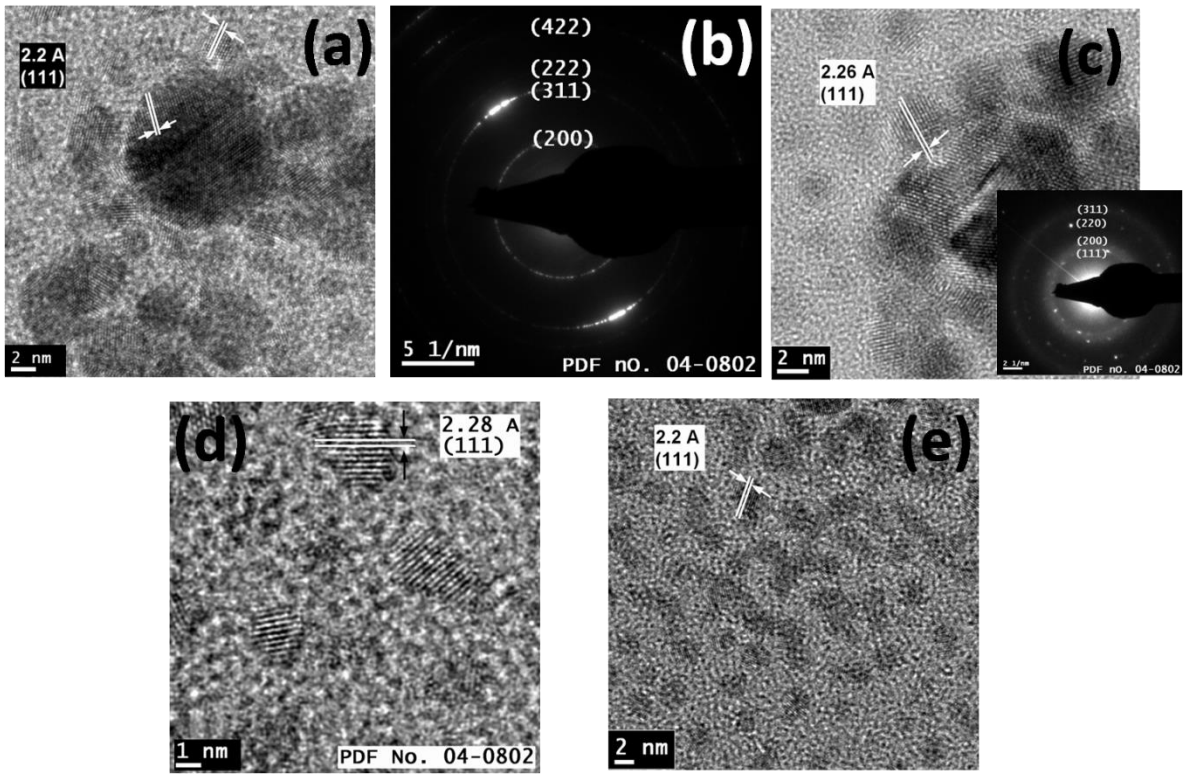

Figure 66. HRTEM and SAED micrographs of Pt nanoparticles synthesized by PLAL in acetone at a) 9, b) 19 and c) 25 J/cm^2 for 5 minutes (532 nm). HRTEM images d) and e) correspond to 25 J/cm^2 for 10 and 15 minutes, respectively.

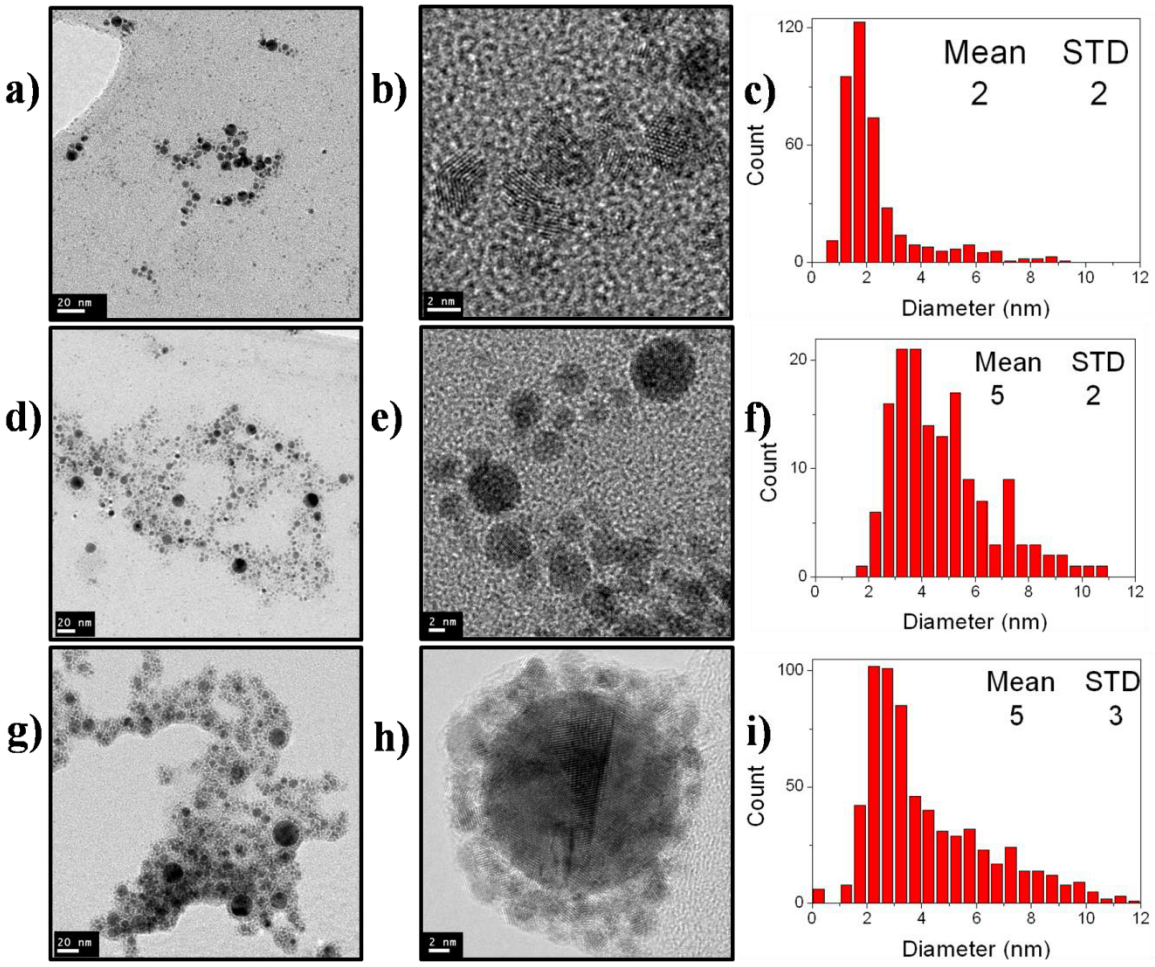

Figure 67. BF, STEM micrographs and size distribution of Pt nanoparticles obtained by PLAL using 532 nm in ethanol at (a, b, c) 9, (d, e, f) 19 and (g, h, i) 25 J/cm^2 of energy fluence.

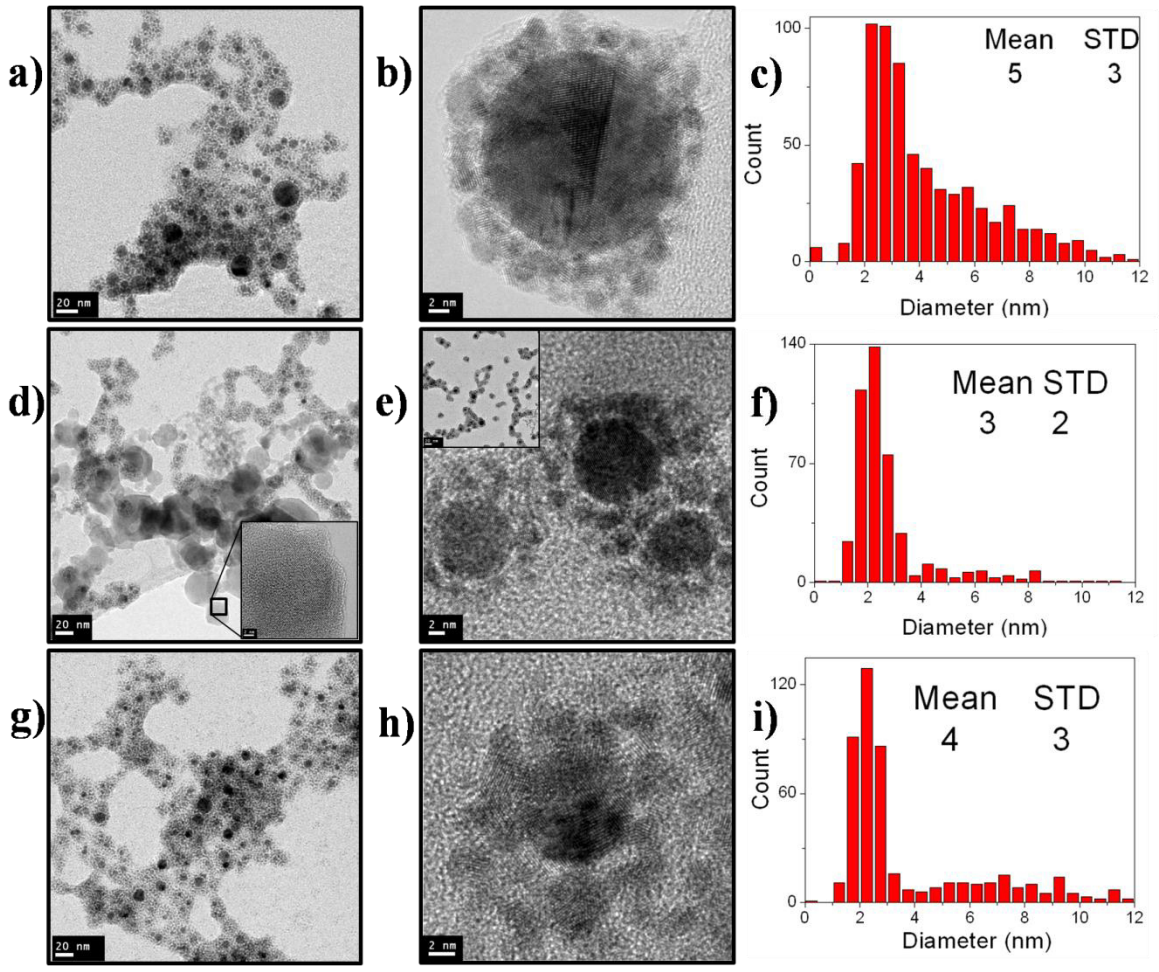

Figure 68. BF and STEM micrographs of Pt nanoparticles obtained by PLAL using 532 nm in ethanol at 25 J/cm^2 of energy fluence with (a, b) 5, (c, d) 10 and (e, f) 15 minutes of laser ablation.

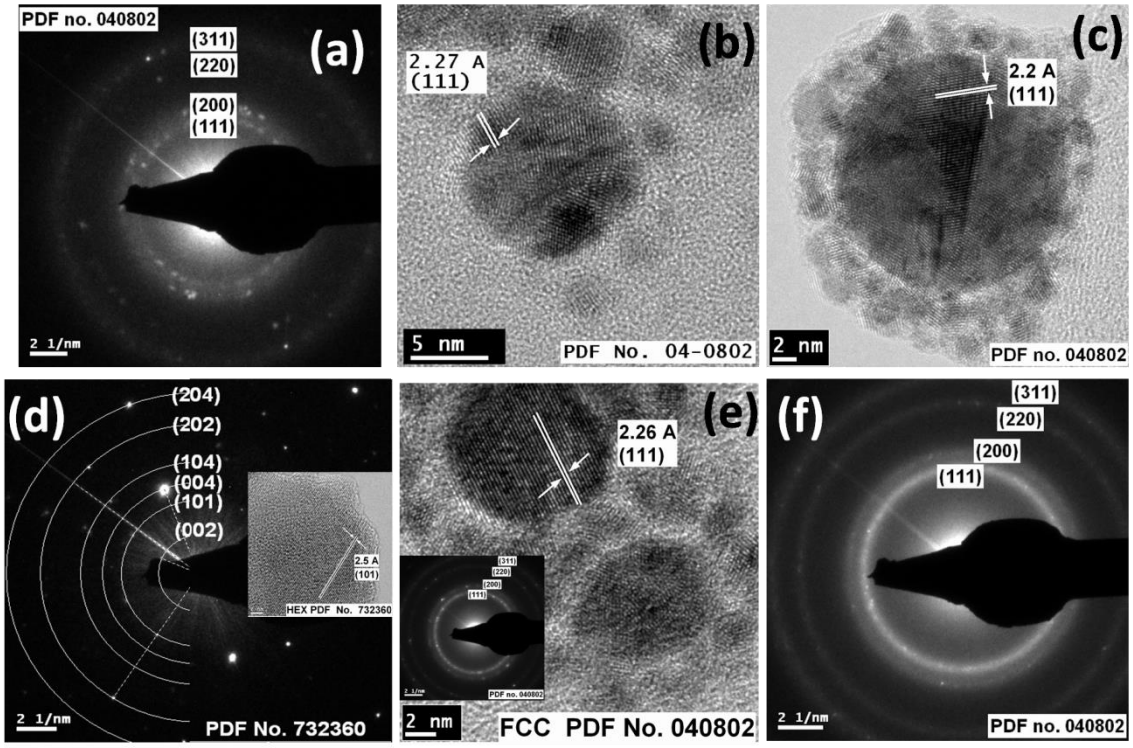

Figure 69. HRTEM and SAED micrographs of Pt nanoparticles synthesized by PLAL in ethanol at a) 9, b) 19 and c) 25 J/cm^2 for 5 minutes (532 nm). Micrographs of Pt NPs obtained at 25 J/cm^2 for (d, e) 10 minutes and f) 15 minutes.

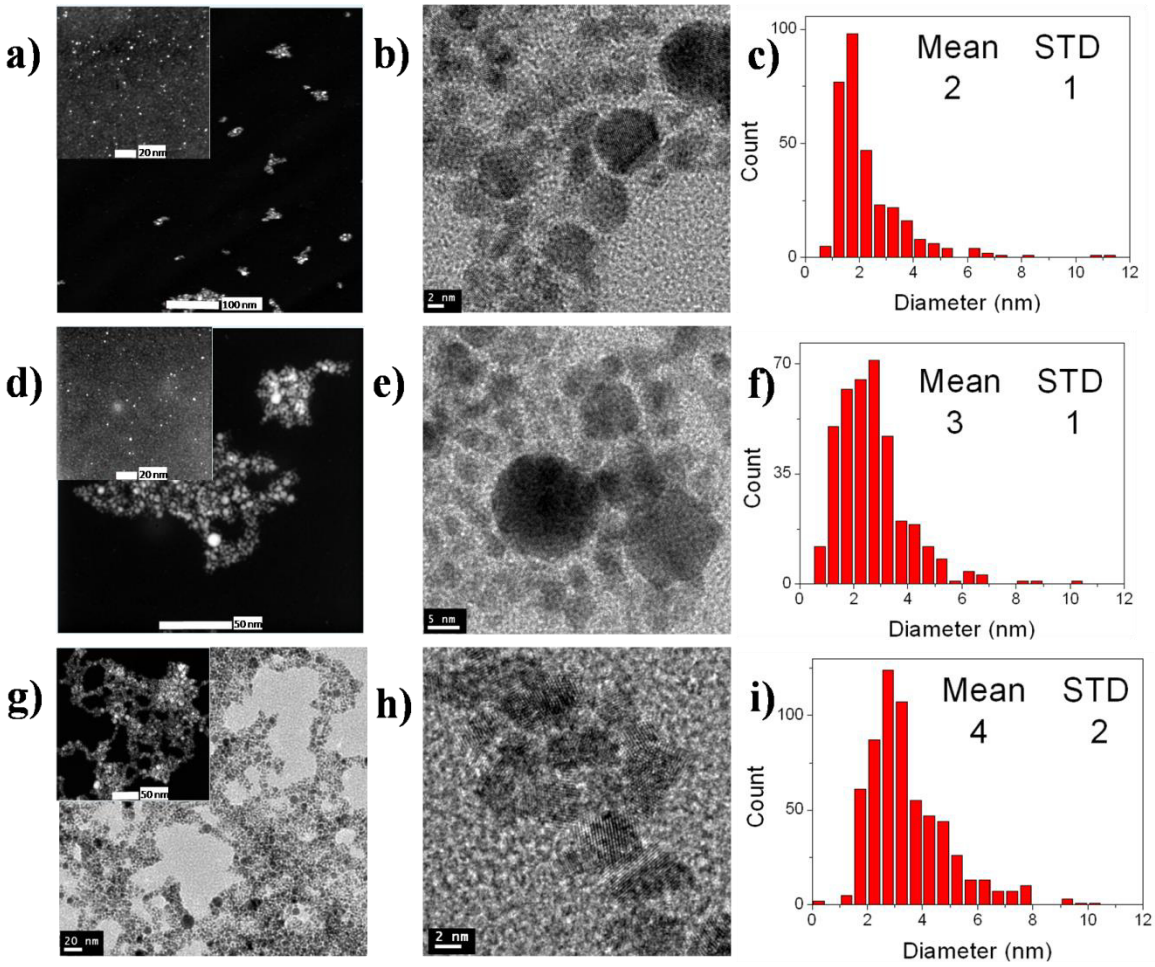

Figure 70. BF, STEM micrographs and size distribution of Pt nanoparticles obtained by PLAL using 532 nm in methanol at (a, b, c) 9, (d, e, f) 19 and (g, h, i) 25 J/cm^2 of energy fluence.

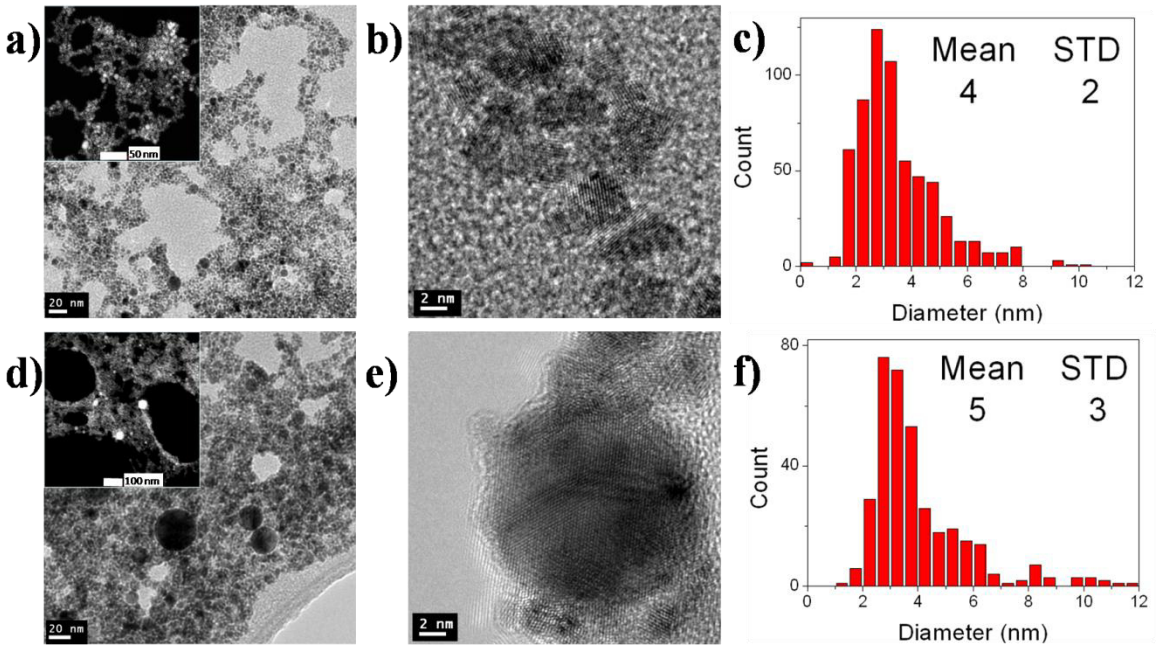

Figure 71. BF, STEM micrographs and size distribution of Pt nanoparticles obtained by PLAL using 532 nm in methanol at 25 J/cm^2 of energy fluence with (a, b, c) 5 and (d, e, f) 15 minutes of laser ablation.

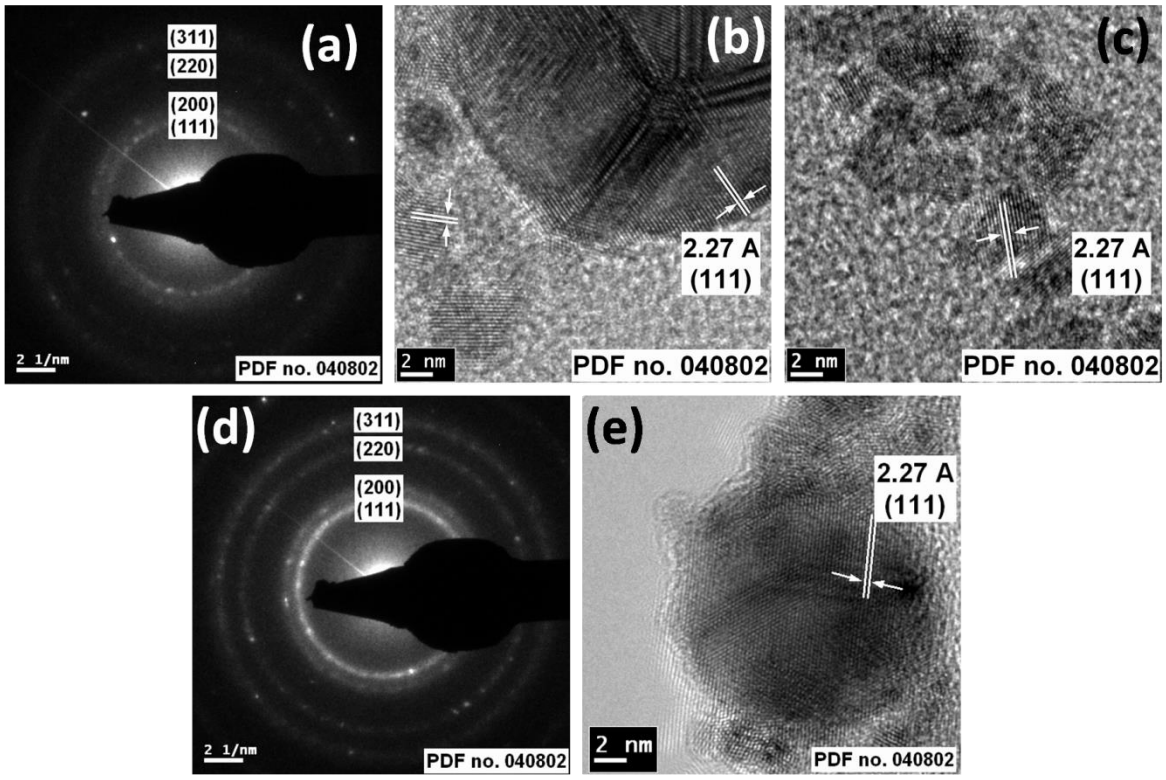

Figure 72. HRTEM and SAED micrographs of Pt nanoparticles synthesized by PLAL in methanol at a) 9, b) 19 and c) 25 J/cm^2 for 5 minutes (532 nm). HRTEM images d) and e) correspond to 25 J/cm^2 for 15 minutes.

5.3.2. Elemental Composition by EDX and XPS

Chemical composition of Pt nanoparticles synthesized by PLAL in different liquid media was determined by EDX detector associated with TEM and X-ray photoelectron spectroscopy. In the case of EDX characterization the NPs sample obtained at 25 J/cm^2 for 15 minutes of ablation was analyzed. STEM micrographs along with its EDX spectrum are shown in figure 73a) smaller NPs groups and b) a big agglomerated of Pt NPs. In both EDX spectra appeared Pt and O signals, this former with less contribution (in %wt) in the spectrum over the big agglomerated probably due the high density of the NPs in comparison with smaller NPs. The presence of oxygen could be in agreement with the detection of PtO_2 in SAED and HRTEM micrographs of flakes Pt NPs. Since EDX is a qualitative analysis technique with no chemical state information, XPS analysis was performed for all the liquid media.

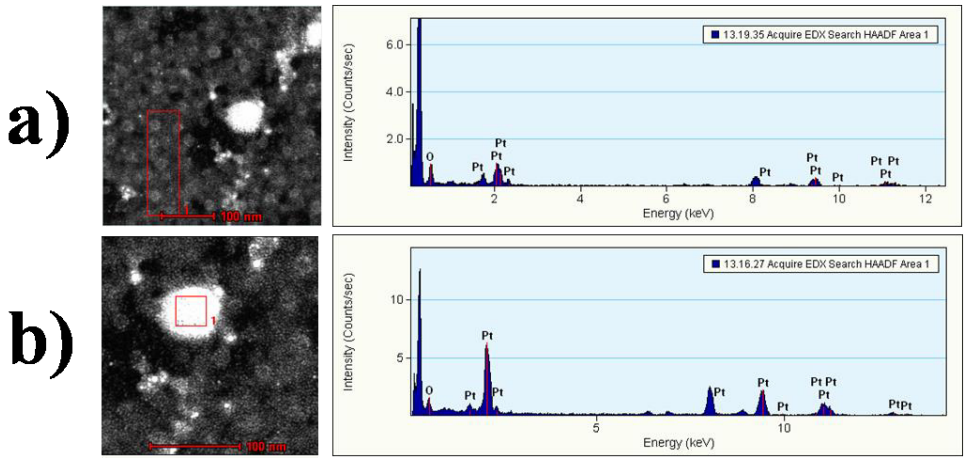

Figure 73. STEM and EDX spectrum of Pt NPs synthesized by PLAL (532 nm) in acetone at 19 J/cm^2 for 15 minutes of ablation.

Pt nanoparticles obtained by PLAL in acetone, ethanol and methanol also were analyzed by XPS. The results obtained were very similar for all the liquid media. Figure 74 shows the XPS spectra of Pt NPs in acetone, in which the high resolution photoelectron peaks $4f_{7/2}$ and $4f_{5/2}$ at 72.02 and 75.22 eV, respectively correspond to Pt^0 [285, 286]. Figures 75 and 76 show the spectrum of Pt NPs in ethanol and methanol, respectively. The peaks at binding energies of 71.22 and 70.86 eV (ethanol and methanol, respectively) for Pt $4f_{7/2}$ were assigned to Pt^0 [287, 288].

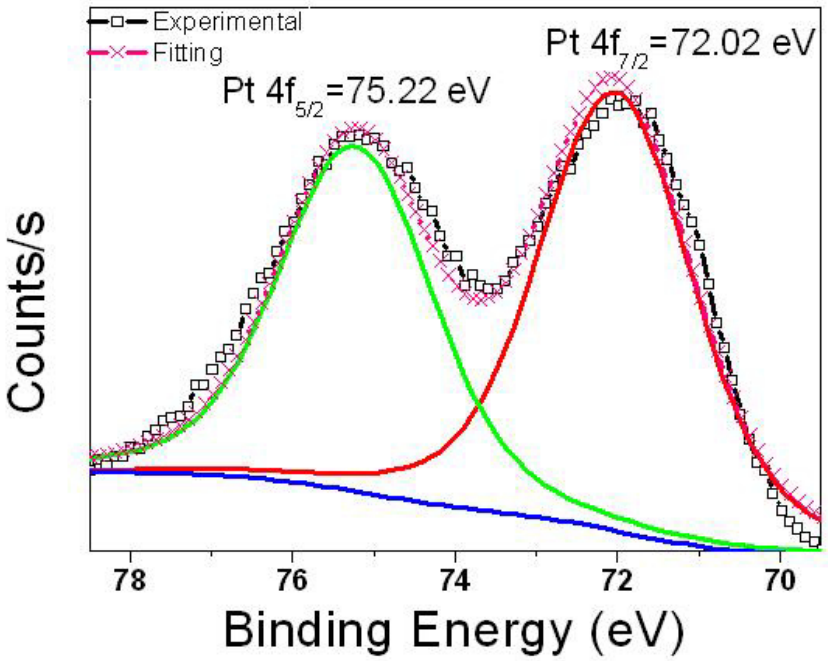

Figure 74. High resolution XPS spectrum of Pt 4f core level correspondent to Pt NPs synthesized by PLAL in acetone.

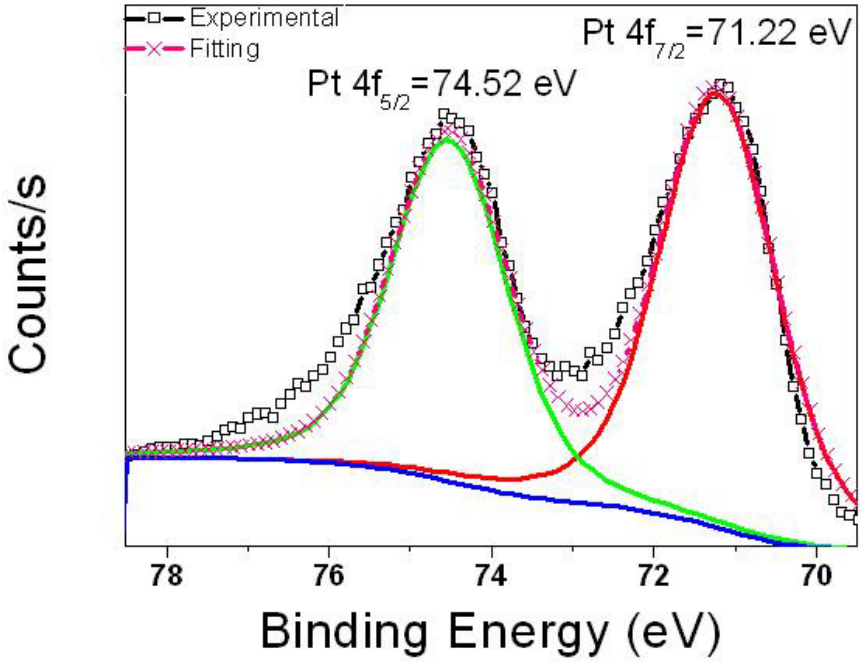

Figure 75. High resolution XPS spectrum of Pt 4f core level correspondent to Pt NPs synthesized by PLAL in ethanol.

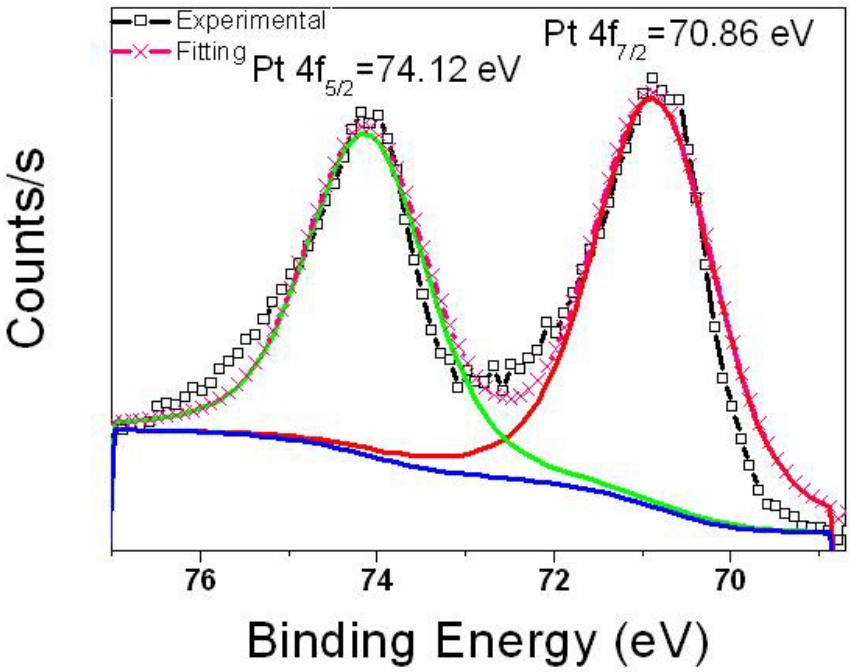

Figure 76. High resolution XPS spectrum of Pt 4f core level correspondent to Pt NPs synthesized by PLAL in methanol.

5.3.3. Optical Properties by UV-Vis

Optical properties of Pt nanocolloids synthesized by PLAL were investigated by UV-Vis absorption spectroscopy. Optical absorption spectra of the Pt nanocolloids were measured immediately after ablation in each liquid media. For Pt nanocolloids obtained in acetone and ethanol measurements were repeated after 49 days. Figure 77 shows UV-Vis absorption spectra of Pt nanocolloids obtained in acetone at different energy fluence: a) as prepared and b) after 49 days of PLAL experiments. The spectra of as-prepared Pt nanocolloids display a broad absorption band with the maximum intensity around 328-335 nm and the intensity continuously decreases from the UV towards the visible region. The maximum absorption intensity (related to higher concentration of NPs) appeared for NPs formed at the lower energy fluence which may be due to increase in the spot area of ablation. According to the literature [252, 253] and theoretical calculations [281], Pt spherical nanoparticles of around 10 nm presented an optical band in the far UV (< 215 nm in water) and was attributed to inter-band transitions. In this case, the peak appeared at around 330 nm, which are in agreement with the reported by J. B. You [289], which

presented a spectra with size dependence and peaks at even 450 nm for Pt NPs with an average size of 8 nm. The spectra of Pt NPs in acetone (b) obtained after 49 days presented the same structure but with a little red shift of around 4-3 nm; which could be related to aggregation of Pt NPs in the solution. Figure 78 (a) illustrates the optical spectrum of Pt NPs obtained in acetone at 25 J/cm^2 for 5, 10 and 15 minutes of PLAL. As expected, high absorption intensity for higher time of ablation was 3 times as that for 5 minutes. The peak appeared at 329, 332 and 334 nm for 5, 10 and 15 minutes, respectively, the small red shift presented in the spectra can be due to an aggregation effect originated from the higher concentration of Pt NPs. This effect is in agreement with observations in TEM images, in which different time of ablation affected size of NPs. Figure 78 (b) shows the spectrum after 49 days of PLAL experiments. The optical spectrum shows a similar structure to the as-prepared Pt NPs in acetone at 25 J/cm^2 which would be related to better stability of nanocolloidal Pt in acetone. Figure 79 (a) corresponds to as-prepared Pt NPs in ethanol at different energy fluence for 5 minutes. The UV-Vis absorption spectra presented a broad peak with the maximum absorption intensity at 241, 246 and 242 nm for NPs formed at 9, 19 and 25 J/cm^2, respectively (similar to reports in literature [281, 290]). Similar to Pt NPs in acetone, higher absorption intensity was obtained at lower energy fluence and medium energy fluence presented a red shifted peak with respect to other ones. Figure 79 (b) shows the spectrum of Pt NPs in ethanol at different energy fluence after 48 days of the experiments. In this case, the single broad absorption peak changed to two narrows peaks. The first and second peaks appeared at 206 nm and 280 nm, respectively for all the energy fluence. E. Gharibshahi et al. [291] reported the optical absorption spectra of Pt NPs with two peaks at 216 and 264 nm. These peaks were attributed to intra-band transitions of conduction electrons to higher energy states. Figure 80 (a) shows the as-prepared Pt NPs in ethanol at 25 J/cm^2 for different time of ablation. The spectrum presented a broad peak at 242, 238 and 230 nm for 5, 10 and 15 minutes, respectively. Contrary to the result obtained in acetone in which the increase in the ablation time induced a red shift in the spectrum, in this case, a blue shift was detected. Figure 80 (b) presents Pt NPs in ethanol at different time of ablation after 48 days. The spectrum also presented the separation of the single peak to two peaks at 205-206 and 276-280 nm (as in figure 79-b). Figure 81 (a) corresponds to Pt NPs in methanol at different energy fluence. The spectrum was similar to that obtained

in acetone, but with the maximum intensity at 231, 234 and 233 nm for 9, 19 and 25 J/cm^2, respectively. The maximum intensity absorption corresponded to lower energy fluence, as the results obtained in the other liquid media. Figure 81 (b) shows Pt nanocolloids in methanol at 25 J/cm^2 with different time of ablation. The maximum intensity absorption was at 233, 228 and 223 nm for 5, 10 and 15 minutes, respectively.

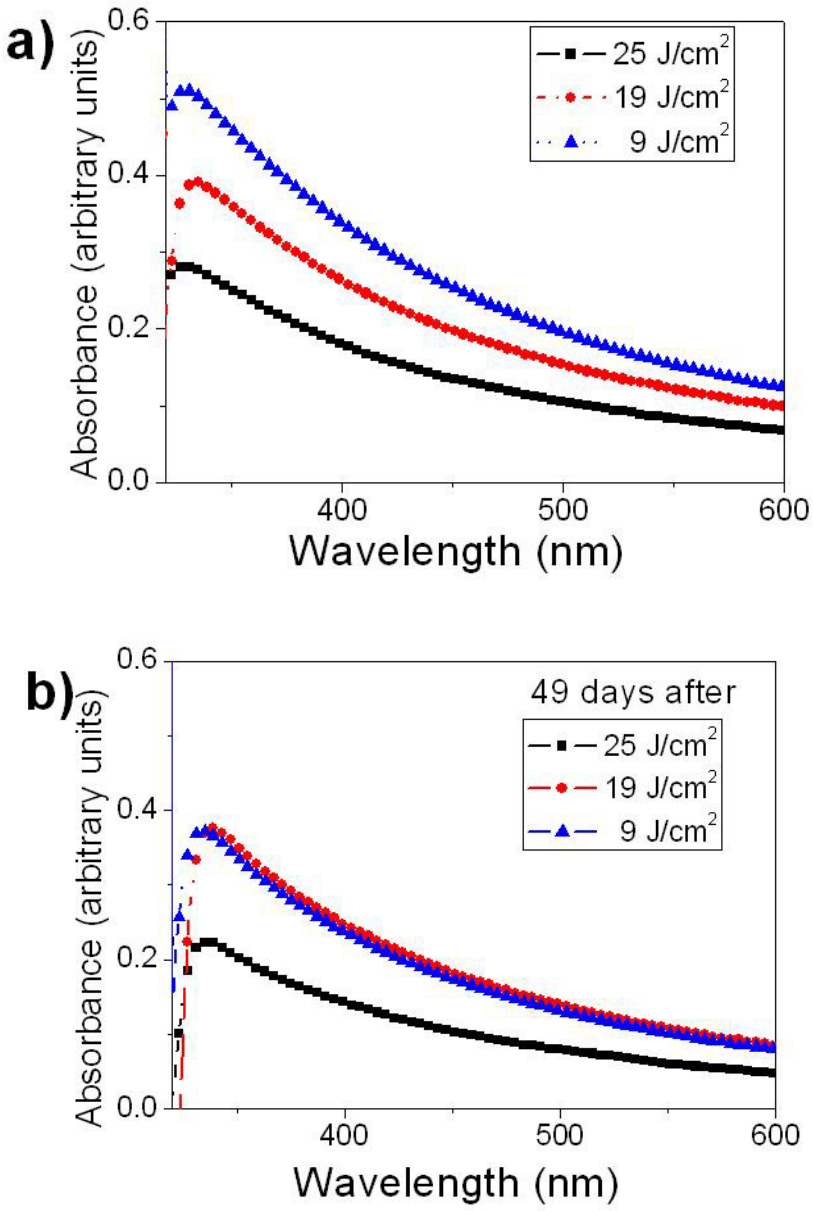

Figure 77. UV-Vis absorption spectra of Pt NPs synthesized by PLAL in acetone with different energy fluence: a) as prepared Pt NPs and b) after 49 days.

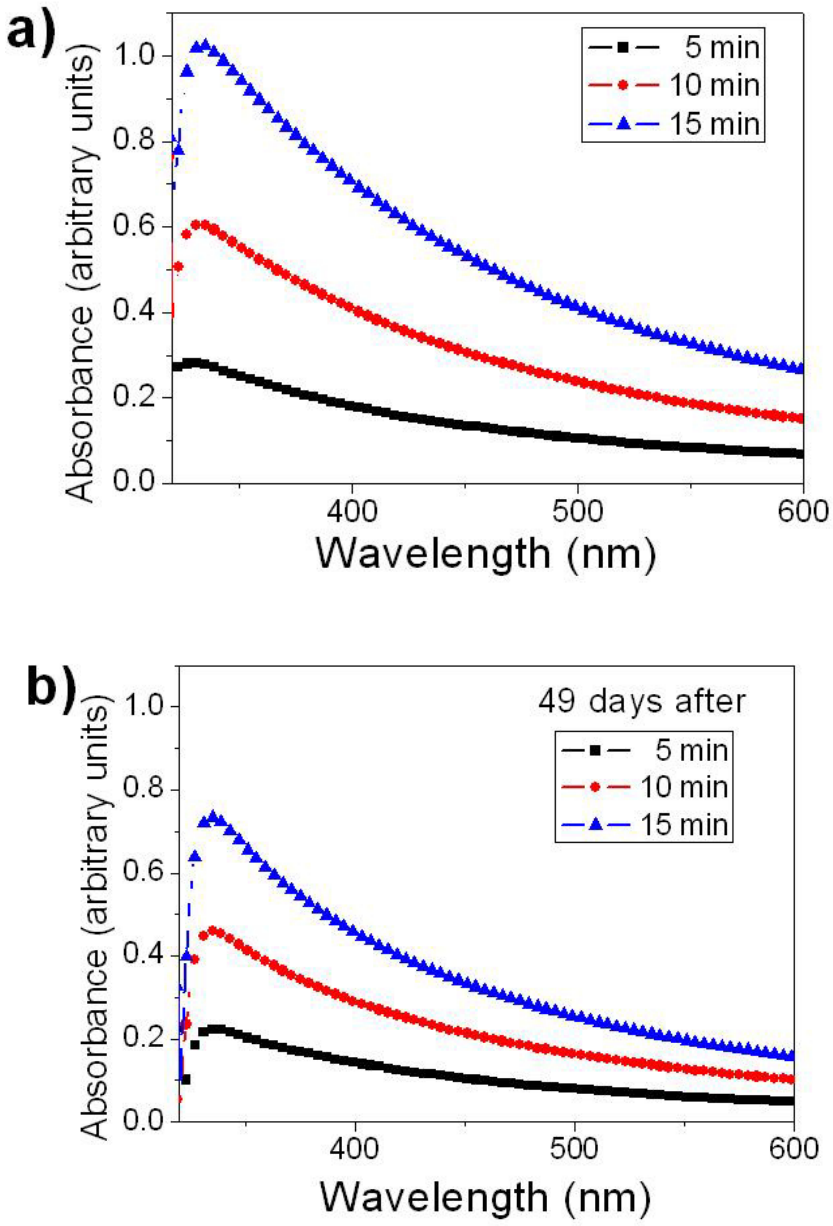

Figure 78. UV-Vis absorption spectra of Pt NPs synthesized by PLAL in acetone at 25 J/cm^2 of energy fluence with different time of ablation: a) as prepared Pt NPs and b) after 49 days.

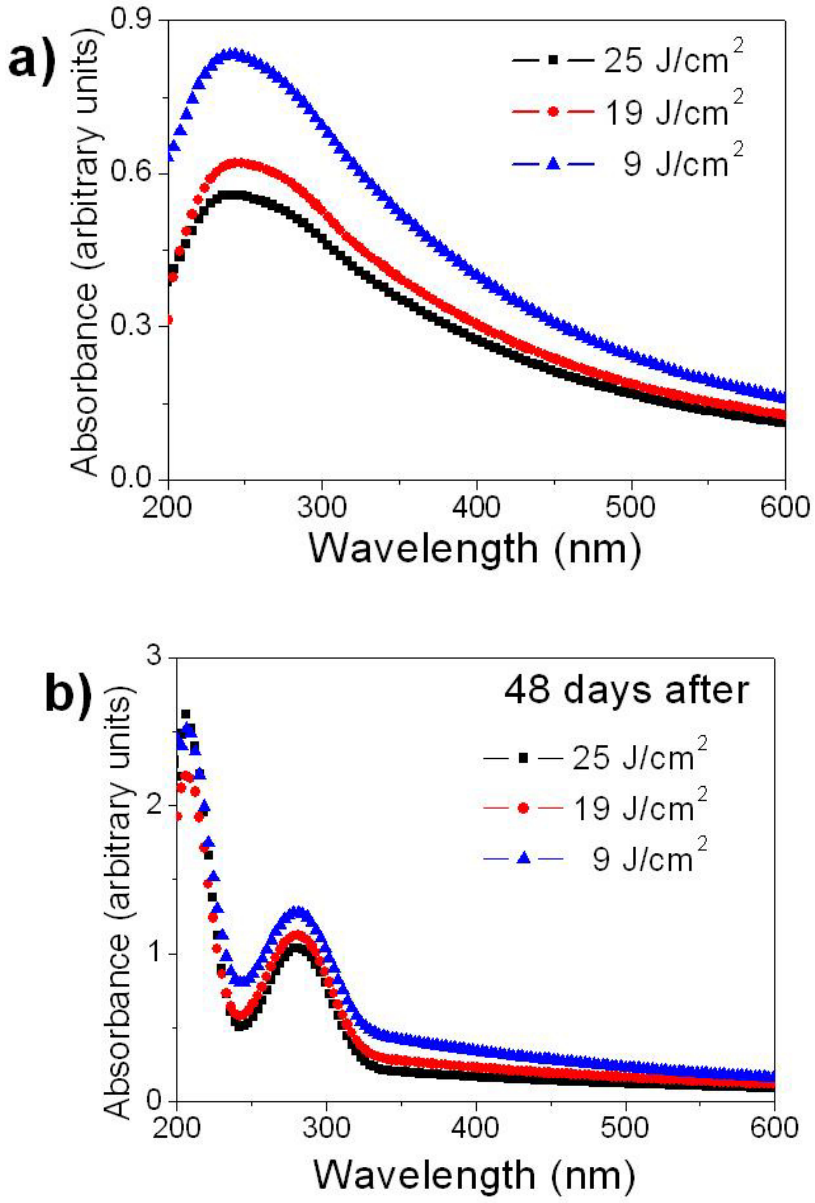

Figure 79. UV-Vis absorption spectra of Pt NPs synthesized by PLAL in ethanol with different energy fluence: a) as prepared Pt NPs and b) after 48 days.

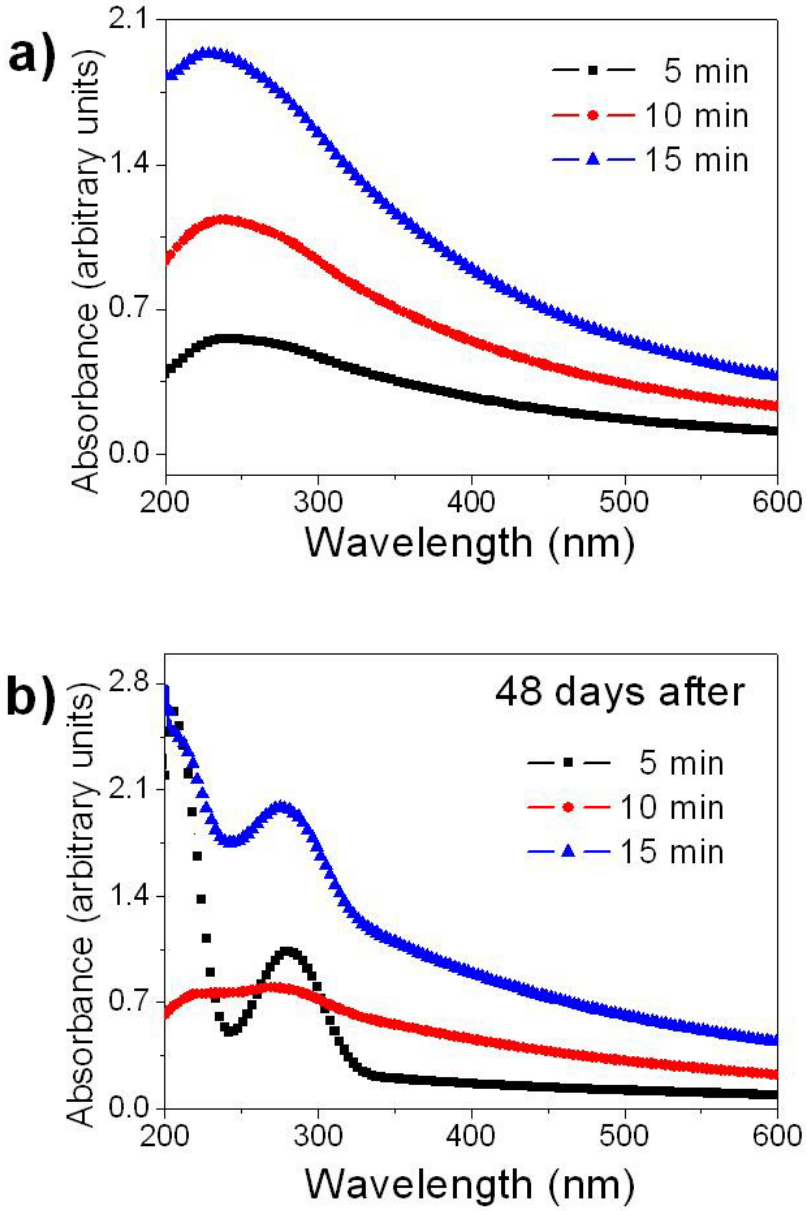

Figure 80. UV-Vis absorption spectra of Pt NPs synthesized by PLAL in ethanol at 25 J/cm^2 of energy fluence with different time of ablation: a) as prepared Pt NPs and b) after 48 days.

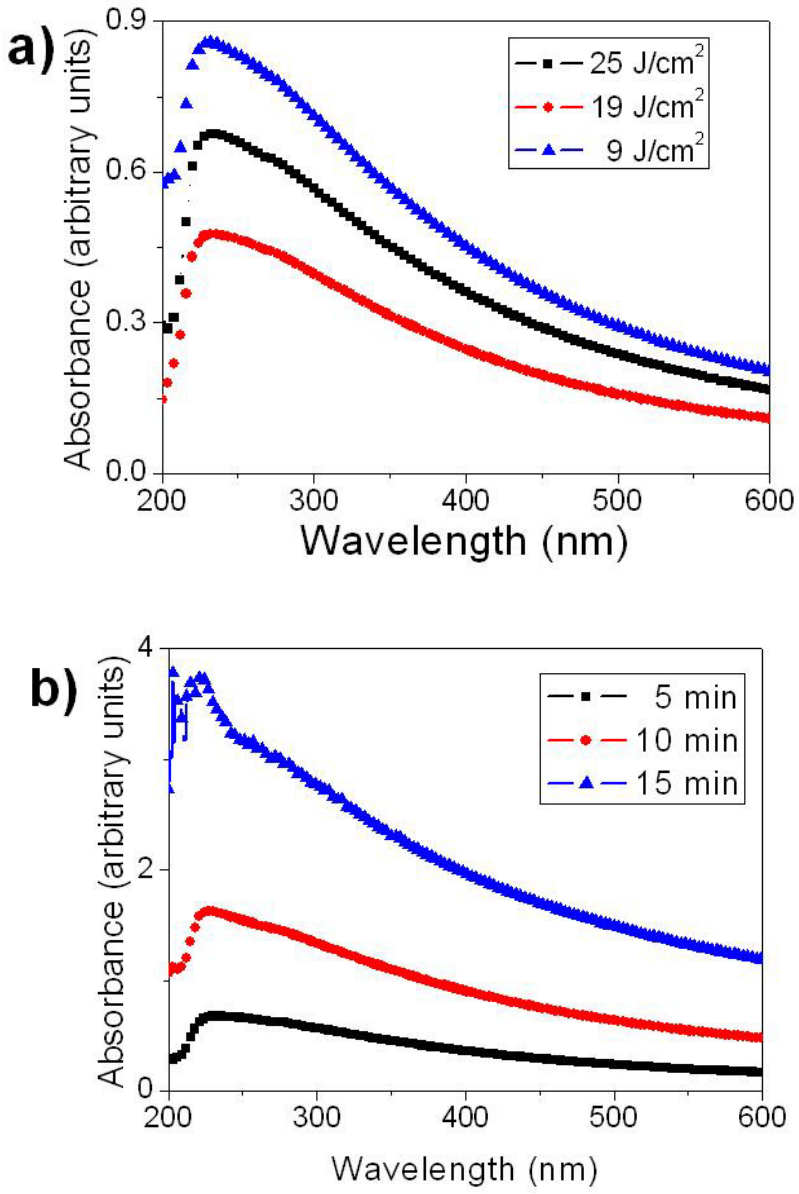

Figure 81. UV-Vis absorption spectra of Pt NPs synthesized by PLAL in acetone: a) with different energy fluence and b) at 25 J/cm^2 of energy fluence with different time of ablation.

In this experiment, Pt nanoparticles were synthesized by PLAL in acetone, ethanol and methanol at different energy fluence and time of ablation. The conclusions were the follow; i) Pt NPs with small average size of around 2-6 nm were obtained for all the liquid media with a narrow size distribution; ii) Contrary to the bimodal size distribution reported

of Pt NPs by PLAL [251, 254], a monomode size distribution for all the liquid media was obtained in these experiments; iii) Elemental composition analyzed by XPS confirmed the formation of Pt^0 NPs for all the liquid media; iv) UV-Vis absorption spectrum of Pt NPs in acetone showed peaks at higher wavelengths in comparison with that obtained for ethanol and methanol; v) For all the liquid media (with respect to energy fluence), higher absorption intensity was obtained for lower energy fluence; vi) Time of ablation showed an effect over the peak position of absorption spectrum, although in TEM images there was a little change in size; vii) Stability of nanocolloids in acetone was confirmed by UV-Vis absorption spectroscopy with measurements after 49 days of PLAL experiments; and finally viii) Absorption spectrum of Pt NPs in ethanol after days presented difference of the as prepared Pt NPs, in which the initial broad peak changed to two narrow peaks.

CHAPTER 6

CONCLUSIONS

Pulsed laser ablation in liquids (PLAL) is a novel technique for synthesis of a great diversity of nanomaterials. This thesis presents the synthesis of nanocolloids of gold, silver, palladium and platinum by PLAL. Gold and silver nanoparticles were synthesized by PLAL using 1064 and 532 nm of wavelength in DW at 40.5 and 27.6 J/cm^2 of energy fluence, respectively. For gold and silver, the effect of in-situ and post-irradiation of a continuous wave laser (at 532 and 457 nm of wavelength) was studied. Morphology (size and size distribution using TEM), crystalline structure (HRTEM and SAED), chemical composition (XPS) and optical properties (UV-Vis absorption) were studied in terms of ablation wavelength. The elemental composition of gold and silver nanoparticles was confirmed as metallic state by XPS spectroscopy. **Gold** nanoparticles obtained at all conditions (wavelength, single PLAL, in-situ and post irradiation of CW lasers) were in general spherical with average size in a range of Ø= 11-16 and 9 nm, respectively for 1064 and 532 nm of ablation wavelengths. In case of gold nanoparticles synthesized by PLAL using 532 nm at different conditions, of in-situ and post-irradiation with CW lasers (532 and 457) there were a few elongated gold nanoparticles. Crystalline structure of gold nanoparticles obtained at all conditions of our PLAL experiments was identified as FCC structure. Higher absorption intensity of gold NPs obtained at 1064 nm in comparison with 532 nm implied that the ablation yield increased when wavelength is increased. Optical spectrum of Au NPs obtained in the set of 1064 nm showed an increase in the absorption intensity for in-situ and post-irradiation for both CW lasers. In the case of Au NPs synthesized using 532 nm, the optical absorbance was higher due to in-situ and post-irradiation by CW 532 nm. In general, absorbance of gold nanocolloids was higher for both in-situ and post-irradiated cases by continuous wave laser in comparison with those or single PL for each set using 1064 and 532 nm. Stability of gold NPs obtained in the set of 532 nm was measured indirectly by UV-Vis absorption spectrum after days. The optical spectrum showed a broadening plasmon peak for single-PL 532 and In-situ CW532 which indicate the agglomeration of nanoparticles and an additional plasmon peak (for in-situ CW457, post CW532 and post CW457) which was related to ellipsoidal NPs. **Silver**

nanoparticles obtained by PLAL using 1064 and 532 nm of pulsed laser wavelength were spherical (both) with average size in a range of 24-8 and 12-5 nm, respectively. Silver nanocolloids obtained using 1064 nm were smaller (Ø= 11-8 nm) due to post-irradiation at both CW. Silver NPs obtained in both cases (1064 and 532 nm) showed higher average size after in-situ CW irradiation by 457 nm. Such NPs possessed hexagonal crystalline structure for in-situ CW 457 condition and both FCC and hexagonal for post-irradiation. As in the case of gold NPs, higher production of Ag NPs resulted at higher ablation wavelength which was evident from the higher optical absorbance in the UV-Vis spectra. The plasmon peaks of silver NPs for single PL1064, after in-situ CW532 and post irradiated CW532 were detected at 396, 395 and 394 nm, respectively in accordance with variation in average size of the NPs. The effect of in-situ and post-irradiation of CW at 457 nm laser was to increase in the optical absorbance of silver nanocolloids. The plasmon peaks of silver NPs obtained using 532 nm ablation for single, in-situ CW532 and post CW were detected at 398, 398 and 400 nm, respectively. Higher absorption intensity was observed for Ag nanocolloids obtained after in-situ CW 457. Plasmon peaks of Ag NPs (set of 532 nm) recorded after 13 days (aging effect) was broader being more evident in the case of NPs after post-irradiation (at both CW) treatments than in the case of the particles obtained with in-situ CW irradiation. **Palladium** nanoparticles were synthesized by PLAL using 1064 nm in different liquid media such as DW, methanol-water mixture, 0.001 M of SDS and ethylene glycol. Morphology (particle shape, size and size distribution), crystalline structure, chemical composition and optical properties were studied as a function of selected laser energy fluence and the nature of liquid media. Post-irradiation and ultrasonic treatments were performed on the precipitates of the as prepared NPs colloids after a few months of aging (2-3 months after the PLAL experiments to obtain the NPs). Results implied that the nature of liquid affects the laser ablation process and thus growth of the nanoparticles: therefore, their dimensions and concentrations changed. Morphology of as-prepared Pd NPs obtained in distilled water and SDS was spherical with an average size in a range of Ø= 17-27 nm and 33-21nm, respectively. In mixture of methanol-water (1:1) spherical and interconnected NPs of Ø= 13±4 nm and 4 nm, respectively in average size were observed. Moreover, as-prepared Pd NPs in EG were spherical, well dispersed and completely embedded in the organic liquid medium. The SAED and HRTEM analysis

showed that Pd NPs present FCC structure irrespective of the liquid media. The average size and yield of Pd nanoparticles depended on the variation of energy fluence. For as-prepared Pd NPs, in DW the average size increased with decrease in fluence while in SDS it decreased as fluence decreased. In methanol-water mixture there was no effect of the ablation fluence on the nanoparticle size. The yield of Pd NPs in DW and SDS was higher for the case obtained at higher energy fluence, contrary to methanol-water mixture and EG. Smaller sizes of as-prepared Pd NPs were obtained in methanol-water mixture compared to other liquid media. XPS analysis of Pd NPs obtained by PLAL using 1064 nm showed elemental Pd^0 for DW and methanol-water mixture, confirmed by EDX spectroscopy. Meanwhile for SDS surfactant Pd NPs showed the presence of palladium in the metallic particles as well as oxidized Pd species. These oxides were formed due to partially oxidized nanoparticles surfaces by air-exposure. Laser post irradiation and ultrasonic treatment were effective to re-disperse the nanoparticles in solution and to retrieve their optical properties. **Platinum** nanoparticles were synthesized by PLAL in acetone, ethanol and methanol at different energy fluence and time of ablation. Morphology, crystalline structure, elemental composition, chemical state and optical properties were characterized by TEM, EDX, XPS and UV-Vis spectroscopy. Spherical Pt NPs with an average size of around 2-6 nm were obtained in all the liquid media showing a narrow size distribution. Elemental composition by XPS confirmed the formation of Pt^0 NPs. UV-Vis absorption spectrum of Pt NPs in acetone showed peaks at higher wavelengths in comparison with that obtained for ethanol and methanol. For all the liquid media (with respect to energy fluence), higher absorption intensity was obtained for lower energy fluence. Time of ablation showed an effect on the peak position of the absorption, although in TEM images there was little change in size. Stability of nanocolloids in acetone was confirmed by UV-Vis absorption spectroscopy with measurements after 49 days aging of the samples. Absorption spectrum of Pt NPs in ethanol after a few days presented a change with respect to the as prepared (freshly) Pt NPs, in which the broad peak changed to two narrow peaks due to aging.

General conclusions

As general conclusions, PLAL is an effective synthesis technique for metal nanoparticles. This is due to the simple and rapid formation of a great variety of nanoparticles as noble metals without changes in their chemical state and crystalline structure. In general Au, Ag, Pd and Pt NPs were spherical, well dispersed and stable for several months. Yield of NPs was affected by some parameters as: wavelength, liquid media, energy fluence and additional CW irradiation. In-situ and post-irradiation affected (in some conditions) both size and yield of metal NPs. Another important characteristic is the feasibility to obtain nanoparticles with narrow size distribution and high purity (in liquids as water and alcohols). Average size and yield of NPs is dominated by wavelength, energy fluence and liquid media.

REFERENCES

[1] G. Cao, Nanostructures & Nanomaterials, Imperial College Press, London, 2004.

[2] S.V. Aradhya, L. Venkataraman, Single-molecule junctions beyond electronic transport, Nature Nano, 8 (2013) 399-410.

[3] Shawn M. Douglas, Ido Bachelet, G.M. Church, A Logic-Gated Nanorobot for Targeted Transport of Molecular Payloads, Science, 335 (2012) 831-834.

[4] R.A. Freitas, Pharmacytes: An Ideal Vehicle for Targeted Drug Delivery, Journal of Nanoscience and Nanotechnology, 6 (2006) 2769-2775.

[5] A. Roy, P.J. Bhattacharya, Nanotechnology in Industrial Wastewater Treatment, IWA Publishing, 2015.

[6] O.V. Salata, Applications of nanoparticles in biology and medicine, Journal of Nanobiotechnology, 2 (2004) 3-3.

[7] Tranum Kaur, Nafiseh Nafissi, Olla Wasfi, Katlyn Sheldon, Shawn Wettig, R. Slavcev, Immunocompatibility of Bacteriophages as Nanomedicines, Journal of Nanotechnology, 2012 (2012) 1-13.

[8] J.B. Sambur, P. Chen, Approaches to Single-Nanoparticle Catalysis, Annual Review of Physical Chemistry, 65 (2014) 395-422.

[9] B. Hvolbæk, T.V.W. Janssens, B.S. Clausen, H. Falsig, C.H. Christensen, J.K. Nørskov, Catalytic activity of Au nanoparticles, Nano Today, 2 (2007) 14-18.

[10] A. Ayati, A. Ahmadpour, F.F. Bamoharram, B. Tanhaei, M. Mänttäri, M. Sillanpää, A review on catalytic applications of Au/TiO2 nanoparticles in the removal of water pollutant, Chemosphere, 107 (2014) 163-174.

[11] X. Lang, W. Xing-Cai, Z. Jun-Jie, Green preparation and catalytic application of Pd nanoparticles, Nanotechnology, 19 (2008) 305603.

[12] P.K. Rastogi, V. Ganesan, S. Krishnamoorthi, Palladium nanoparticles decorated gaur gum based hybrid material for electrocatalytic hydrazine determination, Electrochimica Acta, 125 (2014) 593-600.

[13] S. Cheong, J.D. Watt, R.D. Tilley, Shape control of platinum and palladium nanoparticles for catalysis, Nanoscale, 2 (2010) 2045-2053.

[14] P.S. Roy, J. Bagchi, S.K. Bhattacharya, Synthesis of polymer-protected palladium nanoparticles of contrasting electrocatalytic activity: A comparative study with respect to reflux time and reducing agents, Colloids and Surfaces A: Physicochemical and Engineering Aspects, 359 (2010) 45-52.

[15] F. Christian, Edith, Selly, D. Adityawarman, A. Indarto, Application of nanotechnologies in the energy sector: A brief and short review, Front. Energy, 7 (2013) 6-18.

[16] V. Mlinar, Engineered nanomaterials for solar energy conversion, Nanotechnology, 24 (2013) 042001.

[17] W.A. Badawy, A review on solar cells from Si-single crystals to porous materials and quantum dots, Journal of Advanced Research, 6 (2015) 123-132.

[18] C.S. Sandeep, S. ten Cate, J.M. Schins, T.J. Savenije, Y. Liu, M. Law, S. Kinge, A.J. Houtepen, L.D. Siebbeles, High charge-carrier mobility enables exploitation of carrier multiplication in quantum-dot films, Nature communications, 4 (2013) 2360.

[19] L. Tong, H. Wei, S. Zhang, H. Xu, Recent advances in plasmonic sensors, Sensors (Basel), 14 (2014) 7959-7973.
[20] Matthew E. Stewart, Christopher R. Anderton, Lucas B. Thompson, Joana Maria, Stephen K. Gray, John A. Rogers, R.G. Nuzzo, Nanostructured plasmonic sensors, Chem. Rev., 108 (2008) 494-521.
[21] Yat Li, Fang Qian, Jie Xiang, C.M. Lieber, Nanowire electronic and optoelectronic devices, Materials Today, 9 (2008) 18-27.
[22] V. Stavila, A.A. Talin, M.D. Allendorf, MOF-based electronic and opto-electronic devices, Chemical Society Reviews, 43 (2014) 5994-6010.
[23] P. Bhattacharya, S. Ghosh, A.D. Stiff-Roberts, Quantum Dot Opto-Electronic Devices, Annual Review of Materials Research, 34 (2004) 1-40.
[24] O.Y. Loh, H.D. Espinosa, Nanoelectromechanical contact switches, Nature Nano, 7 (2012) 283-295.
[25] K. L. Ekinci, M. L. Roukes, Nanoelectromechanical systems, Review of Scientific Instruments, 76 (2005) 061101.
[26] J. Ramsden, Nanotechnology: An Introduction, William Andrew, 2011.
[27] A. Pimpin, W. Srituravanich, Review on Micro- and Nanolithography Techniques and their Applications, Engineering Journal, 16 (2012) 37-56.
[28] S. M. Attia, Jue Wang, Guangming Wu, Jun Shen, J. Ma, Review on Sol-Gel derived coatings- process, techniques and optical applications, J. Mater Sci. Technol, 18 (2002) 211-218.
[29] T.K. Tseng, Y.S. Lin, Y.J. Chen, H. Chu, A review of photocatalysts prepared by sol-gel method for VOCs removal, International journal of molecular sciences, 11 (2010) 2336-2361.
[30] Y. Zhang, L. Zhang, C. Zhou, Review of Chemical Vapor Deposition of Graphene and Related Applications, Accounts of Chemical Research, 46 (2013) 2329-2339.
[31] Yi Zhang, L. Zhang, C. Zhou, Review of Chemical Vapor Deposition of graphene and related applications, Accounts of Chemical Research, 46 (2013) 2329-2339.
[32] A.I.Y. Tok, F.Y.C. Boey, X.L. Zhao, Novel synthesis of Al2O3 nano-particles by flame spray pyrolysis, Journal of Materials Processing Technology, 178 (2006) 270-273.
[33] A.K. Keshri, A. Agarwal, Plasma Processing of Nanomaterials for Functional Applications—A Review, Nanoscience and Nanotechnology Letters, 4 (2013) 228-250.
[34] F. Abraham, Homogeneous Nucleation Theory: The Pretransition Theory of Vapor Condensation, Elsevier Science, 2012.
[35] D.W. Oxtoby, Homogeneous nucleation: theory and experiment, Journal of Physics: Condensed Matter, 4 (1992) 7627.
[36] A. Mubarak, E. Hamzah, M.R.M. Toff, Review of Physical Vapour Deposition (PVD) techniques for hard coating, Jurnal Mekanikal, 20 (2005) 42-51.
[37] N. Selvakumar, H.C. Barshilia, Review of physical vapor deposited (PVD) spectrally selective coatings for mid- and high-temperature solar thermal applications, Solar Energy Materials and Solar Cells, 98 (2012) 1-23.
[38] O. Auciello, A.I. Kingon, A critical review of physical vapor deposition techniques for the synthesis of ferroelectric thin films, in: Applications of Ferroelectrics, 1992. ISAF '92., Proceedings of the Eighth IEEE International Symposium on, 1992, pp. 320-331.

[39] K. Thorkelsson, P. Bai, T. Xu, Self-assembly and applications of anisotropic nanomaterials: A review, Nano Today, 10 (2015) 48-66.
[40] H. Hu, M. Gopinadhan, C.O. Osuji, Directed self-assembly of block copolymers: a tutorial review of strategies for enabling nanotechnology with soft matter, Soft Matter, 10 (2014) 3867-3889.
[41] K. Ariga, J.P. Hill, M.V. Lee, A. Vinu, R. Charvet, S. Acharya, Challenges and breakthroughs in recent research on self-assembly, Science and Technology of Advanced Materials, 9 (2008) 014109.
[42] William M. Steen, J. Mazumder, Laser Material Processing, 4 ed., Springer-Verlag London, 2010.
[43] S.C. Singh, H.B. Zeng, C. Guo, W. Cai, Nanomaterials: Processing and Characterization with Lasers, Wiley, 2012.
[44] R. Eason, Pulsed Laser Deposition of Thin Films: Applications-Led Growth of Functional Materials, Wiley, 2007.
[45] D.B. Chrisey, G.K. Hubler, Pulsed Laser Deposition of Thin Films, Wiley, 1994.
[46] P. Afshani, Laser Vaporization Methods for the Synthesis of Metal and Semiconductor Nanoparticles: Graphene, Doped Graphene and Nanoparticles Supported on Graphene, 2013.
[47] C.R. Jones, Analytical Pyrolysis, Elsevier Science, 2012.
[48] R. Smith, Laser Pyrolysis of Methyl Esters and Other Selected Compounds, Chemistry)--University of Auckland, 2007.
[49] P. Colombo, Polymer Derived Ceramics: From Nano-structure to Applications, DEStech Publications, 2010.
[50] D. Straub, V.V. Subramanian, Laser-excited Chemical Vapor Deposition (LECVD) of Carbon Films, Ohio State University, 1991.
[51] J. Mazumder, A. Kar, Theory and Application of Laser Chemical Vapor Deposition, Springer US, 2013.
[52] H. Misawa, S. Juodkazis, 3D Laser Microfabrication: Principles and Applications, Wiley, 2006.
[53] K. Sugioka, M. Meunier, A. Piqué, Laser Precision Microfabrication, Springer Berlin Heidelberg, 2010.
[54] J. Wang, Two-photon Induced Photochemistry, in: Chemistry, University of Arizona, Ann Arbor, E. U. A. , 2007, pp. 298.
[55] A. Shah, C.U. . Interference Assisted Laser Induced Forward Transfer for Line Patterning, Concordia University (Canada), 2008.
[56] G. Yang, Laser Ablation in Liquids: Principles and Applications in the Preparation of Nanomaterials, Pan Stanford, 2012.
[57] C. Liu, A study of particle generation during laser ablation with applications, in: Engineering-Mechanical Enginnering, University of California, Berkeley, 2005, pp. 169.
[58] T. Tsuji, T. Yahata, M. Yasutomo, K. Igawa, M. Tsuji, Y. Ishikawa, N. Koshizaki, Preparation and investigation of the formation mechanism of submicron-sized spherical particles of gold using laser ablation and laser irradiation in liquids, Physical chemistry chemical physics : PCCP, 15 (2013) 3099-3107.
[59] H. Wang, K. Kawaguchi, A. Pyatenko, X. Li, Z. Swiatkowska-Warkocka, Y. Katou, N. Koshizaki, General bottom-up construction of spherical particles by pulsed laser

irradiation of colloidal nanoparticles: a case study on CuO, Chemistry, 18 (2012) 163-169.
[60] I. Yadroitsev, P. Bertrand, I. Smurov, Parametric analysis of the selective laser melting process, Applied Surface Science, 253 (2007) 8064-8069.
[61] Anna Giusti, Emilia Giorgetti, Simona Laza, Paolo Marsili, F. Giammanco, Multiphoton fragmentation of PAMAM G5-capped gold nanoparticles induced by picosecond laser irradiationat 532 nm, Journal of Physical Chemistry C, 111 (2007) 14984-14991.
[62] S. Besner, A.V. Kabashin, M. Meunier, Fragmentation of colloidal nanoparticles by femtosecond laser-induced supercontinuum generation, Applied Physics Letters, 89 (2006) 233122.
[63] S. Hashimoto, T. Uwada, M. Hagiri, R. Shiraishi, Mechanistic Aspect of Surface Modification on Glass Substrates Assisted by Single Shot Pulsed Laser-Induced Fragmentation of Gold Nanoparticles, The Journal of Physical Chemistry C, 115 (2011) 4986-4993.
[64] Kamat P. V., Fluminai M., H.G. V., Picosecond dynamics of silver nanoclusters. Photoejection of electrons and fragmentation, J. Phys. Chem. B., 102 (1998).
[65] Marcos A. Gelesky, Alexandre P. Umpierre, Giovanna Machado, Ricardo R. B. Correia, Wictor C. Magno, Jonder Morais, Gunter Ebeling, J. Dupont, Laser-Induced Fragmentation of Transition Metal Nanoparticles in Ionic liquids, J. Am. Chem. Soc., 127 (2005) 4588.
[66] P. Šmejkal, J. Pfleger, K. Šišková, B. Vlčková, O. Dammer, M. Šlouf, In-situ study of Ag nanoparticle hydrosol optical spectra evolution during laser ablation/fragmentation, Applied Physics A, 79 (2004) 1307-1309.
[67] V. Svrček, D. Mariotti, T. Nagai, Y. Shibata, I. Turkevych, M. Kondo, Photovoltaic Applications of Silicon Nanocrystal Based Nanostructures Induced by Nanosecond Laser Fragmentation in Liquid Media, The Journal of Physical Chemistry C, 115 (2011) 5084-5093.
[68] H. Zeng, S. Yang, W. Cai, Reshaping Formation and Luminescence Evolution of ZnO Quantum Dots by Laser-Induced Fragmentation in Liquid, The Journal of Physical Chemistry C, 115 (2011) 5038-5043.
[69] D.W. Bäuerle, Laser Processing and Chemistry, Springer Berlin Heidelberg, 2013.
[70] J. Fröhlingsdorf, W. Zander, B. Stritzker, Direct preparation of high-Tc-superconducting films by laser ablation, Solid State Communications, 67 (1988) 965-966.
[71] P.F. Bongers, C. Schlenker, B. Stritzker, High Tc Superconductors: Preparation and Application, Elsevier Science, 2012.
[72] M.I. Mendivil, S. Shaji, G.A. Castillo, B. Krishnan, Transmission electron microscopic studies on noble metal nanoparticles synthesized by pulsed laser ablation in liquid, in: A. Méndez-Vilas (Ed.) Microscopy: advances in scientifi research and education, Formatex Research Center, 2014, pp. 911-920.
[73] T. Tsuji, M. Nakanishi, T. Mizuki, S. Ozono, M. Tsuji, Y. Tsuboi, Preparation and Shape-Modification of Silver Colloids by Laser Ablation in Liquids: A Brief Review, Science of Advanced Materials, 4 (2012) 391-400.
[74] Z. Yan, D.B. Chrisey, Pulsed laser ablation in liquid for micro-/nanostructure generation, Journal of Photochemistry and Photobiology C: Photochemistry Reviews, 13 (2012) 204-223.

[75] G.W. Yang, Laser ablation in liquids: Applications in the synthesis of nanocrystals, Progress in Materials Science, 52 (2007) 648-698.
[76] T.H. Mainman, Stimulated Optical Radiation in Ruby, Nature, 187 (1960) 493-494.
[77] S.C. Singh, H. Zeng, Nanomaterials and Nanopatterns Based on Laser Processing: A Brief Review on Current State of Art, Science of Advanced Materials, 4 (2012) 368-390.
[78] A. De Giacomo, M. Dell'Aglio, A. Santagata, R. Gaudiuso, O. De Pascale, P. Wagener, G.C. Messina, G. Compagnini, S. Barcikowski, Cavitation dynamics of laser ablation of bulk and wire-shaped metals in water during nanoparticles production, Physical chemistry chemical physics : PCCP, 15 (2013) 3083-3092.
[79] G.C. Messina, P. Wagener, R. Streubel, A. De Giacomo, A. Santagata, G. Compagnini, S. Barcikowski, Pulsed laser ablation of a continuously-fed wire in liquid flow for high-yield production of silver nanoparticles, Physical chemistry chemical physics : PCCP, 15 (2013) 3093-3098.
[80] S. Barcikowski, A. Hahn, M. Guggenheim, K. Reimers, A. Ostendorf, Biocompatibility of nanoactuators: stem cell growth on laser-generated nickel–titanium shape memory alloy nanoparticles, Journal of Nanoparticle Research, 12 (2010) 1733-1742.
[81] J.G. Walter, S. Petersen, F. Stahl, T. Scheper, S. Barcikowski, Laser ablation-based one-step generation and bio-functionalization of gold nanoparticles conjugated with aptamers, Journal of Nanobiotechnology, 8 (2010) 21.
[82] S. Barcikowski, A. Menéndez-Manjón, B. Chichkov, M. Brikas, G. Račiukaitis, Generation of nanoparticle colloids by picosecond and femtosecond laser ablations in liquid flow, Applied Physics Letters, 91 (2007) 083113.
[83] C.L.s. Sajti, A. Barchanski, P. Wagener, S. Klein, S. Barcikowski, Delay Time and Concentration Effects During Bioconjugation of Nanosecond Laser-Generated Nanoparticles in a Liquid Flow, The Journal of Physical Chemistry C, 115 (2011) 5094-5101.
[84] A. Menéndez-Manjón, A. Schwenke, T. Steinke, M. Meyer, U. Giese, P. Wagener, S. Barcikowski, Ligand-free gold–silver nanoparticle alloy polymer composites generated by picosecond laser ablation in liquid monomer, Applied Physics A, 110 (2012) 343-350.
[85] S. K., Silicon Nanoclusters Selectivity Generated by Laser Ablation in Supercritical Fluid, The journal of physical chemistry. B, 109 (2005) 3731-3733.
[86] Saitow K., Yamamura T., M. T., Gold Nanospheres and Nanonecklaces Generated by Laser Ablation in supercritical Fluid, J. Phys. Chem. C, 112 (2008) 18340-18349.
[87] H. Zeng, X.-W. Du, S.C. Singh, S.A. Kulinich, S. Yang, J. He, W. Cai, Nanomaterials via Laser Ablation/Irradiation in Liquid: A Review, Advanced Functional Materials, 22 (2012) 1333-1353.
[88] D. Werner, S. Hashimoto, Improved Working Model for Interpreting the Excitation Wavelength- and Fluence-Dependent Response in Pulsed Laser-Induced Size Reduction of Aqueous Gold Nanoparticles, The Journal of Physical Chemistry C, 115 (2011) 5063-5072.
[89] M.E. Povarnitsyn, T.E. Itina, P.R. Levashov, K.V. Khishchenko, Mechanisms of nanoparticle formation by ultra-short laser ablation of metals in liquid environment, Physical chemistry chemical physics : PCCP, 15 (2013) 3108-3114.

[90] V. Amendola, M. Meneghetti, Laser ablation synthesis in solution and size manipulation of noble metal nanoparticles, Physical chemistry chemical physics : PCCP, 11 (2009) 3805-3821.
[91] S.K. Sundaram, E. Mazur, Inducing and probing non-thermal transitions in semiconductors using femtosecond laser pulses, Nature Materials, 1 (2002).
[92] V. Amendola, M. Meneghetti, What controls the composition and the structure of nanomaterials generated by laser ablation in liquid solution?, Physical chemistry chemical physics : PCCP, 15 (2013) 3027-3046.
[93] L. Berthe, R. Fabbro, P. Peyre, L. Tollier, E. Bartnicki, Shock waves from a water-confined laser-generated plasma, Journal of Applied Physics, 82 (1997) 2826.
[94] D.N. Patel, R.P. Singh, R.K. Thareja, Craters and nanostructures with laser ablation of metal/metal alloy in air and liquid, Applied Surface Science, 288 (2014) 550-557.
[95] D. Werner, A. Furube, T. Okamoto, S. Hashimoto, Femtosecond Laser-Induced Size Reduction of Aqueous Gold Nanoparticles: In Situ and Pump−Probe Spectroscopy Investigations Revealing Coulomb Explosion, The Journal of Physical Chemistry C, 115 (2011) 8503-8512.
[96] Prashant V. Kamat, Mark Flumiani, G.V. Hartland, Picosecond dynamics of silver nanoclusters- photoejection of electrons and fragmentation, J. Phys. Chem. B., 102 (1998) 3123-3128.
[97] Alexander Pyatenko, Munehiro Yamaguchi, M. Suzuki, Mechanisms of Size Reduction of Colloidal Silver and Gold Nanoparticles Irradiated by Nd:YAG laser, J. Phys. Chem. C, 113 (2009) 9078-9085.
[98] A. De Giacomo, A. De Bonis, M. Dell'Aglio, O. De Pascale, R. Gaudiuso, S. Orlando, A. Santagata, G.S. Senesi, F. Taccogna, R. Teghil, Laser Ablation of Graphite in Water in a Range of Pressure from 1 to 146 atm Using Single and Double Pulse Techniques for the Production of Carbon Nanostructures, The Journal of Physical Chemistry C, 115 (2011) 5123-5130.
[99] V.S. Burakov, N.V. Tarasenko, A.V. Butsen, V.A. Rozantsev, M.I. Nedel'ko, Formation of nanoparticles during double-pulse laser ablation of metals in liquids, The European Physical Journal Applied Physics, 30 (2005) 107-112.
[100] S. Barcikowski, G. Compagnini, Advanced nanoparticle generation and excitation by lasers in liquids, Physical chemistry chemical physics : PCCP, 15 (2013) 3022-3026.
[101] T. Tsuji, Y. Higashi, M. Tsuji, Y. Ishikawa, N. Koshizaki, Preparation of submicron-sized spherical particles of gold using laser-induced melting in liquids and low-toxic stabilizing reagent, Applied Surface Science, 348 (2015) 10-15.
[102] O. Olea-Mejía, M. Fernández-Mondragón, G. Rodríguez-de la Concha, M. Camacho-López, SERS-active Ag, Au and Ag–Au alloy nanoparticles obtained by laser ablation in liquids for sensing methylene blue, Applied Surface Science, 348 (2015) 66-70.
[103] J. Liu, X. Tian, H. Chen, Y. Shao, G. Yang, D. Chen, Near-infrared to visible and near-infrared upconversion of monoclinic Gd2O3:Yb3+/Tm3+ nanoparticles prepared by laser ablation in liquid for fluorescence imaging, Applied Surface Science, 348 (2015) 60-65.
[104] S. Petersen, A. Barchanski, U. Taylor, S. Klein, D. Rath, S. Barcikowski, Penetratin-Conjugated Gold Nanoparticles − Design of Cell-Penetrating Nanomarkers by Femtosecond Laser Ablation, The Journal of Physical Chemistry C, 115 (2011) 5152-5159.

[105] C. Streich, S. Koenen, M. Lelle, K. Peneva, S. Barcikowski, Influence of ligands in metal nanoparticle electrophoresis for the fabrication of biofunctional coatings, Applied Surface Science, 348 (2015) 92-99.
[106] P. Wagener, A. Schwenke, S. Barcikowski, How Citrate Ligands Affect Nanoparticle Adsorption to Microparticle Supports, Langmuir, 28 (2012) 6132-6140.
[107] A.A. Serkov, E.V. Barmina, A.V. Simakin, P.G. Kuzmin, V.V. Voronov, G.A. Shafeev, Generation of core–shell nanoparticles Al@Ti by laser ablation in liquid for hydrogen storage, Applied Surface Science, 348 (2015) 71-74.
[108] M.-C. Wu, I.C. Chang, W.-K. Huang, Y.-C. Tu, C.-P. Hsu, W.-F. Su, Correlation between palladium chemical state and photocatalytic performance of TiO2–Pd based nanoparticles, Thin Solid Films, 570 (2014) 371-375.
[109] G. Marzun, J. Nakamura, X. Zhang, S. Barcikowski, P. Wagener, Size control and supporting of palladium nanoparticles made by laser ablation in saline solution as a facile route to heterogeneous catalysts, Applied Surface Science, 348 (2015) 75-84.
[110] L. Lascialfari, P. Marsili, S. Caporali, M. Muniz-Miranda, G. Margheri, A. Serafini, A. Brandi, E. Giorgetti, S. Cicchi, Carbon nanotubes/Laser ablation gold nanoparticles composites, Thin Solid Films, 569 (2014) 93-99.
[111] Rina Singh, R.K. Soni, Aluminium-Gold nanocomposites prepared by pulsed laser ablation, Journal of Nanoscience Letters, 3 (2013) 11.
[112] R. Zamiri, A. Zakaria, R. Jorfi, G. Zamiri, M. Shokati Mojdehi, H. Abbastabar Ahangar, A. Khorsand Zak, Laser assisted fabrication of ZnO/Ag and ZnO/Au core/shell nanocomposites, Applied Physics A, 111 (2013) 487-493.
[113] T. Sasaki, Y. Shimizu, N. Koshizaki, Preparation of metal oxide-based nanomaterials using nanosecond pulsed laser ablation in liquids, Journal of Photochemistry and Photobiology A: Chemistry, 182 (2006) 335-341.
[114] H. Zeng, W. Cai, Y. Li, J. Hu, P. Liu, Composition/structural evolution and optical properties of ZnO/Zn nanoparticles by laser ablation in liquid media, The journal of physical chemistry. B, 109 (2005) 18260-18266.
[115] S.C. Singh, R. Gopal, Drop shaped zinc oxide quantum dots and their self-assembly into dendritic nanostructures: Liquid assisted pulsed laser ablation and characterizations, Applied Surface Science, 258 (2012) 2211-2218.
[116] S.C. Singh, Effect of oxygen injection on the size and compositional evolution of ZnO/Zn(OH)2 nanocomposite synthesized by pulsed laser ablation in distilled water, Journal of Nanoparticle Research, 13 (2011) 4143-4152.
[117] C. Zhao, Y. Huang, J.T. Abiade, Ferromagnetic ZnO nanoparticles prepared by pulsed laser deposition in liquid, Materials Letters, 85 (2012) 164-167.
[118] Reza Zamiri, Azmi Zakaria, Rahele Jorfi, Golnoosh Zamiri, Masoumeh Shokati Mojdehi, Hossein Abbastabar Ahangar, A.K. Zak, Laser assisted fabrication of ZnO/Ag and ZnO/Au core/shell nanocomposites, Applied Physics A, 111 (2013) 487-493.
[119] X. Zhang, H. Zeng, W. Cai, Laser power effect on morphology and photoluminescence of ZnO nanostructures by laser ablation in water, Materials Letters, 63 (2009) 191-193.
[120] A. Nath, S.S. Laha, A. Khare, Effect of focusing conditions on synthesis of titanium oxide nanoparticles via laser ablation in titanium–water interface, Applied Surface Science, 257 (2011) 3118-3122.

[121] N.G. Semaltianos, S. Logothetidis, N. Frangis, I. Tsiaoussis, W. Perrie, G. Dearden, K.G. Watkins, Laser ablation in water: A route to synthesize nanoparticles of titanium monoxide, Chemical Physics Letters, 496 (2010) 113-116.
[122] A. Nath, S.S. Laha, A. Khare, Synthesis of TiO2Nanoparticles Via Laser Ablation at Titanium-Water Interface, Integrated Ferroelectrics, 121 (2010) 58-64.
[123] C.N. Huang, J.S. Bow, Y. Zheng, S.Y. Chen, N. Ho, P. Shen, Nonstoichiometric Titanium Oxides via Pulsed Laser Ablation in Water, Nanoscale research letters, 5 (2010) 972-985.
[124] P. Liu, W. Cai, M. Fang, Z. Li, H. Zeng, J. Hu, X. Luo, W. Jing, Room temperature synthesized rutile TiO(2) nanoparticles induced by laser ablation in liquid and their photocatalytic activity, Nanotechnology, 20 (2009) 285707.
[125] C.H. Liang, Y. Shimizu, T. Sasaki, N. Koshizaki, Preparation of ultrafine TiO2 nanocrystals via pulsed-laser ablation of titanium metal in surfactant solution, Applied Physics A, 80 (2004) 819-822.
[126] M. Amin, J. Tomko, J.J. Naddeo, R. Jimenez, D.M. Bubb, M. Steiner, J. Fitz-Gerald, S.M. O'Malley, Laser-assisted synthesis of ultra-small anatase TiO2 nanoparticles, Applied Surface Science, 348 (2015) 30-37.
[127] J.M.J. Santillán, F.A. Videla, M.B. Fernández van Raap, D.C. Schinca, L.B. Scaffardi, Analysis of the structure, configuration, and sizing of Cu and Cu oxide nanoparticles generated by fs laser ablation of solid target in liquids, Journal of Applied Physics, 113 (2013) 134305.
[128] S.W. Lee, S.D. Park, I.C. Bang, Critical heat flux for CuO nanofluid fabricated by pulsed laser ablation differentiating deposition characteristics, International Journal of Heat and Mass Transfer, 55 (2012) 6908-6915.
[129] N. Haram, N. Ahmad, Effect of laser fluence on the size of copper oxide nanoparticles produced by the ablation of Cu target in double distilled water, Applied Physics A, 111 (2012) 1131-1137.
[130] M. Kawasaki, Laser-Induced Fragmentative Decomposition of Fine CuO Powder in Acetone as Highly Productive Pathway to Cu and Cu2O Nanoparticles, The Journal of Physical Chemistry C, 115 (2011) 5165-5173.
[131] I.L. Liu, B.C. Lin, S.Y. Chen, P. Shen, NaAlO2and γ-Al2O3Nanoparticles by Pulsed Laser Ablation in Aqueous Solution, The Journal of Physical Chemistry C, 115 (2011) 4994-5002.
[132] D. Amans, C. Malaterre, M. Diouf, C. Mancini, F. Chaput, G. Ledoux, G. Breton, Y. Guillin, C. Dujardin, K. Masenelli-Varlot, P. Perriat, Synthesis of Oxide Nanoparticles by Pulsed Laser Ablation in Liquids Containing a Complexing Molecule: Impact on Size Distributions and Prepared Phases, The Journal of Physical Chemistry C, 115 (2011) 5131-5139.
[133] E. T. Salem, Tin Oxide Nanoparticles Prepared Using Liquid Phase Laser Ablation for Optoelectronic Application, Nanoscience and Nanotechnology, 2 (2012) 86-89.
[134] M.I. Mendivil, B. Krishnan, F.A. Sanchez, S. Martinez, J.A. Aguilar-Martinez, G.A. Castillo, D.I. Garcia-Gutierrez, S. Shaji, Synthesis of silver nanoparticles and antimony oxide nanocrystals by pulsed laser ablation in liquid media, Applied Physics A, 110 (2012) 809-816.
[135] R.-D. Sun, T. Tsuji, Preparation of antimony sulfide semiconductor nanoparticles by pulsed laser ablation in liquid, Applied Surface Science, 348 (2015) 38-44.

[136] M.A. Gondal, T.A. Saleh, Q.A. Drmosh, Synthesis of nickel oxide nanoparticles using pulsed laser ablation in liquids and their optical characterization, Applied Surface Science, 258 (2012) 6982-6986.
[137] M.A. Gondal, T.A. Saleh, Q. Drmosh, Optical Properties of Bismuth Oxide Nanoparticles Synthesized by Pulsed Laser Ablation in Liquids, Science of Advanced Materials, 4 (2012) 507-510.
[138] Z. Swiatkowska-Warkocka, K. Kawaguchi, H. Wang, Y. Katou, N. Koshizaki, Controlling exchange bias in Fe3O4/FeO composite particles prepared by pulsed laser irradiation, Nanoscale research letters, 6 (2011) 226.
[139] V. Amendola, P. Riello, M. Meneghetti, Magnetic Nanoparticles of Iron Carbide, Iron Oxide, Iron@Iron Oxide, and Metal Iron Synthesized by Laser Ablation in Organic Solvents, The Journal of Physical Chemistry C, 115 (2011) 5140-5146.
[140] S. Mollah, S.J. Henley, C.E. Giusca, S.R.P. Silva, Photo-Chemical Synthesis of Iron Oxide Nanowires Induced by Pulsed Laser Ablation of Iron Powder in Liquid Media, Integrated Ferroelectrics, 119 (2010) 45-54.
[141] S.J. Henley, S. Mollah, C.E. Giusca, S.R.P. Silva, Laser-induced self-assembly of iron oxide nanostructures with controllable dimensionality, Journal of Applied Physics, 106 (2009) 064309.
[142] Y. Ishikawa, Y. Shimizu, T. Sasaki, N. Koshizaki, Preparation of zinc oxide nanorods using pulsed laser ablation in water media at high temperature, Journal of colloid and interface science, 300 (2006) 612-615.
[143] S. Link, C. Burda, B. Nikoobakht, M.A. El-Sayed, Laser-Induced Shape Changes of Colloidal Gold Nanorods Using Femtosecond and Nanosecond Laser Pulses, J. Phys. Chem. B., 104 (2000) 6152-6163.
[144] M. Muniz-Miranda, C. Gellini, P. Canton, P. Marsili, E. Giorgetti, SERS and catalytically active Ag/Pd nanoparticles obtained by combining laser ablation and galvanic replacement, Journal of Alloys and Compounds, 615 (2014) S352-S356.
[145] R. Intartaglia, G. Das, K. Bagga, A. Gopalakrishnan, A. Genovese, M. Povia, E. Di Fabrizio, R. Cingolani, A. Diaspro, F. Brandi, Laser synthesis of ligand-free bimetallic nanoparticles for plasmonic applications, Physical chemistry chemical physics : PCCP, 15 (2013) 3075-3082.
[146] Stefanie Dengler, Christian Kûbel, Andreas Schwenke, Gunnar Ritt, B. Eberle, Near- and off-resonant optical limiting properties of gold-silver alloy nanoparticles for intense nanosecond laser pulses, Journal of Optics, 14 (2012) 075203.
[147] E. Messina, L. D'Urso, E. Fazio, C. Satriano, M.G. Donato, C. D'Andrea, O.M. Maragò, P.G. Gucciardi, G. Compagnini, F. Neri, Tuning the structural and optical properties of gold/silver nano-alloys prepared by laser ablation in liquids for optical limiting, ultra-sensitive spectroscopy, and optical trapping, Journal of Quantitative Spectroscopy and Radiative Transfer, 113 (2012) 2490-2498.
[148] S. Dengler, C. Kübel, A. Schwenke, G. Ritt, B. Eberle, Near- and off-resonant optical limiting properties of gold–silver alloy nanoparticles for intense nanosecond laser pulses, Journal of Optics, 14 (2012) 075203.
[149] Yu-Hung Chen, C.-S. Yeh, A new approach for the formation of alloy nanoparticles laser synthesis of gold-silver alloy from gold-silver colloidal mixtures, Chem. Commun., (2001).
[150] J. Jakobi, A. Menendez-Manjon, V.S. Chakravadhanula, L. Kienle, P. Wagener, S. Barcikowski, Stoichiometry of alloy nanoparticles from laser ablation of PtIr in

acetone and their electrophoretic deposition on PtIr electrodes, Nanotechnology, 22 (2011) 145601.
[151] Y. Ishikawa, K. Kawaguchi, Y. Shimizu, T. Sasaki, N. Koshizaki, Preparation of Fe–Pt alloy particles by pulsed laser ablation in liquid medium, Chemical Physics Letters, 428 (2006) 426-429.
[152] Y.-H. Chen, Y.-H. Tseng, C.-S. Yeh, Laser-induced alloying Au–Pd and Ag–Pd colloidal mixtures: the formation of dispersed Au/Pd and Ag/Pd nanoparticles, Journal of Materials Chemistry, 12 (2002) 1419-1422.
[153] H. Acharya, Y.J. Park, Y.S. Choi, J. Sung, T. Kim, D.H. Kim, C. Park, Control over the surface plasmon band of block copolymer/Ag/Au nanoparticles composites by the addition of single walled carbon nanotubes, Reactive and Functional Polymers, 71 (2011) 1195-1201.
[154] N. Hintsho, L. Petrik, A. Nechaev, S. Titinchi, P. Ndungu, Photo-catalytic activity of titanium dioxide carbon nanotube nano-composites modified with silver and palladium nanoparticles, Applied Catalysis B: Environmental, 156-157 (2014) 273-283.
[155] G. Forte, L. D'Urso, E. Fazio, S. Patanè, F. Neri, O. Puglisi, G. Compagnini, The effects of liquid environments on the optical properties of linear carbon chains prepared by laser ablation generated plasmas, Applied Surface Science, 272 (2013) 76-81.
[156] T. Wakabayashi, M. Saikawa, Y. Wada, T. Minematsu, Isotope scrambling in the formation of cyanopolyynes by laser ablation of carbon particles in liquid acetonitrile, Carbon, 50 (2012) 47-56.
[157] E. Fazio, S. Patanè, L. D'Urso, G. Compagnini, F. Neri, Enhanced nonlinear optical response of linear carbon chain colloid mixed with silver nanoparticles, Optics Communications, 285 (2012) 2942-2946.
[158] K. Zhang, X. Liu, Y. Sun, F. Wang, Preparation, characterization, and fluorescence properties of well-dispersed core–shell CdS/carbon nanoparticles, Journal of Materials Science, 46 (2011) 6975-6980.
[159] A. Santagata, A. De Bonis, A. De Giacomo, M. Dell'Aglio, A. Laurita, G.S. Senesi, R. Gaudiuso, S. Orlando, R. Teghil, G.P. Parisi, Carbon-Based Nanostructures Obtained in Water by Ultrashort Laser Pulses, The Journal of Physical Chemistry C, 115 (2011) 5160-5164.
[160] G.X. Chen, Preparation of carbon nanoparticles with strong optical limiting properties by laser ablation in water, Journal of Applied Physics, 95 (2004) 1455.
[161] S. Barcikowski, F. Mafuné, Trends and Current Topics in the Field of Laser Ablation and Nanoparticle Generation in Liquids, The Journal of Physical Chemistry C, 115 (2011) 4985-4985.
[162] Vincenzo Amendola, M. Meneghetti, Laser ablation synthesis in solution and size manipulation of noble metal nanoparticles, Physical chemistry chemical physics : PCCP, 11 (2009) 3805-3821.
[163] M. C. Daniel, D. Astruc, Gold nanoparticles: assembly, supramolecular chemistry, quantum-size-related properties, and applications toward biology, catalysis, and nanotechnology, Chem. Rev. , 104 (2004) 293 - 346.
[164] C.G. Freyschlag, R.J. Madix, Precious metal magic: catalytic wizardry, Materials Today, 14 (2011) 134-142.

[165] Ian Freestone, Nigel Meeks, Margaret Sax, C. Higgitt, The Lycurgus Cup- A Roman Nanotechnology, Gold Bulletin, 40 (2007) 270.
[166] M. Faraday, The Bakerian Lecture: Experimental Relations of Gold (and other metals) to Light, Phil. Trans. R. Soc. Lond., 147 (1857) 145-181.
[167] A. Schrofel, G. Kratosova, I. Safarik, M. Safarikova, I. Raska, L.M. Shor, Applications of biosynthesized metallic nanoparticles - A review, Acta biomaterialia, 10 (2014) 4023–4042.
[168] S. Schrittwieser, J. Schotter, T. Maier, R. Bruck, P. Muellner, N. Kataeva, K. Soulantika, F. Ludwig, A. Huetten, H. Brueckl, Homogeneous biosensor based on optical detection of the rotational dynamics of anisotropic nanoparticles, Procedia Engineering, 5 (2010) 1107-1110.
[169] J. Li, J.-J. Zhu, K. Xu, Fluorescent metal nanoclusters: From synthesis to applications, TrAC Trends in Analytical Chemistry, 58 (2014) 90-98.
[170] V. Biju, T. Itoh, A. Anas, A. Sujith, M. Ishikawa, Semiconductor quantum dots and metal nanoparticles: syntheses, optical properties, and biological applications, Analytical and bioanalytical chemistry, 391 (2008) 2469-2495.
[171] S. Alabbad, S.F. Adil, M.E. Assal, M. Khan, A. Alwarthan, M.R.H. Siddiqui, Gold & Silver Nanoparticles Supported on Manganese Oxide: Synthesis, Characterization and Catalytic Studies for Selective Oxidation of Benzyl Alcohol, Arabian Journal of Chemistry, (2014).
[172] F. Alessandro, C. Gellini, Salvi Pier Remigio, B. Maurizio, Photoacoustic excitation profiles of gold nanoparticles, Photoacoustics, 2 (2014) 47-53.
[173] X. Huang, M.A. El-Sayed, Gold nanoparticles: Optical properties and implementations in cancer diagnosis and photothermal therapy, Journal of Advanced Research, 1 (2010) 13-28.
[174] S. Gioria, H. Chassaigne, D. Carpi, A. Parracino, S. Meschini, P. Barboro, F. Rossi, A proteomic approach to investigate AuNPs effects in Balb/3T3 cells, Toxicology letters, 228 (2014) 111-126.
[175] M. Moritz, M. Geszke-Moritz, The newest achievements in synthesis, immobilization and practical applications of antibacterial nanoparticles, Chemical Engineering Journal, 228 (2013) 596-613.
[176] A. Ayati, A. Ahmadpour, F.F. Bamoharram, B. Tanhaei, M. Manttari, M. Sillanpaa, A review on catalytic applications of Au/TiO nanoparticles in the removal of water pollutant, Chemosphere, 107C (2014) 163-174.
[177] J. Turkevich, Coloidal Gold part I. Historial and preparative aspects, morphology and structure, Gold Bulletin, 18 (1985) 86.
[178] D.L. Feldheim, C.D. Keating, Self-assembly of single electron transistors and related devices, Chem. Soc. Rev, 27 (1998) 1.
[179] Shakibaie M., Forootanfar H., B.Z. Mollazadeh-Moghaddam K., Nafissi Varcheh N., S.A. R., Green synthesis of gold nanoparticles by the marine microalga Tetraselmis suecica, Biotechnology and Applied Biochemistry 57 (2010) 71-75.
[180] G. Veith, A. Lupini, S. Pennycook, G. Ownby, N. Dudney, Nanoparticles of gold on -AlO produced by dc magnetron sputtering, Journal of Catalysis, 231 (2005) 151-158.
[181] U. Shedbalkar, R. Singh, S. Wadhwani, S. Gaidhani, B.A. Chopade, Microbial synthesis of gold nanoparticles: current status and future prospects, Advances in colloid and interface science, 209 (2014) 40-48.

[182] J. Turkevich, J. Hillier, P.C. Stevenson, A study of the nucleation and growth processes in the synthesis of colloidal gold, Discuss. Faraday Soc., 11 (1951) 55.
[183] J. Kimling, M. Maier, B. Okenve, V. Kotaidis, H. Ballot, A. Plech, Turkevich Method for Gold Nanoparticle Synthesis Revisited, The Journal of Physical Chemistry B, 110 (2006) 15700-15707.
[184] S.Y. Li, M. Wang, Branched metal nanoparticles: A reviews on wet-chemical synthesis and biomedical applications, Nano LIFE, 02 (2012) 1230002.
[185] A.D. Pomogailo, G.I. Dzhardimalieva, Nanostructured Materials Preparation via Condensation Ways, Springer Netherlands, 2014.
[186] H. Pan, S.H. Ko, C.P. Grigoropoulos, The Solid-State Neck Growth Mechanisms in Low Energy Laser Sintering of Gold Nanoparticles: A Molecular Dynamics Simulation Study, Journal of Heat Transfer, 130 (2008) 092404.
[187] Jean-Philippe Sylvestre, Suzie Poulin, Andrei V. Kabashin, Edward Sacher, Michel Meunier, J.H.T. Luong, Surface chemistry of gold nanoparticles produced by laser ablation in aqueous media, J. Phys. Chem. B., 108 (2004) 16864-16869.
[188] Andrei V. Kabashin, Michel Meunier, Christopher Kingston, J.H.T. Luong, Fabrication and Characterization of Gold Nanoparticles by Femtosecond Laser Ablation in Aqueous Solution of Cyclodextrins, J. Phys. Chem. B., 107 (2003) 4527-4531.
[189] S. Barcikowski, A. Hahn, A.V. Kabashin, B.N. Chichkov, Properties of nanoparticles generated during femtosecond laser machining in air and water, Applied Physics A, 87 (2007) 47-55.
[190] M.A. Sobhan, M. Ams, M.J. Withford, E.M. Goldys, Ultrafast laser ablative generation of gold nanoparticles: the influence of pulse energy, repetition frequency and spot size, Journal of Nanoparticle Research, 12 (2010) 2831-2842.
[191] G.A. Torchia, L.B. Scaffardi, C. Méndez, P. Moreno, J.O. Tocho, L. Roso, Optical extinction for determining the size distribution of gold nanoparticles fabricated by ultra-short pulsed laser ablation, Applied Physics A, 93 (2008) 967-971.
[192] Ana Menendez-Manjon, Boris N. Chichkov, S. Barcikowski, Influence of water temperature on the hydrodynamic diameter of gold nanoparticles from laser ablation, J. Phys. Chem. C, 114 (2010) 2499-2504.
[193] Fumitaka Mafune, Jun Ya Kohno, Yoshihiro Takeda, T. Kondow, Formation of Gold Nanoparticles by Laser Ablation in Aqueous Solution of Surfactant, J. Phys. Chem. B., 105 (2001) 5114-5120.
[194] K.A. Elsayed, H. Imam, M.A. Ahmed, R. Ramadan, Effect of focusing conditions and laser parameters on the fabrication of gold nanoparticles via laser ablation in liquid, Optics & Laser Technology, 45 (2013) 495-502.
[195] N. Mirghassemzadeh, M. Ghamkhari, D. Dorranian, Dependence of Laser Ablation Produced Gold Nanoparticles Characteristics on the Fluence of Laser Pulse, Soft Nanoscience Letters, 03 (2013) 101-106.
[196] F. Mafune, Kohno J., Takeda Y., K. T., Dissociation and Aggregation of Gold Nanoparticles under Laser Irradiation, J. Phys. Chem. B., 105 (2001) 9050-9056.
[197] Fumitaka Mafuné, Jun Ya Kohno, Y. Takeda, T. Kondow, Full Physical Preparation of Size-Selected Gold Nanoparticles in Solution Laser Ablation: Laser Ablation and Laser-induced Size Control, The Journal of Physical Chemistry B, 106 (2002) 7575-7578.

[198] Natsumi Matsuo, Hitomi Muto, Ken Miyajima, F. Mafuné, Single laser pulse induced aggregation of gold nanoparticles, Physical Chemistry Chemical Physics, 9 (2007) 6027-6031.
[199] N.V. Tarasenko, A.V. Butsen, E.A. Nevar, N.A. Savastenko, Synthesis of nanosized particles during laser ablation of gold in water, Applied Surface Science, 252 (2006) 4439–4444.
[200] K.K. Kim, H.J. Kwon, S.K. Shin, J.K. Song, S.M. Park, Stability of uncapped gold nanoparticles produced by laser ablation in deionized water: The effect of post-irradiation, Chemical Physics Letters, 588 (2013) 167-173.
[201] H. Kurita, A. Takami, S. Koda, Size reduction of gold particles in aqueous solution by pulsed laser irradiation, Applied Physics Letters, 72 (1998) 789.
[202] V. Resta, J. Siegel, J. Bonse, J. Gonzalo, C.N. Afonso, E. Piscopiello, G. Van Tenedeloo, Sharpening the shape distribution of gold nanoparticles by laser irradiation, Journal of Applied Physics, 100 (2006) 084311.
[203] D. Riabinina, J. Zhang, M. Chaker, J. Margot, D. Ma, P. Tijssen, Control of plasmon resonance of gold nanoparticles via excimer laser irradiation, Applied Physics A, 102 (2010) 153-160.
[204] C. Rehbock, V. Merk, L. Gamrad, R. Streubel, S. Barcikowski, Size control of laser-fabricated surfactant-free gold nanoparticles with highly diluted electrolytes and their subsequent bioconjugation, Physical chemistry chemical physics : PCCP, 15 (2013) 3057-3067.
[205] Jean-Philippe Silvestre, Andrei V. Kabashin, Edward Sacher, Michel Meunier, J.H.T. Luong, Stabilization and Size Control of Gold Nanoparticles during Laser Ablation in Aqueous Cyclodextrins, J. Am. Chem. Soc., 126 (2004) 7176-7177.
[206] A.F.M.Y. Haider, S. Sengupta, K.M. Abedin, A.I. Talukder, Fabrication of gold nanoparticles in water by laser ablation technique and their characterization, Applied Physics A, 105 (2011) 487-495.
[207] T.X. Phuoc, Complete Green Synthesis of gold Nanoparticles using Laser Ablation in Deionized Water Containing Chitosan and Starch, J. Mater Sci. Nanotechnol, 1 (2014) 401.
[208] E. Messina, L.D'Urso, E.Fazio, C.Satriano, M.G.Donato, C.D'Andrea , O.M.Marago, P.G. Gucciardi, G.Compagnini, F.Neri, Tuning the structural and optical properties of gold-silver nano-alloys prepared by laser ablation in liquids for optical limiting, ultra-sensitive spectroscopy and optical trapping, Journal of Quantitative Spectroscopy and Radiative Transfer, 113 (2012) 2490-2498.
[209] A.S. Nikolov, N.N. Nedyalkov, R.G. Nikov, I.G. Dimitrov, P.A. Atanasov, K. Maximova, P. Delaporte, A. Kabashin, M.T. Alexandrov, D.B. Karashanova, Processing conditions in pulsed laser ablation of gold in liquid for fabrication of nanowire networks, Applied Surface Science, 302 (2014) 243-249.
[210] T. Salminen, M. Honkanen, T. Niemi, Coating of gold nanoparticles made by pulsed laser ablation in liquids with silica shells by simultaneous chemical synthesis, Physical chemistry chemical physics : PCCP, 15 (2013) 3047-3051.
[211] M. Maciulevičius, A. Vinčiūnas, M. Brikas, A. Butsen, N. Tarasenka, N. Tarasenko, G. Račiukaitis, On-Line Characterization of Gold Nanoparticles Generated by Laser Ablation in Liquids, Physics Procedia, 41 (2013) 531-538.

[212] O Van Overschelde, J. Dervaux, L. Young, D. Thiry, R. Snyders, Screening effect in gold nanoparticles generated in liquid by KrF ablation, Laser Physics, 23 (2013) 055901.
[213] D. Werner, T. Ueki, S. Hashimoto, Methodological Improvement in Pulsed Laser-Induced Size Reduction of Aqueous Colloidal Gold Nanoparticles by Applying High Pressure, The Journal of Physical Chemistry C, 116 (2012) 5482-5491.
[214] A. Henglein, Colloidal silver nanoparticles: photochemical preparation and interaction with O2, CCl4, and some metal ions, Chemistry of Materials, 10 (1998) 444-450.
[215] M.M.H. Khalil, E.H. Ismail, K.Z. El-Baghdady, D. Mohamed, Green synthesis of silver nanoparticles using olive leaf extract and its antibacterial activity, Arabian Journal of Chemistry, 7 (2014) 1131–1139.
[216] M.L. Allen, M. Aronniemi, T. Mattila, A. Alastalo, K. Ojanpera, M. Suhonen, H. Seppa, Electrical sintering of nanoparticle structures, Nanotechnology, 19 (2008) 175201.
[217] Pilar Prieto, Valentin Nistor, Khali Nouneh, Munetaka Oyama, Mohammed Abd-Lefdil, R. Díaz, XPS study of silver, nickel and bimetallic silver-nickel nanoparticles prepared by seed-mediated growth, Applied Surface Science, 258 (2012) 8807-8813.
[218] E. V. Abkhalimov, A. A. Parsaev, B. G. Ershov, Preparation of silver nanoparticles in aqueous solutions in the presence of carbonate ions as stabilizers, Colloid Journal, 73 (2011) 1-5.
[219] R.A. Salkar, P. Jeevanandam, S.T. Aruna, Y. Koltypin, A. Gedanken, The sonochemical preparation of amorphous silver nanoparticles, J. Mater Chem., 9 (1999) 1333.
[220] E. Akman, B.G. Oztoprak, M. Gunes, E. Kacar, A. Demir, Effect of femtosecond Ti:Sapphire laser wavelengths on plasmonic behaviour and size evolution of silver nanoparticles, Photonics and Nanostructures - Fundamentals and Applications, 9 (2011) 276-286.
[221] N. Barsch, J. Jakobi, S. Weiler, S. Barcikowski, Pure colloidal metal and ceramic nanoparticles from high-power picosecond laser ablation in water and acetone, Nanotechnology, 20 (2009) 445603.
[222] E. V. Zavedeev, A. V. Petrovskaya, A. V. Simakin, G.A. Shafeev, Formation of nanostructures upon laser ablation of silver in liquids, Quantum Electronics, 36 (2006) 978-980.
[223] P. Wagener, S. Ibrahimkutty, A. Menzel, A. Plech, S. Barcikowski, Dynamics of silver nanoparticle formation and agglomeration inside the cavitation bubble after pulsed laser ablation in liquid, Physical chemistry chemical physics : PCCP, 15 (2013) 3068-3074.
[224] E. Solati, M. Mashayekh, D. Dorranian, Effects of laser pulse wavelength and laser fluence on the characteristics of silver nanoparticle generated by laser ablation, Applied Physics A, 112 (2013) 689-694.
[225] A.I. Talukder, P. Sultana, A.F.M.Y. Haider, M. Wahadoszamen, K.M. Abedin, S.F.U. Farhad, Power dependence of size of laser ablated colloidal silver nanoparticles, The European Physical Journal D, 60 (2010) 295-300.
[226] R. M. Tilaki, A. Irajizad, S.M. Mahdavi, Stability, size and optical properties of silver nanoparticles prepared by laser ablation in different carrier media, Applied Physics A, 84 (2006) 215-219.

[227] A. Pyatenko, K. Shimokawa, M. Yamaguchi, O. Nishimura, M. Suzuki, Synthesis of silver nanoparticles by laser ablation in pure water, Applied Physics A, 79 (2004) 803-806.
[228] R. A. Ganeev, M. Baba, A.I. Rysasnyansky, M. Suzuki, H. Kuroda, Characterization of optical and nonlinear optical properties of silver nanoparticles prepared by laser ablation in various liquids, Optics Communications, 240 (2004) 437-448.
[229] Fumitaka Mafuné, Jun Ya Kohno, Y. Takeda, T. Kondow, Structure and Stability of Silver Nanoparticles in Aqueous Solution Produced by Laser, J. Phys. Chem. B., 104 (2000) 8333-8337.
[230] Fumitaka Mafuné, Jun Ya Kohno, Y. Takeda, T. Kondow, Formation and Size Control of Silver Nanoparticles by Laser Ablation in Aqueous Solution, J. Phys. Chem. B., 104 (2000) 9111-9117.
[231] Z. Yan, R. Bao, D.B. Chrisey, Generation of Ag-Ag(2)O complex nanostructures by excimer laser ablation of Ag in water, Physical chemistry chemical physics : PCCP, 15 (2013) 3052-3056.
[232] R. Zamiri, A. Zakaria, M.S. Husin, Z.A. Wahab, F.K. Nazarpour, Formation of silver microbelt structures by laser irradiation of silver nanoparticles in ethanol, International journal of nanomedicine, 6 (2011) 2221-2224.
[233] L.C. Courrol, F.R. de Oliveira Silva, L. Gomes, A simple method to synthesize silver nanoparticles by photo-reduction, Colloids and Surfaces A: Physicochemical and Engineering Aspects, 305 (2007) 54-57.
[234] Stamplecoskie K.G., S.J. C., Light emitting diode irradiation can control the morphology and optical properties of silver nanoparticles, J. Am. Chem. Soc., 132 (2010) 1825-1827.
[235] N.K. Mondal, A. Chowdhury, U. Dey, P. Mukhopadhya, S. Chatterjee, K. Das, J.K. Datta, Green synthesis of silver nanoparticles and its application for mosquito control, Asian Pacific Journal of Tropical Disease, 4 (2014) S204-S210.
[236] N.M. Zain, A.G.F. Stapley, G. Shama, Green synthesis of silver and copper nanoparticles using ascorbic acid and chitosan for antimicrobial applications, Carbohydrate Polymers, 112 (2014) 195-202.
[237] Morgan S. Sibbald, George Chumanov, T.M. Cotton, Reduction of Cytochrome c by Halide-Modified, Laser-Ablated Silver Colloids, J. Chem. Phys., 100 (1996) 4672-4678.
[238] B. Pergolese, M. Muniz-Miranda, A. Bigotto, SERS investigation on 4-nitro-3-pyrazolecarboxylic acid adsorbed on palladium-doped silver nanoparticles, Vibrational Spectroscopy, 48 (2008) 107-112.
[239] U. Lange, T. Hirsch, V.M. Mirsky, O.S. Wolfbeis, Hydrogen sensor based on a graphene – palladium nanocomposite, Electrochimica Acta, 56 (2011) 3707-3712.
[240] M.J. Beliatis, N.A. Martin, E.J. Leming, S.R. Silva, S.J. Henley, Laser ablation direct writing of metal nanoparticles for hydrogen and humidity sensors, Langmuir, 27 (2011) 1241-1244.
[241] J. Lan, W. Xu, Q. Wan, X. Zhang, J. Lin, J. Chen, Colorimetric determination of sarcosine in urine samples of prostatic carcinoma by mimic enzyme palladium nanoparticles, Analytica chimica acta, 825 (2014) 63-68.
[242] M. Boutinguiza, R. Comesaña, F. Lusquiños, A. Riveiro, J. del Val, J. Pou, Palladium nanoparticles produced by CW and pulsed laser ablation in water, Applied Surface Science, 302 (2014) 19-23.

[243] G. Cristoforetti, E. Pitzalis, R. Spiniello, R. Ishak, M. Muniz-Miranda, Production of Palladium Nanoparticles by Pulsed Laser Ablation in Water and Their Characterization, The Journal of Physical Chemistry C, 115 (2011) 5073-5083.
[244] S.Z. Mortazavi, P. Parvin, A. Reyhani, A.N. Golikand, S. Mirershadi, Effect of Laser Wavelength at IR (1064 nm) and UV (193 nm) on the Structural Formation of Palladium Nanoparticles in Deionized Water, The Journal of Physical Chemistry C, 115 (2011) 5049-5057.
[245] T. Nishi, A. Takeichi, N. Suzuki, T. Hioki, T. Motohiro, Fabrication of Palladium Nanoparticles by Laser Ablation in Liquid, JLMN- Journal of Laser Micro/Nanoengineering, 5 (2010) 192-196.
[246] N.G. Semaltianos, P. Petkov, S. Scholz, L. Guetaz, Palladium or palladium hydride nanoparticles synthesized by laser ablation of a bulk palladium target in liquids, Journal of colloid and interface science, 402 (2013) 307-311.
[247] P. Ascarelli, V. Contini, R. Giorgi, Formation process of nanocrystalline materials from x-ray diffraction profile analysis: Application to platinum catalysts., J. Appl. Phys., 91 (2002) 4556-4561.
[248] A. Henglein, B.G. Ershov, M. Malow, Absorption Spectrum and Some Chemical Reactions of Colloidal Platinum in Aqueous Solution J. Phys. Chem., 99 (1995) 14129.
[249] Pascale Bommersbach, Mohamed Chaker, Mohamedi, D. Guay, Physico-Chemical and electrochemical properties of Platinum-Tin Nanoparticles Synthesized by Pulsed Laser Ablation for Ethanol Oxidation, J. Phys. Chem. C, 112 (2008) 14672-14681.
[250] Y. Yang, M. Shi, Q.-F. Zhou, Y.-S. Li, Z.-W. Fu, Platinum nanoparticle–graphene hybrids synthesized by liquid phase pulsed laser ablation as cathode catalysts for Li-air batteries, Electrochemistry Communications, 20 (2012) 11-14.
[251] M. Cueto, M. Sanz, M. Oujja, F. Gámez, B. Martínez−Haya, M. Castillejo, Platinum Nanoparticles Prepared by Laser Ablation in Aqueous Solutions: Fabrication and Application to Laser Desorption Ionization, The Journal of Physical Chemistry C, 115 (2011) 22217-22224.
[252] Fumitaka Mafuné, Jun Ya Kohno, Yoshihiro Takeda, T. Kondow, Formation of stable platinum nanoparticles by laser ablation in water, J. Phys. Chem. B., 107 (2003) 4218-4223.
[253] W.T. Nichols, Sasaki Takeshi, N. Koshizaki, Laser ablation of a platinum target in water. I. Ablation mechanisms, J. Appl. Phys., 100 (2006) 114911.
[254] W.T. Nichols, T. Sasaki, N. Koshizaki, Laser ablation of a platinum target in water. II. Ablation rate and nanoparticle size distributions, Journal of Applied Physics, 100 (2006) 114912.
[255] W.T. Nichols, Sasaki Takeshi, N. Koshizaki, Laser ablation of a platinum target in water. III. Laser-induced reactions, J. Appl. Phys., 100 (2006) 114913.
[256] D.L. da Cunha, G.F.C. Pereira, J.F. Felix, J. Albino Aguiar, W.M. de Azevedo, Nanostructured hydrocerussite compound (Pb3(CO3)2(OH)2) prepared by laser ablation technique in liquid environment, Materials Research Bulletin, 49 (2014) 172-175.
[257] P.G. Kuzmin, G.A. Shafeev, G. Viau, B. Warot-Fonrose, M. Barberoglou, E. Stratakis, C. Fotakis, Porous nanoparticles of Al and Ti generated by laser ablation in liquids, Applied Surface Science, 258 (2012) 9283-9287.

[258] B.K. Pandey, A.K. Shahi, R.K. Swarnkar, R. Gopal, Magnetic Property of Novel Cobalt Sulfate Nanoparticles Synthesized by Pulsed Laser Ablation, Science of Advanced Materials, 4 (2012) 537-543.
[259] Q. Li, C. Liang, Z. Tian, J. Zhang, H. Zhang, W. Cai, Core–shell TaxO@Ta2O5 structured nanoparticles: laser ablation synthesis in liquid, structure and photocatalytic property, CrystEngComm, 14 (2012) 3236.
[260] S.Z. Mortazavi, P. Parvin, A. Reyhani, Fabrication of graphene based on Q-switched Nd:YAG laser ablation of graphite target in liquid nitrogen, Laser Physics Letters, 9 (2012) 547-552.
[261] K. Hasna, S.S. Kumar, M. Komath, M.R. Varma, M.K. Jayaraj, K.R. Kumar, Synthesis of chemically pure, luminescent Eu3+ doped HAp nanoparticles: a promising fluorescent probe for in vivo imaging applications, Physical chemistry chemical physics : PCCP, 15 (2013) 8106-8111.
[262] N.V. Tarasenko, A.V. Butsen, M.I. Nedelko, N.N. Tarasenka, Laser-Aided Preparation and Modification of Gadolinium Silicide Nanoparticles in Liquid, The Journal of Physical Chemistry C, 116 (2012) 3897-3902.
[263] V. Švrček, T. Sasaki, R. Katoh, Y. Shimizu, N. Koshizaki, Aging effect on blue luminescent silicon nanocrystals prepared by pulsed laser ablation of silicon wafer in de-ionized water, Applied Physics B, 94 (2008) 133-139.
[264] P.A. Perminov, I.O. Dzhun, S.V. Zabotnov, A.A. Ezhov, E.I. Gatskevich, L.A. Golovan, P.K. Kashkarov, Silicon nanocrystal formation via laser ablation in liquid media, in: Lasers and Electro-Optics 2009 and the European Quantum Electronics Conference. CLEO Europe - EQEC 2009. European Conference on, 2009, pp. 1-1.
[265] Kamal Abderrafi, Raul García Calzada, Maxim B. Gongalsky, Isaac Suarez, Rafael Abarques, Vladimir S. Chirvony, Victor Yu Timoshenko, Rafael Ibañez, J.P. Martínez-Pastor, Silicon Nanocrystals Produced by Nanosecond Laser Ablation in an Organic Liquid, The Journal of Physical Chemistry C, 115 (2011) 5147-5151.
[266] P. Chewchinda, O. Odawara, H. Wada, The effect of energy density on yield of silicon nanoparticles prepared by pulsed laser ablation in liquid, Applied Physics A, 117 (2014) 131-135.
[267] R. Intartaglia, K. Bagga, F. Brandi, G. Das, A. Genovese, E. Di Fabrizio, A. Diaspro, Optical Properties of Femtosecond Laser-Synthesized Silicon Nanoparticles in Deionized Water, The Journal of Physical Chemistry C, 115 (2011) 5102-5107.
[268] E.V. Barmina, C. Fotakis, P.A. Loukakos, E. Stratakis, G.A. Shafeev, Laser-assisted nanostructuring of Silicon in liquid environment, Applied Physics A, 117 (2014) 359-364.
[269] S. Vadavalli, S. Valligatla, B. Neelamraju, M.H. Dar, A. Chiasera, M. Ferrari, N.R. Desai, Optical properties of germanium nanoparticles synthesized by pulsed laser ablation in acetone, Frontiers in Physics, 2 (2014) 57.
[270] Y. Jiang, P. Liu, Y. Liang, H.B. Li, G.W. Yang, Promoting the yield of nanoparticles from laser ablation in liquid, Applied Physics A, 105 (2011) 903-907.
[271] Y. Li, Laser ablation in liquid of germanium in externally applied electric fields, in, University of Missouri-Kansas City, 2013, pp. 57.
[272] O.V. Kharissova, H.V. Dias, B.I. Kharisov, B.O. Perez, V.M. Perez, The greener synthesis of nanoparticles, Trends in biotechnology, 31 (2013) 240-248.

[273] A. Granmayeh Rad, H. Abbasi, M.H. Afzali, Gold Nanoparticles: Synthesising, Characterizing and Reviewing Novel Application in Recent Years, Physics Procedia, 22 (2011) 203-208.
[274] A. Ayati, A. Ahmadpour, F.F. Bamoharram, B. Tanhaei, M. Manttari, M. Sillanpaa, A review on catalytic applications of Au/TiO2 nanoparticles in the removal of water pollutant, Chemosphere, 107 (2014) 163-174.
[275] N. Matsuo, H. Muto, K. Miyajima, F. Mafune, Single laser pulse induced aggregation of gold nanoparticles, Physical chemistry chemical physics : PCCP, 9 (2007) 6027-6031.
[276] Y. Takeuchi, T. Ida, K. Kimura, Colloidal Stability of Gold Nanoparticles in 2-Propanol under Laser Irradiation, J. Phys. Chem. B., 101 (1996) 1322-1327.
[277] José A. Rodríguez, Robert A. Campbell, D.W. Goodman, Electronic interactions in bimetallic systems: core level bindign energy shifts, Journal of Vacuum Science & Technology A, 9 (1991) 1698-1702.
[278] E. Giorgetti, F. Giammanco, P. Marsili, A. Giusti, Effect of Picosecond Postirradiation on Colloidal Suspensions of Differently Capped AuNPs, The Journal of Physical Chemistry C, 115 (2011) 5011-5020.
[279] G. Cristoforetti, E. Pitzalis, R. Spiniello, R. Ishak, F. Giammanco, M. Muniz-Miranda, S. Caporali, Physico-chemical properties of Pd nanoparticles produced by Pulsed Laser Ablation in different organic solvents, Applied Surface Science, 258 (2012) 3289-3297.
[280] M. Martin-Martinez, A. Álvarez-Montero, L.M. Gómez-Sainero, R.T. Baker, J. Palomar, S. Omar, S. Eser, J.J. Rodriguez, Deactivation behavior of Pd-C and Pt-C catalysts in the gas-phase hydrodechlorination of chloromethanes Structure–reactivity relationship, Applied Catalysis B: Environmental, 162 (2015) 532-543.
[281] J. Alan Creighton, D.G. Eadon, Ultraviolet-visible absorption spectra of the colloidal metallic elements, J. Chem. Soc. Faraday Trans., 87 (1991) 3881-3891.
[282] T. Nishi, N. Suzuki, N. Takahashi, K. Yano, Preparation of monodispersed Pd nanoparticles by laser ablation at air–suspension interface, Journal of Nanoparticle Research, 15 (2013).
[283] G. Cárdenas-Triviño, R.A. Segura, J. Reyes-Gasga, Palladium nanoparticles from solvated atoms—stability and HRTEM characterization, Colloid and Polymer Science, 282 (2004) 1206-1212.
[284] L.J. Chen, C.C. Wan, Y.Y. Wang, Chemical preparation of Pd nanoparticles in room temperature ethylene glycol system and its application to electroless copper deposition, Journal of colloid and interface science, 297 (2006) 143-150.
[285] J.B. Yadav, J.-W. Park, Y.-J. Cho, O.-S. Joo, Intermediate hydroxide enforced electrodeposited platinum film for hydrogen evolution reaction, International Journal of Hydrogen Energy, 35 (2010) 10067-10072.
[286] M. Martin-Martinez, A. Álvarez-Montero, L.M. Gómez-Sainero, R.T.Baker, J. Palomar, S. Omar, S. Eser, J.J. Rodriguez, Deactivation behavior of Pd/C and Pt/C catalysts in the gas-phase hydrodechlorination of chloromethanes: Structure–reactivity relationship, Applied Catalysis B: Environmental, 162 (2015) 532-543.
[287] G. Johansson, J. Hedman, A. Berndtsson, M. Klasson, R.l. Nilsson, Calibration of electron spectra, Journal of Electron Spectroscopy and Related Phenomena, 2 (1973) 295-317.

[288] Y. Baer, P.F. Hedén, J. Hedman, M. Klasson, C. Nordling, K. Siegbahn, Band Structure of Transition Metals Studied by ESCA, Physica Scripta, 1 (1970) 55.
[289] J.B. You, X.W. Zhang, J.J. Dong, X.M. Song, Z.G. Yin, N.F. Chen, H. Yan, Localized-Surface-Plasmon Enhanced the 357 nm Forward Emission from ZnMgO Films Capped by Pt Nanoparticles, Nanoscale research letters, 4 (2009) 1121-1125.
[290] N.C. Bigall, A. Eychmuller, Synthesis of noble metal nanoparticles and their non-ordered superstructures, Philosophical transactions. Series A, Mathematical, physical, and engineering sciences, 368 (2010) 1385-1404.
[291] E. Gharibshahi, E. Saion, Influence of dose on particle size and optical properties of colloidal platinum nanoparticles, International journal of molecular sciences, 13 (2012) 14723-14741.

FIGURE CAPTIONS

TABLE CAPTIONS

PUBLICATIONS

ARTICLES

2015 Synthesis and properties of palladium nanoparticles by pulsed laser ablation in liquid, M.I. Mendivil, B. Krishnan, G.A. Castillo, S. Shaji, Applied Surface Science, Vol. 348, Pages 45–53.

2015 Laser Sintering of Magnesia with Nanoparticles of Iron Oxide and Aluminum Oxide, ISSN: 0169-4332, García, L. V. Mendivil, M. I. Roy, T. K. Das, Castillo, G. A., Shaji, S., Int. Applied Surface Science, Vol. 336, Pages 59-66.

2015 Structure and morphologies of ZnO nanoparticles synthesized by pulsed laser ablation in liquid: Effects of temperature and energy fluence, Guillén, G. G., Palma, M. M., Krishnan, B., Avellaneda, D., Castillo, G. A., Roy, T. D. & Shaji, S., Materials Chemistry and Physics, Vol. 162, Pages 561-570.

2015 CdS thin films prepared by laser assisted chemical bath deposition, Garcia, L. V., Mendivil, M. I., Guillen, G. G., Martinez, J. A., Krishnan, B., Avellaneda, D. & Shaji, S., Applied Surface Science, Vol. 336, Pages 329-334.

2015 CuInGaSe2 nanoparticles by pulsed laser ablation in liquid medium, Mendivil, M. I., García, L. V., Krishnan, B., Avellaneda, D., Martinez, J. A. & Shaji, S., Materials Research Bulletin, Vol. 72, Pages 106-115.

2015 Synthesis and Characterization of Hercynite Nanoparticles by Pulsed Laser Ablation in Liquid Technique, Castillo Rodriguez, G. A., Guillen, G. G., Mendivil Palma, M. I., Das Roy, T. K., Guzman Hernandez, A. M., Krishnan, B. & Shaji, S., Int. J. Appl. Ceram. Technol., Vol. 12, No. S2, Pages E34-E43.

2013 Nanoparticles of Antimony Sulfide by Pulsed Laser Ablation in Liquid Media, ISSN 0022-2461, Daniel Garza, G. Grisel García, M. I. Mendivil Palma, D. Avellaneda, G. A. Castillo, T. K. Das Roy, B. Krishnan & S. Shaji, Journal of Materials Science, Vol. 48, No. 18, Pages 6445-6453.

2012 Synthesis of Silver Nanoparticles and Antimony Oxide Nanocrystals by Pulsed Laser Ablation in Liquid Media ISSN: 1432-0630, M. I. Mendivil, B. Krishnan, F. A. Sanchez, S. Martinez, J. A. Aguilar-Martinez, G. A. Castillo, D. I. Garcia-Gutierrez, S. Shaji, Applied Physics A., Vol. 110, No. 4, Pages 809-816

2010 Chemically Deposited Sb_2S_3 Thin Films for Optical Recording, ISSN: 1361-6463, S. Shaji, A. Arato, J.J. O`Brien, J. Liu, G. Alan Castillo, M.I. Mendivil Palma, T.K. Das Roy, B. Krishnan, J. Phys. D, Vol.43, No. 7, Pages 75404.

BOOK CHAPTER

2015 Structure and Properties of Metal, Semiconductor and Ceramic Nanomaterials Synthesized by Pulsed Laser Ablation in Liquid Technique**,** Laser Ablation: Fundamentals, Methods and Applications, Maria. I. Mendivil, Grisel Garcia, Bindu Krishnan, David Avellaneda, Tushar K. Das Roy, Guadalupe A. Castillo, and S. Shaji, Editor Nova Science Publishers, ISBN: 978-1-63482-589-4, p. 101-130

2014 Transmission Electron Microscopic Studies on Noble Metal Nanoparticles Synthesized by Pulsed Laser Ablation in Liquid, Microscopy: Advances in Scientific Research and Education, M.I. Mendivil, S. Shaji, G.A. Castillo and B. Krishnan, Editor A. Méndez-Vilas, Formatex Research Center. p. 911-920.